



HAL
open science

Speciation of plutonium and analogs in phosphate media

Danae Escalante

► **To cite this version:**

Danae Escalante. Speciation of plutonium and analogs in phosphate media. Radiochemistry. Université Paris-Saclay, 2023. English. NNT : 2023UPASP033 . tel-04518035

HAL Id: tel-04518035

<https://theses.hal.science/tel-04518035>

Submitted on 23 Mar 2024

HAL is a multi-disciplinary open access archive for the deposit and dissemination of scientific research documents, whether they are published or not. The documents may come from teaching and research institutions in France or abroad, or from public or private research centers.

L'archive ouverte pluridisciplinaire **HAL**, est destinée au dépôt et à la diffusion de documents scientifiques de niveau recherche, publiés ou non, émanant des établissements d'enseignement et de recherche français ou étrangers, des laboratoires publics ou privés.

Speciation of plutonium and analogs in phosphate media

Spéciation du plutonium et de ses analogues dans le milieu phosphate

Thèse de doctorat de l'université Paris-Saclay

École doctorale n° 576, Particules, Hadrons, Énergie et Noyau : Instrumentation, Imagerie,
Cosmos et Simulation (PHENIICS)

Spécialité de doctorat : Sciences de l'Aval du Cycle Nucléaire,
de la Radioprotection et de la Radiochimie

Graduate School : Physique. Référent : Faculté des Sciences d'Orsay

Thèse préparée dans l'unité de recherche **IJCLab (Université Paris-Saclay, CNRS)**,
sous la direction de **Claire LE NAOUR**, Chargée de recherche HDR

Thèse soutenue à Paris-Saclay, le 22 Mars 2023, par

Danae Carolina ESCALANTE GUTIÉRREZ

Composition du Jury

Membres du jury avec voix délibérative

Pedro DE OLIVEIRA Professeur (HDR), Université Paris-Saclay (LCP)	Président
Christophe DEN AUWER Professeur (HDR), Université Côte d'azur (ICN)	Rapporteur & Examineur
Stéphanie SZENKNECT Directrice de recherche CEA (HDR), Université Montpellier (ICSM)	Rapporteur & Examinatrice
Thomas VERCOUTER Directeur de recherche CEA (HDR), Université Paris-Saclay (CEA-Saclay)	Examineur

Titre: Spéciation du plutonium et de ses analogues dans le milieu phosphate

Mots clés: plutonium, europium, uranium, phosphate, spéciation, solubilité

Résumé: Élément incontournable du cycle du combustible, le plutonium est également présent dans l'environnement, sous différents degrés d'oxydation, suite à des disséminations liées au nucléaire civil et militaire. De même, l'acide phosphorique est formé lors du retraitement du combustible usé et les espèces phosphatées, d'origine naturelle ou anthropique, sont omniprésentes dans les sols et les eaux naturelles. Afin d'étudier l'interaction des ions du plutonium avec les espèces phosphates, différents protocoles expérimentaux ont été développés avec des analogues chimiques présentant un degré d'oxydation stable: Eu(III), Nd(III) et U(VI), pour simuler le comportement de Pu(III) et Pu(VI), respectivement. Les constantes de complexation de Eu(III) et U(VI) avec l'anion dihydrogéo-phosphate ont été déterminées. Le protocole de détermination du produit de solubilité du rhabdophane à base Nd a été appliqué à la monazite PuPO₄.

Title: Speciation of plutonium and analogs in phosphate media

Keywords: plutonium, europium, uranium, phosphate, speciation, solubility

Abstract : Plutonium is present in the environment as well as in the nuclear fuel cycle. Plutonium is release into the environment due to nuclear power accidents and military issues. In another hand, natural and anthropogenic phosphate species are deposited in soils and natural waters. Phosphoric acid can be formed during the reprocessing of spent nuclear fuel.

In order to study Pu-phosphate interaction, different experimental protocols have been developed with chemical analogs with a stable oxidation state: Eu(III), Nd(III), and U(VI), to simulate the behavior of Pu(III) and Pu(VI), respectively. In this context, the speciation of europium (III) with phosphate ligands was performed under two approaches.

The first one is the determination of thermodynamic data by liquid-liquid extraction using ^{152}Eu at trace scale. The second part of the Eu(III)-phosphate study is focused on the development of a protocol that can be applied in low amount of Pu(III)-phosphate compounds. For that purpose, a Nd(III)-based rhabdophane doped with 1% of ^{152}Eu were synthesized.

The solid was characterized by XRD, FTIR, TGA and SEM, and its dissolutions proved to be congruent regardless of the amount of mass used. This protocol was applied to Pu-phosphate compounds.

Then, the study of the complexation of uranium (VI)-phosphate was performed by UV-Vis spectrophotometry. The stability constants were determined at I=1 M in HClO_4 and $(\text{Na,H})\text{ClO}_4$ media and different temperatures.

The uranium-phosphate speciation is complemented by structural study using X-Ray absorption spectroscopy and DFT calculations in order to determine the coordination chemistry and the interatomic distances of the metal-ion. Finally, this investigation conclude, the protocols developed with Eu(III) and U(VI) are approved to be applied with the corresponding Pu-phosphate systems.

Acknowledgement

I would like to express my gratitude to my advisor **Dr. Claire LE NAOUR** for her guidance and support during the preparation of this project. Her invaluable expertise and encouragement helped me to complete this project and write this work.

I would also like to thank all the jury members of my defense **Dr. Pedro DE OLIVEIRA, Dr. Christophe DEN AUWER, Dr. Stéphanie SZENKNECT, Dr. Thomas VERCOUTER and Dr. Thomas DUMAS** for serving on my thesis committee and providing helpful feedback and suggestions.

I am grateful to **Dr. Melody MALOUBIER** for her support and understanding during this process.

I would like to extend my sincere gratitude to **Nicolas DACHEUX, Paul ESTEVENON, Philippe MOISY, Victor HAQUIN and Davide RODRIGUES**. Their willingness to share their experiences and insights has been invaluable to my research and help to make this thesis a success. Thank you for your time and contribution.

I am grateful to **CNRS** for the resources and financial support they provided during the development of this work.

Finally, I would also like to thank my colleague **Meng LUO** for her friendship and emotional support and I am very grateful with **Dr. Victor Fabian RUIZ-RUIZ** for his last minute help which will always be invaluable for me.

Content

Content

i.	List of abbreviations	i
ii.	List of figures	iii
iii.	List of tables	x
	Introduction	1
	References	7
	Chapter I. Bibliographic study	9
	I.1. Actinides	10
	I.1.1 Redox properties	10
	I.1.2. Aquo-ions	13
	I.1.3. Hydrolysis	14
	I.1.4. Actinide complexation	16
	I.1.5 Actinides in the environment	18
	I.2. Phosphate species and phosphoric acid.....	20
	I.2.1. Natural sources	21
	I.2.2. Anthropogenic sources of phosphates.....	22
	I.2.3. Phosphate/phosphoric acid and nuclear industry	23
	I.3 Actinides/lanthanides complexation with phosphate species.....	24
	I.3.1. Speciation of phosphoric acid	24
	I.3.2. Plutonium in phosphate media	27
	I.4 Plutonium analogs in complexing media	30
	I.4.1 Complexation of Pu(III) analogs with phosphate species.....	32
	I.4.2 Complexation of Pu(VI) analog with phosphate species	36
	Summary.....	45
	References	47
	Chapter II. Methodology	58

II.1. Main analytical techniques	63
II.1.1. Determination of the free acidity	63
II.1.2. Gamma spectrometry	64
II.1.3. PERALS.....	69
II.2. Studies in homogeneous solution	71
II.2.1. SIT modelling	73
II.2.2. Complexation of Eu at trace scale	76
II.2.3. Complexation of U and Eu at millimolar scale.....	85
II.3. Studies in heterogeneous systems	89
II.3.1. Determination of solubility products ($K_{s,0}^0$).....	89
II.3.2. Nd-based rhabdophane	91
II.3.3. PuPO ₄ monazite	95
Summary.....	97
References	99
Chapter III. Systems Ln(III)/Pu(III)-phosphate	105
III.1. Complexation of europium (III) with phosphate in aqueous solution.....	106
III.1.1. System Eu(III)/NaH ₂ PO ₄ /(Na,H)ClO ₄ /TTA/toluene.....	106
III.1.2. System Eu(III)/NaH ₂ PO ₄ /(Na,H)Cl/HDEHP/Toluene	112
III.2. Solubility of Nd(III)-based rhabdophane	125
III.2.1. Characterization of Nd-rhabdophane doped with 1% of Eu	125
III.2.2. Dissolution of Nd(III)-based rhabdophane.....	130
III.2.3. Preliminary study in PuPO ₄ monazite	135
III.3. Conclusions and perspectives related to Ln(III)-phosphate systems.....	141
References	142
Chapter IV. System An(VI)-phosphate	146
IV.1. Study of the complexation of uranium(VI) with phosphoric acid by UV-Vis spectrophotometry	147

IV.1.1. Uranium(VI) in 1 M HClO ₄ media	147
IV.1.2. Stability of U(VI)-phosphate complexes.....	148
IV.1.3. Complexation of U(VI) with phosphate in 1 M HClO ₄ , and electrolyte B	152
IV.1.4. Temperature effect on the complexation of U(VI) with phosphate	155
IV.1.5. Structural study of the complexation of UO ₂ (H ₂ PO ₄) ₂	160
IV.2. Conclusions and perspectives related to An(VI)-phosphate systems.....	165
References	167
Chapter V. Conclusion and perspectives.....	169
References	173
Appendix	174
Appendix 1. Calculation of the density of the solutions at different temperatures ..	175
Appendix 2. Preparation of the solutions	176
A.2.1. Preparation of the stock solutions.....	176
A.2.2. Preparation of the electrolytes	177
A.2.3. Preparation of aqueous phases.....	179
A.2.4. Preparation of organic phases	180
Appendix 3. Determination of the amount ¹⁵² Eu in rhabdophane (on HPGe 4000 detector).....	183
Appendix 4. Experimental techniques.....	185
Appendix 5. Supplementary data relative to Eu	189
References	196
Abstract in French.....	198

i. List of abbreviations

ATR-FTIR	Attenuated Total Reflection-Fourier-Transform Infrared Spectroscopy
CEA	Commissariat à l'énergie atomique/ Atomic Energy Commission
CERCA-	Compagnie pour l'Etude et la Réalisation de Combustibles Atomiques
LEA	Laboratoire d'Etalons d'Activité
DBP	Dibutyl phosphate
DFT	Density functional theory
EXAFS	Extended X-Ray Absorption Fine Structure
FTIR	Fourier-Transform Infrared Spectroscopy
HDEHP	Di-(2-ethylhexyl) phosphoric acid
HPGe detector	High Purity Germanium radiation detector
ICP-OES	Inductively Couple Plasma - Optical Emission Spectrometry
ICSM	Institut de Chimie Séparative de Marcoule
JCPDS	Joint Committee on Powder Diffraction Standards
LLE	Liquid-Liquid extraction
M	Molarity (mol L ⁻¹)
m	molality (mol Kg ⁻¹)
MBP	Monobutyl phosphate
NEA-TDB	Nuclear Energy Agency-Thermochemical Database Project
OECD	Organization for Economic Co-operation and Development
PDF	Powder Diffraction File
PERALS	Photon Electron Rejecting Alpha Liquid Scintillation
pK_a	Dissociation constant
PUREX	Plutonium Uranium Extraction Process
rpm	Revolution per minute
SEM	Scanning Electron Microscopy
SIT	Specific Ion Interaction Theory
TBP	Tributyl phosphate
TGA	Thermogravimetric analysis
TRLFS	Time-resolved Laser-induced Fluorescence Spectroscopy

TTA	Thenoyltrifluoroacetone
UV-Vis	Ultraviolet visible
XANES	X-Ray Absorption Near Edge Structure
XAS	X-Ray Absorption Spectroscopy
X-EDS	Energy-dispersive X-ray spectroscopy
XRD	X-Ray diffraction

ii. List of figures

Introduction

Figure 1. Scheme of the nuclear fuel cycle ^[1]	2
Figure 2. Separation of plutonium from uranium ^[16]	4

Chapter I. Bibliographic study

Figure I.1. Periodic table of the elements ^[2]	10
Figure I.2. Potential-pH diagram of uranium at 25 °C ($U_{\text{tot}} 10^{-10}$ M) using database from OECD/NEA ^[5]	12
Figure I.3. Latimer's diagram of Pu in 1 M HClO ₄ ^[6]	13
Figure I.4. (a) The color of non-complexed plutonium at various oxidation states in 1 M HClO ₄ from Pu(III) to Pu(VI) and in strong base for Pu(VII) (b) their corresponding absorption spectra ^[20]	14
Figure I.5. Hydrolysis speciation diagram of mononuclear Pu(III), Eu(III), Pu(VI) and U(VI) without considering colloid or polymer species	16
Figure I.6. Common oxidation states of actinides in the environment under different conditions. States mentioned in bracket (–) are unstable; and with a question mark (?) were not confirmed. The oxidation states bolded correspond to the predominant states ^[36]	19
Figure I.7. Molecular structure of TBP ^[64]	23
Figure I.8. Pu(VI)-phosphate absorption spectra (pH=1, $C_{\text{Pu(VI)}}=1 \times 10^{-3}$ M, and phosphate at a.0 M, b. 0.023 M and c. 0.062 M) ^[82]	28
Figure I.9. Variation of the solubility of PuPO ₄ (cr, hyd) as function of NaH ₂ PO ₄ concentration. The black line corresponds to SIT modeling ^[85]	29
Figure I.10. Optimized structures from DFT calculations of hydrated $\text{Cm}(\text{H}_2\text{PO}_4)_2^{2+}$ (Cm in yellow, O in red and P in violet) ^[98]	34
Figure I.11. Optimized structures from DFT calculations of hydrated $\text{Cm}(\text{H}_2\text{PO}_4)_2^+$ (Cm in yellow, O in red and P in violet) ^[98]	34
Figure I.12. Fluorescence spectra of UO_2^{2+} , $\text{UO}_2\text{H}_2\text{PO}_4^+$, $\text{UO}_2(\text{H}_2\text{PO}_4)_2$, UOHPO_4 and UO_2PO_4^- ^[124]	37
Figure I.13. Effect of phosphate concentration on the UV-Vis absorption spectra of U(VI) in 1 M HClO ₄ (a. free UO_2^{2+} ; b, c, d. Varying the ratio $[\Sigma\text{PO}_4]/\text{U(VI)}$) ^[112]	38

Figure I.14. Speciation diagrams of U(VI)-phosphate at different temperatures ($C_{U(VI)}=5\times 10^{-5}$ M, I=0.5 M NaClO ₄ , pH=1, T=25 and 100) ^[130]	41
Figure I.15. Optimized structure from DFT calculations of UO ₂ (HPO ₄)(H ₂ O) ₃ with bond lengths (in Å) and angles (in degrees) according to a. Jackson et al. ^[109] and b. Majumdar et al. ^[128]	42
Figure I.16. Optimized structures from DFT calculations of hydrated U(VI)-phosphate complexes of stoichiometry 1:1 ^[126]	43
Figure I.17. Optimized structures from DFT calculations of hydrated U(VI)-phosphate complexes of stoichiometry 1:2 ^[126]	44

Chapter II. Methodology

Figure II.1. Calibration curve using 0.5 NaClO ₄ /0.5 M HClO ₄ buffer solutions	63
Figure II.2. Interaction of the radiation with the matter ^[8]	64
Figure II.3. Basic set-up for γ spectrometry ^[7]	66
Figure II.4. Characteristic shape of the coaxial germanium detector efficiency curve ^[11]	69
Figure II.5. Energy transfer in a liquid scintillator cocktail ^[15]	70
Figure II.6. α -liquid scintillation spectrum of the diluted stock solution of U(VI) used in UV-Vis spectrophotometry experiments	71
Figure II.7. Reactions pathways between micro- and macrocomponents ^[18]	72
Figure II.8. Competition of ¹⁵² Eu between to immiscible phases in liquid-liquid extraction experiments.....	78
Figure II.9. Structural formulas of the chelating agent 2-thenoyltrifluoroacetone (HTTA, M=metal, z=charge of M) ^[41]	79
Figure II.10. Structural formula of dimer Bis(2-ethylhexyl)phosphoric acid (HDEHP) ^[53]	80
Figure II.11. Principle of EXAFS ^[71]	88
Figure II.12. Experimental methodology	98

Chapter III. System Ln(III)-phosphate

Figure III.1. UV-Vis absorption spectra of Eu(III)-TTA complex ($C_{HTTA}=5\times 10^{-5}$ M, $0\leq C_{Eu(III)}\leq 0.02$ M, $pC_H=3.7$, I=0.5 M NaClO ₄ / CH ₃ OONa), 1 cm path length	107
---	-----

Figure III.2. Temperature dependency of the stability constant of $\text{Eu}(\text{TTA})^{2+}$	109
Figure III.3. Variation of the distributions ratio of Eu as a function of total concentration of phosphate ($0 \leq [\Sigma\text{PO}_4] \leq 0.1 \text{ M}$, $C_{\text{Eu}} = 10^{-8} \text{ M}$, $C_{\text{TTA}} = 2.5 \times 10^{-2} \text{ M}$, $I = 0.5 \text{ M NaClO}_4\text{-HClO}_4$, $\text{pC}_\text{H} = 3.9$ and $T = 25^\circ\text{C}$)	111
Figure III.4. Percentage of ^{152}Eu activity ($C_{\text{Eu}} = 10^{-8} \text{ M}$, $C_{\text{TTA}} = 2.5 \times 10^{-2} \text{ M}$, $I = 0.5 \text{ M NaClO}_4\text{-HClO}_4$, $\text{pC}_\text{H} = 3.9$ and $T = 25, 40, 50$ and 60°C).....	111
Figure III.5. Variation of the percentage of extracted Eu as a function of pC_H ($C_{\text{Eu}} = 7 \times 10^{-8} \text{ M}$, $C_{\text{HDEHP}} = 0.01 \text{ M}$ in toluene, $I = 1 \text{ M NaCl-HCl}$, $T = 25^\circ\text{C}$)	113
Figure III.6. Variation of the distribution ratio of Eu as a function of phosphate concentration ($0 \leq [\Sigma\text{PO}_4] \leq 0.5 \text{ M}$, $C_{\text{HDEHP}} = 0.0075 \text{ M}$, $I = 1 \text{ M NaCl-HCl}$, $\text{pC}_\text{H} = 3.1$ and $T = 25^\circ\text{C}$).....	114
Figure III.7. Fit example: $[(D_0/D) - 1]$ as a function of $[\Sigma\text{PO}_4]$ ($C_{\text{HDEHP}} = 0.0075 \text{ M}$, $0 \leq [\Sigma\text{PO}_4] \leq 0.1 \text{ M}$, $I = 1 \text{ M NaCl-HCl}$, $\text{pC}_\text{H} = 3.1$ and $T = 25^\circ\text{C}$)	115
Figure III.8. Fit example: $[(D_0/D) - 1]$ as a function of $[\Sigma\text{PO}_4]$ ($C_{\text{HDEHP}} = 0.0075 \text{ M}$, $0 \leq [\Sigma\text{PO}_4] \leq 0.35 \text{ M}$, $I = 1 \text{ M NaCl-HCl}$, $\text{pC}_\text{H} = 3.1$ and $T = 25^\circ\text{C}$)	115
Figure III.9. Variation of the distributions ratio of ^{152}Eu as a function of total phosphate concentration ($C_{\text{Eu}} = 10^{-8} \text{ M}$, $0 \leq [\Sigma\text{PO}_4] \leq 0.5 \text{ M}$, $C_{\text{HDEHP}} = 0.0075 \text{ M}$, $I = 1 \text{ M (Na,H)Cl}$, $\text{pC}_\text{H} = 3.1$, $T = 15$ and 60°C)	118
Figure III.10. Variation of $\log \beta_i^{\text{H-app}}$ as a function of temperature at $I = 1 \text{ M NaCl-HCl}$ according to equilibria III.11 and III.12	121
Figure III.11. Fit example: $[(D_0/D) - 1]$ as a function of $[\Sigma\text{PO}_4]$ ($C_{\text{HDEHP}} = 0.0075 \text{ M}$, $0.35 \leq [\Sigma\text{PO}_4] \leq 0.5 \text{ M}$, $I = 1 \text{ M NaCl-HCl}$, $\text{pC}_\text{H} = 3.1$ and $T = 25^\circ\text{C}$)	123
Figure III.12. Distribution diagram of Eu(III) -phosphate complexes ($C_{\text{Eu}} = 10^{-8} \text{ M}$, $I = 1 \text{ M NaCl-HCl}$, $\text{pC}_\text{H} = 3.1$ and $T = 25^\circ\text{C}$)	125
Figure III.13. FTIR spectra recorded for $\text{Eu}_{0.01}\text{Nd}_{0.99} \cdot n\text{H}_2\text{O}$ and $\text{NdPO}_4 \cdot n\text{H}_2\text{O}$	126
Figure III.14. Experimental XRD patterns obtained for $\text{Eu}_{0.01}\text{Nd}_{0.99} \cdot 0.667\text{H}_2\text{O}$ and $\text{NdPO}_4 \cdot 0.667\text{H}_2\text{O}$ with the theoretical XRD patterns of the hydrated monoclinic Nd-rhabdophane.....	127
Figure III.15. Thermogravimetric analysis of $\text{Eu}_{0.01}\text{Nd}_{0.99} \cdot 0.667\text{H}_2\text{O}$ ($2^\circ\text{K} \cdot \text{min}^{-1}$, argon atmosphere)	129
Figure III.16. SEM micrographs of $\text{Eu}_{0.01}\text{Nd}_{0.99}\text{PO}_4 \cdot 0.667\text{H}_2\text{O}$	129
Figure III.17. Evolution of neodymium, europium, and phosphorous elemental concentrations during the dissolution of $\text{Eu}_{0.01}\text{Nd}_{0.99}\text{PO}_4 \cdot 0.667\text{H}_2\text{O}$ in 0.1 M HCl solution at room temperature.....	130

Figure III.18. SEM micrographs of $\text{Eu}_{0.01}\text{Nd}_{0.90}\text{PO}_4 \cdot 0.667\text{H}_2\text{O}$ before and after the dissolution experiments (0.1 M HCl, room temperature).....	131
Figure III.19. Flowchart for the determination of elemental concentrations.....	131
Figure III.20. Evolution of the dissolution of $\text{Eu}_{0.012}\text{Nd}_{0.988}\text{PO}_4 \cdot 0.667\text{H}_2\text{O}$ doped with ^{152}Eu in 0.15 M HCl at 25°C	132
Figure III.21. X-Ray diffraction pattern of PuPO_4 monazite (experimental, calculated patterns and the difference between them are plotted)	135
Figure III.22. FTIR spectra recorded for PuPO_4 monazite.....	136
Figure III.23. Absorption spectra of the supernatant obtained from dissolution of PuPO_4 in 0.1 M HCl in the presence of 10^{-3} M $\text{NH}_2\text{OH} \cdot \text{HCl}$	137
Figure III.24. PERALS spectra of the supernatant obtained from the dissolution of PuPO_4 in the mixture 4×10^{-4} M NaH_2PO_4 , 10^{-3} M HA and 1.57×10^{-2} M HCl (Counting time: 2000 s).....	139
Figure III.25. PuPO_4 dissolution as a function of NaH_2PO_4 concentration obtained in this work ($4 \times 10^{-4} \leq [\Sigma\text{PO}_4] \leq 0.5$ M, $1.57 \times 10^{-2} \leq [\text{HCl}] \leq 1.99 \times 10^{-1}$ in presence of 10^{-3} M $\text{NH}_2\text{OH} \cdot \text{HCl}$, pH=2 and T=25°C)	140
Figure III.26. PuPO_4 dissolution as a function of NaH_2PO_4 concentration reported by Rai et. al., [39]	140

Chapter IV. System An(VI)-phosphate

Figure IV.1. Absorption spectra of U(VI) at different concentration (I=1 M HClO_4).	148
Figure IV.2. Evolution of the absorbance as a function of $C_{\text{U(VI)}}$ ($\lambda_{\text{max}}=413.8$ nm, $1.74 \times 10^{-3} \text{ M} \leq C_{\text{U(VI)}} \leq 1.75 \times 10^{-2} \text{ M}$, I=1 M HClO_4)	148
Figure IV.3. UV-Vis absorption spectra of U(VI) and U(VI)-phosphate in electrolyte A ($C_{\text{U(VI)}}=7 \times 10^{-3}$ M and ratio $\Sigma\text{PO}_4/\text{U}=40$).....	149
Figure IV.4. UV-Vis absorption spectra over the time of U(VI)-phosphate in electrolyte A at ratio 1:1.....	150
Figure IV.5. UV-Vis absorption spectra over the time of U(VI)-phosphate in electrolyte A at ratio 1:5.....	150
Figure IV.6. UV-Vis absorption spectra over the time of U(VI)-phosphate in electrolyte A at ratio 1:7.....	150
Figure IV.7. UV-Vis absorption spectra over the time of U(VI)-phosphate in electrolyte A at ratio 1:10.....	150

Figure IV.8. UV-Vis absorption spectra over the time of U(VI)-phosphate in electrolyte A at ratio 1:20.	150
Figure IV.9. UV-Vis absorption spectra over the time of U(VI)-phosphate in electrolyte A at ratio 1:40.	150
Figure IV.10. UV-Vis absorption spectra of U(VI)-phosphate in electrolyte A at ratio 1:1 registered at t=0 and 14 days of preparation.	151
Figure IV.11. UV-Vis absorption spectra over the time of U(VI)-phosphate in electrolyte A at ratio 1:10.	151
Figure IV.12. UV-Vis absorption spectra of U(VI)-phosphate system at I= 1 M HClO ₄ (C _{U(VI)} =5.2×10 ⁻³ M, 0≤ΣPO ₄ /U(VI)≤20, T=20°C)	153
Figure IV.13. UV-Vis absorption spectra of U(VI)-phosphate system in electrolyte B (C _{U(VI)} =7.1×10 ⁻³ M, 0≤ΣPO ₄ /U(VI)≤20, T=20°C)	153
Figure IV.14. Molar absorption coefficient of UO ₂ ²⁺ , UO ₂ (H ₂ PO ₄) ⁺ and UO ₂ (H ₂ PO ₄) ₂ in 1 M HClO ₄	154
Figure IV.15. Molar absorption coefficient of UO ₂ ²⁺ , UO ₂ (H ₂ PO ₄) ⁺ and UO ₂ (H ₂ PO ₄) ₂ in 0.5M HClO ₄ /0.5M NaClO ₄	154
Figure IV.16. Variations of stability constant of UO ₂ (H ₂ PO ₄) ⁺ and UO ₂ (H ₂ PO ₄) ₂ complexes as a function of inverse temperature at I=1 M HClO ₄	158
Figure IV.17. Variations of stability constant of UO ₂ (H ₂ PO ₄) ⁺ and UO ₂ (H ₂ PO ₄) ₂ complexes as a function of inverse temperature at I= 0.5 M HClO ₄ /0.5 M NaClO ₄ ...	158
Figure IV.18. Speciation diagram of U(VI)-phosphate complexes in 1 M HClO ₄ at T=20°C and 50°C (C _{U(VI)} =5.2×10 ⁻³ M, Σ(PO ₄)/U=0 to 20, T= 20°C and 50°C)	160
Figure IV.19. Speciation diagram of U(VI)-phosphate complexes in 0.5 M HClO ₄ /0.5 M NaClO ₄ at T=20°C and 50°C (C _{U(VI)} =7.1×10 ⁻³ M, Σ(PO ₄)/U=0 to 20, T=20°C and 50°C)	160
Figure IV.20. Speciation diagram of U(VI)-phosphate complexes calculated at standard conditions from stability constants determined in this work (C _{U(VI)} =7×10 ⁻³ M, [ΣPO ₄]= 1 M, T=25°C, I=1 M HClO ₄)	161
Figure IV.21. UV-Vis absorption spectra of UO ₂ (H ₂ PO ₄) ₂ (C _{U(VI)} =7×10 ⁻³ M, [ΣPO ₄]=1 M, T=25°C)	161
Figure IV.22. Experimental (open circles) and best adjustment (line) of the k ² -weighted EXAFS spectrum and its corresponding Fourier transform at the U L _{III} edge for a solution of U(VI) at 7×10 ⁻³ M in presence of phosphates (ΣPO ₄ =1 M) at pH 2.	163
Figure IV.23. Proposed structure of the U(VI)-diphosphate complex	164

Figure IV.24. UV-Vis-NIR absorption spectra of Pu at different oxidation states in 1 M HCl-1 M NH ₂ OH HCl ^[20]	166
---	-----

VI. Appendix

Figure A.1. Titration curve of HDEHP purified 10-fold diluted in ethanol (reagent used in this work).....	182
Figure A.2. Titration curve of non-purified HDEHP ^[5]	182
Figure A.3. ICP-OES calibration curve for Nd	186
Figure A.4. ICP-OES calibration curve for P	186
Figure A.5. ICP-OES calibration curve for Eu.....	187
Figure A.6. UV-Vis absorption spectra of Eu(III) ($C_{Eu(III)}=2.5 \times 10^{-2}$ M, $T=25^{\circ}\text{C}$, $pC_H=3.52$, $I=0.5$ M NaClO ₄ / CH ₃ OONa).....	189
Figure A.7. UV-Vis absorption spectra of Eu(III)-TTA (keto-hydrate form) complexation ($C_{TTA}=5 \times 10^{-5}$ M, $0 \leq C_{Eu(III)} \leq 0.02$ M, $pC_H=3.7$, $I=0.5$ M NaClO ₄ /CH ₃ OONa at $T=$ a. 40°C , b. 50°C and c. 60°C	190
Figure A.8. Variation of the distributions coefficients of ¹⁵² Eu as a function of total phosphate concentration ($C_{Eu} \approx 10^{-8}$ M, $0 \leq [\Sigma\text{PO}_4] \leq 0.5$ M, $C_{HDEHP}=0.0075$ M, $I=1$ M NaCl-HCl, $pC_H=3.1$, $T=40^*$ and 50^*°C).....	191
Figure A.9. Deduction of $\log \beta_1^{\text{cond}}$ by fitting $(D_0/D)-1$ as a function of total phosphate concentration ($C_{Eu} \approx 10^{-8}$ M, $C_{HDEHP}=0.0075$ M, $10^{-2} \leq [\Sigma\text{PO}_4] \leq 0.1$ M, $I=1$ M NaCl-HCl, $pC_H=3.1$ and $T=15, 40^*, 50^*$ and 60^*°C)	192
Figure A.10. Deduction of $\log \beta_2^{\text{cond}}$ by fitting $(D_0/D)-1$ as a function of total phosphate concentration to second order polynomial ($C_{Eu} \approx 10^{-8}$ M, $C_{HDEHP}=0.0075$ M, $10^{-2} \leq [\Sigma\text{PO}_4] \leq 0.1$ M, $I=1$ M NaCl-HCl, $pC_H=3.1$ and $T=15, 40^*, 50^*$ and 60^*°C).....	193
Figure A.11. Deduction of $\log \beta_3^{\text{cond}}$ by fitting $(D_0/D)-1$ as a function of total phosphate concentration to third order polynomial ($C_{Eu} \approx 10^{-8}$ M, $C_{HDEHP}=0.0075$ M, $10^{-2} \leq [\Sigma\text{PO}_4] \leq 0.1$ M, $I=1$ M NaCl-HCl, $pC_H=3.1$ and $T=15, 40^*, 50^*$ and 60^*°C).....	194
Figure A.12. Experimental and calculate XRD patterns and Rietveld refinement obtained for Eu _{0.01} Nd _{0.99} ·nH ₂ O.....	195

Abstract in French

Figure S.1. Variations du coefficient de distribution de ^{152}Eu en fonction de la concentration totale de phosphate ($C_{\text{Eu}} = 10^{-8} \text{ M}$; $C_{\text{HDEHP}} = 0.0075 \text{ M}$; $I = 1 \text{ M (H,NaCl)}$; $\text{pC}_{\text{H}} = 3,1$; 25°C)..... 201

Figure S.2. Dissolution de PuPO_4 en fonction de la concentration de phosphate (mesures PERALS)..... 203

Figure S.3. Spectres d'absorption de U(VI) 7 mM pour différents ratio phosphate/métal à 20°C en milieu NaClO_4 0.5 M/ HClO_4 0.5 M 203

iii. List of tables

Chapter I. Bibliographic study

Table I.1. Oxidation states of actinides in aqueous solution (the most common ones are denoted in bold) ^[3]	11
Table I.2. Effective charge on actinide ions ^[22]	14
Table I.3. Standard first hydrolysis constants of Eu ³⁺ and actinide ions.....	15
Table I.4. Classification of Bases ^[33]	17
Table I.5. Common phosphate minerals and An-phosphate bearing phases ^[46-50]	21
Table I.6. Standard thermodynamic data associated to the successive dissociation equilibria of phosphoric acid ^[28]	25
Table I.7. Main dimeric species in phosphoric solution.....	26
Table I.8. Dissociation equilibrium of Na-phosphoric acid ion pairs at T=25°C ^[80]	27
Table I.9. Equilibrium reactions and stability constants for Pu-phosphate compounds ^[84]	29
Table I.10. Standard thermodynamic data for plutonium (III) and (VI)-phosphate species in aqueous solution	30
Table I.11. Comparison of thermodynamic data for plutonium(III) and europium(III) complexes	31
Table I.12. Comparison of thermodynamic data for plutonium (VI) and uranium(VI) complexes ^[28]	32
Table I.13. Standard stability constants selected in NEA-TDB and most recent investigations for M(H ₂ PO ₄) ²⁺ and M(H ₂ PO ₄) ₂ ⁺ complexes.....	33
Table I.14. Interatomic distances of Cm(III)-phosphate complexes ^[98]	34
Table I.15. Solubility products determined for Eu(III), Nd(III), Am(III) and Pu(III) in rhabdophane and monazite phases	36
Table I.16. Selected thermodynamic data for uranium-phosphate complexes in aqueous solution (T=25°C, 0.1 MPa, I=0) ^[28]	40

Chapter II. Methodology

Table II.1. Summary of the techniques and studied systems in this work	62
Table II.2. Characteristics of the unsealed standard source of ¹⁵² Eu (CERCA-LEA)....	67
Table II.3. Characteristics gamma rays emission of ¹⁵² Eu isotope.....	68

Table II.4. Efficiency calibration of HPGe detector and associated uncertainty	69
Table II.5. Extraction (in %) of actinides with ALPHAEX from nitric acid solutions ^[16]	70
Table II.6. Ion interaction coefficient (ϵ_{ij}) in kg mol^{-1} used in this work ($T=25^\circ\text{C}$, $P=1$ bar).....	73
Table II.7. Charge of the species and corresponding ion interaction coefficient (ϵ_{ij}) and $\log K_a$ in $\text{m (kg mol}^{-1})$ at $T=25^\circ\text{C}$, $P=1$ bar	74
Table II.8. Debye- Hückel constants as a function of temperature at a pressure of 1 bar ^[20]	75
Table II.9. Dissociation constants of phosphoric acid at $I=1$ M (Na,H)ClO ₄ and different temperatures.....	75
Table II.10. Dissociation constants of phosphoric acid at $I= 1$ M (Na,H)Cl and different temperatures.....	76
Table II.11. Dissociation constants of phosphoric acid at $I=1$ M HClO ₄ and different temperatures.....	76
Table II.12. Acid dissociation constants of HDEHP in different organic diluent and aqueous phases ^[55]	81
Table II.13. Samples preparation for the complexation study of Eu(III)-phosphate.....	84

Chapter III. System Ln(III)-phosphate

Table III.1. Stability constants for Eu(TTA)^{2+} complex formed in aqueous solution at $T=25^\circ\text{C}$ (Equilibrium III.1).....	108
Table III.2. Conditional and apparent stability constant for the formation of $\text{Eu(H}_2\text{PO}_4\text{)}^{2+}$ and $\text{Eu(H}_2\text{PO}_4\text{)}_2^+$ complexes ($I=1$ M (Na,H)Cl, $T=25^\circ\text{C}$)	116
Table III.3. Complexations constants for $\text{M(H}_2\text{PO}_4\text{)}^{2+}$ and $\text{M(H}_2\text{PO}_4\text{)}_2^+$ at $T=25^\circ\text{C}$ according to equilibria III.11 and III.12 and first protonation constant of H_3PO_4	117
Table III.4. Conditional and apparent stability constant for the formation of $\text{Eu(H}_2\text{PO}_4\text{)}^{2+}$ and $\text{Eu(H}_2\text{PO}_4\text{)}_2^+$ complexes ($I=1$ M (Na,H)Cl)	118
Table III.5. Conditional and apparent stability constants for the formation of $\text{Eu(H}_2\text{PO}_4\text{)}^{2+}$ and $\text{Eu(H}_2\text{PO}_4\text{)}_2^+$ at different temperatures ($I=1$ M (Na,H)Cl and first dissociation constant of H_3PO_4	120
Table III.6. Thermodynamic functions for $\text{Eu(H}_2\text{PO}_4\text{)}^{2+}$ and $\text{Eu(H}_2\text{PO}_4\text{)}_2^+$ complexes	122

Table III.7. Thermodynamic parameters calculated from successive complexation constant $K_i^{H\text{-app}}$ of Eu(III)-phosphate complexes	122
Table III.8. Conditional and apparent stability constants for the formation of and $\text{Eu}(\text{H}_2\text{PO}_4)_3^0$ at different temperatures (I=1 M (Na,H)Cl).....	124
Table III.9. Assignment of the vibration bands observed on the FTIR spectra for $\text{Eu}_{0.01}\text{Nd}_{0.99}\cdot n\text{H}_2\text{O}$ and $\text{NdPO}_4\cdot n\text{H}_2\text{O}$ compounds ^[28-31]	127
Table III.10. Unit cell parameters a, b, c, β and lattice volume for Nd and Eu based rhabdophane at room temperature (monoclinic C2 Space group).....	128
Table III.11. Concentration of Nd, Eu and P at the equilibrium	133
Table III.12. Elementary concentrations measured at the equilibrium, calculated molality of the predominant species, equilibrium constants form the predominant aqueous species ($\log_{10}^* K_s$) and standard solubility products obtained at $T=24\pm 1$ for the $\text{Eu}_{0.01}\text{Nd}_{0.99}\text{PO}_4\cdot 0.667\text{H}_2\text{O}$ in 0.1 M HCl and $\text{Eu}_{0.012}\text{Nd}_{0.988}\text{PO}_4\cdot 0.667\text{H}_2\text{O}$ with ^{152}Eu in 0.15 M HCl at different amount of solid	134
Table III.13. Cell parameters of PuPO_4 synthesized in the present work and data available in the literature	135
Table III.14. Composition of the solutions used for PuPO_4 dissolution studies (HA stands for hydroxylammonium hydrochloride $\text{NH}_2\text{OH}\cdot\text{HCl}$).....	137
Table III.15. Isotopic composition of plutonium and nuclear characteristics of each isotope ^[46]	139
Table III.16. Alpha-measurements of Pu supernatant sampling	140

Chapter IV. System An(VI)-phosphate

Table IV.1. Obtained stability constants for $\text{UO}_2(\text{H}_2\text{PO}_4)^+$ and $\text{UO}_2(\text{H}_2\text{PO}_4)_2$ (Equilibrium IV.3).....	155
Table IV.2. Complexation constants according to equations in Table I.16	155
Table IV.3. Stability constant of U(VI)-phosphate complexes at different temperatures and 1 M HClO_4 and electrolyte B(0.5 M HClO_4 /0.5 M NaClO_4)	157
Table IV.4. Thermodynamic parameters for $\text{UO}_2(\text{H}_2\text{PO}_4)^+$ and $\text{UO}_2(\text{H}_2\text{PO}_4)_2$ complexes at $T=25^\circ\text{C}$ in different media.....	159
Table IV.5. EXAFS best fit parameters for the U(VI)-phosphate solutions at pH 2. s_0^2 is the EXAFS global amplitude factor ; $\Delta\chi^2$ is the quality factor and $R_f(\%)$ is the agreement factor of the fit.	163

VI. Appendix

Table A.1. Parameters for density calculation in aqueous solution..... 175

Table A.2. Summary of the reagents and starting materials..... 176

Table A.3. Selected wavelengths for the determination of the element concentrations by ICP-MS 177

Table A.4. Preparation of the electrolytes at fixed ionic strength 178

Table A.5. Absolute activity calculated in total dissolution samples (90µL and 250µL samples) 183

Table A.6. Parameters used for calculation of concentration in dissolution experiments [8] 184

Table A.7. Selected wavelength for the determination of Nd(III), Eu(III) and P concentration by ICP-OES in dissolution experiments. 185

Introduction

Introduction

Human activities related to nuclear issues, civil as well as military, have led to the production of actinides and to their dissemination in the environment. These radioelements are involved in all parts of the nuclear fuel cycle shown in **Figure 1**^[1]. In most of the reactors, the used fuel is in the form of UO₂ with uranium enriched with ²³⁵U. In the steps of extraction and milling of uranium ore, conversion, enrichment and fuel fabrication (with non-reprocessed U), only natural uranium isotopes and their daughters are present^[2].

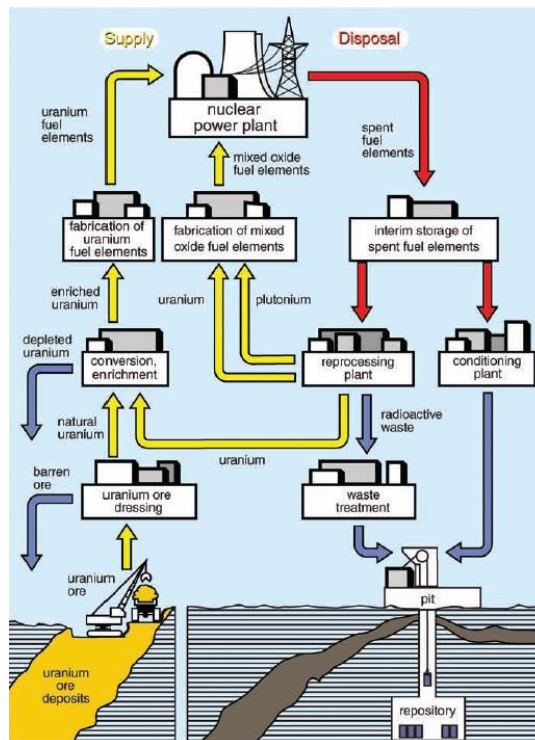
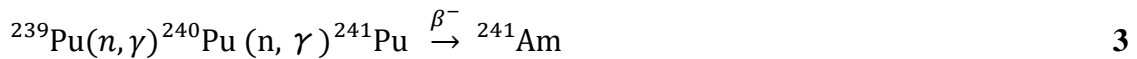


Figure 1. Scheme of the nuclear fuel cycle^[1]

In the nuclear power plant, the splitting of fissile actinide isotopes ²³⁵U, ²³⁹Pu, or ²³³U, under neutron irradiation releases high amount of energy with simultaneous emission of neutrons. However, in addition to these (n,f) reactions that lead to the production of fission products (*e.g.* Tc, Cs, I...), other nuclear reactions occur under neutron flux, especially (n,2n) reactions, successive neutron capture (n,γ) and β-decay that lead to the production of actinide isotopes as illustrated in **Eqs. 1-2** for ²³⁷Np and **Eq. 3** for ²⁴¹Am, two minor actinides and in **Eq. 4** for the fissile isotope ²³⁹Pu.





Then the spent fuel is discharged and stored in cooling basin before reprocessing (or conditioning in deep underground repository), in order to decrease the radiation level and the heat production. The waste is conditioned according to their composition and their radioactivity level for surface storage or future disposal in deep geologic formation [2].

Most of the actinide dissemination in the environment, especially plutonium, is due to the fallout of nuclear weapons tests. However, accidental release of radioactive matter occurred in nuclear power plants (Windscale, Three Mile Island, Chernobyl, Fukushima) and waste storage facility (Kyshtym). In addition, mining and milling operations of uranium ores have generated waste rocks and tailings, leading to uranium contamination of soils and ground waters [3]. The potential migration of actinides from nuclear waste repositories is also of concern.

Phosphorous, a vital element for all living beings, is ubiquitous in the environment, especially in the form of a phosphate derivatives. Very often, soils contain insoluble inorganic phosphates like apatite or monazite. To extract the phosphorus required for their growth, plants exude low-molecular weight organic compounds to enhance phosphate-rich rock dissolution. Physical and chemical weathering of rock and sediments contributes also to the natural release of phosphate in the environment [4, 5]. Since phosphate compounds are sparingly soluble, they are transported as particulate material mainly with organic matter and iron hydroxides [6]. An additional contribution to phosphate release in the environment is related to the industrial production of phosphoric acid and phosphate fertilizers [6-8]. This industrial activity results in deposits of phosphogypsum that can potentially pollute natural waters through leachate [9-11]. Agricultural run-off, discharges of wastewaters also contribute to the overenrichment of waters in phosphate leading to the eutrophication [12-13].

Thus, interactions of actinides -that have been released in the environment- with phosphate are likely to occur. Phosphate derivatives play also an important role in «industrial» actinide chemistry:

-The first separation of plutonium from uranium and fission products was conducted in 1942 at the Hanford site within the frame of the Manhattan Project [14, 15]. The separation was conducted by precipitation of Pu(IV) with bismuth phosphate combined with redox cycles. This compound was selected since the obtained precipitate, crystalline not gelatinous, carried Pu(IV) but not Pu(VI). The oxidation to Pu(VI) by NaBiO_3 led to the dissolution of the precipitate and concentration of Pu(VI) in solution. Then foreign elements that form insoluble compounds with phosphate were separated from Pu(VI) by precipitation. After reduction of Pu(VI) into Pu(IV) using NaNO_2 , the Pu was then precipitated again with BiPO_4 . Several cycles of this procedure were performed as illustrated by the original schema in the patent of Thomson and Seaborg reproduced in **Figure 2** [16].

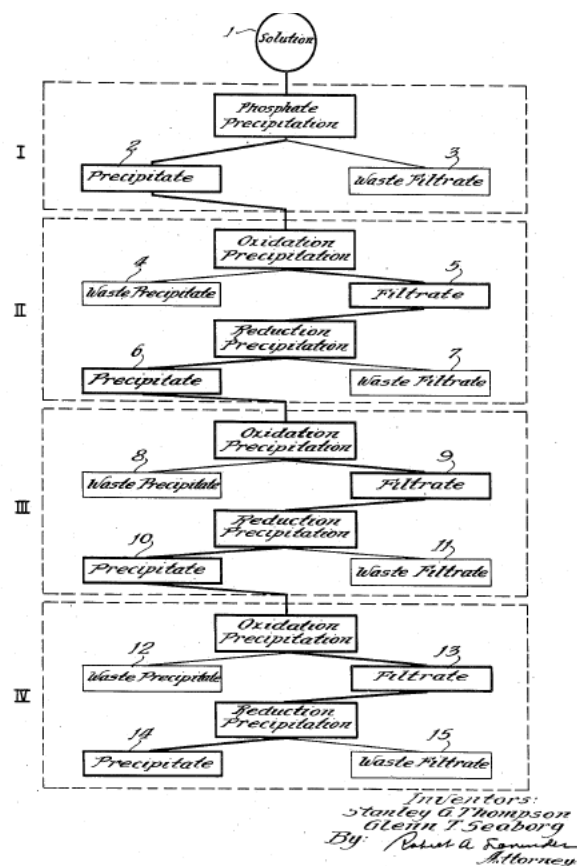


Figure 2. Separation of plutonium from uranium^[16]

- Nuclear fuel undergoes changes in isotopic and chemical composition, and also in structure as consequences of irradiation and thermal effects. Part of the fuel must be removed and replaced by fresh fuel. Unlike the United States, France has opted for spent fuel reprocessing, using the hydrometallurgical PUREX (Plutonium Uranium Reduction EXtraction) process in order to separate U and Pu from the fission products

and from the minor actinides Np, Am and Cm. This process, currently used on industrial scale, has been initially developed to produce plutonium for nuclear weapons purposes [14, 17]. This is a solvent extraction process using a solution of TBP (tributyl phosphate) in paraffinic hydrocarbons. Uranium(VI) and Pu(IV) in 2-4M HNO₃ are extracted by TBP whereas most of the fission products remain in aqueous phase. Then, separation of plutonium from uranium is achieved by reducing Pu(IV) to Pu(III) which is stripped from the organic phase [17, 18]. During reprocessing, TBP undergoes hydrolysis and degradation products, dibutyl phosphate (DBP), monobutyl phosphate (MBP), butanol, and phosphoric acid accumulate overtime [19]. Radiolysis of organic solution of TBP leads to the same degradation products. In addition, various hydrocarbons are also formed [20]. The presence of these compounds interfere with the extraction efficiency leading to unwanted retention of elements in a given phase. In the case of phosphoric acid, precipitation of actinide phosphates or formation of non-extractable species are likely to occur, resulting in a loss in uranium and plutonium [21].

-Phosphate-based compounds like apatite, monazite, cheralite, as well as thorium phosphate-diphosphate can accommodate a great variety of radionuclides (actinides and fission products) without affecting their long-term durability (high resistance towards leaching and radiation). Although the majority of radwaste is conditioned in glasses, these matrices should be used for specific immobilisation of minor actinides as well as of plutonium coming from weapon dismantling [22-25].

-Industrial production of phosphoric acid from phosphate ores that contains natural uranium and thorium generates a by-product: the phosphogypsum in which U and Th are concentrated [9-11]. The environmental contamination of soils and water by U, Th and their daughters in the vicinity of phosphogypsum storage area has already been observed [11]. But most of uranium and thorium ends up in H₃PO₄ which is used in phosphate fertilizer production: these radioelements can be leached, contributing to soils and groundwaters pollution, or taken by plants and transferred into the food chain. However, phosphate rocks can also be considered as unconventional source of uranium. In that case, uranium is a by-product in phosphoric acid production and its health environmental impact is limited [8, 26-28]

Phosphoric acid and phosphate ions, in the environment as well as on industrial scale play an important role in actinide chemistry. However, literature devoted to interaction between phosphate and actinides, especially plutonium, remains scarce. This is partly due to the very low solubility of phosphate compounds. Within this context, the present

work is focused on the determination of fundamental data about the interaction of plutonium cations (Pu^{3+} , and PuO_2^{2+}) with phosphate species (H_3PO_4 , H_2PO_4^- , HPO_4^{2-} and PO_4^{3-}) in order to improve models for predicting the behavior of plutonium in the environment and nuclear industry. However, due to the difficulties in handling this element (complex chemistry, chemical and radio-toxicity) and because of the limited amount allowed in academic laboratory. The present work developed a suitable experimental protocols with chemical analogs of Pu (III) and Pu(VI). These protocols could then be applied to the determination of thermodynamic data on the complexation of Pu ions with phosphate.

This PhD work is organized in four chapters. The **Chapter I** contents a bibliographic study about the actinides and the main chemical properties that govern their behavior in the environment. Some generalities about phosphoric, its sources and its speciation in aqueous solution are also detailed. A state of the art about the interaction of plutonium ions, actinides(III) and lanthanides, and U(VI) with phosphate species is also presented.

In **Chapter II**, the strategy for the determination of the fundamental thermodynamic data is exposed. The general methodology is briefly described as well as the experimental techniques employed to determine the speciation of Eu(III)-phosphate and U(VI)-phosphate in aqueous solution and solid state.

The **Chapter III** is devoted to the study of the complexation of Eu(III)-phosphate as analogous of Pu(III)-phosphate systems.

The **Chapter IV** focuses on to the speciation of U(VI) in the presence of phosphate in aqueous solution.

Finally, the conclusion and perspectives related to the speciation Eu(III)-phosphate and U(VI)-phosphate as analogous of the corresponding Pu(III) and Pu(VI) speciation are presented.

References

- [1] F.A. Settle. Uranium to electricity: The chemistry of the nuclear fuel cycle. *Journal of Chemical Education*, **86**, 316-323 (2009)
- [2] G. Choppin, J.O. Liljenzin, J. Rydberg and C. Eckberg. The nuclear fuel cycle (Chap. 21) in *Radiochemistry and Nuclear Chemistry*, 4th edition. Academic Press Elsevier, 685-751 (2013)
- [3] A. Abdelouas, W. Luzte and E. Nuttall. Chemical reactions of uranium in ground water at a mill tailing site. *Journal of Contaminant Hydrology*, **34**, 343-361 (1998)
- [4] S.M. Singh, L.S. Yadav, S.K. Singh, P. Singh, P.N. Singh and R. Ravindra. Phosphate solubilizing ability of two Arctic *Aspergillus niger* strains, *Polar Research*, **30**:1, 7283 (2011)
- [5] D.A.C. Manning. Phosphate minerals, environmental pollution, and sustainable agriculture. *Elements*, **4**, 105-108 (2008).
- [6] M.P. Bernardo, G.G.F. Guimaraes, V. F. Majaron and C. Ribeiro. Controlled release of phosphate from layered double hydroxide structures: dynamics in soil and application as smart fertilizer. *ACS Sustainable Chemistry and Engineering*, **6**, 5152-5561 (2018).
- [7] A. Dartiguelongue. Etude de la spéciation de l'uranium(VI) dans les solutions d'acide phosphorique et de sa récupération par extraction liquide-liquide. Thèse Ecole Nationale Supérieure de Techniques Avancées (2014).
- [8] S.Gabriel, A. Baschwitz, G. Mathonnière, T. Eleouet and F. Fizaine. A critical assessment of global uranium resources, including uranium in phosphate rocks, and the possible impact of uranium shortages on nuclear power fleets. *Annals of Nuclear Energy* **58**, 213–220 (2013).
- [9] G. Olszewski, A. Boryło and B. Skwarzec. Uranium (^{234}U , ^{235}U and ^{238}U) contamination of the environment surrounding phosphogypsum waste heap in Wislinka (northern Poland). *Journal of Environmental Radioactivity* **146**, 56-66 (2015).
- [10] P.M. Rutherford, M.J. Dudas and R.A. Samek. Environmental impacts of phosphogypsum. *The Science of the Total Environment* **149**, 1-38 (1994).
- [11] H. Tayibi, M. Choura, F.A. Lopez, F.J. Alguacil and A. Lopez-Delgado. Environmental impact and management of phosphogypsum. *Journal of Environmental Management* **90**, 2377–2386 (2009).
- [12] D.L. Correll. The role of phosphorous in the eutrophication of receiving waters: A review. *Journal of Environmental Quality* **27**, 261-266 (1998).
- [13] S. Kundu, M.V. Koumar, S. Rajendiran, A. Rao and A.S. Rao. Phosphates from detergents and eutrophication of surface water ecosystem in India. *Current Science* **108**, 1320-1325 (2015).
- [14] J. M. Cleveland. The chemistry of plutonium. Gordon and Breach, London, Chap.18, 461-525 (1970)
- [15] G.T. Seaborg. Forty years of plutonium chemistry: The beginning. In *Plutonium Chemistry*, W.T. Carnall and G.R. Choppin eds, ACS Symposium series n°216,

- ACS Washington, 1-22 (1983).
- [16] S.G. Thomson and G.T. Seaborg. Bismuth phosphate process for the separation of plutonium from aqueous solution. US Patent 2785951 (1957)
- [17] W.B. Lanham and T.C. Runion. PUREX process for plutonium and uranium recovery. Report ORNL-479 (1949)
- [18] K. L. Nash, C. Madic, J. N. Mathur and J. Lacquement. Actinide separation science and technology in *The Chemistry of Actinide and Transactinide Elements*, 4th edition, L.R. Morss, N.M. Edelstein and J. Fuger Eds, Springer, 2622-2798 (2010)
- [19] R.R. Schoun and M.C. Thomson. Chemical properties and reactions in *Science and Technology of Tributyl Phosphate Volume I*, W.W. Schultz and J.D. Navratil Eds, CRC Press Boca Raton, 137-151 (1984).
- [20] W. Davis Jr. Radiolytic behavior in *Science and Technology of Tributyl Phosphate Volume I*, W.W. Schultz and J.D. Navratil Eds, CRC Press Boca Raton, pp. 221-239 (1984)
- [21] R. Fischer, G.D. Werner, T. Lehmann, G. Hoffman and F. Weigel. The phosphates and arsenates of hexavalent actinides. IV-Plutonium. *Journal of the Less-Common Metals* 80, 121-132 (1981)
- [22] S. Neumeier, Y. Arinicheva, Y. Ji, J.M. Heuser, P.M. Kowalski, P. Kegler, H. Schlenz, D. Bosbach and G. Deissmann. New insights into phosphate based materials for the immobilization of actinides. *Radiochimica Acta* **105**, 961-984 (2017).
- [23] E.H. Oelkers and J.M. Montel. Phosphates and nuclear waste storage. *Elements*, **4**, 113-116 (2008).
- [24] N. Dacheux, R. Podor, B. Chassigneux, V. Brandel and M. Genet. Actinides immobilization in new matrices based on solid solution: $\text{Th}_{4-x}\text{M}^{\text{IV}}_x(\text{PO}_4)_4\text{P}_2\text{O}_7$. ($\text{M}^{\text{IV}} = {}^{238}\text{U}, {}^{239}\text{Pu}$). *Journal of Alloys & Compounds* **236**, 271-273, (1998).
- [25] N. Dacheux, C. Clavier and R. Podor. Versatile Monazite: Resolving geological records and solving challenges in materials science: Monazite as a promising long-term radioactive waste matrix: Benefits of high-structural flexibility and chemical durability. *American Mineralogist* **98**, 833-847 (2013).
- [26] H. Kim, R.G. Eggert, B.W. Carlsen and B.W. Dixon. Potential uranium supply from phosphoric acid: A US analysis comparing solvent extraction and ion exchange recovery. *Resources Policy* **49**, 222-231 (2016)
- [27] B. Huhle, S. Kummer, S. Stadler and B. Merkel. Mobility of uranium from phosphate fertilizers in sandy soils, in *Loads and fate of fertilizer-derived uranium*, L.J. De Kok and E. Schnug Eds, Backhuys Publishers, Leiden, The Netherlands, 47-55 (2008)
- [28] IAEA NEA Report: Uranium 2020: Resources, Production and Demand. OECD (2020)

Chapter I.

Bibliographic study

Chapter I. Bibliographic study

I.1. Actinides

The actinides correspond to the filling of the 5f electron shell as suggested by G.T. Seaborg in 1945 ^[1]. This series occupy the 7th line of the periodic table as illustrated in **Figure I.1**.

IUPAC Periodic Table of the Elements

Key:																																																																																										
atomic number		Symbol		name		standard		atomic weight																																																																																		
1	H	hydrogen	1.008	± 0.0002	2	He	helium	4.0026	± 0.0001	3	Li	lithium	6.94	± 0.006	4	Be	beryllium	9.0122	± 0.0005	5	B	boron	10.81	± 0.002	6	C	carbon	12.011	± 0.002	7	N	nitrogen	14.007	± 0.001	8	O	oxygen	15.999	± 0.001	9	F	fluorine	18.998	± 0.001	10	Ne	neon	20.180	± 0.001																																									
11	Na	sodium	22.990	± 0.002	12	Mg	magnesium	24.305	± 0.002	13	Al	aluminum	26.982	± 0.001	14	Si	silicon	28.086	± 0.002	15	P	phosphorus	30.974	± 0.002	16	S	sulfur	32.06	± 0.002	17	Cl	chlorine	35.45	± 0.01	18	Ar	argon	39.95	± 0.01																																																			
19	K	potassium	39.098	± 0.001	20	Ca	calcium	40.078	± 0.001	21	Sc	scandium	44.956	± 0.001	22	Ti	titanium	47.867	± 0.001	23	V	vanadium	50.942	± 0.001	24	Cr	chromium	51.996	± 0.001	25	Mn	manganese	54.938	± 0.001	26	Fe	iron	55.845	± 0.002	27	Co	cobalt	58.933	± 0.001	28	Ni	nickel	58.693	± 0.001	29	Cu	copper	63.546	± 0.002	30	Zn	zinc	65.38	± 0.02	31	Ga	gallium	69.723	± 0.001	32	Ge	germanium	72.630	± 0.008	33	As	arsenic	74.922	± 0.001	34	Se	selenium	78.96	± 0.008	35	Br	bromine	79.904	± 0.003	36	Kr	krypton	83.798	± 0.002	
37	Rb	rubidium	85.468	± 0.001	38	Sr	strontium	87.62	± 0.001	39	Y	yttrium	88.906	± 0.001	40	Zr	zirconium	91.224	± 0.002	41	Nb	niobium	92.906	± 0.001	42	Mo	molybdenum	95.94	± 0.01	43	Tc	technetium	98	[97]	44	Ru	ruthenium	101.07	± 0.001	45	Rh	rhodium	102.91	± 0.001	46	Pd	palladium	106.42	± 0.001	47	Ag	silver	107.87	± 0.001	48	Cd	cadmium	112.41	± 0.001	49	In	indium	114.82	± 0.001	50	Sn	tin	118.71	± 0.001	51	Sb	antimony	121.76	± 0.001	52	Te	tellurium	127.60	± 0.001	53	I	iodine	126.90	± 0.001	54	Xe	xenon	131.29	± 0.001	
55	Cs	caesium	132.91	± 0.01	56	Ba	barium	137.33	± 0.01	57-71	lanthanoids					72	Hf	hafnium	178.49	± 0.01	73	Ta	tantalum	180.95	± 0.01	74	W	tungsten	183.84	± 0.01	75	Re	rhenium	186.21	± 0.01	76	Os	osmium	190.23	± 0.03	77	Ir	iridium	192.22	± 0.01	78	Pt	platinum	195.08	± 0.02	79	Au	gold	196.97	± 0.01	80	Hg	mercury	200.59	± 0.01	81	Tl	thallium	204.38	± 0.01	82	Pb	lead	207.2	± 0.01	83	Bi	bismuth	208.98	± 1.1	84	Po	polonium	[209]	[210]	85	At	astatine	[210]	[222]	86	Rn	radon	[222]	[222]
87	Fr	francium	[223]	[223]	88	Ra	radium	[226]	[226]	89-103	actinoids					104	Rf	rutherfordium	[261]	[261]	105	Db	dubnium	[262]	[262]	106	Sg	seaborgium	[263]	[263]	107	Bh	bohrium	[264]	[264]	108	Hs	hassium	[265]	[265]	109	Mt	meitnerium	[266]	[266]	110	Ds	darmstadtium	[267]	[267]	111	Rg	roentgenium	[268]	[268]	112	Cn	copernicium	[285]	[285]	113	Nh	nihonium	[286]	[286]	114	Fl	flerovium	[289]	[289]	115	Mc	moscovium	[288]	[288]	116	Lv	livermorium	[293]	[293]	117	Ts	tennessine	[294]	[294]	118	Og	oganeson	[294]	[294]
57	La	lanthanum	138.91	± 0.01	58	Ce	cerium	140.12	± 0.01	59	Pr	praseodymium	140.91	± 0.01	60	Nd	neodymium	144.24	± 0.01	61	Pm	promethium	[145]	[145]	62	Sm	samarium	150.36	± 0.02	63	Eu	europium	151.96	± 0.01	64	Gd	gadolinium	157.25	± 0.03	65	Tb	terbium	158.93	± 0.01	66	Dy	dysprosium	162.50	± 0.01	67	Ho	holmium	164.93	± 0.01	68	Er	erbium	167.26	± 0.01	69	Tm	thulium	168.93	± 0.01	70	Yb	ytterbium	173.05	± 0.02	71	Lu	lutetium	174.97	± 0.01																
89	Ac	actinium	[227]	[227]	90	Th	thorium	[232]	[232]	91	Pa	protactinium	[231]	[231]	92	U	uranium	[238]	[238]	93	Np	neptunium	[237]	[237]	94	Pu	plutonium	[244]	[244]	95	Am	americium	[243]	[243]	96	Cm	curium	[247]	[247]	97	Bk	berkelium	[247]	[247]	98	Cf	californium	[251]	[251]	99	Es	einsteinium	[252]	[252]	100	Fm	fermium	[257]	[257]	101	Md	meitnerium	[258]	[258]	102	No	nobelium	[259]	[259]	103	Lr	lawrencium	[262]	[262]																

INTERNATIONAL UNION OF PURE AND APPLIED CHEMISTRY

For notes and updates to this table, see www.iupac.org. This version is dated 4 May 2022.
Copyright © 2022 IUPAC, the International Union of Pure and Applied Chemistry.

Figure I.1. Periodic table of the elements ^[2]

I.1.1 Redox properties

The light actinides from Pa to Am may exist in solution under different oxidation states that are presented in **Table I.1**. At oxidation states +III and +IV, actinides form aquo ions whereas at oxidation +V and +VI, actinides ions, except Pa, are molecular species characterized by a linear trans-dioxo bond. Americium and curium will be mainly found in the +III oxidation state. The actinides beyond Cm, except No, display similarities with lanthanides and exist in the +III oxidation state.

Table I.1. Oxidation states of actinides in aqueous solution (the most common ones are denoted in bold)^[3]

Actinide	Oxidation state					
⁹⁰Th			IV			
⁹¹Pa			IV	V		
⁹²U		III	IV	V	VI	
⁹³Np		III	IV	V	VI	VII
⁹⁴Pu	II	III	IV	V	VI	VII
⁹⁵Am	II	III	IV	V	VI	
⁹⁶Cm		III	IV			
⁹⁷Bk		III	IV			
⁹⁸Cf		III				
⁹⁹Es		III				
¹⁰⁰Fm	II	III				
¹⁰¹Md	II	III				
¹⁰²No	II	III				
¹⁰³Lr	II	III				

In aqueous solution, thorium has only one stable oxidation state, +IV. Uranium can be found in +III to +VI oxidation states. In oxidic condition, the predominant oxidation state for U is +VI. The stability area of U(III) lies outside of the stability limits of water: it is quickly oxidized in U(IV). U⁴⁺ is also stable in solution if no oxidizing agents are present. The kinetics of redox transformations depends if there is a change in the chemical composition between the oxidized and reduced species. Thus, the reaction between UO₂²⁺ and UO₂⁺ and between U⁴⁺ and U³⁺ are fast whereas the redox reaction between UO₂²⁺ and U⁴⁺ is slow^[3, 4]. U(V) exhibits a strong tendency to disproportionation and exists on a very narrow stability range that cannot be represented in the Pourbaix diagram (**Figure I.2**)^[3, 4].

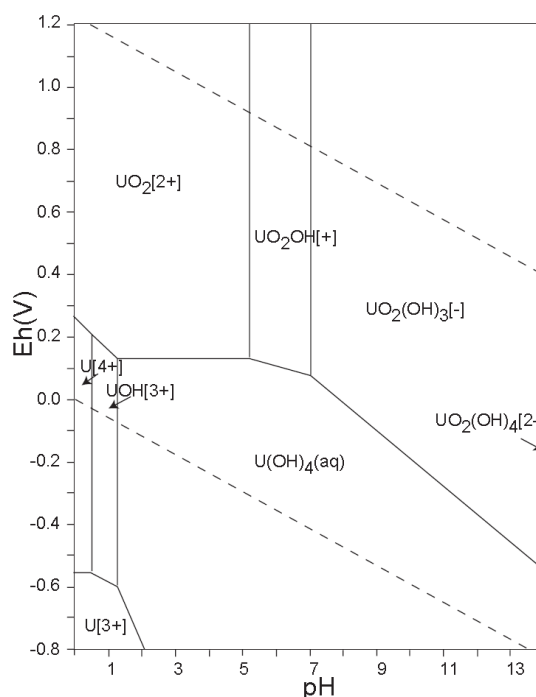


Figure I.2. Potential-pH diagram of uranium at 25 °C ($U_{tot} 10^{-10} M$) using database from OECD/NEA ^[5].

In solution, plutonium might be present in the +III, +IV, +V, +VI and +VII oxidation states as Pu^{3+} , Pu^{4+} , PuO_2^+ and PuO_2^{2+} respectively. Pu(IV) is the most stable species in solution. Usually, Pu(III) and Pu(IV) are more stable in acidic solutions whereas Pu(VI) and Pu(VII) are more stable in alkaline solutions. Pu(V) will be mainly found as the main species in near-neutral solutions at low concentration.

In acidic media, the redox potentials relative to the Pu ions couples involving the oxidation states +III, +IV, +V and +VI are all close to 1 V as it can be shown in the Latimer's diagram in **Figure I.3**. That means that these oxidation states can coexist in solution. This is a unique feature in the periodic table of elements ^[6]. This ability to exist under multiple oxidation states in solution is due to the tendency of Pu(IV) and Pu(V) to disproportionate. In acidic solution without complexing ligands, Pu(IV) disproportionate into Pu(III) and Pu(VI). The disproportionation of Pu(V) takes place in moderately acidic solution leading to Pu(IV) and Pu(VI). Generally, those reactions involve two steps with different kinetics. As uranium, the reactions involving the formation or the breaking of Pu=O bonds are slow, whereas reactions involving a simple electron exchange are fast ^[4].

Actinides aqua ions can exhibit a variety of colors depending on their oxidation states. For example, the solutions containing plutonium ions at oxidation states from +III to +VII in non-complexing media are presented in **Figure I.4.a**. Each oxidation state exhibits a characteristic absorption spectrum (**Figure I.4.b**). The presence of f electrons leads to the presence of sharp absorption bands in the spectrum. Thus, the spectrum of Pu(VII) is the only one without any sharp band. Those sharp bands that can be observed in the visible and near-infrared range reflect the internal 5f transition ^[20].

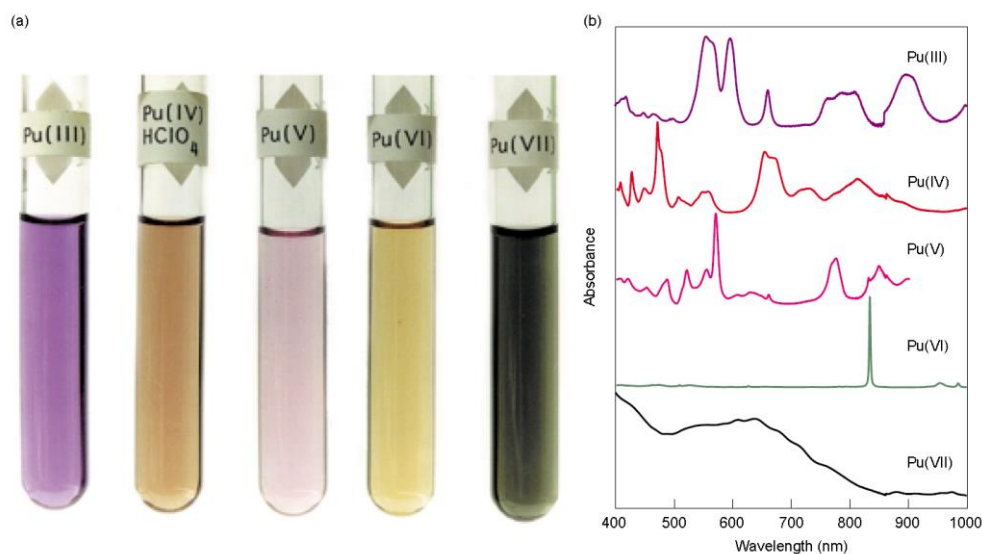


Figure I.4. (a) The color of non-complexed plutonium at various oxidation states in 1 M HClO_4 from Pu(III) to Pu(VI) and in strong base for Pu(VII) (b) their corresponding absorption spectra ^[20].

I.1.3. Hydrolysis

Hydrolysis can be regarded as a complexation with hydroxide in water. For a given actinide, the tendency towards hydrolysis follows the sequence $\text{An}^{4+} > \text{AnO}_2^{2+} > \text{An}^{3+} > \text{AnO}_2^+$ ^[21]. This sequence reflects the variation in effective charge on the metal ions as presented in **Table I.2**.

Table I.2. Effective charge on actinide ions ^[22].

Actinide ion	An^{4+}	AnO_2^{2+}	An^{3+}	AnO_2^+
Effective charge	4	3.3	3	2.3

The hydrolysis behavior of actinides has been studied for many decades and a large amount of hydrolysis constants (not always consistent) are available in the literature. Some critical reviews devoted to the development of thermodynamic database on equilibria involving actinides in aqueous solution include monomers and oligomers [23-25]. In the present work, different concentration scales of lanthanides and actinides have been used. Liquid-liquid extraction experiments were performed with metal at trace and at relative low pH, allowing the condensation of hydrolyzed actinides to be neglected. Higher metal concentrations have been used in spectroscopic measurements, but the use of strongly acidic medium may avoid the formation of colloidal species [26].

First hydrolysis constants at standard state of Eu^{3+} and some actinide ions are listed in **Table I.3**, according to the following equilibrium:

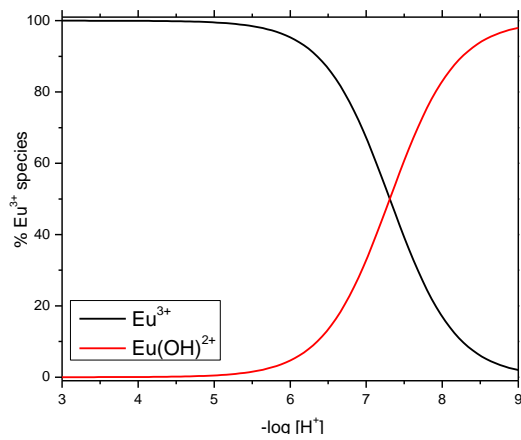


Table I.3. Standard first hydrolysis constants of Eu^{3+} and actinide ions

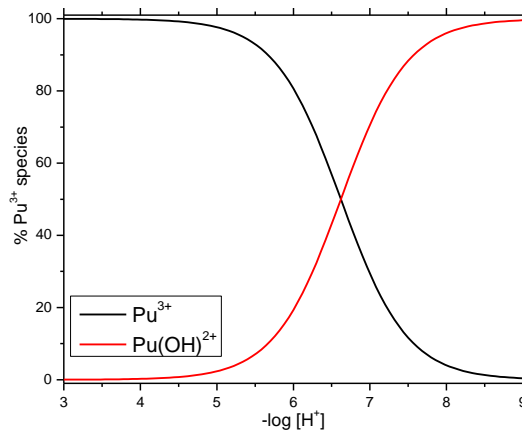
Cation	$\log_{10}\beta_1^0$	Reference
Eu^{3+}	-7.6	[27]
Pu^{3+}	-(6.18±0.5)	[28]
Am^{3+}	-(7.20±0.50)	[24]
U^{4+}	13.46 ± 0.06	[28]
Np^{4+}	10.16	[24]
Pu^{4+}	14.60 ± 0.20	[24]
NpO_2^+	-(11.3 ± 0.7)	[28]
PuO_2^+	≤ -9.73	[28]
UO_2^{2+}	-(5.25 ± 0.24)	[28]
NpO_2^{2+}	-(5.10 ± 0.4)	[28]
PuO_2^{2+}	-(5.5 ± 0.5)	[24]

Hydrolysis constants of An^{4+} , the most reactive oxidation state, are the highest, by several orders of magnitude. According to the first hydrolysis constants in **Table I.3** without considering the formation of colloids or polymeric species, the hydrolysis of An(VI) and An(III) starts at around pH 2 and 4 respectively. This is illustrated by the speciation diagrams of $\text{Eu}^{3+}/\text{Pu}^{3+}$, and U(VI)/Pu(VI) in non-complexing media in **Figure I.5**. Even if these diagrams display strong similarities, some differences can be observed. For example, Pu^{3+} is more readily hydrolyzed than Eu^{3+} . This indicates that

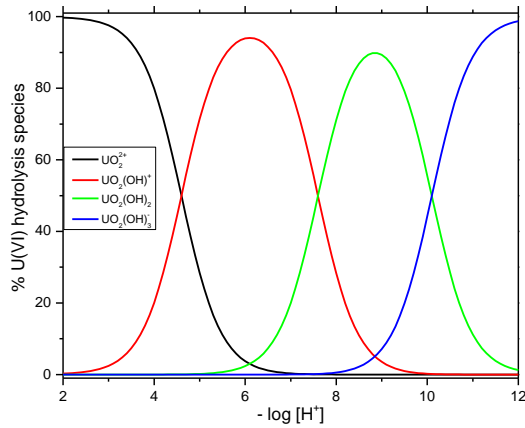
the use of analogs may not be sufficient to characterize plutonium chemistry. A discussion about the validity in using analogs is provided in the next chapter.



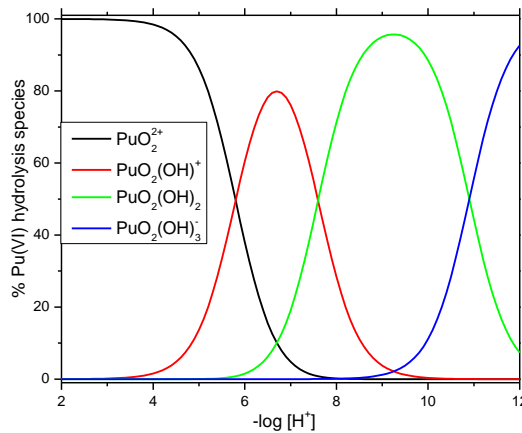
a. $[Eu(III)] = 5 \times 10^{-3} M$, $I = 0.7 M NaCl$
and $T = 25^\circ C$ ^[29]



b. $[Pu(III)] = 5 \times 10^{-3} M$, $I = 0.1 M NaClO_4$
and $T = 25^\circ C$ ^[30]



c. $[U(VI)] = 1 \times 10^{-3} M$, $I = 1 M NaClO_4$
and $T = 25^\circ C$ ^[31]



d. $[Pu(VI)] = 1 \times 10^{-3} M$, $I = 0.01 M NaClO_4$
and $T = 25^\circ C$ ^[32]

Figure I.5. Hydrolysis speciation diagram of mononuclear Pu(III), Eu(III), Pu(VI) and U(VI) without considering colloid or polymer species

I.1.4. Actinide complexation

Hard Soft Acid Base (HSAB) principle has been applied to explain qualitatively the interaction between metal ions and inorganic or organic ligands for many years. Hard acids are characterized by small size and high positive charge whereas hard bases exhibit low polarizability and high electronegativity respectively. On the other hand, soft acids have large size and low positive charge; soft bases have high polarizability and low electronegativity. The general statement of the HSAB principle is that hard acid prefers to coordinate with hard base, and soft acid with soft base ^[33].

The common hard, soft and intermediate electron donors are shown in **Table I.4**. According to HSAB principle, actinides ions, with relative high charges and small sizes belong to the class of hard acids. In particular, they interact strongly with oxygen atoms of a great variety of organic compounds.

Table I.4. Classification of Bases ^[33].

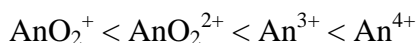
Hard	Soft
H ₂ O, OH ⁻ , F ⁻	R ₂ S, RSH, RS ⁻
CH ₃ CO ₂ ⁻ , PO ₄ ³⁻ , SO ₄ ²⁻	I ⁻ , SCN ⁻ , S ₂ O ₃ ²⁻
Cl ⁻ , CO ₃ ²⁻ , ClO ₄ ⁻ , NO ₃ ⁻	R ₃ P, R ₃ As, (RO) ₃ P
ROH, RO ⁻ , R ₂ O	CN ⁻ , RNC, CO
NH ₃ , RNH ₂ , N ₂ H ₄	C ₂ H ₄ , C ₆ H ₆
	H ⁻ , R ⁻
Borderline	
C ₆ H ₅ NH ₂ , C ₅ H ₅ N, N ₃ ⁻ , Br ⁻ , NO ₂ ⁻ , SO ₃ ²⁻ , N ₂	

Since the strength of the interaction between actinides and a given ligand depends on the effective charge of actinides in the ionic forms, regardless of steric hindrance, the order of the interaction strength should be:



This rule can be commonly observed in aqueous solution without ligands or in the presence of inorganic ligands in aqueous solution since the water molecule or inorganic ligand are small enough to ignore the steric hindrance. Thus, the effective charge decides the strength of interaction in this case.

However, with consideration of steric hindrance, the reactivity order of An³⁺ and AnO₂²⁺ may be reversed and the general tendency of actinides to form complexes follows the sequence:



Thus, the complex with An(IV) should be most stable in solution due to its highest effective charge. On the contrast, An(V) should normally form the weakest complex with ligands.

I.1.5 Actinides in the environment

Actinides released in the environment have several sources. The sources can be natural or anthropogenic. Most environmental contamination is anthropogenic.

The naturally occurring actinides are composed of primordial nuclides. They were created before our solar system. Among those primordial, ^{238}U , ^{235}U and ^{232}Th can be listed. They were produced from neutron capture reactions during supernova explosions. They are featured by a half-life longer than the age of the Earth. By radioactive decay, primordial actinide nuclides can produce other actinides, called radiogenic nuclides (decay chains). The last kind of naturally occurring actinides are the nucleogenic nuclides. They are issued of natural terrestrial nuclear reaction.

The second sources of actinides in the environment are the anthropogenic actinides. They are mainly due to nuclear weapons fallout, nuclear power plant activities and incidents. The anthropogenic actinides are mainly composed of the transuranium elements. One of the main sources of actinides in the environment is the weapon tests. From 1945 to 1980, 543 nuclear tests have been conducted in the Northern hemisphere. After 1963, nuclear tests were mainly underground tests to limit the release in the atmosphere. Those tests are equivalent to 0.1 ton of plutonium released in underground tests and 3.5 tons in atmospheric tests. Radionuclides issued from nuclear tests remaining countable possess long half-lives and are mainly ^{241}Am , $^{239,240}\text{Pu}$, ^{237}Np , but also ^{137}Cs and ^{90}Sr . Accident with nuclear-powered satellites also introduced plutonium in the environment. It was the case in 1964 with the SNAP-9A. Fallouts were mainly located in the Southern hemisphere and were evaluated to 100 TBq of ^{238}Pu [34].

Another source is the release of actinides from nuclear plants during plutonium production or reprocessing steps. Some intentional and accidental releases were observed as airborne and/or liquid discharges. Some examples are Sellafield, in the United Kingdom, with the dissemination from 1952 to 1957 of ^{137}Cs , ^{90}Sr , ^{241}Am , ^{237}Np and $^{239,240}\text{Pu}$ in the North Atlantic Ocean. Other nuclear plants were concerned, such as La Hague in France, Hanford and Rocky Flat in the United States. The last important source of radionuclides in the environment accidents at nuclear power plants with the most recent examples, Chernobyl in 1986 and Fukushima in 2011. The Chernobyl accident is the most important accident involving a nuclear power plant. The inventory is evaluated to 5.6 kg ^{239}Pu , 48.5 kg of ^{236}U , 0.136 kg of ^{237}Np and 0.52 kg of ^{241}Am

(from ^{241}Pu). The composition of the Chernobyl fallout was observed to vary with distance from the accident site [35].

The mobility and toxicity of actinides in the environment are mainly governed by their speciation and depend on several parameters (pH, ionic strength I, Redox potential Eh, inorganic ligands and organic ligands concentrations, etc.). The oxidation state has a strong influence on the mobility of the actinide in the environment. As mentioned previously, some of the light actinides can be present under several oxidation states. Thus, U, Np and Pu can be present under subsurface conditions as An^{3+} , An^{4+} , AnO_2^+ and AnO_2^{2+} .

This feature complicates the prediction of their behavior in the environment. Other actinides of environmental interest are mainly present under one oxidation state, which is the case for Th(IV) and Am(III) for instance (**Figure I.6**). Light actinides in the oxidation states +III and +VI commonly exist in the environment according to the diverse conditions. As regarding the elements used in the present work, U and Eu (as chemical analog of plutonium) are at the +VI and +III oxidation states respectively. Generally, actinides in the +III and +IV states have a lower solubility and a higher tendency to sorb on mineral surfaces, whereas in the +V and +VI states, a higher solubility is observed enhancing their mobility.

	89 Ac	90 Th	91 Pa	92 U	93 Np	94 Pu	95 Am	96 Cm	97 Bk	103 Lr
Valence electrons:	— 6d 7s ²	— 6d ² 7s ²	5f ² 6d 7s ²	5f ³ 6d 7s ²	5f ⁴ 6d 7s ²	5f ⁶ — 7s ²	5f ⁷ — 7s ²	5f ⁷ 6d 7s ²	5f ⁹ — 7s ²	5f ¹⁴ 6d 7s ²
Oxidation States: (all conditions)	III	(III) IV	(III) IV V	III IV V VI	III IV V VI VII	III IV V VI (VII) VII?	III IV V VI VII?	III IV V VI (V)	III	III
Oxic zone: (groundwater)	III	IV	V	VI	V	IV	III	III		
Suboxic zone: (microbially active)	III	IV	IV	IV VI	IV V	III IV	III	III	<i>NO₃ reduction</i> <i>MnO₂ reduction</i> <i>Fe(III)oxide reduction</i>	
Anaerobic zone: (microbially active)	III	IV	IV	IV	(III) IV	III IV	III	III	<i>Fermentation</i> <i>SO₄²⁻ reduction</i> <i>Methanogenesis</i>	

Figure I.6. Common oxidation states of actinides in the environment under different conditions. States mentioned in bracket (—) are unstable; and with a question mark (?) were not confirmed.

The oxidation states bolded correspond to the predominant states [36].

Thus, in reducing environment (anaerobic zone) uranium is mainly present as the low soluble U(IV), whereas in groundwater and in the majority of natural waters, uranium is more soluble in the +VI state. Plutonium may exist under several oxidation states, from +III to +VI (**Figure I.6**). Plutonium(III) is only observed in anaerobic environment or in very acidic waters. Pu(V) is the main species in most of natural waters (aerobic conditions at near-neutral pH) but in very low concentration. The main oxidation state remains Pu(IV) in the environment. Indeed, because of the disproportionation and also because of the low solubility of Pu(IV) the concentration of Pu(V) in natural waters is limited. The low solubility of Pu(IV) can reduce its migration by precipitation ^[36, 37].

In natural waters, the main ligands that can complex with actinides are carbonates and hydroxides. Trivalent actinides form in natural waters mainly $An(OH)^{2+}$, $An(CO_3)_2^-$ and $An(CO_3)^+$ ^[37]. However, hydrolysis remains the most important reaction and hydroxyl species have a high tendency to sorb onto colloids, sediments or humic substances.

For U, Np and Pu, at near neutral pH, the main species are often carbonate species. In natural waters, in presence of carbonate, U(VI) is mainly present as $UO_2(CO_3)_2^{2-}$ and often as $CaUO_2(CO_3)_2$ ^[36-40].

The oxidation state is not the only factor that can influence the migration of actinides in the environment. Another parameter is the sorption of some actinides onto mineral surfaces or colloids. Trivalent and tetravalent actinides are known to sorb readily to surfaces that can reduce their mobility. However, the formation of intrinsic colloids but also the sorption of hydrolyzed species onto colloids leads to further migration of those actinides, especially for plutonium ^[26, 36, 37]. Some studies have shown that Pu migration in the environment could occur by transport on colloidal particles ^[26, 41-44].

Their mobility can also be affected by complexation with inorganic and organic ligands, from simple carboxylic acids to more complex organic molecules (humic substances). A great variety of ligands can be naturally found in the environment among which phosphate species.

I.2. Phosphate species and phosphoric acid

Phosphate species are important in actinides chemistry not only in the environment but also in nuclear technology.

I.2.1. Natural sources

Phosphorous is a minor element on the earth but it is vital for all living beings. For instance, P is essential for plant growth and in the human body, it is an important component in bones and teeth but also a critical component of deoxyribonucleic acid (DNA) and ribonucleic acid (RNA). It is also found as phospholipids which compose cell membranes. P is considered as a source of biochemical energy with the adenosine triphosphate and diphosphate (ATP and ADP). Thus, P is ubiquitous in the environment in a wide variety of organic and inorganic forms. Even if the largest reservoir of P is from the sediments and sedimentary rocks, the one that can be easily taken by plants is the organic P. This natural organic P is mainly from decomposed organic matter but also microbial organisms. Most of the organic P are phosphate esters, or phytins, but the main fraction is still unidentified ^[45].

Concerning the inorganic phosphate sources, several hundred phosphate minerals have been identified. Some of the most common are listed in **Table I.5**: the most important is apatite $\text{Ca}_5(\text{PO}_4)_3\text{X}$ (X=F, Cl OH) whereas some others can be considered as sources of thorium and uranium ^[46].

Table I.5. Common phosphate minerals and An-phosphate bearing phases ^[46-50]

Phosphate mineral	Formula
Apatite	$\text{Ca}_5(\text{PO}_4)_3\text{X}$ (X=F, Cl OH)
Monazite	$(\text{Ce,La,Y,Th})\text{PO}_4$
Rhabdophane	$\text{LnPO}_4.n\text{H}_2\text{O}$ (Ln=Ce, La-Gd)
Xenotime	$\text{LnPO}_4.n\text{H}_2\text{O}$ (Ln=Gd-Lu)
Struvite	$\text{Mg}(\text{NH}_4)\text{PO}_4.6\text{H}_2\text{O}$
Metatorbernite	$\text{Cu}(\text{UO}_2)_2(\text{PO}_4)_2.8-12\text{H}_2\text{O}$
Autunite	$\text{Ca}(\text{UO}_2)_2(\text{PO}_4)_2.10-12\text{H}_2\text{O}$
Cheralite	$\text{CaTh}(\text{PO}_4)_2$

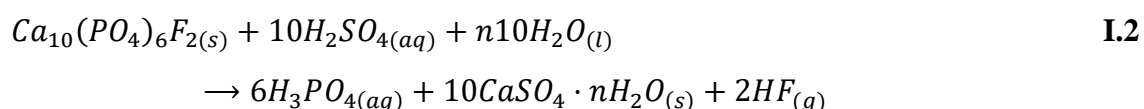
Depending on the geological conditions, phosphate ores can contain natural radioactive impurities such as natural uranium, thorium and their daughters. For example apatite contains 200 ppm of U and less than 10 ppm of Th ^[51]. In contrast, monazite, cheralite or xenotime rocks have relative high concentration of Th and less amount of U (69.2 ppm and 24.8 ppm, respectively) ^[52]. Thus, phosphate rocks are considered as unconventional source of uranium.

The phosphorous cycle in soil can be described first by the chemical weathering of rocks producing the different phosphate species according to the pH. However, even if P is ubiquitous in rocks and soils, due to the low solubility of phosphates, P remains a limiting nutrient in all environmental reservoirs. Moreover, the rocks are often resistant to erosion leading to only small and slow released. Thus, P is more present as particulate phase than dissolved species. However, plants have the ability to exude organic compounds (*e.g.* citric acid) which enhance phosphate dissolution from inorganic and organic solid phases ^[53].

I.2.2. Anthropogenic sources of phosphates

The industrial production of fertilizers and phosphoric acid led to the release of phosphates in the environment. Phosphates rocks are the main sources to produce fertilizers and phosphoric acid, and other further application in food supplements, drinks and other industrial products. The phosphoric acid is mainly manufactured using a wet chemical method ^[46, 54-56].

This method consists in the dissolution of phosphate rock (apatite) with concentrated sulphuric acid. The production of phosphoric acid leads also to the production of phosphogypsum (5 tons of phosphogypsum per ton of phosphoric acid produced) and hydrogen fluoride (**Eq. I.2**) ^[57].



Only 15% of phosphogypsum is recycled as fertilizers, building materials or soil fertilization. The residue is usually not used, because it contains a weak radioactivity caused by natural U and Th and their daughters (Po and Rn) in the phosphate rock. This by-product is usually stored indefinitely in large stock piles exposed to weathering process, causing soils and water contaminations, or taken by plants and transferred into the food chain ^[56].

In another hand, around 90% of the phosphoric acid produced in the world is used for food production, mainly in the manufacturing of agricultural fertilizers and additives for animal feeds. The remaining percentage goes to the industrial used such as detergents, household cleaning products, metal treatment and other industrial applications ^[58]. Those industrial activities contribute to the release of phosphate into the environment by

agriculture runoff, industrial effluents (from fertilizer, detergent and soap industries) and domestic wastewater.

The human activities, by the production and the use of fertilizers, for instance, accelerate the eutrophication of the aquatic system by the excessive presence of phosphate [58, 59]. This phenomenon increases algae bloom, decrease the water quality and has negative impact on aquatic environments.

Thus, the presence of both actinides and phosphates in the environment can lead to possible interactions between them. Moreover, phosphates are also important in the nuclear industry, as described in the following section.

I.2.3. Phosphate/phosphoric acid and nuclear industry

The reprocessing of the nuclear spent fuel with the PUREX process involves tributylphosphate (TBP) as extractant. Its structure is illustrated in **Figure I.7**. This compound belongs to the family of esters that are known to be sensitive to hydrolysis. When a TBP solution is contacted with nitric acid, successive hydrolysis reactions occur by cleavage of C-O bonds, leading to the formation of dibutyl phosphate (DBP), monobutyl phosphate (MBP), butanol and phosphoric acid [60, 61].

In addition to chemical degradation, TBP undergoes radiolysis reactions. Same decomposition products as those produced by hydrolysis are formed. But radiation-induced reaction on TBP as well as on diluent in the presence of nitric acid lead also to the production of saturated and unsaturated, linear and branched hydrocarbons (*e.g.* CH₄, C₂H₆...) as well as polymeric species of unknown composition [62].

All these degradation products are likely to interfere in uranium and plutonium extraction. For example, HDBP, in which structure a butyl chain is removed from TBP, is a relatively strong acid (pK_a = 1), very soluble in aqueous phase. It has been proved to precipitate in the presence of U(VI) leading to the formation of UO₂(DBP)₂ [63]. The solubility of actinides, whatever their oxidation state, is also very limited in the presence of phosphoric acid, the ultimate degradation product of TBP [61-63].

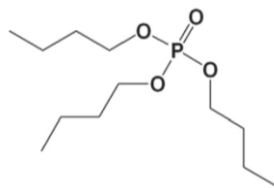


Figure I.7. Molecular structure of TBP [64]

One of the challenges of the nuclear industry is the safe disposal and management of radioactive waste. A variety of materials have been proposed for the disposal in deep geological formation, especially phosphate-based materials due to their long-term durability and their ability to accommodate various radionuclides ^[65]. Monazite can incorporate trivalent minor actinides as well as Pu. For example, Arinicheva *et al.*, ^[66] have synthesized $\text{La}_{1-x}\text{Pu}^{\text{III}}_x\text{PO}_4$ in the form of solid solution if $x \leq 0.15$: in these conditions Pu(III) occupies the sites of the monazite lattice, whereas at higher Pu content, two phases have been obtained ^[66].

Solid solutions with monazite structure can also accommodate tetravalent actinides but with a small content (a few %). Cheralite phase $\text{CaAn}^{\text{IV}}(\text{PO}_4)_2$ can accommodate higher content of tetravalent actinides: single phase compounds $\text{Ca}_{0.5}\text{An}_{0.5}(\text{PO}_4)_2$ have been obtained with Th, U and Np at the +IV oxidation state, but not with Pu. A reduction to Pu(III) occurs during the synthesis leading to the monazite PuPO_4 ^[67].

In thorium-phosphate-diphosphate (TPD), Th^{4+} can be replaced by U^{4+} or Pu^{4+} and solid solutions are formed, both cations taking the place of Th in the structure of TPD. The substitution ratio is higher for U (47.6 wt %) than for Pu (26.1 wt %), the lattice deformation being greater with Pu ^[68, 69]. Whatever the storage matrix considered, aqueous alteration leading potentially to solubilization and re-precipitation at the surface (neoformed phases) must be characterized from the kinetic but also thermodynamic point of view.

I.3 Actinides/lanthanides complexation with phosphate species

The determination of thermodynamic data relative to the interaction between actinides with phosphate species in the environment as well as nuclear industry requires information about the speciation of the ligand itself. That is why the state of the art of An(VI) and An(III) complexation is preceded by a bibliographic survey of the speciation of phosphoric acid in aqueous solution.

I.3.1. Speciation of phosphoric acid

Phosphoric acid can be involved in different equilibria: dissociation, dimerization and also ion pair formation. In diluted solution, phosphoric acid is characterized by three successive dissociation equilibria according to **I.3**, **I.4** and **I.5**.



Standard thermodynamic data relative to these equilibria (equilibrium constants and standard enthalpy variations) selected in the Thermodynamic Data Base of the Nuclear Energy Agency (NEA-TDB) in 1992 are presented in **Table I.6**. The same data is still reported in the recent update in 2021 ^[28].

Table I.6. Standard thermodynamic data associated to the successive dissociation equilibria of phosphoric acid ^[28]

Equilibrium	$\log_{10}K^0$	$\Delta_r H_m^0$ (kJ/M)
$H_3PO_4 \xrightleftharpoons{K_{a1}} H_2PO_4^- + H^+$	-2.140±0.030	-8.480±0.600
$H_2PO_4^- \xrightleftharpoons{K_{a2}} HPO_4^{2-} + H^+$	-7.212±0.013	3.600±1.000
$HPO_4^{2-} \xrightleftharpoons{K_{a3}} PO_4^{3-} + H^+$	-12.350±0.030	14.600±3.800

However, phosphoric acid can also exist as dimeric species. The presence of pyrophosphoric acid $H_4P_2O_7$ and its anion $H_3P_2O_7^-$ has not been considered in this work since the formation of these polyphosphates occur only in concentrated solution of H_3PO_4 at high temperature ^[25, 70]. At room temperature, other dimeric species are described in the literature, but their formulation and their associated stability constant remain controversial. Discrepancies concern also the lowest concentration at which dimeric species can be formed. Polyphosphates have been taken into account to explain and simulate the experimental variations of the dissociation ratio of H_3PO_4 with its total concentration using conductimetry ^[71, 72] or potentiometry ^[73-74].

The changes in Raman and infrared spectra with increasing $H_3PO_4 / K_2H_2PO_4$ concentration have also been attributed to the presence of dimers ^[75, 76]. **Table I.7** presents the different species proposed in the literature. The associated constants are

rather disparate: for example, equilibrium constant relative to the formation of $H_5P_2O_8^{2-}$ ranges between 0.6 and 3. Studies on the thermodynamic modeling of the system H_3PO_4 - H_2O have mainly considered the dimer $H_5P_2O_8^-$ resulting from the interaction between H_3PO_4 and $H_2PO_4^-$. Indeed, according to Pitzer *et al.*, the association between these two species should be twice as great the dimerization of $H_2PO_4^-$ [77].

Table I.7. Main dimeric species in phosphoric solution

Medium	Technique	Equilibria	Reference
H₃PO₄ 0.1-10 M	Conductance pH measurements	$H_5P_2O_8^- \rightleftharpoons H_3PO_4 + H_2PO_4^-$	[71]
H₃PO₄ 1 M	Infrared		[74]
H₃PO₄ 0-10 M	Infrared		[76]
H₃PO₄ 0.3-9.7 M	Raman		[75]
H₃PO₄ 0.05-1 M in 3 M KCl	Potentiometry		[78]
KH₂PO₄	Raman	$H_4P_2O_8^{2-} \rightleftharpoons H_2PO_4^-$ $+ 2H_2PO_4^-$	[79] [73] [72]
H₃PO₄ 0.05-1 M in 3 M KCl	Potentiometry		[78]
H₃PO₄ 1 M	Infrared	$H_2PO_4^- + HPO_4^{2-}$ $\rightleftharpoons H_3(PO_4)_2^{3-}$	[74]
		$H_2PO_4^- + HPO_4^{2-}$ $\rightleftharpoons H_3(PO_4)_2^{3-}$	[73]

The maximal phosphoric acid concentration used in the present work did not exceed 0.5 M, and experiments have been conducted between 15 and 60 °C. The presence of dimer has not been considered in speciation calculations. This assumption is based on the recent work of Dartiguelongue *et al.*, [76] who showed that the amount of the dimer $H_5P_2O_8^-$ remains very low at total H_3PO_4 concentration lower than 1 M at ambient temperature. Moreover, it should be noted that Rudolph, [70] unlike Cherif *et al.*, [75] and Rull *et al.*, [79] associate the change in Raman spectra with increasing H_3PO_4 concentration to the formation of clusters composed of phosphoric acid and water molecules: the strong interaction of phosphoric acid and phosphate anions with water through hydrogen bonding leads to the formation of a three-dimensional network that can affect vibrational properties of phosphate species.

Anionic phosphate species could also interact with electrolyte cations, *e.g.* Na^+ or K^+ leading to the formation of ion pairs ^[80] or complexes ^[81]. The dissociation of sodium H_2PO_4^- and HPO_4^{2-} pairs and their corresponding *K* are presented in **Table I.8**. In the present work, NaCl and NaClO_4 were used as electrolyte. The association between phosphate anions and Na^+ has not been taken into account using the scarce constants available in the literature, but using specific interaction coefficient (SIT modeling).

Table I.8. Dissociation equilibrium of Na-phosphoric acid ion pairs at $T=25^\circ\text{C}$ ^[80]

Equilibrium	<i>K</i> (M)
$\text{NaH}_2\text{PO}_4^0 \rightleftharpoons \text{Na}^+ + \text{H}_2\text{PO}_4^-$	0.56
$\text{NaHPO}_4^- \rightleftharpoons \text{Na}^+ + \text{HPO}_4^{2-}$	0.021

I.3.2. Plutonium in phosphate media

Phosphate compounds of actinides are characterized by a very low solubility. Thus, complexation constants of plutonium cations (Pu^{3+} , Pu^{4+} , PuO_2 and PuO_2^{2+}) with phosphate species (H_3PO_4 , H_2PO_4^- , HPO_4^{2-} and PO_4^{3-}) are scarce and most of the thermodynamic data available in literature have been obtained by solubility measurements of amorphous solid compounds ^[23].

A first approach in aqueous solution was performed by Weger *et al.*, ^[82], using UV-Vis absorption spectrophotometry. The characteristic absorption band at 831 nm of Pu(VI) aquo ion is associated with a large molar absorption coefficient, $\epsilon=550 \text{ M}^{-1}\text{cm}^{-1}$. The formation of Pu(VI) complex leads to a shift in wavelength. **Figure I.8** shows the appearance of an absorption band at 835 nm when phosphate is added. In this case an isobestic point appears at 833 nm, signifying that only one Pu(VI) -phosphate species is formed. The band at 835 nm was assigned to the $\text{PuO}_2(\text{H}_2\text{PO}_4)^+$ species.

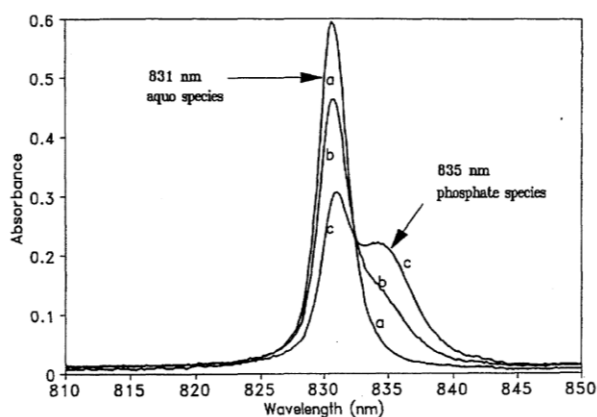


Figure I.8. Pu(VI)-phosphate absorption spectra ($pH=1$, $C_{Pu(VI)}=1 \times 10^{-3} M$, and phosphate at a. 0 M, b. 0.023 M and c. 0.062 M) ^[82]

An extended qualitative study was performed by Weger *et al.*, ^[83] analyzing Pu(VI) present in the supernatant of Pu(VI)-phosphate solid dissolution experiments. In their conditions, the band at 835 nm was shifted at other wavelength for pH values from 2.7 to 11.9. Three bands associated to phosphate complexes were found at 842, 846 and 849 nm. The intensity of the individual bands changed as a function of the pH. This investigation suggested that the band at 842 nm may correspond to the species $PuO_2(H_2PO_4)^+$, the one at 846 nm to $PuO_2(HPO_4)$ complex, and the one at 849 nm to $PuO_2(PO_4)^-$, based only on the predominant phosphate species at the pH of the solutions. In contrast, at $pH > 11.9$, hydrolytic species appear to predominate and the intensity of the bands at 846 and 849 nm decrease significantly. No complexation constants have been proposed by the authors.

Rai *et al.*, ^[84] have performed solubility studies on $(UO_2)_3(PO_4)_2 \cdot 4H_2O$ (crystallized) and on $(PuO_2)_3(PO_4)_2 \cdot 4H_2O$ (amorphous) at different pH (3-10.7) and phosphate concentration ranging from 0.001 M to 1M. Due to the similarity in solubility behavior of U(VI) and Pu(VI), data on plutonium have been processed as the same way as for uranium. Thus, Rai *et al.* have proposed equilibria and associated constants listed in **Table I.9**. But their data have not been retained by the NEA-TDB because of possible formation of secondary phases during the dissolution.

Table I.9. Equilibrium reactions and stability constants for Pu-phosphate compounds^[84]

Reaction	$\log_{10}K^0$
$\text{PuO}_2^{2+} + \text{PO}_4^{3-} \rightleftharpoons \text{PuO}_2\text{PO}_4^-$	11.76±0.70
$(\text{PuO}_2)_3(\text{PO}_4)_2 \cdot 4\text{H}_2\text{O} \rightleftharpoons 3\text{PuO}_2^{2+} + 2\text{PO}_4^{3-} + 4\text{H}_2\text{O}$	-48.97±0.69
$\text{PuO}_2^{2+} + \text{H}_2\text{PO}_4^- \rightleftharpoons \text{PuO}_2\text{H}_2\text{PO}_4^+$	3.260
$\text{PuO}_2^{2+} + 2\text{H}_2\text{PO}_4^- \rightleftharpoons \text{PuO}_2(\text{H}_2\text{PO}_4)_2(\text{aq})$	4.920
$\text{PuO}_2^{2+} + \text{HPO}_4^{2-} \rightleftharpoons \text{PuO}_2\text{HPO}_4(\text{aq})$	7.241

Regarding plutonium at the +III oxidation state, Rai *et al*^[85] studied the solubility of well-characterized $\text{PuPO}_4(\text{cr, hyd})$ as function of time, pH, and phosphate concentration in the presence of a reducing agent (hydroquinone or sodium dithionite)^[85]. They fitted the solubility variations as function of dihydrogenophosphate concentration (**Figure I.9**)

using Pitzer and SIT models for activity coefficient corrections. In the SIT model, the formation of the complex $\text{PuH}_2\text{PO}_4^{2+}$ has been considered, and Rai *et al.*,^[85] proposed the constant $\log_{10}\beta^0 = 2.16 \pm 0.62$ for equilibrium **I.6** and a solubility $\log_{10}K^0$ between pH 1 and 4 equal -4.85 ± 0.38 for equilibrium **I.7**.

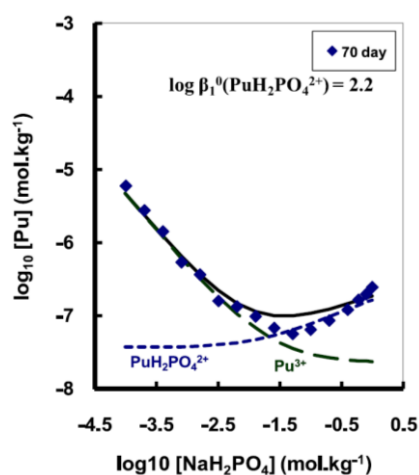
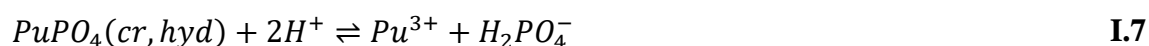


Figure I.9. Variation of the solubility of $\text{PuPO}_4(\text{cr, hyd})$ as function of NaH_2PO_4 concentration. The black line corresponds to SIT modeling^[85]

Concerning Pu^{3+} complexation with phosphates in aqueous solution, Moskvin [86] reports complexes up to stoichiometry 1:4 ($\text{Pu}(\text{H}_2\text{PO}_4)^{2+}$, $\text{Pu}(\text{H}_2\text{PO}_4)_2^+$, $\text{Pu}(\text{H}_2\text{PO}_4)_3^0$, $\text{Pu}(\text{H}_2\text{PO}_4)_4^-$) using a wide range of phosphate concentration (0.05-6.8 M) by cation exchange, but there is not spectroscopic evidence of such complexes.

Thus, standard stability constants of plutonium-phosphate complexes as well as solubility of well-characterized plutonium compounds are scarce. The data related to equilibria involving Pu(III) and Pu(VI) that have been selected in NEA-TDB [28] and the solubility value proposed by Rai *et al.*, [85] are listed in **Table I.10**.

Table I.10. Standard thermodynamic data for plutonium (III) and (VI)-phosphate species in aqueous solution

Species	$\log_{10} K^0$	Reference
$\text{Pu}^{3+} + \text{PO}_4^{3-} \rightleftharpoons \text{PuPO}_4(\text{am}, \text{hyd})$	24.44±0.06	[28]
$\text{Pu}^{3+} + \text{PO}_4^{3-} \rightleftharpoons \text{PuPO}_4(\text{cr}, \text{hyd})$	24.42±0.38	[85]
$\text{Pu}^{3+} + \text{H}_2\text{PO}_4^- \rightleftharpoons \text{Pu}(\text{H}_2\text{PO}_4)^{2+}$	2.20±0.06	[28]
$\text{Pu}^{3+} + \text{H}_2\text{PO}_4^- \rightleftharpoons \text{Pu}(\text{H}_2\text{PO}_4)^{2+}$	2.2 ±0.6	[85]
$\text{Pu}^{4+} + 2\text{HPO}_4^{2-} \rightleftharpoons \text{Pu}(\text{HPO}_4)_2(\text{am}, \text{hyd})$	30.45±0.51	[28]
$\text{Pu}^{4+} + \text{H}_3\text{PO}_4 \rightleftharpoons \text{Pu}(\text{H}_3\text{PO}_4)^{4+}$	2.4±0.3	[28]
$3\text{PuO}_2^{2+} + 2\text{PO}_4^{3-} + 4\text{H}_2\text{O}(\text{l}) \rightleftharpoons (\text{PuO}_2)_3(\text{PO}_4)_2 \cdot 4\text{H}_2\text{O}(\text{am})$	48.97±0.69	[28]

1.4 Plutonium analogs in complexing media

As shown in **Table I.10**, thermodynamic data related to the interaction of plutonium ions with phosphate are rather scarce. Very often, in order to get a better insight into plutonium chemistry, experiments are conducted with chemical analogs that are chosen according to the property investigated. In complexation studies, analogs of Pu ions have usually the same oxidation state and similar radius [87].

This reflects that bonding between f-elements and ligands are mainly electrostatic, especially at oxidation state +III. Am, Cm, Nd, Sm, Eu and Gd display chemical

behavior close to the one of Pu(III), without redox instability. Moreover, characterization techniques, *e.g.* time-resolved laser fluorescence spectroscopy (TRLFS) can be used with these analogs but not with Pu, allowing a deeper understanding of Pu chemistry. Europium(III) is often used as an analog of actinide(III). Indeed, Eu^{3+} has an ionic radius (0.95 Å) close to those of trivalent actinides (1.00 Å for Pu^{3+} , 1.07 for Am^{3+} and 0.97 for Cm^{3+}) [88]. The comparison of the stability constants for Pu^{3+} and Eu^{3+} for several complexes, as presented in **Table I.11**, can either demonstrate a good agreement between the 5f and 4f cations (DTPA) or indicate a stronger interaction with Pu(III) compared to Eu(III) (sulphosalicylic acid, SSA) [89-93]. In the case of the sulphosalicylic acid, the difference observed between Eu(III) and Pu(III) was explained by a higher participation of the 5f orbitals in the bonding compared to the 4f orbitals. In most cases, the use of europium as a plutonium(III) analog seems to be generally justified, however, according to the ligand the analogy still needs to be confirmed.

Table I.11. Comparison of thermodynamic data for plutonium(III) and europium(III) complexes

Species	$\log_{10} \beta$	T(°C)	I	Reference
<i>Pu</i>DTPA²⁻	21.5	25	1.0M KCl	[89] [94]
<i>Eu</i>DTPA²⁻	21.00±0.08	25	1.0 M NaClO ₄	[90]
<i>Pu(III) – SSA</i>	8.56±0.15	25	1.0 M NaClO ₄	[91]
<i>Eu(III) – SSA</i>	6.27±0.08	25	1.0 M NaClO ₄	[91]

The analogs of Pu(V) and Pu(VI) are Np(V) and U(VI). The comparison of some available data for U(VI) and Pu(VI) complexes with a stoichiometry 1:1 shows a good agreement (**Table I.12**). For instance, $\log_{10} K^0$ values involving carbonate as ligand are 9.5 for PuO_2^{2+} and 9.94 for UO_2^{2+} .

Table I.12. Comparison of thermodynamic data for plutonium (VI) and uranium(VI) complexes ^[28]

Reaction	Metal	$\log_{10} K^0$
$MO_2^{2+} + Cl^- \rightleftharpoons MO_2Cl^+$	Pu(VI)	0.23±0.03
	U(VI)	0.17±0.02
$MO_2^{2+} + SO_4^{2-} \rightleftharpoons MO_2SO_4(aq)$	Pu(VI)	3.38±0.20
	U(VI)	3.15±0.10
$MO_2^{2+} + CO_3^{2-} \rightleftharpoons MO_2CO_3(aq)$	Pu(VI)	9.50±0.50
	U(VI)	9.94±0.03

The case of Pu(IV) is more challenging: the ionic radius of Th(IV) is different from that of Pu(IV) and adjustments are required to deduce complexation constants with Pu from those obtained with Th ^[87].

Moreover, CeO₂ is often used as surrogate for PuO₂ in studies on the fabrication of plutonium oxide or mixed oxide (MOX) for nuclear fuel as well as on their dissolution ^[95, 96]. Although CeO₂ and PuO₂ display similar crystallographic properties, PuO₂ is a material more refractory than CeO₂ that can lead to difference in dissolution kinetics. Lastly, a biological analogy between Pu⁴⁺ and Fe³⁺ can be mentioned. More precisely, siderophores are secreted by microorganisms to solubilize iron in order to allow its incorporation to the cell. This process can also occur with Pu(IV) that displays also high affinity towards such ligands, *e.g.* desferrioxamine B ^[92].

In the following section are presented some investigations related to the complexation of trivalent Ln/An-phosphate and U(VI)-phosphate complexation which can assist to study of Pu-phosphate systems.

I.4.1 Complexation of Pu(III) analogs with phosphate species

The available data related to the complexation constants of Ln(III) and An(III) with phosphates have been determined using different techniques: distribution between two phases, Time-Resolved Laser-induced Fluorescence Spectroscopy (TRLFS) and solubility measurements ^[97, 98].

1.4.1.1 In solution

Most of these studies in aqueous solution were performed at low pH and phosphoric acid concentration ranging from 0.05 to 4 M ^[99]. Complexes of stoichiometry 1:1 and 1:2 have been reported for Cm(III), Am(III) and Eu(III). The corresponding stability constants associated to equilibria **I.8** and **I.9** ^[97, 100-105] at I=0 M and T=25°C are shown in **Table I.13**.



It can be seen that $\log \beta_1$ and $\log \beta_2$ tend to decrease according to the sequence Eu(III)>Am(III)>Cm(III) ^[97]. This can be explained because at higher ionic radii the stability constants tend to be decrease.

Table I.13. Standard stability constants selected in NEA-TDB and most recent investigations for $M(H_2PO_4)^{2+}$ and $M(H_2PO_4)_2^+$ complexes

Conditions	$\log_{10}\beta_1^0$	$\log_{10}\beta_2^0$	Method	Reference
Cm(III)	2.59±0.19 ^a		TRLFS	[97]
Eu(III)	3.03±0.13 ^a			
Cm(III)	2.59±0.04 ^a	4.36±0.07 ^a	TRLFS	[98]
Cm(III)	2.40	3.60	Cation exchange	[86]
Pu(III)	2.39	3.70		
Am(III)	2.39	3.63		
Am(III)	2.13±0.08		Solvent extraction	[102]
Am(III)	2.73±0.06 ^b	3.72±0.06 ^b	Spectrophotometry	[104]
Eu(III)	2.65±0.03 ^c	---	Solubility	[105]

a. Values recalculated using $\log_{10}K_{a1}^0=2.14\pm0.030$ ^[28]

b. Values recalculated by NEA-TDB ^[99]

c. Values recalculated using $\log_{10}K_{a1}^0=2.14\pm0.030$, $\log_{10}K_{a2}^0=7.212\pm0.013$ and $\log_{10}K_{a3}^0=-12.35\pm0.030$ ^[28]

Structural data about complexation of Cm(III) with phosphate obtained by DFT calculations have been recently deduced from theoretical calculations ^[98]. Complexes 1:1 and 1:2, with monodentate coordination of phosphate have been found to be the most stable configuration.

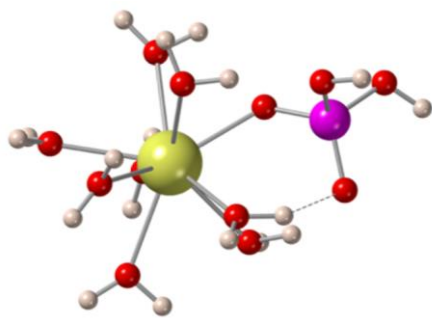


Figure I.10. Optimized structures from DFT calculations of hydrated $\text{Cm}(\text{H}_2\text{PO}_4)^{2+}$ (Cm in yellow, O in red and P in violet)^[98]

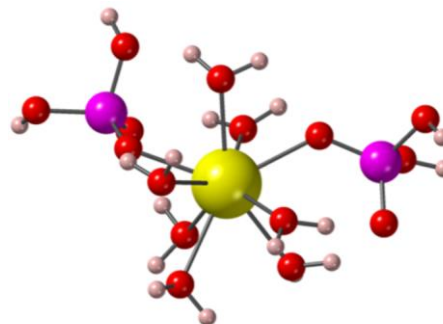


Figure I.11. Optimized structures from DFT calculations of hydrated $\text{Cm}(\text{H}_2\text{PO}_4)_2^+$ (Cm in yellow, O in red and P in violet)^[98]

This study suggested that both complexes can be 8- and 9- coordinates. The interatomic distances of Cm to water molecules ($\text{Cm}-\text{OH}_2$), oxygen and phosphate to H_2PO_4^- species ($\text{Cm}-\text{O}_\text{P}$ and $\text{Cm}-\text{P}_\text{P}$) are presented in **Table I.14**.

Table I.14. Interatomic distances of Cm(III)-phosphate complexes^[98]

	Complex 1:1		Complex 1:2	
	$\text{Cm}(\text{H}_2\text{O})_7(\text{H}_2\text{PO}_4)^{2+}$ CN=8 Å	$\text{Cm}(\text{H}_2\text{O})_7(\text{H}_2\text{PO}_4)_2^+$ CN=9 Å	$\text{Cm}(\text{H}_2\text{O})_6(\text{H}_2\text{PO}_4)_2^+$ CN=8 Å	$\text{Cm}(\text{H}_2\text{O})_7(\text{H}_2\text{PO}_4)_2^+$ CN=9 Å
Cm-OH₂	2.446/2.530	2.447/2.571	2.445/2.521	2.459/2.569
Cm-O_P	2.260	2.297	2.319/2.331	2.365/2.378
Cm-P_P	3.371	3.440	3.428/3.436	3.489/3.530

Studies performed by TRLFS suggested that the luminescence lifetime is correlated with the number of water molecules coordinated to Cm(III)^[98]. The Cm(III) aquo ion 9-fold water coordinated has a lifetime of $67 \pm 2 \mu\text{s}$. The lifetime of the complex $\text{Cm}(\text{H}_2\text{PO}_4)^{2+}$ is $\tau = 73 \pm 3 \mu\text{s}$ that has been assigned to a coordination of 8 water molecules: the replacement of one water molecule by one ligand H_2PO_4^- indicates that the phosphate ligand is monodentate in accordance with theoretical calculations^[97]. The 9-coordination in complex 1:1 is the same whatever the temperature. However, complex 1:2 at $T=25^\circ\text{C}$ is 9-fold coordinated. Then as the temperature increasing one water molecule is replaced by another ligand given a 8-coordination^[106].

I.4.1.2. Pu(III)-rhabdophane and Pu(III)-monazite analogs

Due to the low solubility of M(III)-phosphate complexes, the fundamental thermodynamic data have been determined by solubility measurements of well-characterized solid phosphate compounds. In the present work, the bibliographic study is limited to rhabdophane and monazite.

Rhabdophane structure has a general formula $REPO_4 \cdot nH_2O$ and generally crystallizes in hexagonal system ($P3_121$)^[107]. Recent investigations deduced by X-Ray absorption spectroscopy suggest monoclinic systems ($C2/c$) space group^[48,108]. There are three distinct rhabdophane structures with different hydration state depending on the synthesis conditions: monoclinic hydrated $LnPO_4 \cdot 0.667H_2O$, monoclinic hemihydrate $LnPO_4 \cdot 5H_2O$ and hexagonal anhydrous $LnPO_4$ rhabdophane phases^[100]. Rhabdophane compounds are considered as precursors of monazites phases ($REPO_4$) which crystallize in a monoclinic structure ($P2_1/n$) at low temperature, this irreversible transition occurring between 500 and 900 °C^[48, 108].

At low temperature (typically below 60°C), rhabdophane is the solubility controlling phase for light lanthanide (Ln to Gd)^[109]. The solubility of rhabdophane phases with lanthanides has been investigated systematically by Gausse *et. al.*,^[48] using $LnPO_4 \cdot 0.667H_2O$ (La to Dy) in over and undersaturation experiments at different temperatures (25 to 90°C). Dissolution experiments have been performed in 0.1 M HCl: the dissolution was found to be congruent and the equilibrium reached in 10 days.

Concerning trivalent actinides Rai *et al.*,^[110] have studied the dissolution of Am during 86 days, reporting the equilibrium is reached in 21 days. The solubility products derived from this work responds to the type of reaction **I.7**. The solubility products obtained from these studies are summarized in **Table I.15**, we can notice the values are very similar. Thus, the use of analogs from the lanthanide series can elucidate $PuPO_4$ (monazite) dissolution.

Table I.15. Solubility products determined for Eu(III), Nd(III), Am(III) and Pu(III) in rhabdophane and monazite phases

Compound	$\log_{10}K_{sp}^0$	Type	Reference
EuPO₄·0.667H₂O	-25.5±0.3	Rhabdophane	[48]
NdPO₄·0.667H₂O	-25.6±0.3	Rhabdophane	[48]
EuPO₄·xH₂O	-25.75±0.27	Rhabdophane	[111]
EuPO₄	-26.48	Monazite	
NdPO₄·xH₂O	-25.95±0.06	Rhabdophane	[111]
NdPO₄	-26.38	Monazite	
AmPO₄·xH₂O	-24.79±0.18	Rhabdophane	[110]
PuPO₄	-24.28±0.35	Monazite	[85]

I.4.2 Complexation of Pu(VI) analog with phosphate species

The speciation of uranium (VI) in the presence of phosphate species has been studied using different techniques such as UV-Vis absorption spectroscopy^[112, 113], distribution between two phases^[76, 114-118], potentiometry^[119], solubility^[120-122], TRFLS^[119, 123-125], FTIR spectroscopy^[76, 118] and theoretical quantum chemistry^[126-128].

I.4.2.1. In solution

TRFLS has been used to study the interactions between the uranyl cation (UO₂²⁺) with phosphate ions (H₂PO₄⁻, HPO₄²⁻, PO₄³⁻) at very low uranium concentration (10⁻¹² M)^[123]. The fluorescence properties of UO₂²⁺ strongly depend on the environment of the cation and each uranium species is characterized by its spectra with specific wavelengths and fluorescence lifetime^[129].

In **Figure I.12**, the fluorescence spectra of the free uranyl and three U(VI)-phosphate complexes are presented. According to Scapolan *et al.*,^[123] the emission bands of UO₂²⁺ at 10⁻⁷ M without any complexing ligands are at 488-509-533-559 nm. Then, the addition of phosphates in the solution causes a shift of the spectrum at higher emission wavelengths and it can be assigned to a specific species that will depend then on the pH. For instance, UO₂H₂PO₄⁺ was found to be the major species at pH 1.5 in 10⁻⁴ M H₃PO₄ with its corresponding emission bands at 494-515-539-565 nm, whereas UO₂HPO₄ appears at pH 5 in 10⁻⁷ M H₃PO₄ with bands at 497-519-543-570 nm. The third species,

UO_2PO_4^- is present at pH 7.5 in 10^{-3} M H_3PO_4 and its emission bands shift to 499-520-544-571 nm^[123]. Unfortunately, it seems that the spectra of complexes $\text{UO}_2\text{H}_2\text{PO}_4^+$ and $\text{UO}_2(\text{H}_2\text{PO}_4)_2$ cannot be distinguished^[124].

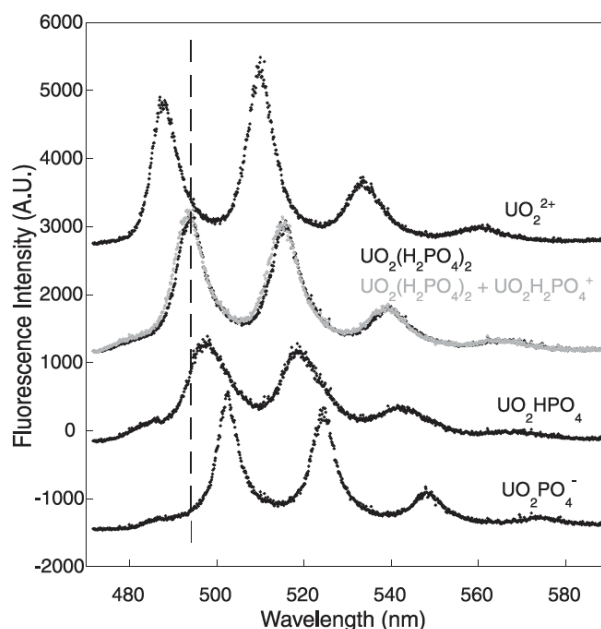


Figure I.12. Fluorescence spectra of UO_2^{2+} , $\text{UO}_2\text{H}_2\text{PO}_4^+$, $\text{UO}_2(\text{H}_2\text{PO}_4)_2$, UO_2HPO_4 and UO_2PO_4^- ^[124]

Moreover, each species can be identified by its fluorescence lifetime. The free uranyl lifetime is known to be short and equal to $2 \pm 0.1 \mu\text{s}$ at $I=1 \text{ NaClO}_4 \text{ M}$, or 1.1 ± 0.1 ^[119, 123, 129].

The fluorescence lifetime of $\text{UO}_2(\text{H}_2\text{PO}_4)^+$ complex has been reported as 11 ± 1 or $14.3 \pm 1.3 \mu\text{s}$ ^[124, 130] similar with the value reported for $\text{UO}_2(\text{HPO}_4)$. This similitude is explained by the difference of only one hydrogen ion between these two aqueous complexes, which is too small to cause detectable changes^[119, 123]. The $\text{UO}_2(\text{H}_2\text{PO}_4)_2$ can be distinguished because it has a bigger lifetime equal to $28 \pm 5 \mu\text{s}$ even $67.9 \pm 11 \mu\text{s}$ have been suggested^[124, 130]. Finally, UO_2PO_4^- has a lifetime reported as $24 \pm 2 \mu\text{s}$ ^[123, 124]. Thus, the general trend is that the fluorescence lifetime of the phosphate complexes increases when the number of phosphate species in the solvation shell increases^[130].

As the previous technique, the UV-Vis absorption spectrum of free uranyl have a characteristic shape with maximum of absorbance around 413.8 nm, as can see in **Figure I.13**^[112]. Then, variation of the phosphate concentration results in a shift of the

spectrum to higher wavelength (420 nm) and a variation of the molar absorbance can be attributed to specific uranium-phosphate complexes [131].

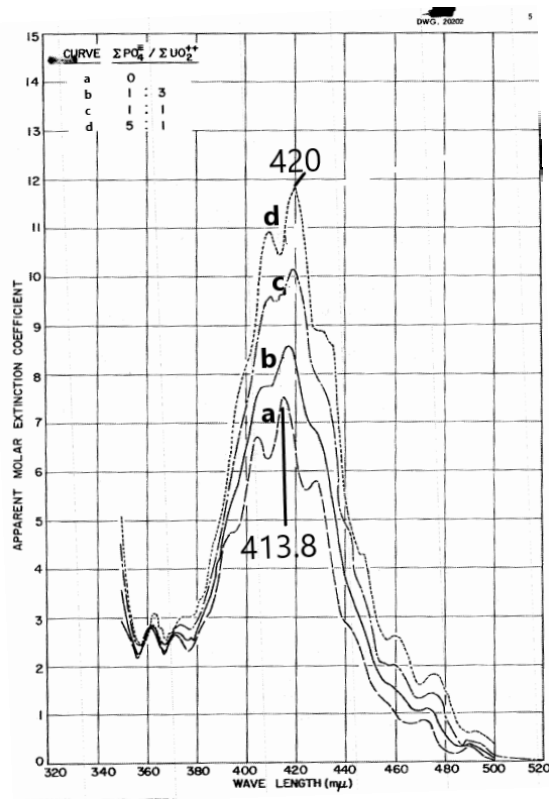


Figure I.13. Effect of phosphate concentration on the UV-Vis absorption spectra of U(VI) in 1 M HClO₄ (a. free UO₂²⁺; b, c, d. Varying the ratio [ΣPO₄]/U(VI)) [112]

Baes Jr., [112] studied U(VI)-phosphate complexation in 1 M HClO₄ and 0.1 M HClO₄/0.9 M NaClO₄ at pH=1-2, using concentration of uranium ($C_{U(VI)}=9.43 \times 10^{-4}$) and moderate phosphate concentration that can vary until 10^{-3} M. A similar experiment was done by Thamer [113] in 1 M (H, Na)ClO₄ at pH 1 with constant $C_{U(VI)}$ around 0.1-0.15 M and extended phosphate concentration between 0.1 and 3.7 M. Their respective analysis of the absorption spectra indicate mainly the presence of aqueous species such as UO₂(H₂PO₄)⁺ at relative low pH (<4) and low-phosphate concentration (<0.02 M) and UO₂(H₂PO₄)₂ at low pH and high phosphate concentration [84, 112, 113]. Complexes with higher stoichiometry are formed at more concentrated phosphoric acid concentration ([ΣPO₄] > 0.5 M). Baes Jr., [112] reported UO₂(H₃PO₄)²⁺ and Thamer [113] suggested UO₂(H₂PO₄)(H₃PO₄)⁺, but those aqueous species are not present in an appreciable amount to distinguish them by UV-Vis spectrophotometry.

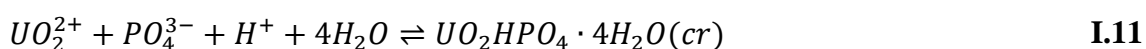
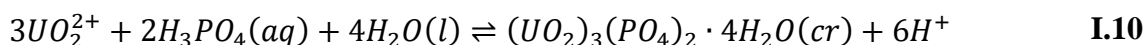
I.4.2.2. Solid compounds

On the other hand, experimental conditions have also been optimized to precipitate stable solid phases and study their solubility. Schreyer *et. al.*, ^[120] reported the preparation of $\text{UO}_2\text{HPO}_4 \cdot 4\text{H}_2\text{O}(\text{cr})$ in 1.1 M H_3PO_4 with U(VI) in nitrate or perchlorate solution in the pH range between 1 and 2. $(\text{UO}_2)_3(\text{PO}_4)_2 \cdot 4\text{H}_2\text{O}(\text{cr})$ was prepared under oxidation conditions by digesting $\text{UO}_2\text{NH}_4\text{PO}_4 \cdot 4\text{H}_2\text{O}(\text{cr})$ in 0.8 M HNO_3 at 100°C . Whereas, Rai *et al.*, ^[84] prepared the same phase mixing 0.7 M H_3PO_4 with 0.05 M $\text{UO}_2(\text{NO}_3)_2$ at 40°C . Schreyer *et. al.*, ^[120] synthesized $\text{UO}_2(\text{H}_2\text{PO}_4)_2 \cdot 3\text{H}_2\text{O}$ from $\text{UO}_2\text{HPO}_4 \cdot 4\text{H}_2\text{O}(\text{cr})$ in excess of H_3PO_4 at 25°C .

The study of the solubility of those solid phases, mainly $(\text{UO}_2)_3(\text{PO}_4)_2 \cdot 4\text{H}_2\text{O}(\text{cr})$ in phosphoric acid solutions (~ 6 M) and low pH (<4), led to the formation of $\text{UO}_2(\text{H}_2\text{PO}_4)^+$ and $\text{UO}_2(\text{H}_2\text{PO}_4)_2$ in aqueous solutions. Other complexes have also been identified, such as $\text{UO}_2(\text{H}_3\text{PO}_4)^{2+}$ and $\text{UO}_2(\text{H}_2\text{PO}_4)(\text{H}_3\text{PO}_4)^+$, but they never became predominant during the experiments ^[84, 120]. The species present in solutions is strongly dependent on the pH. Sandino *et. al* ^[122] performed solubility experiments at extended pH range in 0.5 M NaClO_4 . This investigation reported the formation of $\text{UO}_2\text{HPO}_4(\text{aq})$ at intermediate pH values (~ 4 to 6) and UO_2PO_4^- formed at pH higher than 6.

The stability constant and solubility products associated to those U(VI)-phosphate complexes and compounds can slightly differ for one investigation to another. This is mainly due to variations in experimental conditions, such as ionic strength, background electrolyte, temperature even reaction equilibrium considered by the authors.

The solubility equilibria of the $(\text{UO}_2)_3(\text{PO}_4)_2 \cdot 4\text{H}_2\text{O}(\text{cr})$ and $\text{UO}_2\text{HPO}_4 \cdot 4\text{H}_2\text{O}(\text{cr})$ solid compounds were reported using H_3PO_4 as ligand in the previous NEA-TDB compilations ^[24, 132]. Nevertheless, in the most recently update ^[28], the equilibrium reactions of $\text{UO}_2\text{HPO}_4 \cdot 4\text{H}_2\text{O}(\text{cr})$ were recalculated using PO_4^{3-} . Those equilibria are written as follows:



The corresponding standard stability constants of the equilibria reported in literature and selected by the NEA-TDB compilation ^[28] are listed in **Table I.16**. Those are presented using H₃PO₄ as predominant ligand in acidic media at low pH (<4). In alkaline media, they are written using HPO₄²⁻ at pH around 4-6, and PO₄³⁻ at pH >6.

Table I.16. Selected thermodynamic data for uranium-phosphate complexes in aqueous solution (T=25°C, 0.1 MPa, I=0) ^[28]

Species	log ₁₀ K ⁰
$UO_2^{2+} + H_3PO_4(aq) \rightleftharpoons UO_2(H_2PO_4)^+ + H^+$	1.12±0.06
$UO_2^{2+} + 2H_3PO_4(aq) \rightleftharpoons UO_2(H_2PO_4)_2(aq) + 2H^+$	0.640±0.110
$UO_2^{2+} + 2H_3PO_4 \rightleftharpoons UO_2(H_2PO_4)(H_3PO_4)^+ + H^+$	1.650±0.110
$UO_2^{2+} + H_3PO_4(aq) \rightleftharpoons UO_2(H_3PO_4)^{2+}$	0.760±0.150
$UO_2^{2+} + PO_4^{3-} \rightleftharpoons UO_2PO_4^-$	11.010±0.480
$UO_2^{2+} + HPO_4^{2-} \rightleftharpoons UO_2HPO_4(aq)$	7.240±0.260
$3UO_2^{2+} + 2H_3PO_4(aq) + 4H_2O(l) \rightleftharpoons (UO_2)_3(PO_4)_2 \cdot 4H_2O(cr) + 6H^+$	5.960±0.300
$UO_2^{2+} + PO_4^{3-} + H^+ + 4H_2O \rightleftharpoons UO_2HPO_4 \cdot 4H_2O(cr)$	24.202±0.090

However, other species of stoichiometry higher than 1:2 have been reported in literature, especially in concentrated phosphoric acid ^[113]. Such species have been studied by solvent extraction and their speciation has been determined by UV-Vis spectrophotometry, FTIR spectroscopy, and TRLFS ^[76, 113, 115, 116, 125, 133]. As mentioned in **I.3.1**, dimeric species like H₅P₂O₈⁻ and H₆P₂O₈ can exist in concentrated phosphoric acid solutions leading to the formation of UO₂(H₂PO₄)(H₃PO₄)₂⁺, UO₂(H₂PO₄)₂(H₃PO₄) and UO₂(H₂PO₄)₃⁻.

Investigations conducted in 0.1 to 4 M phosphoric acid range, reported that the predominant species is UO₂(H₂PO₄)(H₃PO₄)⁺ and it is the only one retained by the NEA-TDB. However, species like UO₂(H₂PO₄)(H₃PO₄)₂⁺, UO₂(H₂PO₄)₂(H₃PO₄) and UO₂(H₂PO₄)₃⁻ seem to be predominant in 4.2-7.08 M as suggested by Elyahyaoui *et al.*, ^[115, 116] and Dartiguelongue *et al.*, ^[118]. In this work, these species are not considered since the phosphate concentration is below this range as well as the uranium concentration, in acidic media.

Finally, one can also notice that no enthalpy and entropy variations about U(VI)-phosphate complexation have been retained in NEA-TDB [28]. In literature data, only two studies are focused on the influence of temperature.

Kirishima *et al.*, [130] showed the distribution of UO_2^{2+} , $\text{UO}_2(\text{H}_2\text{PO}_4)^+$ and $\text{UO}_2(\text{H}_2\text{PO}_4)_2$ species at higher temperatures. The authors concluded that no significant variations occur between 25 and 100°C as shown in **Figure I.14**, but values of enthalpy and entropy were not proposed by the authors. The only work where values of these parameters are proposed will be further discussed in part **IV.1.4**.

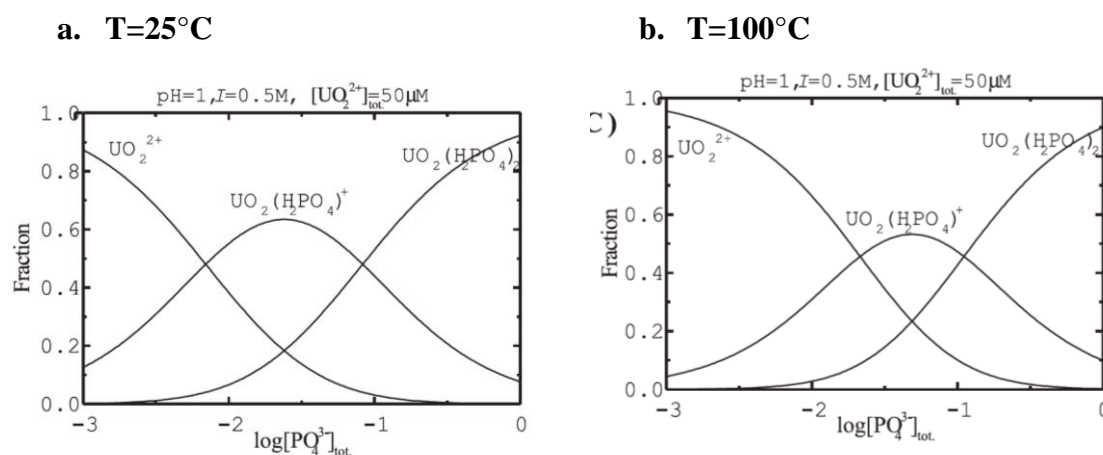


Figure I.14. Speciation diagrams of U(VI)-phosphate at different temperatures
($C_{\text{U(VI)}}=5 \times 10^{-5} \text{ M}$, $I=0.5 \text{ M NaClO}_4$, $\text{pH}=1$, $T=25$ and 100) [130]

I.4.2.1.1 Structural study of uranium (VI) with phosphoric acid

To the best of our knowledge, neither IR, Raman nor XAS spectra relative to U(VI) phosphate complexes in homogeneous solution are available in the literature. But vibration frequencies, interatomic distances have been determined for some solid phase, especially a single crystal of $(\text{UO}_2)_3(\text{PO}_4)_2 \cdot 4(\text{H}_2\text{O})_{(\text{cr})}$ [134].

So far, structural data are deduced from theoretical calculations, which reliability is based on a close comparison to experimental interatomic distances and vibration frequencies determined at solid state or at interface liquid/solid. Monodentate and bidentate binding, bridging, involving the three phosphate species H_2PO_4^- , HPO_4^{2-} and PO_4^{3-} are possible leading to a large variety of combinations. Quantum chemical studies have been performed on uranyl complexes with these three different anionic forms of phosphate [126-128]. Calculations were conducted in the gas phase with explicit water

molecules in order to determine the structural parameters of the complexes (distances, angles), coordination mode of phosphate ligand, vibrational frequencies, associated to anhydrous species and hydrated ones.

a. Complexes of stoichiometry 1:1

Whatever the ligand form, whatever the complex investigated (anhydrous, with 1, 2 or 3 water molecules in the first coordination sphere), the optimized structures are characterized by a bidentate binding of the ligand to uranium, with water molecules in the equatorial plane of the uranyl moiety. As an example, the structure and the interatomic distances of $\text{UO}_2(\text{HPO}_4)(\text{H}_2\text{O})_3$ determined in Jackson *et al.*,^[126] and Majumdar *et al.*,^[128] are presented in **Figure I.15**. Overall both structures agree quite well. However, Jackson *et al.*^[126] found another structure about 15 kcal mol^{-1} more stable: a proton from a water molecule is transferred to the ligand HPO_4^{2-} , leading to H_2PO_4^- that is bound to uranium in a monodentate way. A strong stabilization occurs through hydrogen bond between water molecule and the terminal P-O bond that remains non protonated.

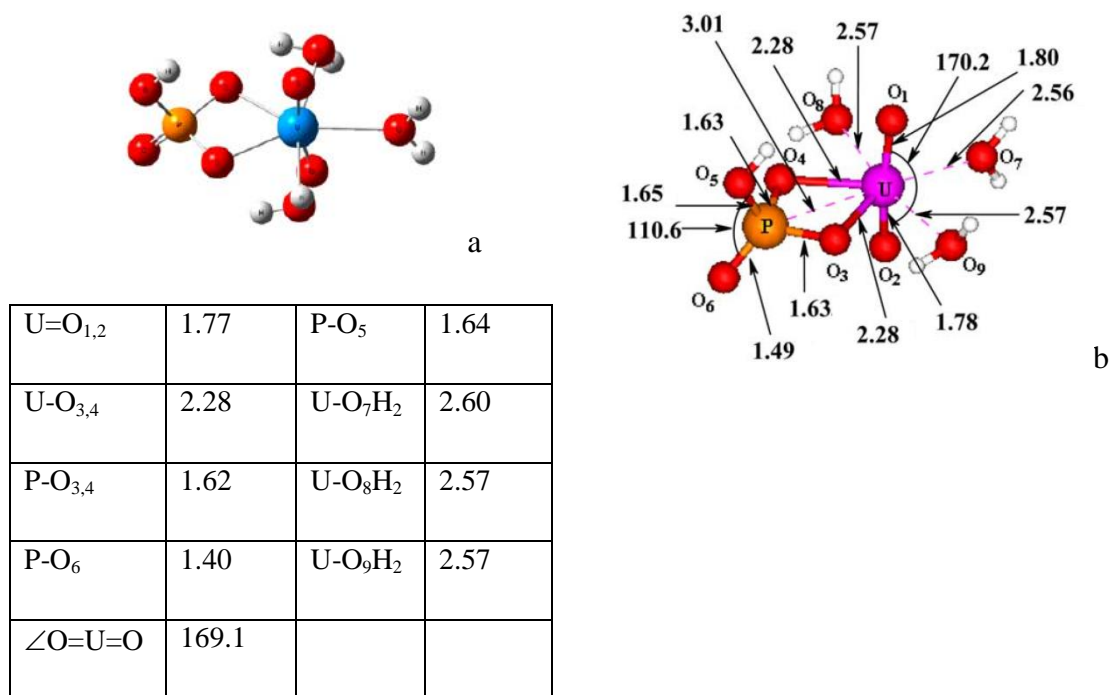


Figure I.15. Optimized structure from DFT calculations of $\text{UO}_2(\text{HPO}_4)(\text{H}_2\text{O})_3$ with bond lengths (in Å) and angles (in degrees) according to a. Jackson *et al.*^[109] and b. Majumdar *et al.*^[128]

According to Jackson *et al.*,^[126] the addition of a fourth water molecules leads to a change in the ligand binding: H_2PO_4^- becomes monodentate in order to reach the coordination number 5 in the equatorial plane (**Figure I.16.a**). HPO_4^{2-} and PO_4^{3-} remain bidentate but in the case of HPO_4^{2-} , a proton transfer from H_2O to the ligand occurs (**Figure I.16.b**). In the case of PO_4^{3-} , the additional water molecule is transferred to the second hydration shell as illustrated in **Figure I.16.c**^[126]. Kubicki *et al.*,^[127] who introduced a second hydration shell with 30 water molecules, also concludes that the bidentate configuration of complexes with HPO_4^{2-} and PO_4^{3-} is more stable than the monodentate one. However, with the ligand H_2PO_4^- , the monodentate binding seems more stable, but the calculated distance U-P does not match with the experimental one of Locock *et al.*:^[134] which found 0.48 Å longer.

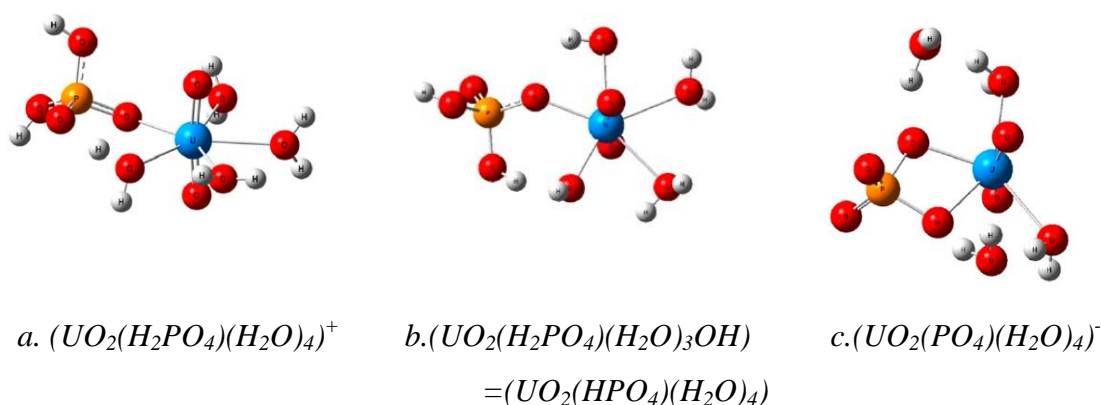


Figure I.16. Optimized structures from DFT calculations of hydrated U(VI)-phosphate complexes of stoichiometry 1:1^[126]

b. Complexes of stoichiometry 1:2

All phosphate ligands in anhydrous complexes of stoichiometry 1:2 display bidentate configuration^[126]. This configuration tends to turn to monodentate depending on the number of water molecules and the form of phosphate ligand. The presence of 2 water molecules in the first coordination sphere leads to one bidentate and one monodentate H_2PO_4^- , the latter being stabilized by the hydrogen bond between the terminal P-O and water molecule (**Figure I.17.a**). By adding a third water molecule, both ligand become monodentate.

The hydrated complexes with hydrogenophosphate ligands are characterized by proton transfer from water to the ligand, leading to the formation of «hydroxide species» bound to uranium. In some complexes, only 4 coordination sites are filled in the equatorial

plan. According to Jackson *et al.*,^[126] a strong stabilization through several hydrogen bonds could favor this unusual coordination. This is illustrated in **Figure I.17.b**, for the complex $(\text{UO}_2(\text{HPO}_4)_2(\text{H}_2\text{O}))^{2-}$ which structure corresponds to the formulation $(\text{UO}_2(\text{H}_2\text{PO}_4)(\text{HPO}_4)(\text{OH}))^{2-}$. In the complex with one water molecule, both ligands PO_4^{3-} are bidentate, and surprisingly, while the equatorial plane could accommodate H_2O , this latter is expelled to the second solvation sphere. The optimized structure with an additional water molecule leads to a proton transfer to PO_4^{3-} : the non-protonated phosphate remains bidentate, the protonated one become monodentate and the coordination sphere of U is supplemented by a hydroxide.

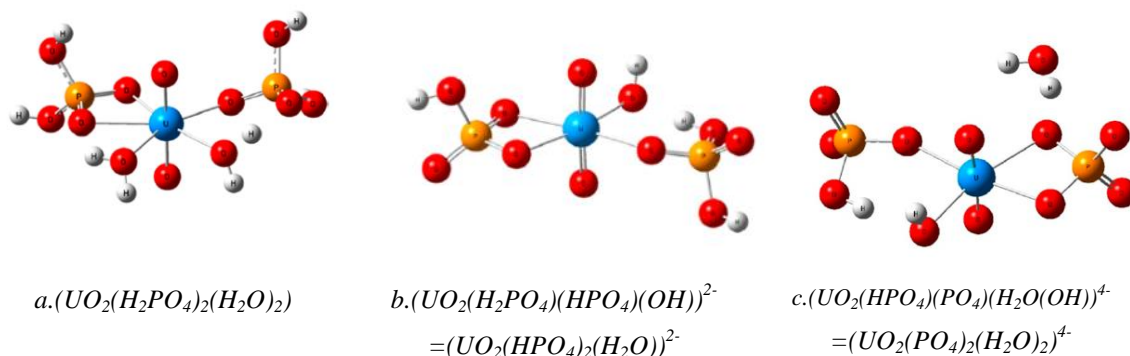


Figure I.17. Optimized structures from DFT calculations of hydrated U(VI)-phosphate complexes of stoichiometry 1:2^[126]

c. Complexes of stoichiometry 1:3 and 1:4

The existence of the complex 1:3 is proposed in only one paper published in 1957: Thamer proposed the species $(\text{UO}_2(\text{H}_2\text{PO}_4)_2(\text{H}_3\text{PO}_4))$ to interpret his solvent extraction data collected in the system DBP/kerosene/ H_3PO_4 ^[113]. But this assumption has been discarded in the critical OCDE review^[132] since it is not consistent with some solubility data, and the large range of phosphoric acid concentration used in Thamer's work did not ensure that activity coefficients remained constant. Nevertheless, Jackson *et al.*,^[126] have also determined the optimized geometry of anhydrous complexes of stoichiometry 1:3 and 1:4. Except for the complex $(\text{UO}_2(\text{H}_2\text{PO}_4)_3)^-$ where 2 ligands are bidentate and the third monodentate, only monodentate binding is observed in all other complexes.

Summary

Chapter 1 is devoted to the bibliographic study about actinides and phosphate in the environment as well as in the nuclear industry. Actinides are released by natural sources but most of the environmental contaminations are caused by anthropogenic activities mainly due to nuclear weapons fallout or nuclear plants during plutonium production or reprocessing steps. The migrations and toxicity of actinides are mainly governed by their speciation and depend on several parameters such oxidation state, redox properties, hydration structure, hydrolysis and complexation with organic and inorganic ligands naturally found in the environment such phosphate species

Phosphate species are released in soils, waters and sediments by natural weathering of phosphate rocks (*e.g.* monazite or apatite) and by the industrial production of fertilizers and phosphoric acid. Phosphate species are present in the nuclear fuel cycle since they play an important role during the reprocessing of the nuclear spent fuel with the PUREX process which involves tributylphosphate (TBP) as extractant and the safe disposal using phosphate matrices for their immobilizations at long term.

Phosphate can be involved in different equilibria such dissociation (H_2PO_4^- , HPO_4^{2-} , PO_4^{3-}), dimerization ($\text{H}_5\text{P}_2\text{O}_8^{2-}$, $\text{H}_4\text{P}_3\text{O}_8^{2-}$, $\text{H}_3(\text{PO}_4)_2^{3-}$) and also ion pair formation with cations (Na^+ or K^+) and those species can interact with plutonium ions (An^{3+} , An^{4+} , AnO_2^+ and AnO_2^{2+}). However, thermodynamic data related to Pu-phosphate interaction is limited due to low solubility of Pu-phosphate compounds and the most of the data has been obtained by solubility measurements. In order to understand Pu-phosphate interactions, some investigations have been performed experiments using chemical analogs at the same oxidation state and similar radius. This investigation is focused in Eu(III) and U(VI) since those display chemical behavior close to the one of Pu(III) and Pu(VI), without redox instability.

Investigations related to Ln/An-phosphate systems (Ln/An=Am, Cm, Pu and Eu) in aqueous solutions reveal the formation of complexes with stoichiometric 1:1 and 1:2 using distribution between two phases and TRLFS. However, studies performed by cation exchanged suggested the formation of complexes up to 1:4. Structural data about complexation of Cm(III) with phosphate obtained by theoretical calculations suggested monodentate coordination for complexes of stoichiometric 1:1 and 1:2. This chapter also presents solubility studies in solid phosphate compounds such monazite ($\text{An}^{(\text{III})}\text{PuO}_4$)

and rhabdophane ($\text{REEPO}_4 \cdot x\text{H}_2\text{O}$). The solubility products obtained from these studies are very similar which confirm the use of analogs from lanthanide series can elucidate $\text{Pu}^{(\text{III})}\text{PO}_4$ dissolution.

Concerning the speciation of U(VI) with phosphate species, more species have been identified and retained by NEA-TDB that can help to interpret Pu(VI)-phosphate systems. However, the concentration of phosphate and pH play an important role during the complexation process. In acidic conditions, complexes of stoichiometry 1:1 and 1:2 are found at very low phosphate concentration involved H_3PO_4 as main ligand. The increasing of pH leads with the formation of species with HPO_4^- and PO_4^{3-} as ligand. At higher concentrations, dimeric species or even the formation of solid compounds can be found. Structural information about complexes of stoichiometry 1:1 reveals whatever the water molecules in the first coordination sphere; the complex is characterized by a bidentate binding of the ligand to uranium. In case of stoichiometry 1:2, the anhydrous complexes display bidentate configuration and this configuration tends to turn to monodentate depending on the number of water molecules and the form of phosphate ligand.

References

- [1] G. T. Seaborg, The chemical and radioactive properties of the heavy elements, *Chemical and Engineering News Archive*, **23**, 2190-2193 (1945).
- [2] IUPAC, International Union of Pure and Applied Chemistry, 2022. [On line]. Available: <https://iupac.org/what-we-do/periodic-table-of-elements/>. [Last access: 12 10 2022].
- [3] G. R. Choppin and M. P. Jensen, Actinides in solution: complexation and kinetics, *The chemistry of the actinide and transactinide elements*, 4th ed., Netherlands, Springer, 2524-2621, (2010).
- [4] T. Newton and S. Rabideau, A review of the kinetics of the aqueous oxidation–reduction reactions of uranium, neptunium, and plutonium, *Journal of Physical Chemistry*, **63**, 365-370 (1959).
- [5] N. Takeno, Atlas of Eh-pH diagrams, *Geological Survey of Japan Open File report*, **419**, 102 (2005).
- [6] J. M. Cleveland. The chemistry of plutonium. Gordon and Breach, London (1970)
- [7] Z. Szabó, T. Toraiishi, V. Vallet and I. Grenthe, Solution coordination chemistry of actinides: Thermodynamics structure and reaction mechanisms, *Coordination Chemistry Reviews*, **250**, 784-815 (2006).
- [8] K. E. Knope and L. Soderholm, Solution and solid-state structural chemistry of actinide hydrates and their hydrolysis and condensation products, *Chemical Reviews*, **113**, 944-994 (2013).
- [9] L. Galbis, J. Hernandez-Cobos, C. Den Auwer, C. Le Naour, D. Guillaumont, E. Simoni and E. S. Marcos, Solving the hydration structure of the heaviest actinide aqua ion known: the californium (III) case, *Angewandte Chemie-International Edition*, **49**, 3811-3815 (2010).
- [10] H. Moll, M. A. Denecke, F. Jalilehvand, M. Sandstrom and I. Grenthe, Structure of the aqua ions and fluoride complexes of uranium(IV) and thorium(IV) in aqueous solution: an EXAFS study, *Inorganic Chemistry*, **38**, 1795-1799 (1999).
- [11] V. Neck, R. Muller, M. Bouby, M. Altmaier, J. Rothe, M. A. Denecke and J. I. Kim, Solubility of amorphous Th(IV) hydroxide application of LIBD to determine the solubility product and EXAFS for aqueous speciation, *Radiochimica Acta*, **90**, 485-494 (2002).
- [12] J. Rothe, M. A. Denecke, V. Neck, R. Muller and J. I. Kim, XAFS investigation of the structure of aqueous thorium(IV) species, colloids, and solid thorium(IV) oxide/hydroxide, *Inorganic Chemistry*, **41**, 249-258 (2002).

- [13] C. Hennig, K. Schmeide, V. Brendler, H. Moll, S. Tsushima and A. C. Scheinost, EXAFS investigation of U(VI), U(IV), and Th(IV) sulfate complexes in aqueous solution, *Inorganic Chemistry*, **46**, 5882-5892 (2007).
- [14] N. Torapava, I. Person, L. Eriksson and D. Lundberg, Hydration and hydrolysis of thorium(IV) in aqueous solution and the structures of two crystal-line thorium(IV) hydrates, *Inorganic Chemistry*, **48**, 11712-11723 (2009).
- [15] K. E. Knope, M. Vasiliu, D. A. Dixon and L. Soderholm, Thorium(IV)-selenate clusters containing an octanuclear Th(IV) hydroxide/oxide core, *Inorganic Chemistry*, **51**, 4239-4249 (2012).
- [16] J. Chaboy and S. Díaz-Moreno, Ab initio X-ray absorption spectroscopy study of the solvation structure of Th(IV), U(IV), and Np(IV) in aqueous solution, *The Journal of Physical Chemistry A*, **115**, 2345-2349 (2011).
- [17] M. R. Antonio, L. Soderholm, C. W. Williams, J. P. Blaudeau and B. E. Bursten, Neptunium redox speciation, *Radiochimica Acta*, **89**, 17-25 (2001).
- [18] A. Ikeda-Ohno, C. Hennig, S. Tsushima, A. C. Scheinost, G. Bernhard and T. Yaita, Speciation and structural study of U(IV) and -(VI) in perchloric and nitric acid solutions, *Inorganic Chemistry*, **48**, 7201-7210 (2009).
- [19] S. D. Conradson, I. Almahamid, D. L. Clark, N. J. Hess, E. A. Hudson, M. P. Neu, P. D. Palmer, W. H. Runde and C. D. Tait, Oxidation state determination of plutonium aquo ions using X-ray absorption spectroscopy, *Polyhedron*, **17**, 599-602 (1998).
- [20] D. L. Clark, The chemical complexities of plutonium, *Los Alamos Science*, **26**, 364-381 (2000).
- [21] J. J. Katz, G. T. Seaborg and L. R. Morss, Summary and comparative aspects of the actinide elements, *The chemistry of the actinide elements*, 2nd ed., New York, Springer, (1986).
- [22] G. R. Choppin, Solution chemistry of the actinides, *Radiochimica Acta*, **32**, 43-53 (1983).
- [23] R. J. Lemire, J. Fuger, H. Nitsche, P. Potter, M. H. Rand, J. Rydberg, K. Spahiu, J. C. Sullivan, W. J. Ullman, P. Vitorge and H. Wanner, Chemical Thermodynamics of Neptunium and Plutonium, vol. 4, Amsterdam: Elsevier, (2001).
- [24] R. Guillaumont, T. Fanghänel, J. Fuger, I. Grenthe, V. Neck, D. A. Palmer and M. H. Rand, Update on the chemical thermodynamics of Uranium, Neptunium, Plutonium, Americium and Technetium, vol. 5, Amsterdam: Elsevier Science, (2003).
- [25] M. Rand, J. Fuger, I. Grenthe, V. Neck and D. Rai, Chemical

- Thermodynamics of Thorium, vol. 11, Paris: OECD/NEA, (2008).
- [26] A. B. Kersting, Plutonium Transport in the Environment, *Inorganic Chemistry*, **52**, 3533-3546 (2013).
- [27] W. Hummel, U. Berner, E. Curti, F. J. Pearson and T. Thoenen, Nagra/PSI Chemical thermodynamic data base 01/01, *Radiochimica Acta*, **90**, 805-813 (2002).
- [28] I. Grenthe, X. Gaona, L. Rao, V. Plyasunov, W. H. Runde, B. Grambow, R. J. M. Konings, A. L. Smith and E. E. Moore, Second update on the chemical thermodynamics of uranium, neptunium, plutonium, americium and technetium. Chemical Thermodynamics, vol. 14, Paris: OECD/NEA (2021).
- [29] M. Caceci and G. R. Choppin, The determination of the first hydrolysis constant of Eu(III) and Am(III), *Radiochimica Acta*, **33**, 101-104 (1983).
- [30] H. R. Cho, Y. S. Youn, E. C. Jung and W. Cha, Hydrolysis of trivalent plutonium and solubility of Pu(OH)₃(am) under electrolytic reducing conditions, *Dalton Transactions*, **45**, 19449-19457 (2016).
- [31] B. Drobot, A. Bauer, R. Steudtner, S. Tsushima, F. Bok, M. Patzschke, J. Raff and V. Brendler, Speciation studies of metals in trace concentrations: the mononuclear uranyl(VI) hydroxo complexes, *Analytical Chemistry*, **88**, 3548–3555, (2016).
- [32] H. R. Cho, E. C. Jung, K. K. Park, W. H. Kim, K. Song and J. I. Yun, Spectroscopic study on the mononuclear hydrolysis species of Pu(VI) under oxidation conditions, *Radiochimica Acta*, **98**, 765-770 (2010).
- [33] R. G. Pearson, Chemical Hardness, Weinheim: Wiley-VCH, (1997).
- [34] D. A. Atwood, Radionuclides in the Environment, Chichester: John Wiley & Sons, (2013).
- [35] M. A. Denecke, N. Bryan, S. Kalmykov, K. Morris and F. Quinto, Sources and behavior of actinide elements in the environment, *Experimental and theoretical approaches to actinide chemistry*, John Wiley & Sons Ltd, 378-444, (2018).
- [36] K. Maher, J. Bargar and G. E. Brown Jr., Environmental speciation of actinides, *Inorganic Chemistry*, **52**, 3510–3532 (2013).
- [37] G. R. Choppin, Actinide speciation in the environment, *Journal of Radioanalytical and Nuclear Chemistry*, **273**, 695–703 (2007).
- [38] G. Bernhard, G. Geipel, V. Brendler and H. Nitsche, Speciation of uranium in seepage waters of a mine tailing pile studied by Time-Resolved Laser-Induced Fluorescence Spectroscopy, *Radiochimica Acta*, **74**, 87-91 (1996).

- [39] O. Prat, T. Vercouter, E. Ansoborlo, P. Fichet, P. Perret, P. Kurttio and L. Salonen, Uranium speciation in drinking water from drilled wells in southern Finland and its potential links to health effects, *Environmental science & Technology*, **43**, 3941-3946 (2009).
- [40] M. Maloubier, P. L. Solari, P. Moisy, M. Monfort, C. Den Auwer and C. Moulin, XAS and TRLIF spectroscopy of uranium and neptunium in seawater, **44**, 5417-5427 (2015).
- [41] A. B. Kersting, D. W. Efurud, D. L. Finnegan, D. J. Rokop, D. K. Smith and J. L. Thompson, Migration of plutonium in ground water at the Nevada Test Site, *Nature*, **397**, 56-59 (1999).
- [42] P. H. Santschi, K. A. Roberts and L. D. Guo, Organic nature of colloidal actinides transported in surface water environments, *Environmental Science and Technology*, **36**, 3711-3719 (2002).
- [43] A. P. Novikov, S. N. Kalmykov, S. Utsunomiya, R. C. Erwing, F. Horreard, A. Merkulov and B. F. Myasoedov, Colloid transport of plutonium in the far-field of the Malak production association, *Russia Science*, **314**, 638-641 (2006).
- [44] A. I. Abdel-Fattah, D. X. Zhou, H. Boukhalfa, S. Tarimala, S. D. Ware and A. A. Keller, Dispersion stability and electrokinetic properties of intrinsic plutonium colloids: implications for subsurface transport, *Environmental Science and Technology*, **47**, 5626-5634 (2013).
- [45] M. P. Bernardo, G. G. F. Guimarães, V. F. Majaron and C. Ribeiro, Controlled release of phosphate from layered double hydroxide structures: dynamics in soil and application as smart fertilizer, *ACS Sustainable Chemistry and Engineering*, **6**, 5152-5561 (2018).
- [46] S. Gabriel, A. Baschwitz, G. Mathonnière, T. Eleouet and F. Fizaine, A critical assessment of global uranium resources, including uranium in phosphate rocks, and the possible impact of uranium shortages on nuclear power fleets, *Annals of Nuclear Energy*, **58**, 213-220 (2013).
- [47] E. Valsami-Jones, Phosphates *Encyclopedia of Geology (Second Edition)*, **2**, 422-427 (2021).
- [48] C. Gausse, S. Szenknect, D. W. Qin, A. Mesbah, N. Clavier, S. Neumeier, D. Bosbach and N. Dacheux, Determination of the solubility of rhabdophanes $\text{LnPO}_4 \cdot 0.667\text{H}_2\text{O}$ (Ln=La to Dy), *European Journal of Inorganic Chemistry*, **28**, 4615-4630 (2016).
- [49] A. Shelyug, A. Mesbah, S. Szenknect, N. Clavier, N. Dacheux and A. Navrotsky, Thermodynamics and stability of rhabdophanes, hydrated rare earth phosphates $\text{REPO}_4 \cdot n\text{H}_2\text{O}$, *Frontiers in Chemistry*, **6**, 1-11 (2018).
- [50] F. Cretaz, S. Szenknect, N. Clavier, P. Vitorge, A. Mesbah, M. Descostes, C. Poinsot and N. Dacheux, Solubility properties of synthetic and natural meta-

- torbernite *Journal of Nuclear Materials*, **442**, 195–207 (2013).
- [51] R. G. Menzel, Uranium, radium, and thorium content in phosphate rocks and their possible radiation hazard, *Journal of Agricultural and Food Chemistry*, **16**, 231-234 (1968).
- [52] K. Singh-Patel, S. Sharma, J. Prakash-Maitty, P. Martín-Ramos, Z. Fiket, P. Bhattacharya and Y. Zhu, Occurrence of uranium, thorium and rare earth elements in the environment: A review, *Frontiers in Environmental Science*, **10**, 1-18 (2023).
- [53] B. O. Ferguson, L. C. Murdoch, M. Trumm, F. Liu, A. M. Rao and B. A. Powell, Mechanisms and kinetics of citrate-promoted dissolution of a uranyl phosphate mineral, *Geochimica et Cosmochimica Acta*, **318**, 247-262 (2022)
- [54] D. A. C. Manning, Phosphate minerals, environmental pollution, and sustainable agriculture, *Elements*, **4**, 105-108 (2008).
- [55] P. M. Rutherford, M. J. Dudas and R. A. Samek, Environmental impacts of phosphogypsum, *The Science of the Total Environment*, **149**, 1-38 (1994).
- [56] H. Tayibi, M. Choura, R. A. López, F. J. Alguacil and A. López-Delgado, Environmental impact and management of phosphogypsum, *Journal of Environmental Management*, **90**, 2377-2386 (2009).
- [57] S. V. Dorozhkin, Fundamentals of the wet-process phosphoric acid production. 2. Kinetics and mechanism of $\text{CaSO}_4 \cdot 0.5\text{H}_2\text{O}$ surface crystallization and coating formation, *Industrial and Engineering Chemistry Research*, **36**, 467-473 (1997).
- [58] S. Kundu, M. V. Coumar, S. Rajendiran, A. Rao and S. Rao, Phosphates from detergents and eutrophication of surface water ecosystem in India, *Current Science*, **108**, 1320-1325 (2015).
- [59] D. L. Correll, The role of phosphorous in the eutrophication of receiving waters: A review, *Journal of Environmental Quality*, **27**, 261-266 (2009).
- [60] K. George, A. J. Masters, F. R. Livens, M. J. Sarsfield, R. J. Taylor and C. A. Sharrad, A review of technetium and zirconium extraction into tributyl phosphate in the PUREX process, *Hydrometallurgy*, **211**, 105892 (2022).
- [61] R. R. Shoun and M. C. Thompson, Chapter 5: Synthesis, properties and reactions, *Science and Technology of Tributyl Phosphate*, United States, CRC Press, 137-151 (1984).
- [62] W. Davis Jr., Chapter 7: Radiolytic behaviour, *Science and Technology of Tributyl Phosphate*, United States, CRC Press, 221-239 (1984).
- [63] B. A. Powell, J. D. Navratil, D. Thompson and C. Major, Compounds of hexavalent uranium and dibutylphosphate in nitric acid systems, *Solvent*

- Extraction and Ion Exchange*, **21**, 347-368 (2003).
- [64] A. G. Badwin, M. J. Servis, Y. Yang, N. J. Bridges, D. T. Wu and J. C. Shafer, The structure of tributyl phosphate solutions: Nitric acid, uranium (VI), and zirconium (IV), *Journal of Molecular Liquids*, **246**, 225-235 (2017).
- [65] S. Neumeier, Y. Arinicheva, Y. Ji, J. M. Heuser, P. M. Kowalski, P. Kegler, H. Schlenz, D. Bosbach and G. Deissmann, New insights into phosphate based materials for the immobilisation of actinides, *Radiochimica acta*, **105**, 961-984 (2017).
- [66] Y. Arinicheva, K. Popa, A. Scheinost, A. Rossberg, O. Dieste-Blanco, P. Raison, A. Cambriani, J. Somers, D. Bosbach and S. Neumaier, Structural investigations of (La, Pu)PO₄ monazite solid solutions: XRD and XAFS study, *Journal of Nuclear Materials*, **493**, 404-411 (2017).
- [67] D. Bregiroux, O. Terra, F. Audubert, N. Dacheux, V. Serin, R. Podor and D. Bernache-Assolant, Solid-state: Synthesis of Monazite-type compounds containing tetravalent elements, *Inorganic Chemistry*, **46**, 10312-10282 (2007).
- [68] N. Dacheux, R. Podor, B. Chassigneux, V. Brandel and M. Genet, Actinides immobilization in new matrices based on solid solutions: Th_{4-x}M_x^{IV}(PO₄)₂P₂O₇ (M^{IV}=²³⁸U, ²³⁹Pu), *Journal of Alloys and Compounds*, **271-273**, 236-239 (1998).
- [69] N. Dacheux, R. Podor, V. Brandel and M. Genet, Investigations of systems ThO₂-MO₂-P₂O₅ (M=U, Ce, Zr, Pu). solid solutions of thorium-uranium (VI) and thorium-plutonium (IV) phosphate-diphosphates, *Journal of Nuclear Materials*, **252**, 179-186 (1998).
- [70] W. W. Rudolph, Raman-spectroscopic measurements of the first dissociation constant of aqueous phosphoric acid solution from 5 to 301°C, *Journal of Solution Chemistry*, **41**, 630-645 (2012).
- [71] K. L. Elmore, J. D. Hatfield, R. L. Dunn and A. D. Jones, Dissociation of phosphoric acid solutions at 25°C, *The Journal of Physical Chemistry*, **69**, 3520-3525 (1965).
- [72] M. Selvaratnam and M. Spiro, Transference numbers of orthophosphoric acid and the limiting equivalent conductance of the H₂PO₄⁻ ion in water at 25°C, *Transaction of the Faraday Society*, **61**, 360-373 (1965).
- [73] C. W. Childs, Equilibriums in dilute aqueous solutions of orthophosphates, *The Journal of Physical Chemistry*, **73**, 2956-2960 (1969).
- [74] J. Baril, J. J. Max and C. Chapados, Titration infrarouge de l'acide phosphorique, *Canadian Journal of Chemistry*, **78**, 490-507 (2000).
- [75] M. Cherif, A. Mgaidi, N. Ammar, G. Vallée and W. Fürst, A new investigation of aqueous orthophosphoric acid speciation using raman

- spectroscopy, *Journal of Solution Chemistry*, **29**, 255-269 (2000).
- [76] A. Dartiguelongue, E. Provost, A. Chagnes, G. Cote and W. Fürst, Experimental determination and modeling of the speciation of uranium (VI) in phosphoric acid medium, *Solvent Extraction and Ion Exchange*, **34**, 241-259 (2016).
- [77] K. S. Pitzer and L. F. Silvester, Thermodynamics of electrolytes. VI. Weak electrolytes including H_3PO_4 , *Journal of Solution Chemistry*, **5**, 269-278 (1976).
- [78] G. Ferroni, Potentiometric studies on association and dissociation equilibria of orthophosphoric acid, in water-KCl 3 M medium at 25°C, *Electrochimica Acta*, **21**, 283-286 (1976).
- [79] F. Rull, A. Del Valle, F. Sobron and S. Veintemillas, Raman study of phosphate dimerization in aqueous KH_2PO_4 solutions using a self-deconvolution method, *Journal of Raman Spectroscopy*, **20**, 625-631 (1989).
- [80] A. D. Pethybridge, J. D. R. Talbot and W. A. House, Precise conductance measurements on dilute aqueous solutions of sodium and potassium hydrogenphosphate and dihydrogenphosphate, *Journal of Solution Chemistry*, **35**, 381-393 (2006).
- [81] P. G. Daniele, A. De Robertis, C. De Stefano, A. Gianguzza and S. Sammartano, Salt effects on the protonation of orthophosphate between 10 and 50°C in aqueous solution. A complex formation model, *Journal of Solution Chemistry*, **20**, 495-515 (1991).
- [82] H. T. Weger and D. Reed, Absorption spectra and speciation of plutonium (VI) with phosphate, United States Department of Energy, **40**, 1-27 (1996).
- [83] H. T. Weger, S. Okajima, J. C. Cunnane and D. T. Reed, Bulk solubility and speciation of plutonium(VI) in phosphate-containing solutions, MRS Online Proceedings Library, **294**, 739-745 (1992).
- [84] D. Rai, Y. Xia, L. Rao, N. J. Hess, A. R. Felmy, D. A. Moore and D. E. McCready, Solubility of $(\text{UO}_2)_3(\text{PO}_4)_2 \cdot 4\text{H}_2\text{O}$ in H^+ - Na^+ - OH^- - H_2PO_4^- - HPO_4^{2-} - PO_4^{3-} - H_2O and its comparison to the analogous PuO_2^{2+} system, *Journal of Solution Chemistry*, **34**, 469-498 (2005).
- [85] D. Rai, D. A. Moore, A. R. Felmy, K. M. Rosso and H. Bolton Jr, PuPO_4 (cr, hyd.) Solubility product and Pu^{3+} complexes with phosphate and ethylenediaminetetraacetic acid, *Journal of Solution Chemistry*, **39**, 778-807 (2010).
- [86] A. Moskvina, Complex formation of the actinides with anions of acids in aqueous solutions, *Soviet Radiochemistry*, **11**, 447-449 (1969).
- [87] G. R. Choppin, Utility of oxidation state analogs in the study of plutonium

- behaviour, *Radiochimica Acta* , **65**, 89-95 (1999).
- [88] R. D. Shannon, Revised effective ionic radii and systematic studies of interatomic distances in halides and chalcogenides, *Acta Crystallographica Section A*, **32**, 751-767 (1976).
- [89] E. Merciny, J. M. Gatez and G. Duyckaerts, Constantes de formation des complexes de stoechiometrie 1:1 et 1:2 ainsi que des complexes mixtes formes entre le plutonium(III) et divers acides amino-polyacetiques, *Analytica Chimica Acta*, **100**, 329-342 (1978).
- [90] G. Tian, L. R. Martin, Z. Zhang and L. Rao, Thermodynamic, spectroscopic, and computational studies of lanthanide complexation with diethylenetriaminepentaacetic acid: temperature effect and coordination modes, *Inorganic Chemistry*, **50**, 3087-3096 (2011).
- [91] G. M. Nair and K. Chander, Stability constants of complexes of plutonium(III) and americium(III) with 5-sulphosalicylic acid, *Journal of the Less Common Metals*, **92**, 29-34 (1983).
- [92] H. Boukhalfa , S. D. Reilly and M. P. Neu, Complexation of Pu(IV) with the natural siderophore desferrioxamine B and the redox properties of Pu(IV)(siderophore) complexes, *Inorganic Chemistry*, **46**, 1018-1026 (2007).
- [93] M. A. Brown, A. Paulenova and A. V. Gelis, Aqueous Complexation of Thorium(IV), Uranium(IV), Neptunium(IV), Plutonium(III/IV), and Cerium(III/IV) with DTPA, *Inorganic Chemistry*, **51**, 7741-7748 (2012).
- [94] NIST, NIST Standard Reference Data, [On line]. Available: <https://webbook.nist.gov/chemistry/>. [Last access: 29 05 2023] (2023).
- [95] H. S. Kim, C. Y. Joung, B. H. Lee, J. Y. Oh, Y. H. Koo and P. Heimgartner, Applicability of CeO₂ as a surrogate for PuO₂ in a MOX fuel development, *Journal of Nuclear Materials*, **378**, 98-104 (2008).
- [96] L. Claparede, N. Clavier, N. Dacheux, A. Mesbah, J. Martinez, S. Szenknect and P. Moisy, Multiparametric dissolution of thorium–cerium dioxide solid solutions, *Inorganic Chemistry*, **50**, 11702-11714 (2011).
- [97] N. Jordan, M. Demnitz, H. Lössch, S. Starke, V. Brendler and N. Huittinen, Complexation of trivalent lanthanides (Eu) and actinides (Cm) with aqueous phosphates at elevated temperatures, *Inorganic Chemistry* , **57**, 7015-7024 (2018).
- [98] N. Huittinen, I. Jessat, F. Réal, V. Vallet, S. Starke, M. Eibl and N. Jordan, Revisiting the complexation of Cm(III) with aqueous phosphates: What can we learn from the complex structures using luminescence spectroscopy and Ab initio simulations, *Inorganic Chemistry*, **60**, 10656-10673 (2021).
- [99] R. J. Silva, G. Bidoglio, M. H. Rand, P. B. Robouch, H. Wanner and I. Puigdomènech, Chemical Thermodynamics of Americium, vol. 2,

Amsterdam: Elsevier (1995).

- [100] N. Huittinen, A. C. Scheinost, Y. Ji, P. M. Kowalski, Y. Arinicheva, A. Wilden, S. Neumeier and T. Stumpf, A spectroscopic and computational study of Cm^{3+} incorporation in lanthanide phosphate rhabdophane ($\text{LnPO}_4 \cdot 0.67\text{H}_2\text{O}$) and Monazite (LnPO_4), *Inorganic Chemistry*, **57**, 6252-6265 (2018).
- [101] H. Moll, V. Brendler and G. Bernhard, Aqueous curium (III) phosphate species characterized by time-resolved laser-induced fluorescence spectroscopy, *Radiochimica Acta*, **99**, 775-782 (2011).
- [102] V. K. Rao, G. R. Mahajan and P. R. Natarajan, Phosphate complexation of americium (III), *Radiochimica Acta*, **40**, 145-149 (1986).
- [103] M. S. Borisov, A. A. Elesin, I. A. Lebedev, V. T. Filimonov and G. N. Yakovlev, Investigation of the complexing of trivalent actinides and lanthanides in phosphoric acid solutions, *Soviet Radiochemistry*, **8**, 40-44 (1966).
- [104] I. A. Lebedev, V. Y. Frenkel, Y. M. Kulyako and B. F. Myasoedov, Investigation of the complex formation of americium (III) and americium (IV) in phosphoric acid solutions, *Soviet Radiochemistry*, **21**, 692-698 (1979).
- [105] X. Liu and R. H. Byrne, Rare earth and yttrium phosphate solubilities in aqueous solution, *Geochimica et Cosmochimica Acta*, **61**, 1625-1633 (1997).
- [106] T. Kimura and G. R. Chappin, Luminescence study on determination of the hydration number of Cm(III), *Journal of Alloys and Compounds*, **2213-214**, 313-317 (1994).
- [107] R. C. Mooney, X-ray diffraction study of cerous phosphate and related crystals. I. Hexagonal modification, *Acta Crystallographica*, **3**, 337-340 (1950).
- [108] A. Mesbah, N. Clavier, E. Elkaim, C. Gausse, I. B. Kacem, S. Szenknect and N. Dacheux, Monoclinic form of the rhabdophane compounds: $\text{REEPO}_4 \cdot 0.667\text{H}_2\text{O}$, *Crystal growth and design*, **14**, 5090-5098 (2014).
- [109] C. Gausse, S. Szenknect, A. Meshbah, N. Clavier, S. Neumeier and N. Dacheux, Dissolution kinetics of monazite LnPO_4 (Ln=La to Gd): a multiparametric study, *Applied Geochemistry*, **93**, 81-93 (2018).
- [110] D. Rai, A. R. Felmy and R. W. Fulton, Solubility and ion activity product of $\text{AmPO}_4 \cdot x\text{H}_2\text{O}$, *Radiochimica Acta*, **56**, 7-14 (1992).
- [111] F. H. Firsching and S. N. Brune, Solubility products of the trivalent rare-earth phosphates, *Journal of Chemical and Engineering Data*, **36**, 93-95 (1991).
- [112] C. F. Baes Jr., A spectrophotometric investigation of uranyl phosphate complex formation in perchloric acid solution, *Journal of Physical Chemistry*,

- 60**, 878-883 (1956).
- [113] B. J. Thamer, Spectrophotometric and solvent-extraction studies of uranyl phosphate complexes, *Journal of the American Chemical Society*, **79**, 4298-4305 (1957).
- [114] Y. Marcus, Anion exchange of metal complexes: The uranyl phosphate system, *2nd United Nations International Conference on the Peaceful Uses of Atomic Energy*, **3**, 465-471 (1958).
- [115] A. Elyahyaoui, S. Bouhlassa, M. Hussonnois, L. Brillard and R. Guillaumont, Complexation de l'uranium hexavalent par l'acide phosphorique concentré, *Journal of the Less Common Metals*, **135**, 147-160 (1987).
- [116] A. Elyahyaoui, S. Bouhlassa, M. Hussonnois, L. Brillard and R. Guillaumont, Complexes de l'uranium hexavalent dans les acides phosphoriques industriels, *Journal of the Less Common Metals*, **99**, 195-206 (1988).
- [117] J. N. Mathur, Complexation and thermodynamics of the uranyl ion with phosphate, *Polyhedron*, **1**, 47-53 (1991).
- [118] A. Dartiguelongue, A. Chagnes, E. Provost, W. Fürst and G. Cote, Modelling of uranium (VI) extraction by D2EHPA/TOPO from phosphoric acid within a wide range of concentrations, *Hydrometallurgy*, **165**, 57-63 (2016).
- [119] V. Brendler, G. Geipel, G. Bernhard and H. Nitsche, Complexation in the system $\text{UO}_2^{2+}/\text{PO}_4^{3-}/\text{OH}^-$ (aq): Potentiometric and spectroscopy investigations at very low ionic strengths, *Radiochimica Acta*, **74**, 75-80 (1996).
- [120] J. M. Schreyer and C. F. Baes Jr, The solubility of uranium(VI) orthophosphates in phosphoric acid solutions, *Journal of the American Chemical Society*, **76**, 354-357 (1954).
- [121] M. Markovic and N. Pavkovic, Solubility and equilibrium constants of uranyl(2+) in phosphate solutions, *Inorganic Chemistry*, **22**, 978-982 (1983).
- [121] A. Sandino and J. Bruno, The solubility of $(\text{UO}_2)_3(\text{PO}_4)_2 \cdot 4\text{H}_2\text{O}(\text{s})$ and the formation of U (VI) phosphate complexes: Their influence in uranium speciation in natural waters, *Geochimica et Cosmochimica Acta*, **56**, 4135-4145 (1992).
- [123] S. Scapolan, E. Ansoborlo, C. Moulin and C. Madic, Investigation by Time-Resolved Laser-Induced Fluorescence and capillary electrophoresis of uranyl-phosphate species: application to blood serum, *Journal of Alloys and Compounds*, **271-273**, 106-111 (1998).
- [124] I. Bonhoure, S. Meca, V. Marti, J. De Pablo and J. L. Cortina, A new Time-Resolved Laser-Induced Fluorescence Spectrometry (TRLFS) data acquisition procedure applied to the uranyl-phosphate system, *Radiochimica Acta*, **95**, 165-172 (2007).

- [125] D. Beltrami, F. Mercier-Bon, G. Cote, H. Mokhtari, B. Courtaud, E. Simoni and A. Chagnes, Investigations of the speciation of uranium (VI) in concentrated phosphoric acid and in synergistic extraction systems by time-resolved laser-induced fluorescence spectroscopy (TRLFS), *Journal of Molecular Liquids*, **190**, 42-49 (2014).
- [126] V. E. Jackson, K. E. Gutowski and D. A. Dixon, Density Functional Theory Study of the complexation of the uranyl dication with anionic phosphate ligands with and without water molecules, *The journal of Physical Chemistry A*, **117**, 8939-8957 (2013).
- [127] J. D. Kubicki, G. P. Halada, P. Jha and B. L. Phillips, Quantum mechanical calculation of aqueous uranium complexes: carbonate, phosphate, organic and biomolecular species, *Chemistry Central Journal*, **3**, 1-29 (2009).
- [128] D. Majumdar and K. Balasubramanian, Theoretical studies on the nature of uranyl-silicate, uranyl-phosphate and uranyl-arsenate interactions in the model $\text{H}_2\text{UO}_2\text{SiO}_4 \cdot 3\text{H}_2\text{O}$, $\text{HUO}_2\text{PO}_4 \cdot 3\text{H}_2\text{O}$, and $\text{HUO}_2\text{AsO}_4 \cdot 3\text{H}_2\text{O}$ molecules, *Chemical Physics Letters*, **397**, 26-33 (2004).
- [129] C. Moulin, P. Decambox, V. Moulin and J. G. Decaillon, Uranium speciation in solution by Time-Resolved Laser-Induced Fluorescence, *Analytical Chemistry*, **67**, 348-353 (1995).
- [130] A. Kirishima, T. Kimura, O. Tochiyama and Z. Yoshida, Speciation study on complex formation of uranium (VI) with phosphate and fluoride at high temperature and pressures by time-resolved laser induced fluorescence spectroscopy, *Radiochimica Acta*, **92**, 889-896 (2004).
- [131] G. Meinrath, Uranium(VI) speciation by spectroscopy, *Journal of Radioanalytical and Nuclear Chemistry*, **224**, 119-126 (1997).
- [132] I. Grenthe, J. Fuger, R. J. M. Konings, R. Lemire, R. Muller, C. Ngunyen-Trungh and H. Wanner, *Chemical Thermodynamics of Uranium*, Amsterdam: Elsevier Science (1992).
- [133] D. Beltrami, G. Cote, H. Mokhtari, B. Courtaud, B. A. Moyer and A. Chagnes, Recovery of uranium from wet phosphoric acid by solvent extraction processes, *Chemical Reviews*, **114**, 12002-12023 (2014).
- [134] A. Locock and P. C. Burns, Crystal structures of three framework alkali metal uranyl phosphate hydrates, *Journal of Solid State Chemistry*, **167**, 226-236 (2002).

Chapter II

Methodology

Chapter II. Methodology

This work is focusing on the establishment of fundamental data about the interaction of plutonium cations with phosphate species in order to improve models for predicting the behavior of plutonium in the environment and industry. Indeed, in the previous chapter, it has been emphasized that thermodynamic data, stability constants as well as solubility products, are scarce. This is due to the low solubility of phosphate compounds whatever the actinide, to the complex redox chemistry of plutonium that can be simultaneously present in solution under several oxidation states. Moreover, in an academic laboratory such as IJCLab, the amount of plutonium that can be handled is limited to 2 mg.

Therefore, this work was initially devoted to the development of protocols with chemical analogues that could subsequently be applied to plutonium studies. Only 2 oxidation states have been considered: +III and +VI. The choice fell on redox stable cations that possess the same charge of plutonium ions: Nd and Eu for Pu(III) and U(VI) for Pu(VI). These analogues have been suggested by Choppin ^[1] because of the strong similarity in their chemical behavior. However, it should be borne in mind that the behavior of lanthanides (Ln^{3+}) is not strictly identical to that of An^{3+} . It is on the basis of their differences that separation processes like TALSPEAK (Trivalent Actinide Lanthanide Separations by Phosphorus reagent Extraction from Aqueous Komplexes) ^[2] have been implemented. Concerning the oxidation state +VI, data available on U(VI) can be used as a first approximation, but direct measurements are obviously preferable ^[1].

The present study has been conducted according to two experimental approaches, bearing in mind that the techniques used must be applicable to plutonium:

i. In homogeneous aqueous phase, the complexation constants of Eu^{3+} and UO_2^{2+} with phosphates are determined as function of temperature using different element concentrations and thus suitable techniques.

In the case of Eu, experiments have been conducted with the element at tracer scale using the radionuclide ^{152}Eu . Liquid-liquid extraction combined with gamma spectrometry has been used. The complexation constants have been deduced from the variations of the partition of Eu between organic and aqueous phase, as function of the

phosphate concentration, at different temperatures but constant ionic strength and acidity.

Concerning U(VI), the study of the complexation was performed by UV- Visible absorption spectrophotometry at the millimolar range, varying electrolyte and temperature. An additional study was conducted using X-Ray absorption spectroscopy (XAS) to get structural information about the U(VI)-phosphate complex of higher stoichiometry.

ii. In heterogeneous phase, solubility measurements have been conducted on Nd-based rhabdophane and PuPO_4 monazite. The rhabdophane, a hydrated rare earth phosphate, has been chosen since this phase plays an important role in the environment. For example, it has been identified in contaminated sediments at Hanford site ^[3]. Rhabdophane is also formed during leaching of phosphate-based ceramics ^[4]. Moreover, Nd-based rhabdophane is easy to synthesize ^[5] and the solubility of rhabdophane $\text{LnPO}_4 \cdot 0.667\text{H}_2\text{O}$ with $\text{Ln}=\text{La}$ to Dy is well known ^[6]. Since the amount of Pu that can be handled in our laboratory is limited, a protocol has been developed in order to combine small amount of solid and detection feasibility. For that purpose, Nd-based rhabdophane has been doped first with 1% stable Eu. In order to check that the incorporation of Eu does not change the structure of Nd-rhabdophane, the solid was characterized by X-ray diffraction (XRD), Thermogravimetric analysis (TGA), Fourier-transform infrared spectroscopy (FTIR) and Scanning Electron Microscopy (SEM). And its dissolution behavior was monitored using ICP OES. Then a Nd-rhabdophane doped with 1% stable Eu and ^{152}Eu was synthesized: the dissolution was conducted with decreasing amount of solid, from 50 mg to less than 2, and monitored using gamma spectrometry.

This protocol was initially developed to be applied to plutonium rhabdophane, the preparation of this compound being conducted at CEA Marcoule by Paul Estevenon and Thomas Dumas. But because of difficulties in maintaining plutonium at the +III oxidation state in rhabdophane, another phase has been prepared: the monazite. Dissolution have been conducted on PuPO_4 and the solubility followed using UV-Vis spectrophotometry and Photon-Electron Rejecting Alpha Liquid Scintillation (PERALS)

The techniques applied, the studied systems and the corresponding experimental conditions used in this work are summarized in **Table II.1**. The principle of the techniques and experimental details are described in the following sections.

Table II.1. Summary of the techniques and studied systems in this work

Objective	Technique	System	Conditions
Complexation constants Enthalpy and entropy variations	UV-Vis absorption spectrophotometry	U(VI)-phosphate	T=20, 30, 40 and 50°C I=1 M HClO ₄ , C _{U(VI)} =5.2×10 ⁻³ M, 0≤[ΣPO ₄]/U(VI)≤20 I=0.1 M HClO ₄ , C _{U(VI)} =7×10 ⁻³ M, 0≤[ΣPO ₄]/U(VI)≤20 I=0.9 M NaClO ₄ / 0.1 M HClO ₄ , C _{U(VI)} =7×10 ⁻³ M, 0≤[ΣPO ₄]/U(VI)≤50 I=0.5 M NaClO ₄ / 0.5 M HClO ₄ , C _{U(VI)} =7.1×10 ⁻³ M, 0≤[ΣPO ₄]/U(VI)≤20
	LLE combined with γ-spectrometry	¹⁵² Eu(III)-phosphate/TTA-Toluene ¹⁵² Eu(III)-phosphate/HDEHP-Toluene	T= 25, 40, 50 and 60 °C I=0.5 M NaClO ₄ -HClO ₄ pC _H = 3.9 T=15, 25, 40*, 50* and 60*°C I= 1 M NaCl-HCl pC _H = 3.1
Structural information	X-Ray absorption spectroscopy	U(VI)-phosphate	C _{U(VI)} = 7×10 ⁻³ M [ΣPO ₄]= 1 M pH 2
Solubility products	ICP-OES	Eu _{0.01} Nd _{0.99} PO ₄ ·nH ₂ O	Dissolution in 0.1 M HCl
	γ-spectrometry PERALS α-spectrometry	Eu _{0.012} Nd _{0.988} PO ₄ ·nH ₂ O with ¹⁵² Eu PuPO ₄	Dissolution in 0.15 M HCl Dissolution in 0.1 M HCl Dissolution HCl+NaH ₂ PO ₄ In presence of NH ₂ OH·HCl
Structural information	SEM, FTIR, XRD, TGA	Eu _x Nd _{1-x} PO ₄ ·nH ₂ O	

*The real temperatures measured by a conventional thermometer in our experimental conditions were 38, 46 and 56°C

II.1. Main analytical techniques

II.1.1. Determination of the free acidity

The pH measurements were carried out by a conventional pH-meter (Seven Multi S47-Mettler Toledo) with a glass electrode combined with a reference Ag/AgCl with a saturated 3 M NaCl solution. The electrode was first calibrated with pH buffer solutions pH=1.679, 4.005, 7.000 and 10.000 at 25° (Hanna instruments) in order to check that it worked properly. Then, the electrode was calibrated in protons concentration (pC_H (-log $[H^+]$)) at ionic strengths used in the present work: 0.5 and 1M NaClO₄ and NaCl. For this calibration, a series of buffer solutions were prepared at proton concentration equal to 0.1, 0.01, 0.003 and 0.001 in NaClO₄ and NaCl by mixing the stock solution of NaClO₄ and HClO₄ at I=0.5 M and NaCl and HCl at I=1 M. The potential was measured for each protons concentration, allowing plotting a calibration line as illustrated in **Figure II.1**. The value of pC_H (-log $[H^+]$) was determined by measuring the potential (ΔE) of the solution according with the calibration line. Adjustments with NaOH or HCl or HClO₄ were performed if required. A tolerance of ± 2 mV around has been chosen for pC_H adjustments.

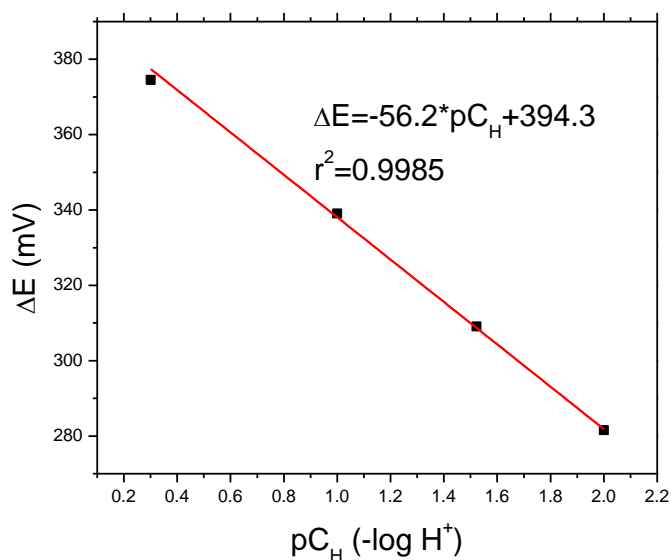


Figure II.1. Calibration curve using 0.5 NaClO₄/0.5 M HClO₄ buffer solutions

II.1.2. Gamma spectrometry

Gamma ray spectrometry is an analytical method that allows the identification and quantification of gamma emitting isotopes in a variety of matrices, based on the determination of both the count rate and the energy of the radiation.

A gamma ray is a penetrating electromagnetic radiation arising from the radioactive decay of atomic nuclei. After a nucleus has emitted a beta particle or an alpha particle, more often it is slightly unstable and in order to get to a stable state it will get rid of its excess energy by emitting a gamma ray immediately afterwards. The energy range for γ -rays emitted by nuclei is 0.1~20 MeV ^[7].

II.1.2.1. Interaction of gamma radiation with matter

There are three fundamental interactions: photo-electric effect, Compton scattering and pair ion production illustrated in **Figure II.2** ^[7].

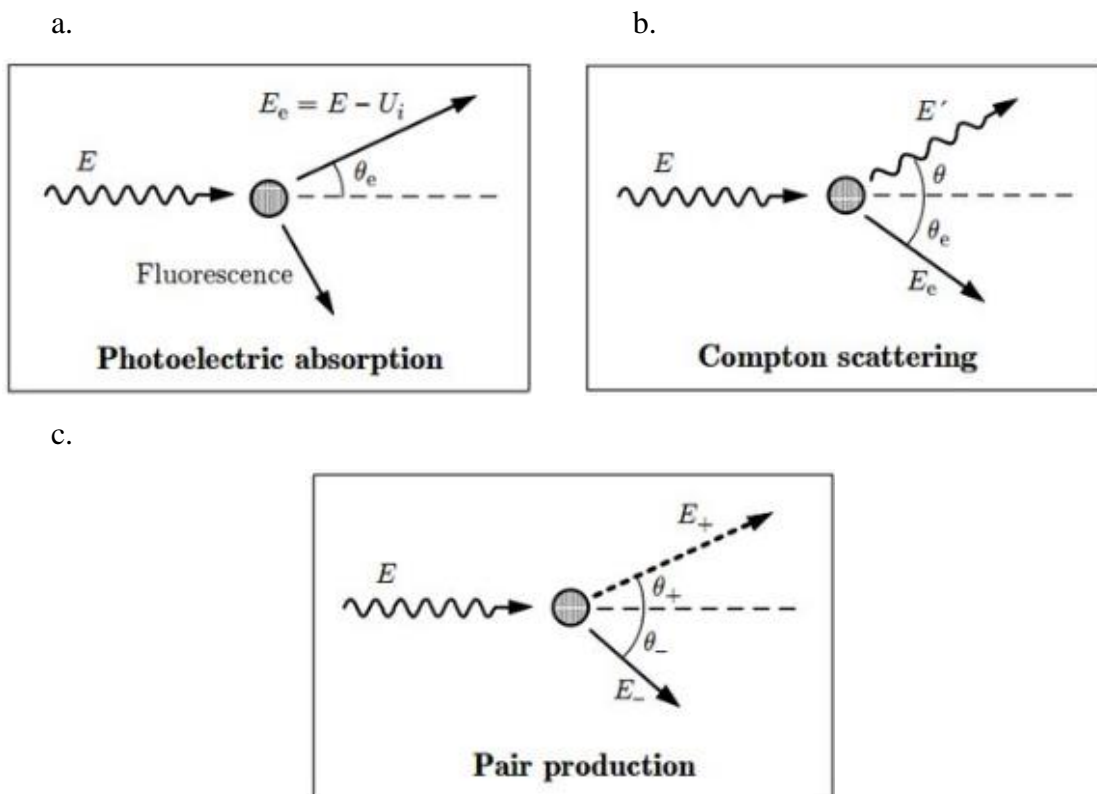


Figure II.2. Interaction of the radiation with the matter ^[8]

In the photoelectric process, the gamma ray interacts with one of the bound electrons and transfers all its energy to it, ejecting it from its shell. It means that electron has the same amount of kinetic energy as the incident gamma-ray, minus the energy needed to

eject it from the shell (so called binding energy). Since the interaction creates a vacancy in one of the electron shells, typically the K or L, an electron moves down to fill in. The drop in energy of the filling electron often produces a characteristic x-ray photon. Assuming an ideal detector, the sum of these energies will equal the energy of the original gamma-ray^[7].

The Compton effect also called Compton scattering, describes the phenomenon of transferring just a part of the gamma-ray energy into the electron, causing its (gamma's) recoil. Evidently, in such a case, the detection of full energy is impossible, as gamma escapes with part of it. The electron that was ejected from the atom produces ionizations in just the same way as a beta particle^[7].

Pair-production occurs when when gamma ray which is passing through the Coulomb field of the nuclei carries the energy equal to at least twice the rest mass of an electron, *i.e.* 1022 keV . The gamma ray is converted into electron and positron. The electron and positron move in different paths away from each other. The positron immediately joins with electron it meets on its way through a process called annihilation. This results in the emission of two new photons, each with equal energy (511keV)^[7].

The photoelectric effect is dominant for low energy photons and high Z materials. Furthermore, pair production is dominant for high energy photons and high Z materials. Also the Compton scattering interaction is dominant for moderate energies^[7].

II.1.2.2. Detection

A typical gamma-ray spectrometry system consists of a detector (for example High-purity Germanium (HPGe) with a lead shielding container to reduce the background interferences, high voltage power supply, electronics for signal processing (preamplifier, amplifier, multichannel analyzer), computer and dedicated software (**Figure II.3**). These gamma rays are detected by the detector, treated by the electronic setup and then observed in the form of a spectrum.

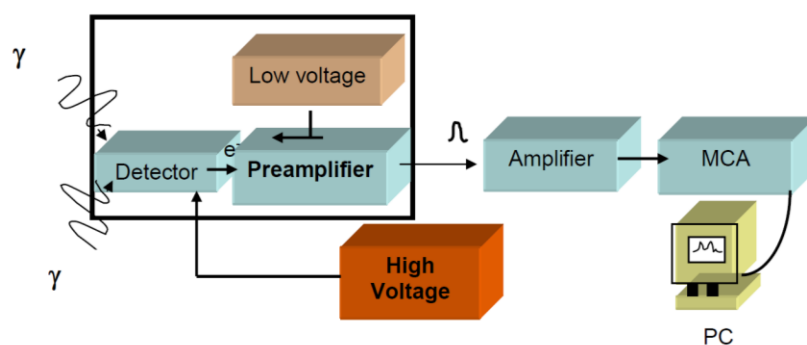


Figure II.3. Basic set-up for γ spectrometry^[7]

The instrument used for ^{152}Eu activity detection was an HPGe 40% from ORTEC connected with High voltage supplier (459, ORTEC) and Amplifier (672, ORTEC) and a multichannel analyzer (ASPEC MCA 927, Ortec, 8192 channels) that is directly connected to the computer. The interface used was Interwinner 8.0 Software from Itech Instruments.

II.1.2.3. Efficiency calibration

The efficiency of the detector depends on the geometry conditions and energy of the gamma ray. In liquid-liquid extraction experiments, the distribution ratio of ^{152}Eu is deduced from the activity measurements of the organic phase and the aqueous phase in strictly identical geometrical conditions (volume, distance sample-detector). The impact of the difference in density of organic and aqueous samples can be neglected. In that case, relative activities and not absolute ones are determined. The use of the detector efficiency is not necessary.

In contrast, solubility experiments involving Nd-based rhabdophane doped with ^{152}Eu , have been performed with different volumes of samples, thus in different geometry. In that case, the use of the detector efficiency is necessary. Thus, the Full Energy Peak efficiency (ϵ^{FEP}) calibration of the HPGe detector has been performed for each volume in the conditions used in solubility experiments.

For that purpose, 10 μL of a standard solution of ^{152}Eu (CERCA-LEA) which characteristics are presented in **Table II.2** have been 10-fold diluted in 0.1 M HCl (all volumes being weighted). This dilution factor allowed gamma measurements in the same geometric arrangement as solubility experiments with a dead time lower than 2 %.

Then, 9 μl of this diluted solution have been taken and used for efficiency calibration. The absolute activity determined from the data in **Table II.2** and the weighed volumes is $A_{\text{ref}}=524\pm 9$ Bq at the date of the measurement using $T_{1/2}$ for ^{152}Eu equal to 13.54 years.

Table II.2. Characteristics of the unsealed standard source of ^{152}Eu (CERCA-LEA)

Specification	Certificated value
Masse	5.091 g
Composition	EuCl_3 10 $\mu\text{g g}^{-1}$ in 1 N HCl
Density	1.02
Specific activity	637.7 kBq g^{-1} on 22/10/2019
Relative uncertainty	± 1.5

The spectrum corresponding to 9 μL aliquot was registered and the efficiency ε^{FEP} (full-energy peak) of the HPGe detector was determined according to equation **II.1** with associated propagation error **II.2** [9]. This efficiency $\varepsilon^{\text{FEP}}(E_\gamma)$ is the ratio of the number of events when the energy E_γ is deposited in the detector to the number of photons of energy E_γ emitted by the source. Where $N(E_\gamma)$ is the number of counts in the full energy peak (or net area), t is the measuring time (in seconds), P_{E_γ} is the photon emission intensity at the energy E , A_{ref} is the radionuclide activity. In our experimental conditions, the decay-correction factor (C_i) can be neglected since the half-life ($T_{1/2}=13.54$ y) of ^{152}Eu is high enough with respect to measurement time.

$$\varepsilon^{\text{FEP}}(E_\gamma) = \frac{N(E_\gamma)}{t * A_{\text{ref}} * P_{E_\gamma}} * C_i \quad \text{II.1}$$

$$\left(\frac{\Delta\varepsilon^{\text{FEP}}(E_\gamma)}{\varepsilon^{\text{FEP}}(E_\gamma)}\right)^2 = \left(\frac{\Delta N(E_\gamma)}{N(E_\gamma)}\right)^2 + \left(\frac{\Delta A_{\text{ref}}}{A_{\text{ref}}}\right)^2 + \left(\frac{\Delta P_{E_\gamma}}{P_{E_\gamma}}\right)^2 \quad \text{II.2}$$

The gamma-ray energies (E_γ) of ^{152}Eu and their associated emission intensity used for calibration are presented in **Table II.3** [10].

Table II.3. Characteristics gamma rays emission of ^{152}Eu isotope

Energy (keV)	Uncertainty $\mu(\text{E})$	Number of photons per 100 decays ($\text{P}_{\text{E}\gamma}$)	Uncertainty $\mu(\text{P}_{\text{E}\gamma})$
121.7817	0.0003	0.2841	1.3×10^{-3}
244.6974	0.0008	0.0755	4.0×10^{-4}
344.2785	0.0012	0.2659	1.2×10^{-3}
443.9650	0.0030	0.0312	2.8×10^{-4}
778.9045	0.0024	0.1297	6.0×10^{-4}
964.0790	0.0180	0.1450	6.0×10^{-4}
1112.076	0.0030	0.1341	6.0×10^{-4}
1408.013	0.0030	0.2085	8.0×10^{-4}

The volume of the initial aliquot of 9 μL was then increased to 45, 90, 250 and 450 μL , by dilution with 0.1 M HCl. These volumes are those used in solubility experiments. For each volume, the efficiency was calculated according to equation II.1 using $A_{\text{ref}} = 524 \pm 9$ Bq. The uncertainty on efficiency mostly comes from the count rate, in other words the net area of peaks ($\mu(\text{N})$). It has been calculated according to equation II.3.

$$\Delta \varepsilon^{FEP} = \frac{\mu(\text{N})}{A_{\text{ref}} * t} \quad \text{II.3}$$

The uncertainty in the net area is provided by the software Interwinner. The counting time has been chosen in order to minimize the statistical error in peak area. Whatever the volume, the minimum value considered for the peak at 444 keV (less intense) was $\text{N} \sim 8000$ that corresponds to 1.1 % uncertainty maxima.

The efficiency of a HPGe detector is known to increase until around 100 keV, then a linear decrease is observed as illustrated schematically in **Figure II.4**. Since the values around the knee of the curve vary in a significant way, the region on both sides of the curvature must be adequately covered to allow reliable fitting ^[11].

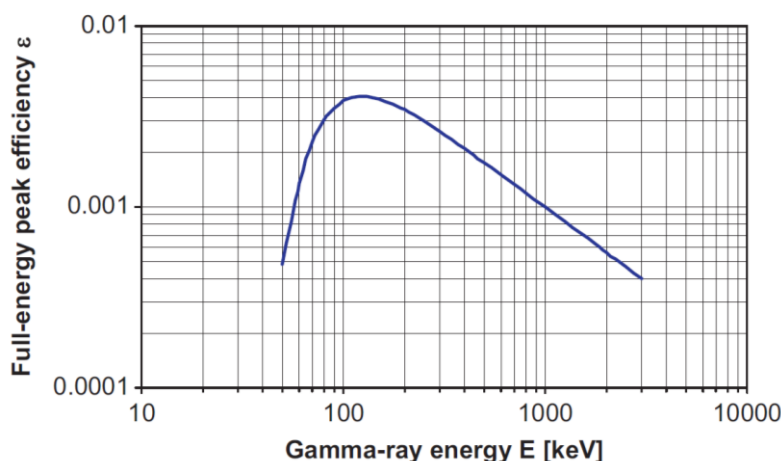


Figure II.4. Characteristic shape of the coaxial germanium detector efficiency curve ^[11].

But the nuclear characteristics of ¹⁵²Eu do not allow efficiency determination at energy lower than 121.8 keV (**Table II.3**). Since only an unsealed standard source of this isotope is available in the laboratory, the efficiency calibration has been performed as following.

A linear fitting of the variations of $\ln(\varepsilon^{\text{FEP}})$ with $\ln(E\gamma)$ has been conducted at energy higher than 200 keV. For each volume, the value at 121.8 keV has been considered separately. Results are presented in **Table II.4**.

Table II.4. Efficiency calibration of HPGe detector and associated uncertainty

Volume (μL)	ε^{FEP} (121.8 keV)	$\mu(\varepsilon^{\text{FEP}})$ (121.8keV)	$\ln \varepsilon^{\text{FEP}}$ (E>150 keV)
9	0.1186	3×10^{-4}	$(-0.7455 \pm 0.0257) \ln E\gamma + (1.6392 \pm 0.1562)$
45	0.1167	3×10^{-4}	$(-0.6867 \pm 0.0529) \ln E\gamma + (1.3015 \pm 0.3238)$
90	0.1138	2×10^{-4}	$(-0.7015 \pm 0.0493) \ln E\gamma + (1.3550 \pm 0.3017)$
250	0.1075	1×10^{-4}	$(-0.7167 \pm 0.0616) \ln E\gamma + (1.3428 \pm 0.3730)$
450	0.1031	2×10^{-4}	$(-0.6973 \pm 0.0393) \ln E\gamma + (1.2015 \pm 0.2404)$

II.1.3. PERALS

PERALS (Photon Electron Rejecting Alpha Liquid Scintillator) is a technique allowing the detection of alpha particles by discriminating beta and gamma emissions associated to that alpha radiation. The process is illustrated in **Figure II.5**. In the scintillation mixture, the α particle transfers its energy to the solvent leading to excitation or

ionization of solvent molecules. Then the energy released by solvent de-excitation is transferred to the scintillator that produces photons (fluorescence). The number of the emitted photon (the counts) is proportional to the concentration of the radionuclide analyzed. ^[12-14].

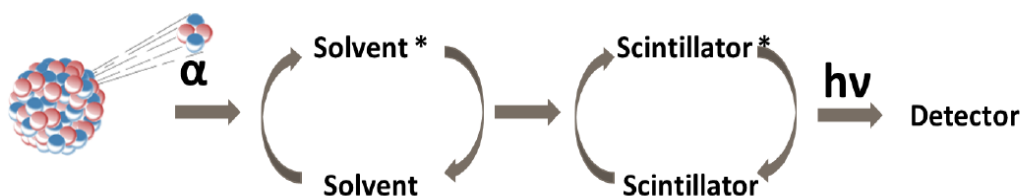


Figure II.5. Energy transfer in a liquid scintillator cocktail ^[15]

In PERALS spectrometry, the scintillator cocktail acts both as scintillator and extractant. In the present work, the cocktail ALPHAEX containing the extractant HDEHP in toluene has been used. It is known that the extraction yield with HDEHP depends on the acidity of the aqueous phase and the oxidation state of the actinide ^[16]. Some extraction yields are reported in **Table II.5**.

Table II.5. Extraction (in %) of actinides with ALPHAEX from nitric acid solutions ^[16]

HNO ₃ concentration (M)	Am ³⁺ and Cm ³⁺	Th ⁴⁺	Pu ⁴⁺	UO ₂ ²⁺
10 ⁻³	99	90	94	97
0.1	0	90	90	97
1	0	90	90	82

In this investigation, we have used PERALS spectrometry to determine the concentration of the U(VI) stock solution and to check plutonium oxidation state.

The liquid-liquid extraction experiments were performed following the methodology proposed by Dacheux *et. al.* ^[16]: 4.8 mL of aqueous phase containing U(VI) or Pu were contacted with 1.2 mL of ALPHAEX.

After strong stirring for 10 minutes, the samples were centrifuged at 3000 rpm. Then 1 mL of ALPHAEX was collected and transferred into culture tube for PERALS counting and each added volume was weighed.

Figure II.6 illustrates the PERALS spectrum corresponding to U(VI) sample. The two peaks correspond to of the isotopes ^{238}U and ^{234}U . The fact that the areas of both peaks are very close indicates that these isotopes are in secular equilibrium: the activity in both isotopes is the same. It is therefore natural uranium. But the low resolution of PERALS spectroscopy causes an overlapping of the peaks and makes difficult the attribution of counts to a specific isotope. Thus, the net area of each peak was obtained by deconvolution of the spectra ^[16].

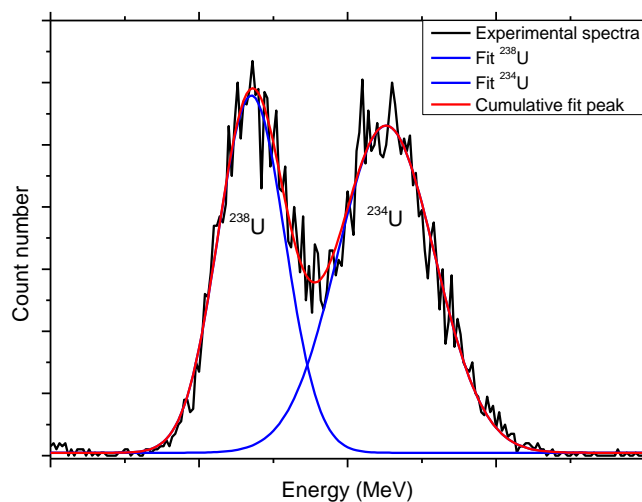


Figure II.6. α -liquid scintillation spectrum of the diluted stock solution of U(VI) used in UV-Vis spectrophotometry experiments

Taking into account the net area of ^{238}U (3240 ± 72 in 3600s), all dilution factors and assuming a % of extraction equal 97%, the concentration of the stock solution was found equal 0.17 ± 0.02 M. PERALS spectra of plutonium will be described in **Chapter III**, part **III.2.3.1**.

II.2. Studies in homogeneous solution

In solution, the concentration ranges for an element with, for instance an atomic mass $Z=100$, can be classified into categories. The macroscale are amounts higher than 100 milligrams (mg) per mL, which corresponds to concentrations 10^{-1} to 10^{-3} M. The microscale is found between $100 \mu\text{g mL}^{-1}$ and 10 ng mL^{-1} being 10^{-4} to 10^{-8} M. The

tracer scale refers to amounts less than 10 picograms (pg) per mL, corresponding to concentrations between 10^{-10} to 10^{-16} M [17, 18].

In aqueous solution, the system can be composed of microcomponent and macrocomponent. For instance, an element (M^+) with a concentration lower than 10^{-8} M will be considered as a microcomponent, whereas a ligand, an oxidizing/reducing or an impurity might be macrocomponents. The macro and microcomponent can interact in three possible pathways as shown in **Figure II.7**. The pathway 1 corresponds to the reaction between microcomponents and refers to sub-tracer scale chemistry. The pathway 2 are the reactions between macrocomponents, which occur in classical chemistry. Then, the pathway 3 are the reactions between a microcomponent and a macrocomponent, which is relevant for tracer scale chemistry. The reactions of interest in radiochemistry between macro and microcomponents can be hydrolysis, complexation, redox process and dissociation reactions. The consumption of the microcomponent is undetectable [17, 18].

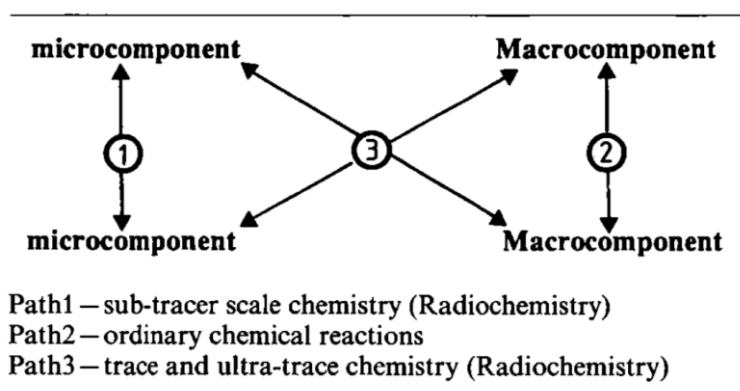


Figure II.7. Reactions pathways between micro- and macrocomponents [18]

In the present work, the complexation of Eu and U with phosphate corresponds to path 3 and path 2, respectively. The general equilibria of complexation of a metal M with a ligand L can be written as **Eq. II.4**, with a constant β defined as **Eq. II.5**.



$$\beta = \frac{[ML_n]}{[M][L]^n} \quad \text{II.5}$$

In practice, the equilibrium constants are determined in various media at different ionic strength. SIT (Specific Interaction Theory) is one of the methods used for activity corrections and extrapolation of the constants to the experimental conditions used.

II.2.1. SIT modelling

The fundamental thermodynamic data in aqueous solution were obtained at constant ionic strength and different media ((Na,H)Cl, HClO₄ or (Na,H)ClO₄). To be able to use the dissociations constants of phosphoric acid whatever the conditions, the constants have been corrected using Specific Ion Interaction Theory (SIT modelling). The impact of the temperature has also been considered.

According to SIT, the equilibrium constant at zero ionic strength is related to the constant at the ionic strength I_m by the Eq. **II.6**.

$$\log_{10} K(T) - \Delta z_i^2 D_H = \log_{10} K^0(T) - \Delta \varepsilon_{ij} I_m \quad \text{II.6}$$

where z_i stands for the charge of the species i , ε_{ij} represents the ion interaction coefficient between ions of opposite charge, I_m the ionic strength in molal units and D_H is the Debye-Hückel term^[19, 20] defined in equation **II.7**. The terms A is $0.509 \text{ kg}^{1/2} \text{ mol}^{-1/2}$ and Ba_j is $1.5 \text{ kg}^{1/2} \text{ mol}^{1/2}$ at $T=25^\circ\text{C}$, as recommended by Grenthe *et. al.*,^[20].

$$D_H = \frac{A\sqrt{I_m}}{1 + Ba_j\sqrt{I_m}} \quad \text{II.7}$$

II.2.1.1. Application of SIT to phosphoric acid dissociation at 25°C

The dissociation constant of phosphoric acid have been extrapolated to $I=1 \text{ M}$ (Na,H)ClO₄, 1 M (Na,H)Cl and 1 M HClO₄ using the standard values listed in **Table I.6** and specific interaction coefficients taken from Puigdomènech *et. al.*,^[21] listed in **Table II.6**.

Table II.6. Ion interaction coefficient (ε_{ij}) in kg mol^{-1} used in this work ($T=25^\circ\text{C}$, $P=1 \text{ bar}$)

Ion interaction coefficient (ε_{ij})	Value kg mol^{-1}
$\varepsilon(\text{H}^+, \text{ClO}_4^-)$	0.14 ± 0.02
$\varepsilon(\text{H}^+, \text{Cl})$	0.12 ± 0.01
$\varepsilon(\text{Na}^+, \text{H}_2\text{PO}_4^-)$	$-(0.08 \pm 0.04)$
$\varepsilon(\text{Na}^+, \text{HPO}_4^{2-})$	$-(0.15 \pm 0.06)$
$\varepsilon(\text{Na}^+, \text{PO}_4^{3-})$	$-(0.25 \pm 0.03)$

Those values as well as Δz^2 , $\Delta \epsilon$ used for the calculations are summarized in **Table II.7**.

Table II.7. Charge of the species and corresponding ion interaction coefficient (ϵ_{ij}) and $\log K_a$ in m (kg mol^{-1}) at $T=25^\circ\text{C}$, $P=1$ bar

Medium	1 M (Na,H)ClO ₄		1 M (Na,H)Cl		1 M HClO ₄		
I	1 M NaClO ₄		1 M NaCl		1 M HClO ₄		
I _m	1.0515 m NaClO ₄		1.0213 m NaCl		1.0508 m HClO ₄		
	Δz^2	$\Delta \epsilon$		$\Delta \epsilon$		$\Delta \epsilon$	
$\log K_{a1}$	2	0.06	-1.792±0.158	0.04	-1.772±0.153	0.14	-1.876±0.205
$\log K_{a2}$	4	0.07	-6.463±0.150	0.05	-6.445±0.163	0.14	-6.536±0.695
$\log K_{a3}$	6	0.04	-11.158±0.167	0.02	-11.143±1.148	0.14	-11.263±1.236

Once the SIT model applied, the equilibrium constants are in molal units (mol kg^{-1}). To convert them in to molar unit, the relation **II.8** is used. Where $\xi = \frac{m_B}{c_B}$, m_B refers to the concentration of the electrolyte in molal units (mol kg^{-1}) and c_B in molar units (mol L^{-1}) and $\sum_B \nu_B$ is the sum of the stoichiometric coefficient of the corresponding reactions.

$$\log_{10} K_m = \log_{10} K_c + \sum_B \nu_B \log_{10} \xi \quad \text{II.8}$$

$$m_B = \frac{c_B}{\rho - c_B M} \quad \text{II.9}$$

The density of electrolytes has been calculated using the parameters reported by Novotny *et al.* [22] as described in **Appendix 1**.

II.2.1.2. Phosphoric acid dissociation as a function of temperature

Depending of the system under investigation the dissociation constants of H₃PO₄ are required from 15°C to 60°C. The value of $\log_{10}K(T)$ at different temperatures can be extrapolated using the Van't Hoff equation (**II.10**), neglecting the variation of $\Delta_r H_m^0$ with the temperature and $\Delta_r C_{p,m}^0=0$. The term $\Delta_r H_m^0$ is the molal standard enthalpy of the corresponding dissociation reaction presented in **Table I.6**. The parameter R is the universal molar gas constant ($8.31451 \text{ J K}^{-1} \text{ mol}^{-1}$) and T is the temperature in Kelvin ($T_0=298.15 \text{ K}$) [20, 21].

$$\log_{10} K^0(T) = \log_{10} K^0(T_0) - \frac{\Delta_r H_m^0(T_0)}{R \ln 10} \left[\frac{1}{T} - \frac{1}{T_0} \right] \quad \text{II.10}$$

Nonetheless, the dissociation constants at different temperatures deduced by equation **II.10** are at zero ionic strength. The SIT method needs to be applied to perform ionic strength corrections depending on our experimental. However, the Debye-Hückel term (D_H) must to be adjusted because the parameters A and I_m have temperature dependence. The variations of the parameter A from 15°C to 50°C were taken from Grenthe *et. al.*^[20], but at 60°C it was deduced by linear regression of A vs T . The A values are presented in **Table II.8**. The empirical parameter B_{aj} is kept constant at $1.5 \text{ kg}^{1/2} \text{ mol}^{-1/2}$ for all temperatures up to 90°C^[19].

Table II.8. Debye- Hückel constants as a function of temperature at a pressure of 1 bar^[20]

Temperature	$A \text{ (Kg mol}^{-1}\text{)}^{1/2}$
10	0.498
15	0.501
20	0.505
25	0.509
30	0.513
40	0.525
50	0.534
60	0.542

The summary of the dissociation constant of H_3PO_4 at $I=1 \text{ M (Na,H)ClO}_4$, 1 M (Na,H)Cl and 1 M HClO_4 and their corresponding variations with the temperature are summarized in **Table II.9** to **Table II.11** in molar units.

Table II.9. Dissociation constants of phosphoric acid at $I=1 \text{ M (Na,H)ClO}_4$ and different temperatures

T (°C)	I= 1 M (Na,H)ClO ₄		
	log ₁₀ K _{a1}	log ₁₀ K _{a2}	log ₁₀ K _{a3}
10	-1.742±0.160	-6.535±0.152	-11.342±0.196
15	-1.767±0.160	-6.518±0.150	-11.287±0.180
20	-1.791±0.160	-6.501±0.150	-11.233±0.170
25	-1.813±0.160	-6.484±0.150	-11.179±0.168
30	-1.835±0.161	-6.468±0.151	-11.127±0.171
40	-1.874±0.162	-6.431±0.153	-10.020±0.192
50	-1.913±0.164	-6.400±0.157	-10.925±0.226
60	-1.947±0.166	-6.365±0.162	-10.827±0.264

Table II.10. Dissociation constants of phosphoric acid at $I= 1\text{ M (Na,H)Cl}$ and different temperatures

I= 1 M (Na,H)Cl			
T (°C)	$\log_{10} K_{a1}$	$\log_{10} K_{a2}$	$\log_{10} K_{a3}$
10	-1.710±0.155	-6.505±0.165	-11.315±0.179
15	-1.735±0.154	-6.488±0.163	-11.260±0.162
20	-1.758±0.154	-6.471±0.163	-11.206±0.151
25	-1.781±0.154	-6.454±0.163	-11.152±0.148
30	-1.803±0.155	-6.437±0.163	-11.100±0.152
40	-1.841±0.156	-6.400±0.165	-10.992±0.175
50	-1.880±0.158	-6.369±0.169	-10.898±0.211
60	-1.914±0.160	-6.335±0.173	-10.800±0.252

Table II.11. Dissociation constants of phosphoric acid at $I=1\text{ M HClO}_4$ and different temperatures

I= 1 M HClO ₄			
T (°C)	$\log_{10} K_{a1}$	$\log_{10} K_{a2}$	$\log_{10} K_{a3}$
10	-1.825±0.201	-6.608±0.772	-11.446±1.707
15	-1.850±0.203	-6.591±0.708	-11.391±1.458
20	-1.874±0.205	-6.575±0.701	-11.338±1.294
25	-1.897±0.208	-6.558±0.698	-11.284±1.238
30	-1.919±0.210	-6.541±0.699	-11.233±1.286
40	-1.959±0.217	-6.505±0.713	-11.126±1.600
50	-1.998±0.226	-6.475±0.741	-11.032±2.049
60	-2.033±0.235	-6.441±0.777	-10.934±2.520

II.2.2. Complexation of Eu at trace scale

II.2.2.1. Liquid-liquid extraction: general points

The liquid-liquid extraction technique is based on the distribution of a metal between two immiscible phases, usually an aqueous solution and an organic solvent which consists in an extractant solubilized in a diluent ^[25, 26]. Solvent extraction is the major hydrometallurgical process used in nuclear industry ^[27] for the reprocessing of nuclear fuel: as examples we can mention the separation of Pu and U in the PUREX process (Plutonium, Uranium, Reduction EXtraction) ^[26], the selective extraction of Cm(III) and Am(III) by DIAMEX-SANEX process (DIAMide Extraction Selective Actinide Extraction) ^[28] or the selective separation of americium by the EXAm process

(EXtraction of Americium) ^[29]. According to the extraction mechanism involved, extractants can be classified into four categories ^[30].

-Simple partition: the separation is based on the difference in solubility of a molecule between organic and aqueous phases.

-Ion-pair formation (anion exchange) between an alkylammonium as the cationic part and an anionic metallic complex. For example, ternary amines and quaternary ammoniums have been used in TRAMEX process in order to carry out the selective extraction of trivalent transplutonium elements over fission products including lanthanides, from concentrated LiCl solutions ^[31].

-Solvation of neutral metal species (metallic ion with its counter ion) by an extractant with donor atoms O, N, S or P whose electron pairs coordinate the metal ion. Tri-n-butyl-phosphate (TPB) is the organophosphorous extractant used in the PUREX process: for example, it extracts the aqua cation U(VI) and Pu(IV) in the form $UO_2(NO_3)_2 \cdot 2TBP$ and $Pu(NO_3)_4 \cdot 2TBP$ respectively ^[32].

-Extraction by compound formation with chelating agent (*e.g.* beta diketone) or acidic organophosphorous compounds (*e.g.* dialkyl phosphoric acid) ^[33]. Formally, these extractants behave as liquid cation exchanger: protons from extractant are released in the aqueous phase during extraction. In TALSPEAK process (Trivalent Actinide Lanthanide Separation with phosphorous-reagent Extraction from Aqueous Komplexes), HDEHP (bis(2-ethylhexyl)phosphoric acid) extracts selectively lanthanides whereas trivalent actinides are retained in aqueous phase in the form of complexes with polyaminopolycarboxylic acid ^[34].

In biphasic system, the partition of a metal M is quantified by the distribution ratio D expressed in equation **II.11**, where C_M and \overline{C}_M refer to the concentration of M^{n+} in the aqueous and organic phase, respectively. In some cases, the distribution ratio can also be expressed as the percentage of extraction, %E, according to equation **II.12** ^[17, 35].

$$D_M = \frac{\overline{C}_M}{C_M} \quad \text{II.11}$$

$$\%E = \left(\frac{D_M}{1 + D_M} \right) \times 100 \quad \text{II.12}$$

In the present work, liquid-liquid extraction is used as a tool for complexation study in aqueous phase, not for separation purpose ^[36] as illustrated in **Figure II.8**. This

technique is based in the distribution of ^{152}Eu between two immiscible phases, where the organic phase is composed of an extractant and the aqueous phase contains the ligand.

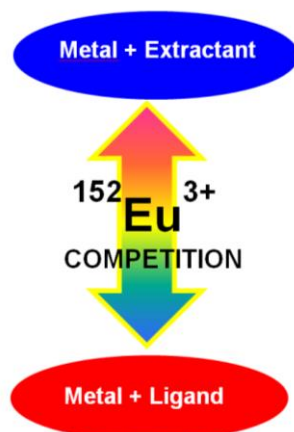


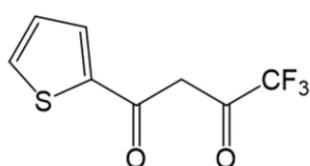
Figure II.8. Competition of ^{152}Eu between two immiscible phases in liquid-liquid extraction experiments

In this work, the experiments have been performed with ^{152}Eu at trace scale, to study the complexation of Eu(III) with phosphates. Two acidic extractants, TTA and HDEHP, that leads to compound formation in organic phase, were used. Some generalities about the extractants used in this investigation are presented below.

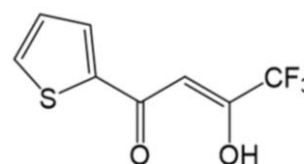
II.2.2.2. Properties of extractant TTA and HDEHP

a. TTA

The chelating agent 2-thenoyltrifluoroacetone (TTA, or sometimes abbreviated as HTTA) is a β -diketone widely used for extraction of metal ion from acidic media in radiochemical separations, that leads to the formation of a neutral chelate in organic phase^[37, 38]. In its β -diketone form (**Figure II.9**), TTA is a solid displaying color from straw-yellow to amber, with molecular weight 222.2 g mol^{-1} . It is also sensitive to light and must be stored in brown bottles^[39, 40]. Depending on the medium, TTA can exist under different forms, β -diketone, enol and keto-hydrate as illustrated in **Figure II.9**^[39, 41].



a. Keto



b. Enol

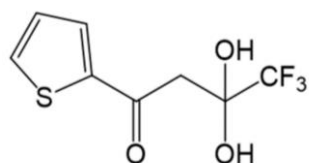
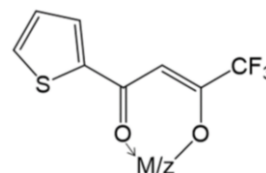
c. *Keto hydrate*d. *Enolate*

Figure II.9. Structural formulas of the chelating agent 2-thenoyltrifluoroacetone (HTTA, M =metal, z =charge of M)^[41]

In inert organic solvents, around 94.6% of the TTA is present in enol form, whereas only 1.6% of this form is present in aqueous solutions. In benzene solutions, the enol form of TTA exhibits a maximum of absorbance at 325 nm with a shoulder at 355 nm. The molar absorption coefficient (ϵ) at 325 nm is around $12000 \text{ M}^{-1} \text{ cm}^{-1}$ [40, 42]. By contrast, keto-hydrate is the predominant form of TTA in aqueous phase. In solid state, it is a white powder with molar weight of 240.2 g mol^{-1} . Its UV-Vis spectrum in slightly acidic aqueous solution presents two absorption bands in the region of 260-270 and 285-295 nm, with molar absorption coefficient equal to 10000 and $8000 \text{ M}^{-1} \text{ cm}^{-1}$ at 267 nm and 292 nm respectively. [40, 42].

In alkaline solutions (buffer at pH 8), enol and keto-hydrated forms of TTA are converted into enolate form. The UV-Vis absorption spectrum of this form exhibits a band at 340 nm, with a molar absorption coefficient of $20000 \text{ M}^{-1} \text{ cm}^{-1}$ at pH=8 [42, 43]. TTA in its enol form, behaves as a weak acid. In the system benzene/1 M NaClO_4 , the recommended value of pKa is 6.2 at 25°C [44], 6.3 with 0.1 M NaClO_4 [36], and 6.38 at zero ionic strength [43].

The extraction of trivalent actinides and lanthanides by TTA occurs according to the equilibrium **II.13** [41, 45]. The formation of the chelate in organic phase is accompanied by the release of 3 protons in aqueous phase. The extracted cation is also coordinated by water molecules: 3 in the case of europium for example [46].



In the presence of ligand in aqueous phase, whatever its concentration, the extracted species is always the same. Moreover, since no aggregation of the extractant occurs in organic phase, TTA is considered to behave ideally [30]. However, at 25°C , the distribution ratio of TTA between benzene or toluene and $\text{NaClO}_4/\text{HClO}_4$ mixtures (I

$\leq 1\text{M}$), lies in the range 30-50, leading to the presence of 2-3 % of TTA in aqueous phase that could interfere with the complexation under study ^[47-49].

In kinetic terms, the rate of conversion of enol to keto-hydrate form in aqueous solution is rapid. By contrast, the transformation of keto-hydrate form into enol form in non-polar solvent such benzene is slower (2 or 3 days) ^[38, 40, 47]. The rate of ketonization (enol \rightarrow keto-hydrate) is about two hundred times higher than of enolization in the aqueous phase. It is the opposite in the organic phase: the rate of enolization (keto-hydrate \rightarrow enol) is about one hundred times higher than that of ketonization. This reaction is the rate limiting step in our experimental conditions, where the extractant is introduced in organic phase as keto-hydrate form ^[47, 50].

b. HDEHP

HDEHP (bis(2-ethylhexyl)phosphoric acid) is an organophosphorus compound that tends to form dimer through hydrogen bonds in most organic solvents, leading to the formation of eight-membered ring (**Figure II.10**) ^[51, 52].

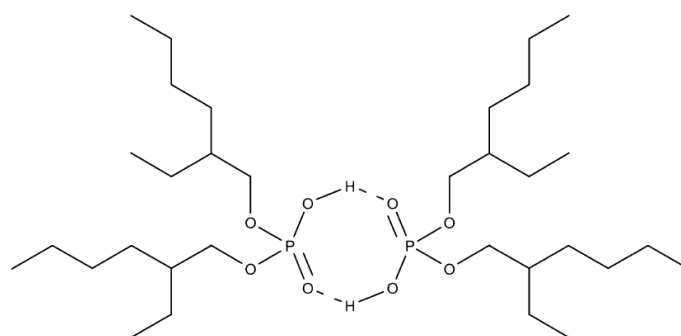


Figure II.10. Structural formula of dimer Bis(2-ethylhexyl)phosphoric acid (HDEHP) ^[53]

The acid dissociation constants of HDEHP are reported as $\text{pK}_a=1.4$ in **Table II.12** ^[54]. However, data obtained by partition experiments reveal that, depending on the organic diluent used and the composition of the aqueous phase, pK_a values can differ as shown in **Table II.12** ^[55]. A large difference exists between chloroform and toluene, but for n-hexane, isooctane, n-octane and chloroform, the difference between pK_a values is relative small.

Table II.12. Acid dissociation constants of HDEHP in different organic diluent and aqueous phases ^[55].

Aqueous phase	T (°C)	Diluent	pKa
0.1 M (H ⁺ ,Na ⁺)Cl ⁻	30	Kerosene	1.70
0.1 M (H ⁺ ,Na ⁺)ClO ₄ ⁻	25	Toluene	0.47
0.1 M (H ⁺ ,Na ⁺)ClO ₄ ⁻	20	<i>n</i> -hexane	1.30
		isooctane	
		<i>n</i> -octane	
		chloroform	
0.1 M (H,Na)NO ₃ ⁻	25	<i>n</i> -heptane	1.49
0.50 M (H,Na)SO ₄ ²⁻	25	Kerosene	1.27±0.03

The extraction with HDEHP is carried out by exchanging the proton of the extractant (the proton is transfer to the aqueous phase) with a metal cation which passes from aqueous phase to organic phase. The distribution of the metal cation between the aqueous phase and the organic diluent depends on the pH ^[56]. The HDEHP has been widely used in the reprocessing of the nuclear spent fuel. It is used in the TALSPEAK process ^[34] and in the DIAMEX-SANEX process, to separate actinides (III) from lanthanides (III), from a weakly acid aqueous phase containing an actinide (III) selective complexing agent ^[57]. The extraction of Ln³⁺ and An³⁺ by HDEHP can be described as **II.14** ^[58, 59].



$$K_{ex} = \frac{[\overline{\text{Ln}((\text{DHEP})(\text{HDEHP}))_3}][\text{H}^+]^3}{[\text{Ln}^{3+}][(\overline{\text{HDEHP}})_2]^3}$$

The kinetic of Ln³⁺ extraction with HDEHP is usually fast ^[37]. Kneißl *et al.* ^[60] demonstrated that the extraction is faster when the speed of the stirring is increased.

In the present work, liquid-liquid extraction experiments have been performed with ¹⁵²Eu at trace scale using TTA and HDEHP as extractant in order to get information about the complexation of Eu(III) with phosphate in aqueous phase. The principles of trace chemistry and of the method of exploiting partition data are outlined in the following paragraph.

II.2.2.3. Rydberg's formalism

The analysis of the variations of the distribution ratio that has been performed, is based on Rydberg's formalism.

According to Rydberg's formalism the species involved in partition and complexation equilibria can be written as $\overline{M(H_pL)_l(HA)_xH_{-N}}$ (neutral extracted chelate) and $M(H_pL)_l(HA)_xH_{-y}^{(N-y)+}$ (complex in aqueous phase). Where M is the metal at the oxidation state N , H_pL the ligand (stands for the neutral form of the ligand, e.g. H_3PO_4) in the aqueous phase and HA the chelating agent (non-dissociated form of HTTA or HDEHP) in the organic phase, l and x are the numbers of the ligand and the chelating molecules per metal atom respectively and y the number of hydroxo groups ($y > 0$) or the number of protons ($y < 0$).

Rydberg's formalism is only valid at constant temperature and ionic strength. The thermodynamic activity of the species is also constant.

Using this formalism, the distribution ratio becomes **II.15** [61]:

$$D = \frac{\sum_l \sum_x \left[\overline{M(H_pL)_l(HA)_xH_{-N}} \right]}{\sum_l \sum_x \sum_y \left[M(H_pL)_l(HA)_xH_{-y} \right]} \quad \text{II.15}$$

Introducing the individual distribution ratio of each species ($P_{l,x,N}$) and their formation constant ($\beta_{l,x,y}$), D can be written as **II.16**, with $\beta_{l,x,y}$ as **II.17** [62].

$$D = \frac{\langle \sum_{l=0} \sum_{x=0} P_{l,x,N} \beta_{l,x,N} [H_pL]^l [HA]^x [H]^N \rangle_{org}}{\sum_{l=0} \sum_{x=0} \sum_{y=0} \beta_{l,x,N} [H_pL]^l [HA]^x [H]^{-y}} \quad \text{II.16}$$

$$\beta_{l,x,y} = \frac{\left[\overline{M(H_pL)_l(HA)_xH_{-y}} \right]}{[M][H_pL]^l [HA]^x [H]^{-y}} \quad \text{II.17}$$

The logarithmic variations of D as a function of ligand, or extractant concentration, or free proton provide information about the mean number of ligands **II.18**, the predominant species in organic and aqueous phase **II.19**, or the mean charge of the predominant complex in aqueous phase **II.20** since the species in organic phase are assumed to be neutral. It is possible to choose experimental conditions in order to have $\langle x_{aq} \rangle = 0$, which means that the proportion of the chelate M - HA in aqueous phase can be neglected. When $\langle l_{org} \rangle = 0$, the chelates extracted in the organic phase are identical

to those extracted in the absence of complexing agent: the extracted species does not contain H_pL ^[61].

$$\frac{\partial \log D}{\partial \log[H_pL]} = \langle l_{org} \rangle - \langle l_{aq} \rangle \quad \text{II.18}$$

$$\frac{\partial \log D}{\partial \log[HA]} = \langle x_{org} \rangle - \langle x_{aq} \rangle \quad \text{II.19}$$

$$\frac{\partial \log D}{\partial \log[H^+]} = -(N - \langle y \rangle) \quad \text{II.20}$$

The species formed differing by only one water molecule cannot be distinguished. For example, the species $M(OH)(H_2PO_4)$ is equivalent to $M(HPO_4)$ species. The technique is limited by the fact that the exact composition of the complexes is unknown. It gives for instance, only access to the difference of mean ligand number between species in organic and aqueous phase as shown in **II.18**.

The determination of the complexation constants $\beta_{l,x,y}$ from partition data will be developed in **Chapter 3**, simultaneously with the presentation of the results on Eu(III) complexation.

II.2.2.4. Experimental conditions

The preparation of the aqueous phase and organic phase is described in **Appendix 2**. Extraction experiments have been performed with equal volumes (1 mL) of organic and aqueous phases, by series of 20 samples.

The electrolyte consists in mixtures of $HClO_4/NaClO_4/NaH_2PO_4$ or $HCl/NaCl/NaH_2PO_4$ at fixed pC_H and ionic strength. As mentioned in **Table II.2**, the ^{152}Eu source contains also 10 $\mu g/g$ $EuCl_3$ with stable isotopes of Eu. For each series, between 10 and 50 μL of the calibrated source of ^{152}Eu are evaporated to dryness and the residue taken up in 1300 μL of $HClO_4$ or HCl at the same acidity as the electrolyte under study. Then 50 μl of this solution are introduced in extraction vials. This leads to a Eu concentration between $1.5 \cdot 10^{-8}$ and $7.4 \cdot 10^{-8}$ M. The organic phase consists in TTA or HDEHP diluted in toluene. In the case of TTA, only the diluent was pre-equilibrated with the aqueous phase during 2 days ^[47]. For HDEHP, the solvent (extractant and diluent) was pre-equilibrated twice during 24 hours ^[63].

Samples were stirred at 50 rpm in a temperature controlled bath (HUBER programmable from -30°C to 150°C). The stirring time for TTA systems was 24 h at 25°C, 15 h at 40, 50 and 60°C^[47]. For HDEHP systems the stirring time was 150 min at 25°C and 120 min at 40, 50 and 60°C displayed by the temperature controlled bath but the real temperature measured by an conventional thermometer was 38, 46 and 56°C, respectively^[60, 63]. A summary of the composition of the samples and on the conditions of extraction are presented in **Table II.13**.

Table II.13. Samples preparation for the complexation study of Eu(III)-phosphate

Systems and objective	Aqueous phase	Organic phase	Contact time and temperature
Eu(III)-phosphate/TTA-toluene Complexation constants	$0 \leq [\Sigma\text{PO}_4] \leq 0.1$ I=0.5 M NaClO ₄ -HClO ₄ pC _H =3.9	0.0025 M TTA in pre-equilibrated toluene	t= 20-24 hours T=25, 40, 50 and 60 °C
Eu(III)-HDEHP Experimental conditions for quantitative extraction	I=0.5 M NaCl-HCl pC _H = 1, 2, 3, 4 and 5	0.0075 M HDEHP diluted in Toluene Twice pre-equilibrated in 0.5 M NaCl-HCl	t= 120-150 min T=25 °C
Eu(III)-phosphate/HDEHP-toluene Complexation constants	$10^{-4} \leq [\Sigma\text{PO}_4] \leq 0.5$ I=1 M NaCl-HCl pC _H =3.1	0.0075 M HDEHP diluted in Toluene Twice pre-equilibrated in 0.5 M NaCl-HCl	t= 120-150 min T=15, 25, 40*, 50* and 60* °C

**The real temperatures measured by a conventional thermometer in our experimental conditions were 38, 46 and 56°C.*

Once the equilibrium was reached, the phases were separated by centrifugation (ALLEGRA 6R-centrifuge, Beckman Coulter) at 3000 rpm during 5 minutes. An aliquot (500 µL) of each phase was then collected in polypropylene tubes and analyzed

by gamma spectrometry. The distribution ratio (D) of ^{152}Eu was determined from the activities measured in each phase at 121.8 keV according to Equation **II.21**. Values of the net peak areas at this energy were in the range 500-20000, for a counting time between 200 s and 2000 s. The associated error of the distribution coefficient was estimated to 10%.

$$D = \frac{A_{org}}{A_{aqu}} \quad \text{II.21}$$

II.2.3. Complexation of U and Eu at millimolar scale

II.2.3.1. Ultraviolet-visible absorption spectrophotometry: principle

UV-Visible absorption spectrophotometry was mainly used to determine the speciation and the stability constants of the U(VI)-phosphate systems.

This technique refers to the absorption of light by matter^[64] in the ultraviolet and visible ranges of the electromagnetic spectrum, meaning from 180 to 750 nm^[65]. This technique is commonly used for chemical speciation and determination of stability constants^[66]. In general, the Beer-Lambert law specifies that the absorbance of a solution is directly proportional to the concentration of the absorbing species in the solution and the path length^[67].

$$A = \varepsilon Cl = -\log T = \log \frac{1}{T} = \log \frac{I_0}{I} \quad \text{II.22}$$

Where A is the measured absorbance, I_0 and I are the intensities of the monochromatic light before and after the sample, respectively, ε is the molar absorption coefficient ($\text{M}^{-1} \text{cm}^{-1}$), C is the concentration (M), l is the path length (1 cm) and T is the transmittance. In the case of a mixture of absorbing species, the total absorbance at a given wavelength is the sum of the absorbance of each individual species according to their proportion in the solution as shown in equation **II.23**.

$$A_{tot}(\lambda) = \sum A_i(\lambda) = \sum \varepsilon_i(\lambda)c_i l \quad \text{II.23}$$

Where ε_i and C_i are the molar absorption coefficient and the concentration of each species, respectively. A_{tot} is the total absorbance of the system.

Most of lanthanides and actinides exhibit characteristic absorption bands in the UV-Vis-NIR region due to f-f transitions^[68]. The formation of a new species due to complexation, should lead to variations of the absorbance at specific wavelengths.

Depending on the optical properties on the investigated system, experimental studies are conducted at fixed metal concentration varying ligand's one, or on the opposite, at fixed ligand concentration varying the metal's one. Both approaches have been used in the present work. And stability constants, β_n , can be deduced from the variation of the total absorbance as a function of ligand or metal concentration according to equations **II.24** to **II.26**.



$$A_{tot}(\lambda) = \varepsilon(\lambda) \times l \times [M] + \sum_n \varepsilon_n(\lambda) \times l \times [ML_n] \quad \text{II.25}$$

$$A_{tot}(\lambda) = C_M \times l \times \varepsilon(\lambda) + \frac{(\sum_n \varepsilon_n(\lambda) \times l \times \beta_n \times [L]^n)}{1 + \sum_n \beta_n [L]} \quad \text{II.26}$$

II.2.3.2. Experimental conditions

The preparation of the stock solution of acids, salts, Eu are described in **Appendix 2**. The experimental conditions and the preparation of the samples used for the study of the complexation of Eu-TTA and U(VI)-phosphate by UV-Vis spectrophotometry are described in the following paragraphs.

- **Complexation of Eu with TTA**

In aqueous phase, the anionic form (TTA⁻) is likely to interact with Eu³⁺ and compete with Eu(III)-phosphate complexation. The possible contribution of Eu(TTA)²⁺ complex should be studied in order to correct the conditional stability constant of Eu(III)-phosphate complexes. However, due to the spectroscopy properties of Eu(III) (low absorbance) and TTA (high absorbance, pH dependency), the complexation was studied following the absorbance variation of the ligand.

Each series were measured with fixed TTA/NaClO₄-CH₃OONa concentration (5×10⁻³ M) and by varying the europium concentration from 0 to 0.02 M. The ionic strength of the samples was fixed at 0.5 M with HClO₄/NaClO₄ solution and pC_H=3.7.

- **Complexation of U(VI) with phosphate**

Because of the low solubility of phosphate compounds and the need to be at the millimolar range to have useful absorption spectra, it was necessary to verify the stability of the U(VI)-phosphates samples first. The stability of U(VI)-phosphate over

time was studied in different media: 1 M HClO₄, 0.1 M HClO₄, 0.9 M NaClO₄/0.1 M HClO₄, and 0.5 M NaClO₄/0.5 M HClO₄. The samples were prepared at fixed uranium concentration equal to 7×10^{-3} M and by varying the ratio $\Sigma\text{PO}_4/\text{U}$ from 0 to 50.

Once the appropriate conditions determined, the complexation was studied in two electrolytes by varying the ratio $\Sigma\text{PO}_4/\text{U}$ from 0 to 20:

- 1 M HClO₄ media at fixed $C_{\text{U(VI)}} = 5.22 \times 10^{-3}$ M.
- 0.5 M NaClO₄/0.5 M HClO₄ media at $C_{\text{U(VI)}} = 7.1 \times 10^{-3}$ M.

Absorption spectra have been registered at 20, 30, 40 and 50°C. Before the measurement, the samples were maintained in a water bath at the corresponding temperature during 20 minutes.

- **Data acquisition**

All the measurements were performed with a UV-2501-PC spectrophotometer (Shimadzu, Deuterium-Tungsten lamp) using a quartz cell with 1 cm path length. The baseline was defined as the electrolyte. The UV-Vis spectra were collected from 200 to 400 nm for Eu(III)-TTA system, and from 350 to 480 nm for U(VI)-phosphate system. The spectra were recorded with a slow speed and 0.05 nm step. The instrument is equipped with a Peltier control temperature chamber to perform the experiments at 25, 40, 50 and 60°C.

The UV-Vis spectra were processed by the HypSpec software ^[69, 70] to determine the stability constants. Depending on the studied system, the input data are the protonation constants of H₃PO₄ (**Table 11.9** and **Table 11.1**) or TTA extrapolated to our experimental conditions. The stability constants of Eu-TTA and U(VI)-phosphate reported in literature have been used to initiate the calculation. The output data are the number of species formed, their associated stability constants and their individual absorption spectrum ^[69, 70].

II.2.3.3. X-ray absorption spectroscopy (XAS)

X-ray absorption spectroscopy (XAS) is a suitable technique used to determine the speciation of elements in different kind of samples such as gas, solutions, amorphous or crystalline solid. This technique can provide information about electronic properties (oxidation state) or local structural information (coordination number, distances, and

species of the atoms surrounding the absorber element) ^[71]. This technique uses synchrotron radiation and is based on photoelectric effect. This is also an element specific technique that can be performed at large concentration range (down to 10^{-5} M).

X-ray absorption spectroscopy works in the x-ray spectral region from 0.25 Å to 25Å. The principle can be explained as an incident x-ray photon absorbed by an atom causing the excitation or ejection of a core electron. The photo-electron ejected can be considered as a wave emitted in all directions, which can be scattered by neighboring atoms, returning to the absorbing atom. Thus, it can alter the density of electrons and affect the absorption coefficient (μ). The principle is summarized in **Figure II.11**. In absence of nearby atoms, the XAS signal is represented in blue. The presence of neighboring atoms can modulate the amplitude of the photo-electron wave-function at the absorbing atom, leading to the absorption spectrum represented in red ^[71].

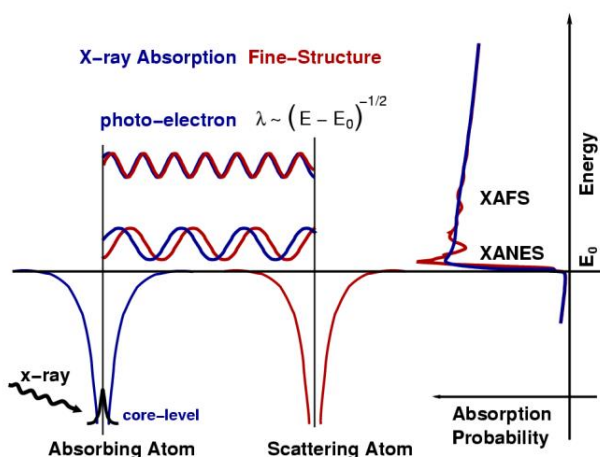


Figure II.11. Principle of EXAFS ^[71]

The electronic and structural information can be deduced from the absorption spectrum in **Figure II.11**. The spectrum can be divided into two parts: the X-ray absorption Near-Edge structure (XANES) and the Extended X-Ray absorption Fine Structure (EXAFS) ^[72]. The XANES allows to mainly determine the oxidation state of the absorbing atom, and the EXAFS oscillations provide information on the local structure around the absorbing atom ^[71].

XAS analysis has been used to study the structure of U(VI)-phosphate complexes in aqueous solution. The sample studied by EXAFS was prepared at 7×10^{-3} M uranium concentration and 1 M phosphoric acid ($\Sigma\text{PO}_4/\text{U} = 142$) and the pH was adjusted to 2.

XAS at the uranium L_{III} edge (17.2 keV) was performed at the SOLEIL synchrotron facility, on the MARS beamline. The beamline is equipped with a Si(220) monochromator. Higher harmonics were rejected by two Pt coated mirrors. The first mirror collimates the x-ray beam onto the monochromator crystal, and the second focuses the beam vertically to the sample. Energy calibrations were conducted at the Y K edge (17 038 eV). The measurement was performed in fluorescence mode using a 13-element high purity germanium detector (ORTEC).

Data processing was carried out using the Athena code ^[73]. The E_0 energy was identified at the maximum of the absorption edge. Fourier transformation was performed in k^2 between 2.667 and 13.299 \AA^{-1} with Hanning windows using the ARTEMIS code ^[73]. The r factor and the quality factor ($\Delta\chi^2$) of the fit were provided from ARTEMIS. Phases and amplitudes were calculated from the FEFF9 simulation code ^[73] using the $UO_2(H_2PO_4)_2(H_2O)_3$ structure predicted by Jackson *et al.* using DFT calculations ^[74]. Three single scattering paths were used during the data adjustment, corresponding to the axial oxygen of the uranyl groups, the equatorial oxygen atoms and the phosphorous. The adjustment includes the four-legged multiple scattering path of the uranyl group, as well as the multiple scattering path of the phosphate groups (U-P-Oeq).

Before analysis, the stability of the sample over time was verified by UV-Vis spectrophotometry.

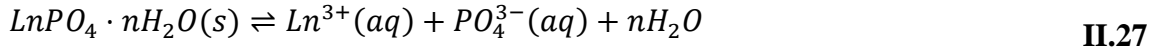
II.3. Studies in heterogeneous systems

Due to the low solubility of phosphate compounds, the determination of thermodynamic data in homogeneous aqueous solution remains delicate. Another approach to collect those data on phosphate systems is to study the solubility of these compounds. For that purpose, rhabdophane and monazite solids ($MPO_4 \cdot nH_2O$ or MPO_4) were synthesized and characterized. These solids were subsequently used for dissolution experiments. The details of the synthesis and the techniques employed are described in the following sections.

II.3.1. Determination of solubility products ($K_{s,0}^0$)

The calculation of the solubility products requires that the steady state is reached ^[75]. In this investigation, the thermodynamic data were determined as described by Gausse *et al.* ^[6].

According to the Nuclear Energy Agency-Thermodynamic Data Base (NEA-TDB), the dissolutions reactions of $\text{LnPO}_4 \cdot n\text{H}_2\text{O}$ can be written using non-complexed aqueous species as presented in **II.27**.

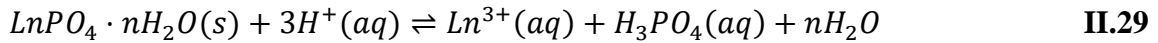


The *standard solubility product* ($K_{s,0}^0$) associated to the reaction **II.27** can be calculated as equation **II.28**. The subscript “0” implies that the equilibrium reaction involves only non-complexed aqueous species, the index “s” indicates that the constant refers to solubility process and “0” implies standard conditions.

$$K_{s,0}^0 = (\text{Ln}^{3+})(\text{PO}_4^{3-})(\text{H}_2\text{O})^n = (\gamma_{\text{Ln}^{3+}}m_{\text{Ln}^{3+}})(\gamma_{\text{PO}_4^{3-}}m_{\text{PO}_4^{3-}})(\text{H}_2\text{O})^n \quad \text{II.28}$$

Where (i) denotes the activity of the ion i , m_i (mol kg^{-1}) is the molality, and γ_i is the activity coefficient of the considered species i . By definition, the water activity at zero ionic strength is 1.

Considering that the dissolution was performed at very low pH, the predominant species in solution are Ln^{3+} ions and H_3PO_4 . Thus, the dissolution reaction of $\text{LnPO}_4 \cdot n\text{H}_2\text{O}$ in acidic medium can be written as equilibrium **II.29**.



In order to reduce systematic errors from ionic strength corrections, the *equilibrium constants* ($*K_s$) for the predominant species was calculated from molalities of the predominant species as shown in equation **II.30**. The asterisk (*) indicated that the solubility constant involves protonation equilibrium.

$$*K_s = \frac{m_{\text{Ln}^{3+}}m_{\text{H}_3\text{PO}_4}}{m_{\text{H}^+}^3} \quad \text{II.30}$$

The molalities (mol.kg^{-1}) and molarities (mol.L^{-1}) of all species were calculated from pH measurements and from the experimental concentrations obtained by gamma spectrometry and ICP-OES (see **Appendix 3** and **Appendix 4**). During the experiment, all volumes (corresponding HCl solution and dissolution uptakes) were weighted, which allowed a direct calculation of the molarity and molality. Thus, the *standard solubility product* ($*K_s^0$) associated to reaction **II.29** may be written as equation **II.31**.

$$*K_s^0 = \frac{(\text{Ln}^{3+})(\text{H}_3\text{PO}_4)(\text{H}_2\text{O})^n}{(\text{H}^+)^3} \quad \text{II.31}$$

To extrapolate the equilibrium constants determined in this work to infinite dilution, activity corrections were performed using the Specific Interaction Theory (SIT). The comparison between $\log_{10} {}^*K_s$ and $\log_{10} {}^*K_s^0$ gives the magnitude of the ionic strength correction through expression **II.32**, obtained by combination of equations **II.30**, **II.31** and **II.6**. The values of the specific ion interaction are in **Table II.6**.

$$\log {}^*K_s = \log {}^*K_s^0 + 6D + [3\varepsilon(H^+, Cl^-) - \varepsilon(Ln^{3+}, Cl^-)]m_{Cl^-} - n \log(H_2O) \quad \text{II.32}$$

The water activity in 0.1 M HCl solution is 0.9966 and it is 0.9914 in 0.25 M HCl solutions ^[18]. In this work, it is assumed that the variation of the ionic strength and associated systematic error can be neglected. Thus, the water activity in 0.1 M solution was used for the calculation of *K_s values for the dissolution experiments. The value of ${}^*K_{s,0}^0$ was deduced from ${}^*K_s^0$ by combining **II.30** with successive phosphoric acid dissociations constants (**Table I.6**) obtaining **II.33** and **II.34** in log units.

$$K_{s,0}^0 = {}^*K_s^0 \times K_{a1}K_{a2}K_{a3} \quad \text{II.33}$$

$$\log_{10} K_{s,0}^0 = \log_{10} {}^*K_s^0 + \log_{10} K_{a1} + \log_{10} K_{a2} + \log_{10} K_{a3} \quad \text{II.34}$$

The molar Gibbs energy of reaction **II.27** was calculated from the standard solubility product with equation **II.34**, where R is the ideal gas constant ($8.314 \text{ J K}^{-1} \text{ mol}^{-1}$), and T the absolute temperature (K). The uncertainty of $K_{s,0}^0$ was estimated by propagating experimental errors associated with pH measurements and elementary concentration at equilibrium.

$$\Delta_r G^0 = -RT \times \ln K_{s,0}^0 \quad \text{II.35}$$

II.3.2. Nd-based rhabdophane

II.3.2.1. Synthesis and characterization

Several studies reported the synthesis of rhabdophane samples via wet chemical process usually at low temperature ($\leq 170^\circ\text{C}$). The synthesis consists on the mixtures of lanthanide salts with an excess of phosphoric acid (between 2-5%) ^[76].

In this work, the synthesis of Nd(III)-based rhabdophane structures ($\text{NdPO}_4 \cdot n\text{H}_2\text{O}$) was carried out according to the methodology proposed by Gause *et al.*, ^[6]. The protocol was slightly modified to get Nd-based rhabdophane doped with 1 % of stable Eu(III) or

with both stable and ^{152}Eu isotope. The preparation of Nd(III) and Eu(III) salt solutions and H_3PO_4 stock solutions are described in **Appendix 2**. Two solids were synthesized by mixing solutions of LnCl_3 (4mmol) at the appropriate concentration with a 5 M H_3PO_4 solutions (4.08 mmol), corresponding to 2% molar excess of phosphate ^[6]. For the typical rhabdophane, the concentration of NdCl_3 is 4mM, while for the solid doped with Eu, both solutions of NdCl_3 at 3.96 mM and EuCl_3 at 0.04 mM were added. These solids are then identified as $\text{NdPO}_4 \cdot n\text{H}_2\text{O}$ and **$\text{Eu}_{0.01}\text{Nd}_{0.99}\text{PO}_4 \cdot n\text{H}_2\text{O}$** . A third solution was prepared with ^{152}Eu isotope by mixing solutions of NdCl_3 (8.16×10^{-4} M), EuCl_3 (8.25×10^{-6} M) with a ^{152}Eu solution (1.30 mL of CERCA LEA source described in **Table II.2** added into a 5 M H_3PO_4 solution. Among this work, it will be referred as **$\text{Eu}_{0.012}\text{Nd}_{0.988}\text{PO}_4 \cdot n\text{H}_2\text{O}$ doped with ^{152}Eu** . The total amount of ^{152}Eu in $\text{Eu}_{0.012}\text{Nd}_{0.988}\text{PO}_4 \cdot n\text{H}_2\text{O}$ doped with ^{152}Eu was determined as described in **Appendix 3** using the efficiency calibration of HPGe detector presented in **II.1.2.3**. A value of 7404 ± 159 Bq per mg of doped rhabdophane was found. This corresponds to an additional amount of stable Eu of 0.12 μg per mg of doped rhabdophane. Thus in the calculation of europium and neodymium concentration in solubility experiment involving rhabdophane doped with ^{152}Eu , the stoichiometry of Eu was considered equal to 0.012.

For all systems, the mixture was stirred into polytetrafluoroethylene (PTFE) containers from Savillex (120 mL) and placed in an oven for 14 days at 90 °C. Then, the precipitate was separated from the solution by centrifugation at 14000 rpm for 5 min. The solid was washed twice with MilliQ water and then once with ethanol. Finally, obtained powders were air dried at room temperature.

In order to check that $\text{Eu}_{0.01}\text{Nd}_{0.99}\text{PO}_4 \cdot n\text{H}_2\text{O}$ has the same structure as typical rhabdophane ($\text{NdPO}_4 \cdot n\text{H}_2\text{O}$), the powders were characterized by FTIR, XRD and TGA.

For the identification of the functional groups of $\text{Eu}_{0.01}\text{Nd}_{0.99}\text{PO}_4 \cdot n\text{H}_2\text{O}$, a powder layer bed was deposited on the surface of a ATR diamond module (single reflection, Miracle10, Shimadzu) and analyzed on an IR affinity 1 spectrometer (Shimadzu) thanks to a DLATGS detector. The infrared spectra were recorded in the range $4000\text{-}700\text{ cm}^{-1}$ (resolution 2 cm^{-1} , 64 scans per spectrum).

To check that $\text{Eu}_{0.01}\text{Nd}_{0.99}\text{PO}_4 \cdot n\text{H}_2\text{O}$ has the same structure as $\text{NdPO}_4 \cdot n\text{H}_2\text{O}$, powder X-Ray diffraction (PXRD) patterns were recorded by using a BRUKER AXS- D8 advance

diffractometer equipped with the LynxEye detector adopting the Bragg-Brentano geometry. All the data were recorded at room temperature using a $\text{CuK}\alpha_{1,2}$ radiation ($\lambda=1.5418 \text{ \AA}$), operating at 40kV and 40 mA, in the $5^\circ < 2\theta < 75^\circ$ range with a step size of $\Delta(2\theta)=0.01^\circ$. The unit cell parameters were refined by the Rietveld method using PROFEX-BGMN program^[77].

In order to determine the degree of hydration of $\text{Eu}_{0.01}\text{Nd}_{0.99}\text{PO}_4 \cdot n\text{H}_2\text{O}$, thermogravimetric analysis was performed in argon on a NETZSCH STA 449 F3 Jupiter. After recording a baseline using an empty alumina crucible, about 15 mg of powder was heated at a rate of $2^\circ\text{K}\cdot\text{min}^{-1}$ from 20°C up to 500°C to follow the dehydration steps.

The morphology and chemical composition of $\text{Eu}_{0.01}\text{Nd}_{0.99}\text{PO}_4 \cdot n\text{H}_2\text{O}$, before and after the dissolution was obtained at the ICSM laboratory with the use of a FEI Quanta 200 electron microscope. The powder for morphological analysis were deposited on a carbon tape and analyzed directly. The acceleration voltage of the electron beam was fixed to 8-10 kV while the pressure in the chamber was under 100 Pa. X-EDS analyzer (BRUKER X Flash 5010 SDD) was used for quantitative chemical analysis, with an acceleration voltage of 15 kV and a chamber pressure below 2×10^{-4} Pa (2 spots were analyzed before dissolution and 4 spots after dissolution).

II.3.2.2. Solubility of Nd-based rhabdophane

The dissolution experiments were carried out in two steps. The first one is the dissolution of $\text{Eu}_{0.01}\text{Nd}_{0.99}\text{PO}_4 \cdot n\text{H}_2\text{O}$ to verify that all components (Nd, Eu and P) are dissolved with the same tendency as typical rhabdophane structures. The second step is to demonstrate that dissolutions reach the equilibrium at the same rate when reducing the amount of solid, without having any impact on the solubility products in order to validate the protocol for further studies with low amount of plutonium compounds. This part was done using $\text{Eu}_{0.012}\text{Nd}_{0.988}\text{PO}_4 \cdot n\text{H}_2\text{O}$ doped with ^{152}Eu .

The dissolution experiments of rhabdophane compounds were performed according to the methodology reported by Gausse *et al.*^[6] and Cretaz *et al.*,^[75].

The dissolutions of $\text{Eu}_{0.01}\text{Nd}_{0.99}\text{PO}_4 \cdot n\text{H}_2\text{O}$ was carried out by contacting 50.2 mg of solid with 50.2 mL of 0.1 M HCl in sealed PTFE-Saville containers. In parallel, dissolutions of $\text{Eu}_{0.012}\text{Nd}_{0.988}\text{PO}_4 \cdot n\text{H}_2\text{O}$ doped with ^{152}Eu were performed by reducing

the amount of mass and volume maintaining the ratio equal to 1. The samples were prepared from 50.1 to 1.8 mg of solid contacting with the corresponding volume (mL) of 0.15 M HCl solutions in suitable size PTFE-Savillex containers.

The containers were shaken in an orbital shaking incubator (IKA KS 4000i control) at 150 rpm at 25°C. The evolution of the dissolution was monitored through regular uptakes of the leachate; each sampling being replaced by the same volume of fresh HCl solution to maintain a constant total volume throughout the experiment. More precisely, an **aliquot A** (corresponding to around 1% of the leachate), was first centrifuged for 5 min at 14000 rpm to eliminate possible particles taken during the sampling. After centrifugation, an **aliquot B** (around 95% of **aliquot A**) was taken for subsequent analysis. During the experiment all volumes were weighted.

Under these conditions, less than 3% of the leachate was renewed to limit any perturbation in the establishment of dissolution process at the solid/liquid interface^[6, 75]. The pH of the solutions was measured, at the beginning of the dissolution and once the steady state was reached, using a conventional pH-meter calibrated with standard pH buffer solutions, as explained in **II.1.1**.

The evolution of the dissolution of $\text{Eu}_{0.01}\text{Nd}_{0.99}\text{PO}_4 \cdot n\text{H}_2\text{O}$ was monitored using Inductively-Coupled Plasma Optical Emission Spectrometry (ICP-OES, Spectro Arcos EOP) at ICSM laboratory. An **aliquot C** (from **aliquot B**) was 5-fold diluted in 1% HNO_3 solutions for the determination of the concentrations of Nd, Eu and P. The instrument was calibrated using certified standard solutions of Nd, Eu and P at 1000 ppm diluted in 1% HNO_3 solution. The selected emission wavelengths, as well as, the calibration curves are presented in **Appendix 4**. In these conditions, the detection limits for Nd and P reach 10^{-8} M, while the detection limit for europium is 10^{-9} M. However, due to the low concentration of Eu compared to Nd and P, uncertainties on Eu concentrations are higher (9×10^{-9} M) compared to Nd and P (2×10^{-8} M).

The dissolution of $\text{Eu}_{0.012}\text{Nd}_{0.988}\text{PO}_4 \cdot n\text{H}_2\text{O}$ with ^{152}Eu was monitored by γ -spectrometry. The calibration of the gamma spectrometer and the calculation of the absolute activities in samples at different volumes (9, 45, 90 and 450 μL) are detailed in **II.1.2.3**.

II.3.3. PuPO₄ monazite

As already mentioned, the aim was initially to prepare the rhabdophane phase and conduct solubility experiments in the same way as for Nd-based rhabdophane.

II.3.3.1. Synthesis and characterization of PuPO₄ monazite

PuPO₄ monazite was synthesized by Paul ESTEVENON and Thomas DUMAS at CEA-Marcoule. First, a solution 0.2 M Pu(III) in 0.2 M HCl was prepared electrochemically. Then, the synthesis was performed by mixing the Pu(III) solution with 5 M H₃PO₄ solution considering 5% molar excess of phosphate. Unfortunately, the powder obtained was a mixture containing both Pu(III) and Pu(IV). In order to obtain a pure Pu(III) solid, the powder was heated at 1100°C under hydrogenated argon flow, leading to the formation of PuPO₄. The final solid was characterized by X-Ray diffraction, UV-Vis spectrophotometry, Fourier Transform infra-red spectroscopy and Raman spectroscopy at CEA-Marcoule.

II.3.3.2. Solubility of PuPO₄ monazite

The dissolution of PuPO₄ monazite was performed by putting in contact 0.9-4 mg of solid in 4 mL of different electrolytes. All electrolytes contain hydroxylamine hydrochloride (NH₂OH·HCl) 4×10⁻³ M to stabilize plutonium at the +III oxidation state and have been de-aerated by bubbling water-saturated Argon during 45 minutes prior to use. The investigated media were 0.1 M HCl, 0.01 M HCl and 5 mixtures HCl/NaH₂PO₄ with pH =2. After orbital stirring for several months at 25°C, the supernatants were withdrawn and centrifuged at 14000 rpm during 10 minutes. Then different analyses have been conducted. UV-Vis absorption spectra have been registered using a Shimadzu 3101 (nuclearized) in order to check the oxidation state of plutonium at 582-602 nm.

Analysis using PERALS spectrometry (Photon Electron Rejecting Alpha Liquid Scintillation) has been performed with the ALPHAEX cocktail at pH 3 (quantitative extraction of An³⁺)^[16]. In both cases, aqueous and organic phase have been deaerated with water and toluene saturated Argon respectively. Extraction has been conducted with 4.8 mL aqueous phase containing 50 µL of supernatant at pH 3 and 1.2 mL ALPHAEX. A strong stirring was performed by hand during 10 min, followed by a centrifugation at 3500 rpm (10 min). One mL of organic phase was then taken off and

transferred to a counting tube for PERALS analysis (Ordela, 8100AB). All volumes have been weighed.

In addition, alpha-spectra have been registered on sources obtained by evaporation of 2 μL of the supernatant using ATHENA instrument (ITECH) and Interwinner software.

Summary

Chapter 2 was devoted to the description of the experimental strategies employed for the determination of stability constants of Pu-phosphate in solution and solubility products of Pu-phosphate compounds. However, due to the difficulties to manipulate plutonium and the limit amount available in academic laboratory, experimental protocols were developed using chemical analogous with similar chemical behavior in the same stable oxidation state. In this work, Eu(III), Nd(III) and U(VI) were used to simulate Pu(III) and Pu(VI), respectively. The experimental methodology employed consisted in two approaches:

The complexation study in homogeneous aqueous phase of Eu(III) and U(VI) with phosphates at different temperatures. For that purpose, the experimental conditions were chosen to ensure the absence of precipitation, but also to be then applied for plutonium. Eu(III)-phosphate complexation was studied by liquid-liquid extraction combined with gamma spectrometry using ^{152}Eu at tracer scale. For U(VI), the study was performed by UV-Visible spectrophotometry at milimolar range. Some structural information about U(VI)-phosphate system were determined by X-Ray absorption spectroscopy (XAS).

The second approach consist in develop a suitable protocol for the study of the solubility of Pu(III)-phosphate compounds limiting the amount of Pu used in the experiments to less than 2 mg. For that purpose, the experimental conditions were establish from a Nd-based rhabdophane doped with 1% of Eu(III). The impact of the amount of solid was monitored by incorporating ^{152}Eu isotope in the solid. To corroborate Eu(III) doping do not change the typical rhabdophane structure, the solid was characterized by XRD, TGA, FTIR and SEM. The evolution of the dissolution was monitored by gamma spectrometry and ICP-OES. This protocol was applied to PuPO_4 monazite system, which was synthetized at CEA-Marcoule, and its dissolution, was followed by UV-Vis spectrophotometry and PERALS.

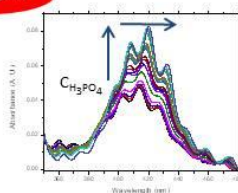
Determination of thermodynamic data

Homogeneous aqueous solution

- ✓ Complexation of $^{152}\text{Eu(III)}\text{-NaH}_2\text{PO}_4 \rightarrow$ Stability constants
- ✓ Complexation of $\text{U(VI)}\text{-H}_3\text{PO}_4$
- ✓ Influence of T → Enthalpy and entropy
- Liquid-liquid extraction at ultra-trace scale ($C_{\text{Eu}} \approx 10^{-8}$ M) monitored with gamma spectrometry



- UV-Vis spectrophotometry at microconcentration ($C_{\text{U(VI)}} \approx 10^{-3}$ M)



Heterogeneous systems (solid/liquid)

- Dissolution with low amount Pu-phosphate to get solubility products
- ✓ Impact of Eu(III) in $\text{NdPO}_4 \cdot 0.667\text{H}_2\text{O}$
 - Synthesis and structural characterization
 - XRD
 - TGA
 - SEM
 - Dissolution monitored by ICP-OES
- ✓ Influence of reducing the amount of solid
 - $\text{Eu}_{0.012}\text{Nd}_{0.988}\text{PO}_4 \cdot 0.667\text{H}_2\text{O}$ doped with $^{152}\text{Eu(III)}$
- ✓ Application to Pu-phosphate solid



Figure II.12. Experimental methodology

References

- [1] G. Choppin, Utility of oxidation state analogs in the study of plutonium behavior, *Radiochimica Acta*, **85**, 89-96 (1999).
- [2] G. Tian, L. R. Martin, Z. Zhang and L. Rao, Thermodynamic, spectroscopic, and computational studies of lanthanide complexation with diethylenetriaminepentaacetic acid: temperature effect and coordination modes, *Inorganic Chemistry*, **50**, 3087-3096 (2011).
- [3] E. C. Buck, D. A. Moore, K. R. Czerwinski, S. D. Conradson, O. N. Batuk and A. R. Felmy, Nature of nano-sized plutonium particles in soils at the Hanford Site, *Radiochimica Acta*, **102**, 1059-1068 (2014).
- [4] E. Du Fou de Kerdaniel, N. Clavier, N. Dacheux, O. Terra and R. Podor, Actinide solubility-controlling phases during the dissolution of phosphate ceramics, *Journal of Nuclear Materials*, **362**, 451-458 (2007).
- [5] N. Dacheux, Personal communication, *ICSM* (2023).
- [6] C. Gausse, S. Szenknect, D. W. Qin, A. Mesbah, N. Clavier, S. Neumeier, D. Bosbach and N. Dacheux, Determination of the solubility of rhabdophanes $\text{LnPO}_4 \cdot 0.667\text{H}_2\text{O}$ (Ln=La to Dy), *European Journal of Inorganic Chemistry*, **28**, 4615-4630 (2016).
- [7] N. Reguigui, Gamma ray spectrometry, *Practical Information*, **1**, 1-79 (2006).
- [8] D. De Paiva-Magalhães, Study and Characterization via monte carlo simulation of ionizing radiation damages in hybrid pixel detectors. Ph.D. Thesis, Campinas: Universidade Estadual de Campinas (2018).
- [9] A. M. El-Khatib, M. S. Badawi and M. A. Elzaher, A study of the validity of the efficiency transfer method to calculate the peak efficiency using γ -ray detectors at extremely large distances, *Journal of Theoretical and Applied Physics*, **8**, 1-9 (2014).
- [10] M. M. Be, V. Chiste, C. Dulieu, E. Browne, V. Chechev, N. Kuzmenko, R. Helmer, A. Nichols, E. Schonfeld and R. Dersch, Table of Radionuclides (Vol.2-A=151 to 242), de *Monographie BIPM-5*, vol. 2, Sévres, Bureau International des Poids et Mesures (2004)
- [11] A. Švec, Analytical efficiency curve for coaxial germanium detectors, *Applied Radiation and Isotopes*, **66**, 786-791 (2008).
- [12] N. N. Mirashi, K. Chander and S. K. Aggarwal, Liquid Scintillation counting techniques for the determination of some alpha emitting actinides. A review, *Radiochemistry and nuclear chemistry*, **33**, 1-30 (2000).
- [13] S. Delpech, C. Cannes, D. Rodrigues, J. F. Le Du and G. Charles, Master I: Nuclear Energy, *Analytical Chemistry of Radiactive Elements* (2021).

- [14] M. L'Annunziata, A. Tarancón, H. Bagán and J. F. García, Chapter 6. Liquid scintillation analysis: principles and practice, *Volume 1: Radiation Physics and Detectors*, **1**, 575-801 (2020).
- [15] A. Reboli, Utilisation de nouveaux détecteurs et de nouvelles molécules scintillantes associées pour la mesure des émetteurs alpha par scintillation liquid alpha. Ph.D.Thesis, Université Paris Sud. Orsay. France (2005).
- [16] N. Dacheux and J. Aupiais, Determination of uranium, thorium, plutonium, americium, and curium ultratraces by photon electron rejecting a liquid scintillation, *Analytical Chemistry*, **69**, 2275-2282 (1997).
- [17] J. P. Adloff and R. Guillaumont, Fundamentals of radiochemistry, USA: CRC Press (1993).
- [18] R. Guillaumont, J. P. Adloff, A. Peneloux and P. Delamoye, Sub-tracer scale behaviour of radionuclides. Application to actinide chemistry, *Radiochimica Acta*, **54**, 1-15 (1991).
- [19] R. J. Silva, G. Bidoglio, M. H. Rand, P. B. Robouch, H. Wanner and I. Puigdomènech, Chemical Thermodynamics of Americium, vol. 2, Amsterdam: Elsevier (1995).
- [20] I. Grenthe, X. Gaona, L. Rao, V. Plyasunov, W. H. Runde, B. Grambow, R. J. M. Konings, A. L. Smith and E. E. Moore, Second update on the chemical thermodynamics of uranium, neptunium, plutonium, americium and technetium. Chemical thermodynamics, vol. 14, Paris: OECD/NEA (2021).
- [21] I. Puigdomènech, J. A. Rard, A. V. Plyasunov and I. Grenthe, TDB-4 Temperature corrections to thermodynamic data and enthalpy calculations, Issy-les-Moulineaux: NEA-OCDE (1999).
- [22] P. Novotný and O. Sönel, Density of binary aqueous solutions of 306 inorganic substances, *Journal of Chemical and Engineering Data*, **33**, 49-55 (1988).
- [23] A. Shelyug, A. Mesbah, S. Szenknect, N. Clavier, N. Dacheux and A. Navrotsky, Thermodynamics and stability of rhabdophanes, hydrated rare earth phosphates REPO₄.nH₂O, *Frontiers in Chemistry*, **6**, 1-11 (2018).
- [24] A. Mesbah, N. Clavier, E. Elkaim, G. Clemence, I. Benkacem, S. Szenknect and N. Dacheux, The monoclinic form of the rhabdophane compounds: REEPO₄.0.667 H₂O, *Crystl Grown Design*, **14**, 5090–5098 (2014).
- [25] J. Starý, The Solvent Extraction of Metal Chelates, New York: Elsevier, (1964).
- [26] L. R. Morss, N. M. Edelstein and J. Fuger, *The chemistry of the actinoid and transactinoid elements*, Netherlands, Springer, 813-1264 (2006)
- [27] C. Madic, M. Lecomte, P. Baron and B. Boullis, Separation of long-lived radionuclides from high active nuclear waste, *Compte Rendu Physique*, **3**, 397-

- 811 (2002).
- [28] P. Baron, M. Lecomte, B. Boullis, N. Simon and D. Warin, Separation of the long lived radionuclides: Current status and future R&D program in France, New Orleans, United States, (2003).
- [29] M. Miguiditchian, V. Vanel, C. Marie, V. Pacary, M. C. Charbonnel, L. Berthon, X. Hérès, M. Montuir, C. Sorel, M. J. Bollesteros, S. Costenoble, C. Rostaing, M. Masson and C. Poinssot, Americium recovery from highly active PUREX raffinate by solvent extraction: The EXAm Process. A review of 10 years of R&D, *Solvent Extraction and Ion Exchange*, **38**, 365-387 (2020).
- [30] Y. Marcus and A. S. Kertes, Ion Exchange and Solvent Extraction of Metal Complexes, New York: Wiley-Interscience, (1969).
- [31] R. E. Leuze, R. D. Baybarz and B. Weaver, Application of amine and phosphonate extractants to transplutonium element production, *Nuclear Science and Engineering*, **17**, 252-258 (1963).
- [32] J. M. Mckibben, Chemistry of the PUREX process, *Radiochimica Acta*, **36**, 3-15 (1984).
- [33] Y. Miyake and Y. Baba, Rate processes in solvent extraction of metal ion, *Mineral Processing and Extractive Metallurgy Review: An International Journal*, **21**, 351-380 (2000).
- [34] K. Nash, The chemistry of TALSPEAK: A review of the science, solvent extraction and ion exchange, *Solvent Extraction and Ion Exchange*, **33**, 1-55 (2015).
- [35] F. Xie, T. A. Zhang, D. Dreisinger and F. Doyle, A critical review on solvent extraction of rare earths from aqueous solutions, *Minerals Engineering*, **56**, 10-28 (2014).
- [36] J. Rydberg, M. Cox, C. Musikas and G. R. Choppin, Principles and Practices of Solvent Extraction, 2 ed., USA: Marcel Dekker, (1992).
- [37] A. S. Kertes, Chapter 2: The chemistry of solvent extraction, *Recent advances in liquid-liquid extraction*, Hungary, Pergamon Press, 15-92 (1971).
- [38] R. A. Tournier and M. W. Davis Jr., Distribution, rate of extraction, and complexing action of thenoyltrifluoroacetone in the synergistic system kerosine/thenoyltrifluoroacetone/tributylphosphate/dilute HNO₃, *Separation Science*, **7**, 159-186 (1972).
- [39] A. M. Poskanzer and B. M. Foreman Jr., A summary of TTA extraction coefficients, *Journal of Inorganic and Nuclear Chemistry*, **16**, 323-336 (1961).
- [40] E. King and W. Reas, The hydration of thenoyltrifluoroacetone in benzene solution, *Journal of the American Chemical Society*, **73**, 1806-1808 (1951).

- [41] M. Attanassova, Thenoyltrifluoroacetone: Preferable molecule for solvent extraction of metals. Ancient Twist to New Approaches, *Separations*, **9**, 1-40 (2022).
- [42] P. J. Elving and P. G. Grodzka, Thenoyltrifluoroacetone: Polarographic and spectrophotometric behavior, and dissociation equilibria. Mechanisms of electrolytic reduction, *Analytical Chemistry*, **33**, 2-11 (1961).
- [43] E. H. Cook and R. W. Taft Jr., Concerning the behavior of aqueous thenoyltrifluoroacetone, *Journal of the American Chemical Society*, **74**, 6103-6104, (1952).
- [44] J. Rydberg, Hydrophilic actinide complexation studied by solvent extraction radiotracer technique, *Mineral Processing and Extractive Metallurgy Review: An International Journal*, **21**, 167-215 (2000).
- [45] V. K. Manchanda and C. Allen Chang, Solvent extraction studies of lanthanum(III) and neodymium(III) with ionizable macrocyclic ligands and thenoyltrifluoroacetone, *Analytical Chemistry*, **58**, 2269-2275 (1986).
- [46] S. Lis, J. N. Mathur and G. R. Choppin, Luminiscence study of Eu(III) complexes extracted in the organic phase, *Solvent Extraction and Ion Exchange*, **9**, 637-647, (1991).
- [47] C. Jaussaud, Contribution a l'étude thermodynamique de l'hydrolyse de Pa(V) a l'échelle des traces par la technique d'extraction liquide-liquide avec la thenoyltrifluoroacetone (TTA). Ph.D Thesis, Orsay, France: Université Paris-Sud. U.F.R. Scientifique d'Orsay (2003).
- [48] T. Wakahayashi, S. Oki and N. Suzuki, Some applications of the regular solution theory to solvent extraction-I. Distribution of β -diketones, *Journal of Inorganic and Nuclear Chemistry*, **26**, 2255-2264 (1964).
- [49] T. Sekine, Y. Hasegawa and N. Ihara, Acid dissociation and two-phase distribution constants of eight β -diketones in several solvent extraction systems, *Journal of Inorganic and Nuclear Chemistry*, **35**, 3968-3970 (1973).
- [50] T. Sekine, A. Hokura and I. Tanaka, Rate and equilibrium of the distribution of 2-thenoyltrifluoroacetone in carbon tetrachloride-aqueous perchlorate solution systems, *Analytical Science*, **12**, 747-753 (1996).
- [51] K. Rama Swami, R. Kumaresan, P. K. Nayak, K. A. Venkatesan and M. Antony, Effect of pK_a on the extraction behavior of Am(III) in organo phosphorus acid and diglycolamide solvent system, *Radiochimica Acta*, **106**, 107-118 (2017).
- [52] D. F. Peppard, J. R. Ferraro and G. W. Mason, Hydrogen bonding in organophosphoric acid, *Journal of Inorganic and Nuclear Chemistry*, **7**, 231-244 (1958).
- [53] P. Tkac, G. F. Vandergrift, G. J. Lumetta and A. L. Gelis, Study of the interaction between HDEHP and CMPO and its effect on the extraction of

- selected lanthanides, *Industrial and Engineering Chemistry Research*, **51**, 10433-10444 (2012).
- [54] R. Kusaka and Watanabe, The structure of a lanthanide complex at an extractant/water interface studied using heterodyne-detected vibrational sum frequency generation *Physical Chemistry Chemical Physics*, **20**, 2809-2813 (2018).
- [55] R. K. Biswas, M. A. Habib and M. N. Islam, Some physicochemical properties of (D2EHPA). 1. Distribution, dimerization, and acid dissociation constants of D2EHPA in a kerosene/0.10 kmol m⁻³ (Na⁺, H⁺)Cl⁻ system and the extraction of Mn(II), *Industrial and Engineering Chemistry Research*, **39**, 155-160 (2000).
- [56] M. D. Williams-Wynn, P. Naidoo and D. Ramjugernath, The distribution coefficients of Y³⁺ and Eu³⁺ between HNO₃ and HDEHP, *Minerals Engineering*, **153**, 106285 (2020).
- [57] J. D. Law, Chapter I. Aqueous reprocessing of used nuclear fuel, *Nuclear fuel reprocessing and waste management*, Virginia, Word Scientific Publising, 1-22 (2019).
- [58] D. F. Peppard, G. W. Mason, J. L. Maier and W. J. Driscoll, Fractional extraction of the lanthanides as their di-alkyl orthophosphates, *Journal of Inorganic and Nuclear Chemistry*, **4**, 334-343 (1957).
- [59] A. T. Kandil and K. Farah, The solvent extraction of terbium and europium by di-(2-ethylhexyl)-phosphoric acid and various organophosphorous compounds, *Journal of Inorganic and Nuclear Chemistry*, **42**, 277-280 (1980).
- [60] F. Kneißl, A. Geist and W. Nitsch, Europium extraction into D2EHPA: Kinetics of mass transfer in a stirred cell, *Solvent Extraction and Ion Exchange*, **17**, 475-493 (1999).
- [61] R. Guillaumont, R. Muxart and G. Bouissieres, Extraction par solvant d'un élément à l'état de chélate, *Bulletin de la Société Chimique de France*, **5**, 1952-1956 (1968).
- [62] S. Leguay, Complexation des actinides (III, IV et V) par des acides organiques. Ph.D Thesis, Orsay, France: Université Paris Sud, (2012).
- [63] M. Aguilar and D. H. Liem, Studies on the solvent extraction of europium (III) by di-(2-ethylhexyl)phosphoric acid (HDEHP) in toluene, *Acta Chemica Scandinavica*, **30**, 313-321 (1976).
- [64] T. Owen, Fundamentals of modern UV-Visible spectroscopy, Germany: Agilent Technologies, (2000).
- [65] M. Tissue, Ultraviolet and Visible Absorption Spectroscopy, *Characterization of Materials*, Virginia, E. N. Kaufmann, 1-13 (2012)

- [66] T. K. Nedeltcheva, A. R. Surleva, L. G. Nikolova, R. G. Borissova and S. I. Georgieva, Spectrophotometric study of competitive complexation equilibria involving overlapped spectral responding species: Determination of the stability constant of bismuth-pyrophosphate complex, *Central European Journal of Chemistry*, **10**, 1875-1881, (2012).
- [67] M. He, Complexation d'actinides et d'analogues par des ligands hydroxamates. Ph.D Thesis, Orsay, France: Université Paris Saclay (2019).
- [68] D. L. Clark, S. S. Hecker, G. D. Jarvinen and M. P. Neu, Plutonium, *The chemistry of the actinide and transactinide elements*, Netherlands, Springer, **2**, 813-1264 (2010)
- [69] P. Gans, A. Sabatini and A. Vacca, Determination of equilibrium constant from spectrophotometric data obtained from solutions of known pH: The program pHab, *Annali di Chimica*, **89**, 45-49 (1999).
- [70] P. Gans, A. Sabatini and A. Vacca, Investigation of equilibria in solution. Determination of equilibrium constants with the HYPERQUAD suite of programs, *Talanta*, **43**, 1739-1753 (1996).
- [71] M. Newville, Fundamentals of XAFS, Chicago: Consortium for Advanced Radiation Sources, (2004).
- [72] F. De Groot, High-Resolution X-ray Emission and X-ray Absorption Spectroscopy, *Chemical Reviews*, **101**, 1779-1808 (2001).
- [73] B. Ravel and M. Newville, ATHENA, ARTEMIS, HEPHAESTUS: data analysis for X-ray absorption spectroscopy using IFEFFIT, *Journal of Synchrotron Radiation*, **12**, 537-541 (2015).
- [74] V. E. Jackson, K. E. Gutowski and D. A. Dixon, Density Functional Theory Study of the complexation of the uranyl dication with anionic phosphate ligands with and without water molecules, *The Journal of Physical Chemistry A*, **117**, 8939-8957 (2013).
- [75] F. Cretaz, S. Szenknect, N. Clavier, P. Vitorge, A. Mesbah, M. Descostes, C. Poinssot and N. Dacheux, Solubility properties of synthetic and natural meta-torbernite *Journal of Nuclear Materials*, **442**, 195-207 (2013).
- [76] C. Gausse, S. Szenknect, A. Mesbah, N. Clavier, S. Neumeier and N. Dacheux, Dissolution kinetics of monazite LnPO_4 (Ln= La to Gd): A multiparametric study, *Applied Geochemistry*, **93**, 81-93 (2018).
- [77] N. Döbelin and R. Kleeberg, Profex: a graphical user interface for the Rietveld refinement program BGMN, *Journal of Applied Crystallography*, **48**, 1573-1580, (2015).

Chapter III

Systems Ln(III)/Pu(III)-phosphate

III. Systems Ln(III)/Pu(III)-phosphate

This chapter presents the results of studies on Eu(III)/Nd(III)/Pu(III)-phosphate systems. The first part is devoted to the study of Eu complexation with phosphate species in aqueous solution, using liquid-liquid extraction combined with γ -spectrometry. The second part focus on the synthesis and solubility of Nd(III)-based rhabdophane compounds. Finally, preliminary results on PuPO₄ are described.

III.1. Complexation of europium (III) with phosphate in aqueous solution

This study, performed using liquid-liquid extraction has involved the use of ¹⁵²Eu. Since this source contains also stable Eu isotopes as mentioned in **Table II.2**, the total concentration of Eu in the samples was in the range 10^{-8} - 7×10^{-8} M. Thus the consumption of macrocomponents in reactions with europium, was considered as negligible. TTA and HDEHP have been used as extractants.

III.1.1. System Eu(III)/NaH₂PO₄/(Na,H)ClO₄/TTA/toluene

The distribution of thenoyltrifluoroacetone between toluene and acidic aqueous solution is characterized by a distribution ratio ranging between 30 and 40 ($C_{TTA}=5$ to 100 mM and $I=0.1$ to 1 M) ^[1]. In aqueous solution the keto-hydrate form of TTA is involved in acidic dissociation equilibrium ($pK_a = 6.2$). The anionic form (TTA⁻) is likely to interact with metallic cations and to compete with the complexation under study. In order to correct the constants of Eu(III)-phosphate complexes from a possible contribution of a Eu(TTA)²⁺, the stability constant of the latter has been determined using UV-Vis spectrophotometry.

III.1.1.1. Complexation of Eu with TTA in aqueous solution

Due do the spectroscopic properties of europium (low absorbance) and TTA (high absorbance, dependence on pH), the study was performed using TTA concentration fixed at 5×10^{-5} M and $C_{Eu(III)}$ varying between 0 and 0.02 M. The pC_H was fixed at 3.7 and $I=0.5$ M HClO₄/NaClO₄. The large excess of Eu concentration favors the formation of only one complex: Eu(TTA)²⁺ ^[2]. **Figure III.1** presents absorption spectra of TTA with increasing Eu concentration. In absence of Eu, two large absorption bands at 266 and 294 nm are observed. These bands can be assigned to the undissociated form of TTA (HTTA keto-hydrate), as mentioned by different authors ^[3-5]. The order of magnitude of the molar extinction coefficient at 266 nm is $8000 \text{ M}^{-1} \text{ cm}^{-1}$ ^[3]. Besides,

the europium absorption spectra presented in **Appendix 5** shows a maximum absorbance at 394 nm and small bands at 267, 298 and 348 nm. The molar extinction coefficient of $\text{Eu}(\text{NO}_3)_3$ at 394 nm is reported as $2.2 \pm 0.2 \text{ M}^{-1} \text{ cm}^{-1}$ [6].

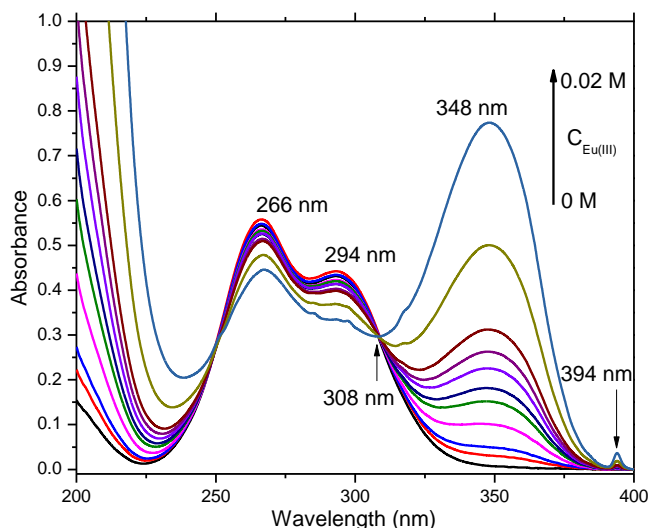
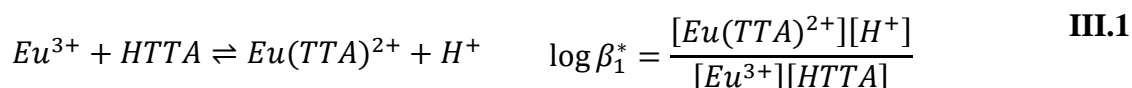
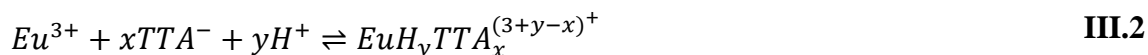


Figure III.1. UV-Vis absorption spectra of $\text{Eu}(\text{III})$ -TTA complex ($C_{\text{HTTA}} = 5 \times 10^{-5} \text{ M}$, $0 \leq C_{\text{Eu}(\text{III})} \leq 0.02 \text{ M}$, $pC_H = 3.7$, $I = 0.5 \text{ M NaClO}_4 / \text{CH}_3\text{OONa}$), 1 cm path length

The addition of europium results in a decrease in absorbance at 266 and 294 nm and in the appearance of a new band with a maximum at 348 nm. This new band is close to the one of the enolate form (340 nm) [4]. Since the absorption of $\text{Eu}(\text{III})$ in this wavelength range is negligible, the presence of the enolate band in slightly acidic medium can be explained by the formation of a complex $\text{Eu}(\text{III})$ -TTA that involves the deprotonation of the keto-hydrate leading to the enolate. The isobestic point at 308 nm indicates that the sum of the absorbances of the components remains unchanged at this wavelength whatever the ratio $\text{Eu}(\text{III})$ -TTA. Assuming that all components involved in the reaction are absorbing species, and according to literature data, the observed spectral variations have been attributed to the equilibrium **III.1** [2, 7, 8].



The experimental absorption spectra in **Figure III.1** have been processed using HypSpec software [9, 10]. The calculation procedure in this software is based on the formal complex formation equilibrium **III.2**. Thus the ligand appears in its deprotonated form.



$$\beta_x = \frac{[EuH_yTTA_x^{(3+y-x)^{+}}]}{[Eu^{3+}][TTA^{-}]^x[H^{+}]^y}$$

The input data were the protonation constant of TTA^{-} ($pK_a = 6.20$), the composition of each sample and their associated spectrum. The output data were the constant of the equilibrium **III.2**.

The stability constant of $Eu(TTA)^{2+}$ in aqueous solution determined in this work is listed in **Table III.1** with the data available in the literature. The value of $Eu(TTA)^{2+}$ complex at $T=25^{\circ}C$ and $I=0.5$ M obtained in this work agrees with $\log \beta_1=4.93\pm 0.04$ reported by Lutoshkin *et al.*,^[7] at the same ionic strength.

*Table III.1. Stability constants for $Eu(TTA)^{2+}$ complex formed in aqueous solution at $T=25^{\circ}C$ (Equilibrium **III.1**)*

Complex	$\log \beta_1$	Ionic strength	Technique	Reference
$Eu(TTA)^{2+}$	4.27 ± 0.10	0.5 M NaClO ₄ / CH ₃ OONa	UV-Vis spectrophotometry	This work
	4.93 ± 0.04	0.5 M NaCl	UV-Vis spectrophotometry	[7]
	4.65	0.1 M (H,Na)ClO ₄	Solvent extraction	[8]
	4.4	0.1 M NaClO ₄	Solvent extraction	[11]

The same procedure was applied at 40, 50 and 60°C, leading to estimate the corresponding stability constants 4.61 ± 0.14 , 4.83 ± 0.10 and 4.88 ± 0.10 at $I=0.5$ M NaClO₄/ CH₃OONa with the equilibrium **III.1**. Due to the small number of experimental data and the narrow range of investigated temperature, the variation of ΔH with temperature has been assumed to be constant ($\Delta C_p=0$). Thus, the variation of the stability constants versus $1/T$ has been adjusted using Van't Hoff equation (**III.3**), where R is the universal molar gas constant $8.314 \text{ J K}^{-1} \text{ mol}^{-1}$, T the temperature in Kelvin and $T_0=298.15$ K. This adjustment has been performed using the academic software from Kuban State University^[12].

$$\log \beta_i = \frac{-\Delta H}{RT \ln 10} + \frac{\Delta S}{R \ln 10}$$

The positive enthalpy variation obtained for the complexation of $\text{Eu}(\text{TTA})^{2+}$ indicates an endothermic reaction ($\Delta H=35\pm 4 \text{ kJ mol}^{-1}$) combined with high entropic contribution ($\Delta S= 200\pm 14 \text{ J mol}^{-1} \text{ K}^{-1}$). The positive enthalpy variation reflects that the energy released by the formation of new bondings in the complex is lower than the energy required for dehydration of the aquo cation Eu^{3+} and of TTA^- . The large entropy variation can be correlated with the coordination mode of Eu in $\text{Eu}(\text{TTA})^{2+}$ chelate that is likely bidentate. The formation of the complex leads to the release of 2 water molecules, increasing the disorder.

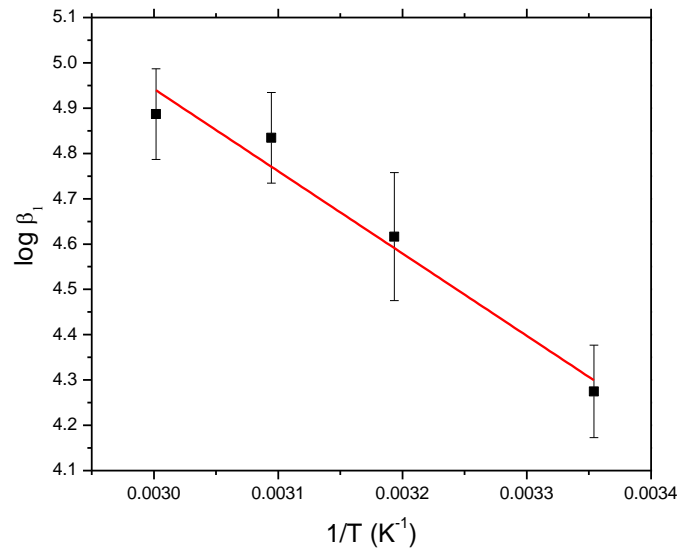


Figure III.2. Temperature dependency of the stability constant of $\text{Eu}(\text{TTA})^{2+}$

III.1.1.2. Quantification of $\text{Eu}(\text{TTA})^{2+}$ in aqueous phase

In liquid-liquid extraction experiments, a fraction of TTA remains in aqueous phase. This fraction has been quantified using the systematic study of TTA partition between toluene and $(\text{Na,H})\text{ClO}_4$ solution conducted by Jaussaud ^[1]. The mean value of the distribution ratio of TTA is 34.2 ± 1.6 ^[1]. This corresponds to a total concentration of TTA ($\text{HTTA}+\text{TTA}^-$) in aqueous phase at equilibrium equal to $7.1\times 10^{-4} \pm 0.1\times 10^{-4} \text{ M}$, and thus $[\text{TTA}^-] = 3.3\times 10^{-6} \text{ M}$ at equilibrium. Using β_1 at $T=25^\circ\text{C}$ in **Table III.1**, the corresponding percentage of $\text{Eu}(\text{TTA})^{2+}$ reaches 7% of total Eu(III) in aqueous solution. Since TTA^- could compete with phosphate ligand, these value must be considered to

correct the conditional stability constant of Eu(III)-phosphate complexes in aqueous solution.

III.1.1.3. Complexation of Eu(III) with phosphate using liquid-liquid extraction with TTA

The low percentage of $\text{Eu}(\text{TTA})^{2+}$ complex in aqueous phase allows the competition between the formation of Eu(III)-TTA chelate in organic phase and Eu(III)-phosphate complexation in aqueous phase to occur. In this context, the study of the complexation of Eu(III) with phosphate was performed by liquid-liquid extraction combined with γ -spectrometry using ^{152}Eu at trace scale using TTA as extractant. The organic phase consisted in TTA 2.5×10^{-2} M diluted in toluene. The aqueous phases were prepared varying the concentration of phosphate from 0 to 0.1 M at $I=0.5$ M $\text{NaClO}_4\text{-HClO}_4$, $\text{pC}_\text{H}=3.9$.

The variation of the distribution ratio (D) of ^{152}Eu as a function of the total phosphate concentration $[\Sigma\text{PO}_4]$ is presented in **Figure III.3**. The error bars do not appear since they have the same size as the experimental points. The value of D_0 corresponding to the distribution ratio in absence of complexing ions has been arbitrarily represented at $[\Sigma\text{PO}_4]=10^{-8}$ M. At low phosphate concentration ($10^{-8} \leq [\Sigma\text{PO}_4] \leq 10^{-3}$ M), a plateau is observed with an average value close to D_0 . Then, the decrease of the D value with increasing ligand concentration $10^{-8} \leq [\Sigma\text{PO}_4] \leq 10^{-3}$ M can be correlated with the formation of Eu complexes in aqueous phase.

According to equation **II.18**, the slopes of the logarithmic variations of the distribution ratio D with total phosphate concentration indicate the mean number of ligands per europium atom in the predominant species in aqueous phase. The slopes corresponding to 1:1 and 1:2 complexes can be observed in **Figure III.3**.

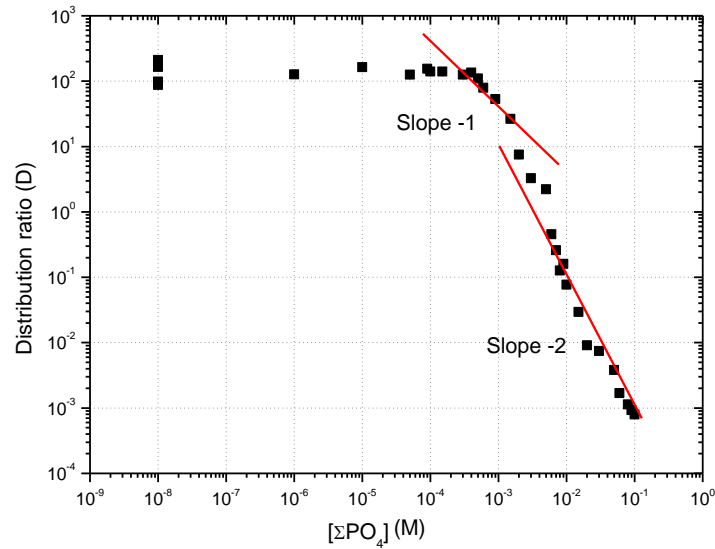


Figure III.3. Variation of the distributions ratio of Eu as a function of total concentration of phosphate ($0 \leq [\Sigma\text{PO}_4] \leq 0.1\text{M}$, $C_{\text{Eu}}=10^{-8}\text{M}$, $C_{\text{TTA}}=2.5 \times 10^{-2}\text{M}$, $I=0.5\text{M}$ $\text{NaClO}_4\text{-HClO}_4$, $pC_{\text{H}}=3.9$ and $T=25^\circ\text{C}$)

However, a systematic deviation of mass balance was observed. Indeed, the total activity of ^{152}Eu ($A_{\text{aq}}+A_{\text{org}}$) did not remain constant with increasing phosphate concentration. **Figure III.4** illustrates the variation of the percentage of the activity in ^{152}Eu ($(A_{\text{aq}}+A_{\text{org}})/A_{\text{ini}} \times 100$) as function of the total phosphate concentration. The mass balance is respected at very low phosphate concentration from 10^{-8} to around 10^{-4}M , and then a sudden decline is observed at 10^{-4}M . Between 10^{-3} and a few 10^{-2}M in phosphate, almost all the activity is lost. At higher phosphate concentration, the total activity of ^{152}Eu tends to increase, with some fluctuations but it does not correspond to the initial activity.

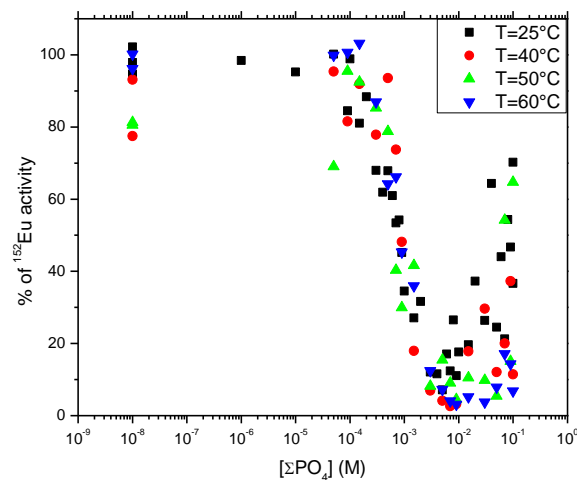


Figure III.4. Percentage of ^{152}Eu activity ($C_{\text{Eu}}=10^{-8}\text{M}$, $C_{\text{TTA}}=2.5 \times 10^{-2}\text{M}$, $I=0.5\text{M}$ $\text{NaClO}_4\text{-HClO}_4$, $pC_{\text{H}}=3.9$ and $T=25, 40, 50$ and 60°C)

In order to identify the causes of the atypical behavior of mass balance, some additional experiments were performed: different TTA concentration have been considered, glass vials and parylene-coated vials have been used to check a possible sorption on the walls. A deviation of the mass balance was systematically observed when the complex 1:1 starts to form. This investigation suggests that the loss of ^{152}Eu activity could be due to the formation of a ternary complex $\text{Eu-TTA-H}_2\text{PO}_4$. This complex could be sorbed at the interface. Due to this systematic deviation in mass balance, the use of TTA in liquid-liquid extraction has been abandoned. Then experiments have been performed with HDEHP as extractant.

III.1.2. System $\text{Eu(III)/NaH}_2\text{PO}_4/(\text{Na,H})\text{Cl/HDEHP/Toluene}$

In order to determine the formation constant of Eu(III)-phosphate by liquid-liquid extraction using HDEHP as extractant, some preliminary experiments were performed to establish conditions that allows the competition between the formation of Eu-HDEHP chelate in organic phase and the Eu(III)-phosphate complex in aqueous phase to occur.

III.1.2.1. System $\text{Eu(III)/(Na,H)Cl/HDEHP/Toluene}$

The extraction of Eu with HDEHP was performed at fixed concentration of HDEHP equal to 0.01 M diluted in toluene. The ionic strength was maintained constant to 1 M in NaCl-HCl medium and the pC_H was varying from 1 to 5. **Figure III.5** presents the percentage of extracted Eu(III) as a function pC_H . The maximum extraction is reached at pC_H higher than 3. However, the distribution ratio ($D \sim 480$) is high and may shift the competition towards chelate formation in organic phase, preventing phosphate complexation in aqueous phase. Therefore, the study in the presence of phosphate was conducted with a lower HDEHP concentration (7.5×10^{-3} M) at $\text{pC}_\text{H} = 3.1$.

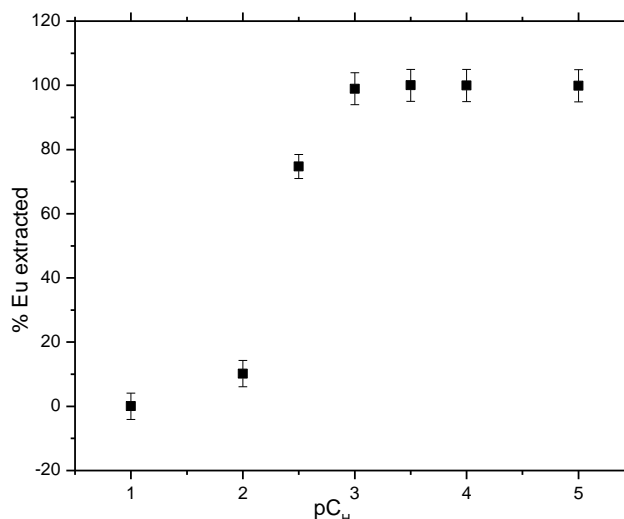


Figure III.5. Variation of the percentage of extracted Eu as a function of pC_H ($C_{Eu} = 7 \times 10^{-8}$ M, $C_{HDEHP} = 0.01$ M in toluene, $I = 1$ M NaCl-HCl, $T = 25$ °C)

III.1.2.2. Complexation of Eu(III) with phosphate using liquid-liquid extraction with HDEHP

Liquid-liquid extraction experiments have been performed with equal volumes of aqueous and organic phase having the following composition: 1 M NaCl-HCl, $pC_H = 3.1$, $0 \leq [\Sigma PO_4] \leq 0.5$ M, and $C_{HDEHP} = 0.0075$ M. The pC_H was monitored before and after the extraction: it was found constant equal to 3.1 ± 0.05 . **Figure III.6** presents the variation of distribution ratio of ^{152}Eu as a function of total phosphate concentration. D_0 is arbitrarily represented at $[\Sigma PO_4] = 10^{-8}$ M. A plateau is observed for $[\Sigma PO_4]$ ranging from 10^{-8} to 10^{-2} M. Then, a slope of -1 is observed from 10^{-2} to 10^{-1} M, followed by a slope -2 up to $[\Sigma PO_4] = 0.4$ M. This corresponds to the formation of complexes of stoichiometry 1:1 and 1:2, respectively. The last three experimental points from 0.35 to 0.5 M of NaH_2PO_4 seem to align along a straight line of slope -3 suggesting the formation of a complex 1:3.

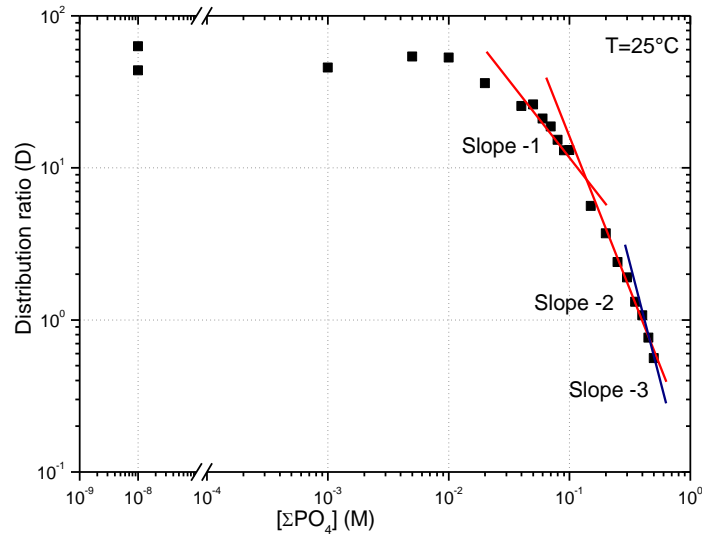


Figure III.6. Variation of the distribution ratio of Eu as a function of phosphate concentration ($0 \leq [\Sigma PO_4] \leq 0.5$ M, $C_{HDEHP} = 0.0075$ M, $I = 1$ M, NaCl-HCl, $pC_H = 3.1$ and $T = 25^\circ\text{C}$)

The observation of complexes with stoichiometry 1:1 and 1:2 agrees with literature data whatever the technique used (*e. g.* TRLFS ^[13, 14], UV-Vis spectrophotometry ^[15] or cation exchange ^[16]). Higher stoichiometry is not excluded. Moskvin ^[16] reported complexes up to the stoichiometry 1:4 using cation exchange. In the present work, the complex 1:3 seems to be present, but in a very narrow range of phosphate concentration. For this reason, at first, this complex was not considered, but an estimation of its stability constant is provided in section III.1.2.4.

The determination of Eu(III)-phosphate stability constants has been conducted in two steps. First, the conditional stability constants (β_i^{cond}) related to the general equilibrium III.4 have been considered. In this equation, (PO_4) stands for phosphate species regardless of its chemical form (the charges are omitted). The β_i^{cond} values can be deduced from the variation of $(D_0/D-1)$ as a function of total concentration of phosphate $[\Sigma PO_4]$ by fitting with a polynomial whose order corresponds to the maximum stoichiometry of the complexes, according to equation III.5:



$$\frac{D_0}{D} - 1 = \sum \beta_i^{cond} \times [\Sigma PO_4]^i \quad \text{III.5}$$

The adjustment of $[D_0/D-1]$ was first conducted on the range of $[\Sigma PO_4]$ corresponding to the predominance of the complex of stoichiometry 1:1. This lead to linear variations as illustrated in **Figure III.7**, whose slope represents β_1^{cond} . Then, the variations of $[(D_0/D-1)-\beta_1^{cond} \times [\Sigma PO_4]]$ were adjusted with a polynomial of second order to get β_2^{cond} as illustrated in **Figure III.8**. The extraction data obtained at $[\Sigma PO_4]$ higher then 0.35 M were excluded due to the possible formation of phosphate complex of higher stoichiometry.

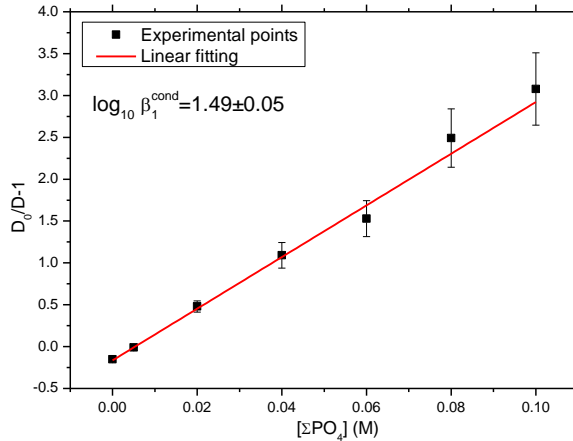


Figure III.7. Fit example: $[(D_0/D)-1]$ as a function of $[\Sigma PO_4]$ ($C_{HDEHP}=0.0075$ M, $0 \leq [\Sigma PO_4] \leq 0.1$ M, $I=1$ M NaCl-HCl, $pC_H=3.1$ and $T=25^\circ C$)

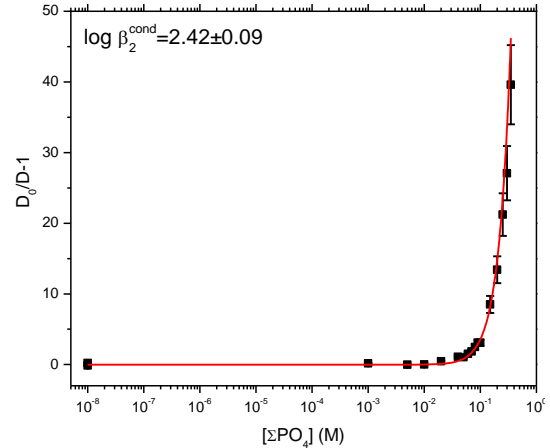


Figure III.8. Fit example: $[(D_0/D)-1]$ as a function of $[\Sigma PO_4]$ ($C_{HDEHP}=0.0075$ M, $0 \leq [\Sigma PO_4] \leq 0.35$ M, $I=1$ M NaCl-HCl, $pC_H=3.1$ and $T=25^\circ C$)

In a second step, the apparent stability constants (β_i^{app}), which involves a defined chemical form of the metallic ion, of the ligand and of the complex, have been determined. In our experimental conditions, the predominant species was $H_2PO_4^-$. It was therefore decided to write the corresponding equilibria as follows:



The conditional and apparent constants are related by the factor $\alpha_{H_2PO_4}^*$ according to the equations **III.8** and **III.9**.

$$\beta_1^{app} = \alpha_{H_2PO_4}^* \times \beta_1^{cond} \quad \text{III.8}$$

$$\beta_2^{app} = (\alpha_{H_2PO_4}^*)^2 \times \beta_2^{cond} \quad \text{III.9}$$

The factor alpha ($\alpha_{H_2PO_4^-}^*$) represents the inverse of the mole fraction of a defined form of the ligand, $H_2PO_4^-$ in this case. The parameter $\alpha_{H_2PO_4^-}^*$ has been calculated using the following equation:

$$\alpha_{H_2PO_4^-}^* = 1 + K_{a1}^{-1}[H^+] + K_{a2}[H^+]^{-1} + K_{a2}K_{a3}[H^+]^{-2} \quad \text{III.10}$$

where K_{ai} stand for the successive acid dissociation constants of phosphoric acid.

The values used in our experimental conditions (1 M (Na,H)Cl, 25°C) can be found in **Table II.10**. The values of the conditional and apparent constants associated to equilibria **III.6** and **III.7** are summarized in **Table II.2**.

Table III.2. Conditional and apparent stability constant for the formation of $Eu(H_2PO_4)_2^{2+}$ and $Eu(H_2PO_4)_2^+$ complexes (I=1 M (Na,H)Cl, T=25°C)

$\log_{10} \beta_1^{cond}$	$\log_{10} \beta_2^{cond}$	$\alpha_{H_2PO_4^-}^*$	$\log_{10} \beta_1^{app}$	$\log_{10} \beta_2^{app}$
1.49±0.05	2.42±0.09	1.05±0.11	1.51±0.12	2.46±0.14

In the literature, most of the available data correspond to the following equilibria:



Thus, for comparison purpose, the conditional and apparent stability constants associated to equations **III.8** and **III.9** determined in the present work, have been converted in β_i^H according to equation **III.13** where K_{a1} stands for the first constant of deprotonation of phosphoric acid.

$$\beta_i = \frac{\beta_i^H}{(K_{a1})^i} \quad \text{III.13}$$

Data on trivalent actinides have also been included in **Table III.3**. All published data have been obtained in perchlorate/perchloric media but the difference in electrolyte cannot explain the discrepancy with our data obtained in chloride media. The complexes between Eu(III) chloride indeed are known to be very weak and can be neglected in our experimental conditions^[17].

One could notice that the stability constants relative to Eu determined in the present work are closer to those of trivalent actinides as compared to Eu reported by Jordan *et al.*,^[14] and Liu *et al.*,^[18] whatever the used technique. Bingler *et al.*,^[19] found also a value of -0.08 for gadolinium using liquid-liquid extraction. At the present time, no

explanation can be proposed regarding the difference of half an order of magnitude in Eu-phosphate stability constants.

Table III.3. Complexations constants for $M(H_2PO_4)^{2+}$ and $M(H_2PO_4)_2^+$ at $T=25^\circ C$ according to equilibria III.11 and III.12 and first protonation constant of H_3PO_4

Cation	Ionic strength	$\log \beta_1^{H\text{-app}}$	$\log \beta_2^{H\text{-app}}$	$\log K_{a1}$	Method	Ref.
Eu(III)	1 M (Na,H)Cl	-0.29±0.05	-1.14±0.24	-1.78±0.19	Extraction	This work
	0.1 M HClO ₄	0.248	---	-1.943 ^a	Solubility	[18]
	1.1 M NaClO ₄	0.29±0.11	---	-1.64±0.03 ^b	TRLFS	[14]
Cm (III)	1.1 M NaClO ₄	-0.14±0.10	---	-1.64±0.03 ^b	TRLFS	[14]
	1 M NaClO ₄	-0.16±0.15	-0.82±0.25	-1.81±0.03 ^b	TRLFS	[13]
	0.1 M NaClO ₄	0.32±0.02	---	-2.0±0.1 ^c	TRLFS	[20]
Am(III)	0.5 M HClO ₄	-0.15	---	-2.12 ^g	Solubility	[21]

a. $\log K_{a1}$ value from Liu et al. [18]

b. The values of $\log_{10} K_{a1}$ was estimated applying SIT model using D , A , B_{aj} , ϵ parameters provided by the author.

c. The author mentioned that the values of $\log K_{a1}=2.0\pm 0.1$, $\log K_{a2}=5.72\pm 0.5$ and $\log K_{a3}=11.74\pm 0.08$ were taken from Smith et al. [22]

III.1.2.3. Temperature effect on the complexation of Eu(III) with phosphate

Liquid-liquid extraction experiments with HDEHP have been conducted at 15, 38, 46 and 56°C, in the same way as at 25°C. **Figure III.8** illustrates the variation of D of ^{152}Eu as a function of total phosphate concentration at 15°C and 56°C. All the curves follow the same trend as in **Figure III.6**, leading to the formation of complexes 1:1 and 1:2, and probably 1:3, but the latter was not considered for the calculation of the associated thermodynamic parameters. The individual curves for 38 and 46°C are presented in **Appendix 5**. An slight increase in D_0 with increasing temperature is observed.

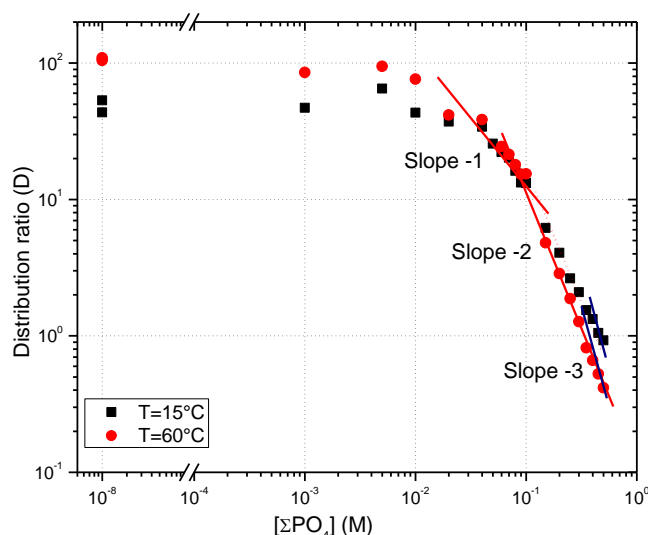


Figure III.9. Variation of the distributions ratio of ^{152}Eu as a function of total phosphate concentration ($C_{\text{Eu}}=10^{-8}\text{ M}$, $0\leq[\Sigma\text{PO}_4]\leq 0.5\text{ M}$, $C_{\text{HDEHP}}=0.0075\text{ M}$, $I=1\text{ M}(\text{Na,H})\text{Cl}$, $pC_{\text{H}}=3.1$, $T=15$ and 60°C)

The calculation procedure used at 25°C has been applied to the data collected at other temperatures. Raw extraction curves as well as adjustments are summarized in **Appendix 5**. The conditional and apparent stability constants of the complexes 1:1 and 1:2 according to equilibria **III.6** and **III.7** are presented in **Table III.4**.

Table III.4. Conditional and apparent stability constant for the formation of $\text{Eu}(\text{H}_2\text{PO}_4)^{2+}$ and $\text{Eu}(\text{H}_2\text{PO}_4)_2^+$ complexes ($I=1\text{ M}(\text{Na,H})\text{Cl}$)

T ($^\circ\text{C}$)	$\log_{10} \beta_1^{\text{cond}}$	$\log_{10} \beta_2^{\text{cond}}$	$\alpha_{\text{H}_2\text{PO}_4}^*$	$\log_{10} \beta_1^{\text{app}}$	$\log_{10} \beta_2^{\text{app}}$
15	1.31 ± 0.03	2.27 ± 0.16	1.04 ± 0.11	1.33 ± 0.12	2.31 ± 0.16
40*	1.60 ± 0.08	2.59 ± 0.11	1.06 ± 0.11	1.63 ± 0.13	2.64 ± 0.16
50*	1.68 ± 0.01	2.68 ± 0.11	1.06 ± 0.12	1.71 ± 0.13	2.73 ± 0.16
60*	1.78 ± 0.04	2.94 ± 0.10	1.07 ± 0.12	1.81 ± 0.13	2.99 ± 0.16

*The real temperatures measured by a conventional thermometer in our experimental conditions were 38, 46 and 56°C

In order to compare our data with those reported in literature, the stability constants in **Table III.4** have been converted in β_1^{H} according to equation **III.13** since the data on trivalent actinides at other temperatures in literature have been reported using the equilibria **III.11** and **III.12**. The $\log \beta_1^{\text{H-app}}$ values presented in **Table III.5** tend to

decrease with the temperature as reported for Eu(III) and Cm(III) in 1.1 M NaClO₄ media by Jordan *et al.*,^[14]. As mentioned in the previous sections, no explanation can be proposed regarding the difference of half an order of magnitude in Eu-phosphate stability constants.

Table III.5. Conditional and apparent stability constants for the formation of $\text{Eu}(\text{H}_2\text{PO}_4)^{2+}$ and $\text{Eu}(\text{H}_2\text{PO}_4)_2^+$ at different temperatures ($I=1\text{ M (Na,H)Cl}$ and first dissociation constant of H_3PO_4)

T (°C)	This work						Jordan <i>et al.</i> , ^[14]		
	Eu(III)		Eu(III)				Eu(III)	Cm(III)	
	$\log_{10} \beta_1^{H-\text{cond}}$	$\log_{10} \beta_2^{H-\text{cond}}$	$\alpha_{\text{H}_2\text{PO}_4}^*$	$\log_{10} \beta_1^{H-\text{app}}$	$\log_{10} \beta_2^{H-\text{app}}$	$\log_{10} K_{a1}$	$\log_{10} \beta_1^{H-\text{app}}$	$\log_{10} \beta_1^{H-\text{app}}$	$\log_{10} K_{a1}$
15	-0.43±0.08	-1.20±0.29	1.04±0.11	-0.41±0.08	-1.16±0.28	-1.73±0.19			
25	-0.29±0.06	-1.10±0.24	1.05±0.11	-0.27±0.05	-1.10±0.23	-1.78±0.19	0.29±0.11	-0.14±0.10	-1.64±0.03
40*	-0.24±0.05	-1.09±0.22	1.06±0.11	-0.21±0.05	-1.05±0.21	-1.84±0.20	0.35±0.15	-0.12±0.10	-1.70±0.03
50*	-0.20±0.04	-1.08±0.25	1.06±0.12	-0.17±0.04	-1.03±0.24	-1.88±0.21	0.39±0.15	-0.08±0.20	-1.73±0.04
60*	-0.14±0.03	-0.89±0.21	1.07±0.12	-0.11±0.02	-0.83±0.20	-1.91±0.22	0.45±0.18	-0.02±0.10	-1.77±0.05

*The real temperatures measured by a conventional thermometer in our experimental conditions were 38, 46 and 56°C

The changes of equilibrium constants with the temperature have been adjusted using Van't Hoff's equation (III.3). **Figure III.10** illustrates the variations of $\log \beta_i^{H\text{-app}}$ relative to equilibria III.11 and III.12 as function of $1/T$. The linear variations observed in this figure justify a posteriori the assumption that ΔC_p variations can be neglected over a narrow range of temperature. The enthalpies (ΔH) and entropies (ΔS) with their standard deviations were computed using an academic software developed by Kuban State University [12].

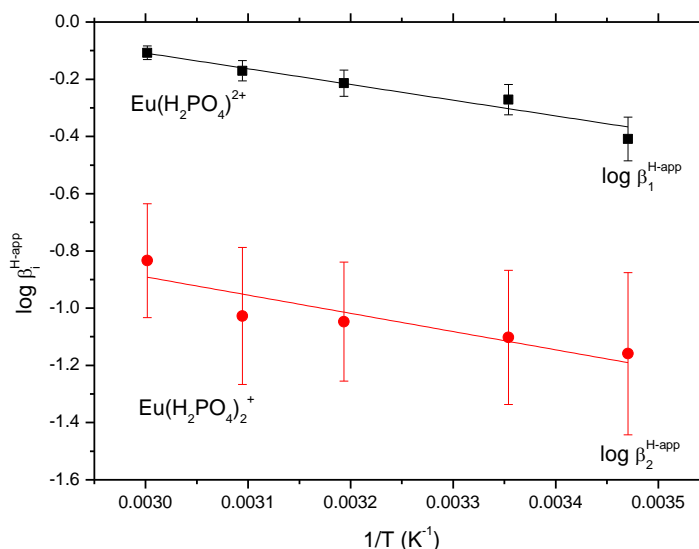


Figure III.10. Variation of $\log \beta_i^{H\text{-app}}$ as a function of temperature at $I=1$ M NaCl-HCl according to equilibria III.11 and III.12

The derived thermodynamic data for both complexes obtained in this work are summarized in **Table III.6**. The entropy (ΔH) and enthalpy (ΔS) values seems to have the same order of magnitude with those reported for Eu(III) and Cm(III) reported in standard conditions by Jordan *et. al.* [14] and Huittinen *et. al.*, [13]. The positive enthalpy and entropy indicate the both reactions are endothermic with a moderate entropic contribution [23]. The positive enthalpy variation indicates that the energy released by the formation of new bonding in the complex is lower than the energy required for dehydration of the aqua cation Eu^{3+} and the ligand H_3PO_4 .

Table III.6. Thermodynamic functions for $\text{Eu}(\text{H}_2\text{PO}_4)_2^{2+}$ and $\text{Eu}(\text{H}_2\text{PO}_4)_2^+$ complexes

Equilibrium	H_3PO_4 species	
	ΔH (kJ mol^{-1})	ΔS ($\text{J mol}^{-1} \text{K}^{-1}$)
III.11	11±1	29±4
III.12	12±3	20±2

In order to bypass the contribution of the dehydration of the phosphate ligand to the thermodynamic parameters, the successive complexations reactions have been considered. In that case, the constant $K_1^{\text{H-app}}$ is equivalent to $\beta_1^{\text{H-app}}$ and $K_2^{\text{H-app}} = \beta_2^{\text{H-app}} / \beta_1^{\text{H-app}}$. The corresponding enthalpy and entropy variations are summarized in **Table III.7**. With this formalism, the formation of the complex 1:2 becomes athermic: the energy spent in the dehydration step of the complex 1:1 is similar to the energy released to form the complex 1:2. As regards the entropic variations, they pass from positive to negative with increasing ligand number. According to the theoretical calculations presented in part **I.4.1**, phosphate ligands should be coordinated to Eu in a monodentate fashion, as for Cm. Thus, for both complexes, there is a release of one water molecule from the hydration sphere of Eu that is replaced by a monodentate phosphate ligand that contributes to an entropic gain. In the case of the complex 1:2, this effect is totally counterbalanced by an ordering due to the symmetry in the complex 1:2^[24].

Table III.7. Thermodynamic parameters calculated from successive complexation constant $K_i^{\text{H-app}}$ of Eu(III)-phosphate complexes

$K_i^{\text{H-app}}$	Successive reactions	
	ΔH (kJ mol^{-1})	ΔS ($\text{J mol}^{-1} \text{K}^{-1}$)
$\text{Eu}(\text{H}_2\text{PO}_4)_2^{2+}$	11±1	29±4
$\text{Eu}(\text{H}_2\text{PO}_4)_2^+$	0	-9±0.9

III.1.2.4. Formation of Eu-phosphate complexes with stoichiometry 1:3

As mentioned in the previous section, an Eu(III)-phosphate complex with stoichiometry 1:3, should be formed in our experimental conditions that allow a large excess in phosphate with respect to the cation to be reached. However, the following results must be regarded with caution since only the last three experimental points in **Figure III.6** tend to align along a straight line of slope -3. The extraction data have been adjusted with **Eq. III.5** with $i=3$ and using the values of β_1^{cond} and β_2^{cond} previously determined. The β_3^{cond} values are deduced from the variation of $D_0/D-1$ versus $[\Sigma PO_4]$ adjusted with a third order polynomial as illustrated in **Figure III.11**.

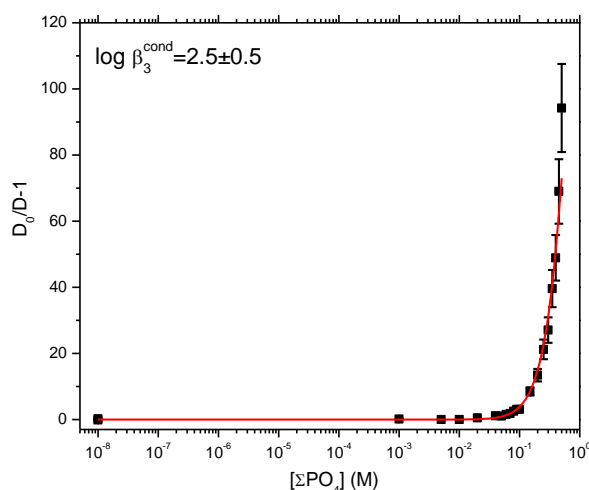


Figure III.11. Fit example: $[(D_0/D)-1]$ as a function of $[\Sigma PO_4]$ ($C_{HDEHP}=0.0075$ M, $0.35 \leq [\Sigma PO_4] \leq 0.5$ M, $I=1$ M NaCl-HCl, $pC_H=3.1$ and $T=25^\circ\text{C}$)

The apparent stability constant was deduced considering the equilibrium **III.14** and the relation **III.15**.



$$\beta_3^{app} = (\alpha_{H_2PO_4^-}^*)^3 \times \beta_3^{cond} \quad \text{III.15}$$

The same procedure was applied for all the temperatures studied in this work. The $\log \beta_3^{app}$ values obtained are presented in **Table III.8**. Our $\log \beta_3^{app}$ at $T=25^\circ\text{C}$ has the same order of magnitude of those for Pu(III), Am(III) and Cm(III) equal to 2.90, 2.85 and 2.84 reported

by Moskvin ^[16] at I=1 M and T=25°C. The proposed values at other temperatures are suggested for the first time. They tend to decrease with temperature as for the formation of complexes 1:1 and 1:2. But it requires further study to clearly establish the existence of the complex 1:3.

Table III.8. Conditional and apparent stability constants for the formation of and $\text{Eu}(\text{H}_2\text{PO}_4)_3^0$ at different temperatures (I=1 M (Na,H)Cl)

Temperature (°C)	$\log_{10} \beta_3^{\text{cond}}$	$\alpha_{\text{H}_2\text{PO}_4^-}^*$	$\log_{10} \beta_3^{\text{app}}$	$\log_{10} \beta_3^{\text{H-app}}$
15	2.5±0.2	1.04±0.11	2.5±0.2	-2.7±0.3
25	2.5±0.1	1.05±0.11	2.8±0.3	-2.5±0.3
40*	2.6±0.2	1.06±0.11	2.9±0.3	-2.6±0.3
50*	2.7±0.2	1.06±0.12	2.7±0.3	-2.9±0.3
60*	2.3±0.3	1.07±0.12	3.3±0.3	-2.4±0.3

*The real temperatures measured by a conventional thermometer in our experimental conditions were 38, 46 and 56°C

This investigation proposes a distribution diagram from the stability constants obtained for complexes of stoichiometry 1 to 3 in **Figure III.12**. The $\text{Eu}(\text{H}_2\text{PO}_4)_3^{2+}$ complex is predominant at phosphate concentration lower than 0.1 M. Then, $\text{Eu}(\text{H}_2\text{PO}_4)_2^+$ is formed as the phosphate concentration is increasing. According to the present speciation diagram, the $\text{Eu}(\text{H}_2\text{PO}_4)_3^0$ complex tends to be formed at higher phosphate concentration (>0.35 M). However, more experimental points will be required to ensure that the calculated stability constants are reliable. To be able to work with larger phosphate concentration range, the fixed ionic strength of the media needs to be increased.

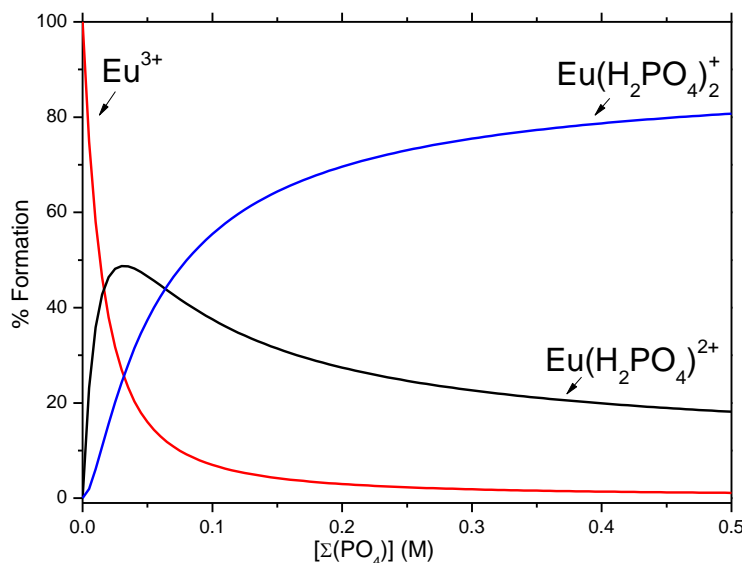


Figure III.12. Distribution diagram of Eu(III)-phosphate complexes ($C_{Eu} = 10^{-8} M$, $I=1 M$ NaCl-HCl, $pC_H=3.1$ and $T=25^\circ C$)

III.2. Solubility of Nd(III)-based rhabdophane

In order to develop an experimental protocol that can be applied to Pu(III)-phosphate compounds, rhabdophane phase was chosen because it is easy to synthesize especially with Nd(III). Its dissolution behavior -thermodynamic, kinetics and mechanism- is well known. In addition, rhabdophane phase is present as secondary phase during the dissolution of monazite^[25-27]. The strategy used for the determination of fundamental thermodynamic data from solubility measurements was as follows. First the synthesis, characterization and dissolution of the rhabdophane $Eu_{0.01}Nd_{0.99}PO_4 \cdot nH_2O$ were performed and its properties carefully compared to those of $NdPO_4 \cdot 0.667H_2O$. Then, the synthesis of $Eu_{0.012}Nd_{0.988}PO_4 \cdot nH_2O$ doped with ^{152}Eu was conducted and dissolution experiments were performed with decreasing amounts of solid for further application to Pu(III) phosphate compound in accordance with rules in IJCLab.

III.2.1. Characterization of Nd-rhabdophane doped with 1% of Eu

The ATR-FTIR spectra of $Eu_{0.01}Nd_{0.99}PO_4 \cdot nH_2O$ and $NdPO_4 \cdot nH_2O$ are presented in **Figure III.13**. These spectra can be divided in three domains: the deformation and stretching modes of PO_4 group, around 600 and 1000 cm^{-1} , respectively, and the vibrations of water molecules around 3500 and 1620 cm^{-1} ^[28]: The sharp peak at 1037 cm^{-1} can be assigned to

antisymmetric stretching mode ($\nu_{as}(\text{PO}_4)$) and the band at 970 cm^{-1} to the symmetric stretching mode $\nu_s(\text{PO}_4)$; the deformation vibrations of PO_4 are observed at lower wavenumber [28, 29]. Clavier *et al.* [28] have recently demonstrated that the vibrations assigned to PO_4 can hardly be used to discriminate the structural types of Gd-phosphates: rhabdophane, churchite, monazite and xenotime. However, the presence of water molecules in both compounds that can be attested by the bending and stretching vibration at 1620 and 3550 cm^{-1} allows excluding the anhydrous monazite and xenotime. Moreover, the presence of a single band at 1620 cm^{-1} has been proved to characterize the rhabdophane structure [28]. These results confirm that both compounds correspond to rhabdophane and there is no significant effect of the presence of 1% Eu.

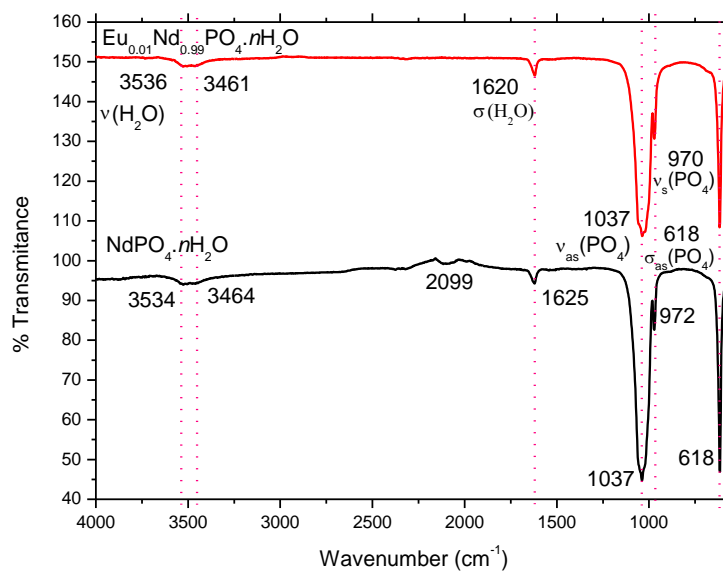


Figure III.13. FTIR spectra recorded for $\text{Eu}_{0.01}\text{Nd}_{0.99}\cdot n\text{H}_2\text{O}$ and $\text{NdPO}_4\cdot n\text{H}_2\text{O}$

The assignment of the vibration bands observed on the FTIR spectra recorded for $\text{Eu}_{0.01}\text{Nd}_{0.99}\cdot n\text{H}_2\text{O}$ and $\text{NdPO}_4\cdot n\text{H}_2\text{O}$ are summarized in **Table III.9**. The proximity of the bands between both compounds confirms that the presence of 1% Eu does not change the rhabdophane's chemical bonds.

Table III.9. Assignment of the vibration bands observed on the FTIR spectra for $\text{Eu}_{0.01}\text{Nd}_{0.99}n\text{H}_2\text{O}$ and $\text{NdPO}_4 \cdot n\text{H}_2\text{O}$ compounds^[28-31]

Wavenumber (cm^{-1})		Band assignment	Group
$\text{Eu}_{0.01}\text{Nd}_{0.99}\text{PO}_4 \cdot n\text{H}_2\text{O}$	$\text{NdPO}_4 \cdot n\text{H}_2\text{O}$		
3536	3534	$\nu(\text{H}_2\text{O})$	O-H stretching
3461	3464		
---	2099	$\nu_{\text{as}}(\text{PO}_4)$	P-O stretching
1620	1625	$\delta(\text{H}_2\text{O})$	O-H bending
1037	1037	$\nu_{\text{as}}(\text{PO}_4)$	P-O stretching
970	972	$\nu_{\text{s}}(\text{PO}_4)$	P-O stretching
618	618	$\delta_{\text{s}}(\text{PO}_4)$	O-P-O bending

Both solids were analyzed by XRD. The XRD patterns of $\text{Eu}_{0.01}\text{Nd}_{0.99}\text{PO}_4 \cdot n\text{H}_2\text{O}$ and $\text{NdPO}_4 \cdot n\text{H}_2\text{O}$ are presented in **Figure III.14**. No reflections other than those belonging to the hydrated monoclinic rhabdophane (PDF-00-050-0620) can be seen in the diffractograms, indicating that single-phase rhabdophane are formed during the synthesis of both solids.

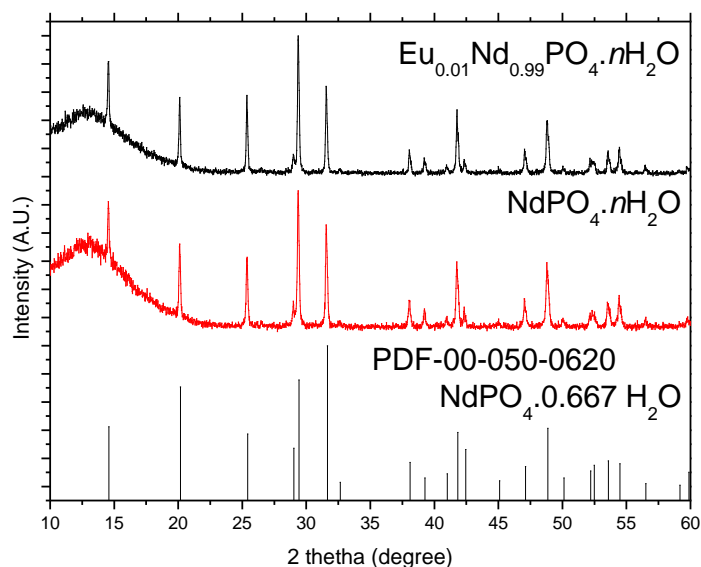


Figure III.14. Experimental XRD patterns obtained for $\text{Eu}_{0.01}\text{Nd}_{0.99} \cdot 0.667\text{H}_2\text{O}$ and $\text{NdPO}_4 \cdot 0.667\text{H}_2\text{O}$ with the theoretical XRD patterns of the hydrated monoclinic *Nd-rhabdophane*

The Rietveld refinement of X-Ray patterns of $\text{Eu}_{0.01}\text{Nd}_{0.99}\text{PO}_4 \cdot n\text{H}_2\text{O}$ in **Appendix 5** allowed to determine the unit cell parameters and the lattice volume presented in **Table III.10**. Those values confirm $\text{Eu}_{0.01}\text{Nd}_{0.99}\text{PO}_4 \cdot n\text{H}_2\text{O}$ is in monoclinic C2 space group characteristic of rhabdophane phase ^[28, 32]. Our values align to cell of type $\text{NdPO}_4 \cdot n\text{H}_2\text{O}$ as can see in **Table III.10**. Thus, the incorporation of Eu atoms do not disturb the structure of Nd-based rhabdophane ^[32-35].

Table III.10. Unit cell parameters a, b, c, β and lattice volume for Nd and Eu based rhabdophane at room temperature (monoclinic C2 Space group)

Rhabdophane	a (Å)	b (Å)	c (Å)	β (deg)	Volume (Å ³)	Reference
$\text{Eu}_{0.01}\text{Nd}_{0.99}\text{PO}_4 \cdot n\text{H}_2\text{O}$	28.279	7.012	12.124	115.242	2174.5	This work
$\text{NdPO}_4 \cdot \text{H}_2\text{O}$	28.309	7.028	12.100	115.4	2174.6	[33]
$\text{NdPO}_4 \cdot 0.667\text{H}_2\text{O}$	28.2769	7.0033	12.1326	115.28	2172.5	[32]
$\text{NdPO}_4 \cdot 0.667\text{H}_2\text{O}$	28.3889	7.0294	12.1786	115.31	2197.1	[34]
$\text{NdPO}_4 \cdot 0.746\text{H}_2\text{O}$	28.2882	7.0048	12.1380	115.28	2174.7	[35]
$\text{EuPO}_4 \cdot 0.667\text{H}_2\text{O}$	28.1187	6.9466	12.0257	115.20	2125.3	[34]
$\text{EuPO}_4 \cdot 0.667\text{H}_2\text{O}$	28.0245	6.9212	11.9853	115.22	2103.1	[32]
$\text{EuPO}_4 \cdot 0.555\text{H}_2\text{O}$	28.0108	6.9194	11.9803	115.21	2100.9	[35]

In order to specify the number of water molecules in the crystal structure characteristic of rhabdophane phases, a thermogravimetric analysis of $\text{Eu}_{0.01}\text{Nd}_{0.99} \cdot n\text{H}_2\text{O}$ was conducted from 0 to 300°C. Under these temperature conditions there is no transition to monazite that occurs at 700-800°C and remains in rhabdophane phase ^[25, 27, 32]. The TGA curve corresponding to the thermal behavior of $\text{Eu}_{0.01}\text{Nd}_{0.99} \cdot n\text{H}_2\text{O}$ is presented in **Figure III.15**.

The water molecules are eliminated in two steps: firstly 0.167 H₂O molecules are removed between room temperature and 100°C assigned to the water absorbed onto the powder's surface due to the storage conditions ^[32]. Then, the remaining ~0.5 water molecules are eliminated between 100 and 250 °C. By decreasing again the temperature, a partial rehydration of the sample was observed that indicates that this process is reversible. This

two steps dehydration process was already observed in the literature for hydrated rhabdophane structure [36]. In conclusion, for Nd-rhabdophane doped with 1% of Eu, the experimental amount of water molecules was found to be 0.667 which is in a good agreement with the typical rhabdophane structure [36].

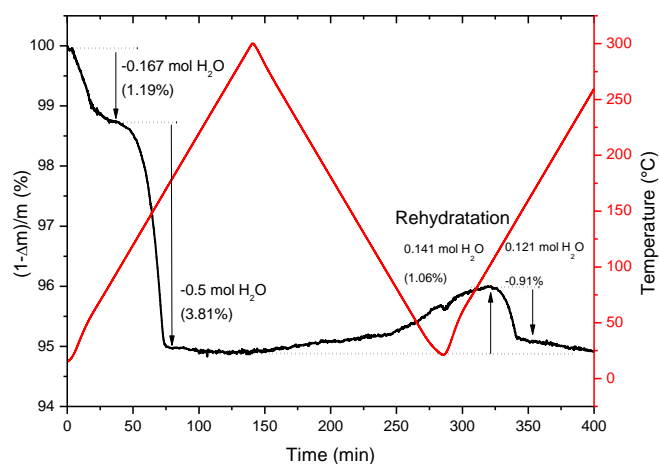


Figure III.15. Thermogravimetric analysis of $\text{Eu}_{0.01}\text{Nd}_{0.99}\cdot 0.667\text{H}_2\text{O}$ ($2^\circ\text{K}\cdot\text{min}^{-1}$, argon atmosphere)

The morphology of $\text{Eu}_{0.01}\text{Nd}_{0.99}\text{PO}_4\cdot 0.667\text{H}_2\text{O}$ was observed by SEM. The micrograph in **Figure III.16** shows needle-like crystals characteristics of the rhabdophane phase [27, 36]. The composition was determined by X-EDS analysis couple with SEM. It confirms the expected stoichiometry of the solid $\text{Eu}_{0.01}\text{Nd}_{0.99}\text{PO}_4\cdot 0.667\text{H}_2\text{O}$ [27, 36]. The grain size of the needle-like crystals is around $1.5\pm 0.2\ \mu\text{m}$, a little bit longer than the value of $1\ \mu\text{m}$ reported by Gausse *et al.*, [27] for La-Nd series.

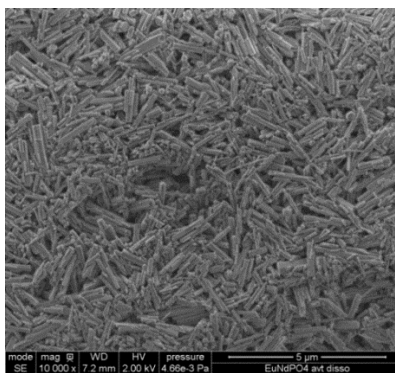


Figure III.16. SEM micrographs of $\text{Eu}_{0.01}\text{Nd}_{0.99}\text{PO}_4\cdot 0.667\text{H}_2\text{O}$

The experimental techniques employed for the characterization of $\text{Eu}_{0.01}\text{Nd}_{0.99}\text{PO}_4 \cdot 0.667\text{H}_2\text{O}$ confirm that the doping with 1% Eu(III) does not change the rhabdophane structure. In addition, the number of water molecules and the morphology of our solid are as expected. Therefore, a second solid was synthesized incorporating ^{152}Eu isotope into Nd(III)-based rhabdophane assuming it will have same crystal structure, composition and morphology as $\text{Eu}_{0.01}\text{Nd}_{0.99}\text{PO}_4 \cdot n\text{H}_2\text{O}$. However, the additional amount of stable Eu of 0.12 μg per mg of doped rhabdophane give a solid with stoichiometry of $\text{Eu}_{0.012}\text{Nd}_{0.988}\text{PO}_4 \cdot n\text{H}_2\text{O}$ doped with ^{152}Eu .

III.2.2. Dissolution of Nd(III)-based rhabdophane

In our investigations, the dissolution experiments were conducted under low-pH conditions in 0.1 M HClO_4 for Nd^{3+} ion is the dominant aqueous species. This approach simplifies the calculations to determine the solubility products ^[26].

III.2.2.1. Dissolution of $\text{Eu}_{0.012}\text{Nd}_{0.988}\text{PO}_4 \cdot n\text{H}_2\text{O}$

The evolution of the elemental concentration during the dissolution of $\text{Eu}_{0.01}\text{Nd}_{0.99}\text{PO}_4 \cdot 0.667\text{H}_2\text{O}$ in 0.1 M HCl is presented in **Figure III.17**. The elemental concentrations increased gradually until reaching a plateau after around 11 days at room temperature. Nd, Eu and P tend to dissolve at the same rate which means the dissolution of $\text{Eu}_{0.01}\text{Nd}_{0.99}\text{PO}_4 \cdot 0.667\text{H}_2\text{O}$ is congruent. The pH at the equilibrium was 0.993.

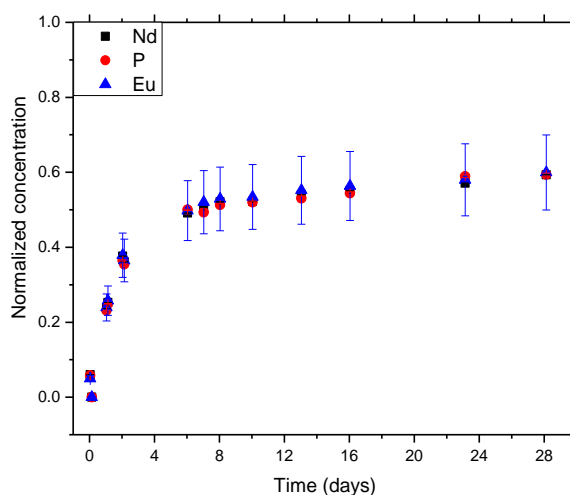


Figure III.17. Evolution of neodymium, europium, and phosphorous elemental concentrations during the dissolution of $\text{Eu}_{0.01}\text{Nd}_{0.99}\text{PO}_4 \cdot 0.667\text{H}_2\text{O}$ in 0.1 M HCl solution at room temperature

The morphology of $\text{Eu}_{0.01}\text{Nd}_{0.99}\text{PO}_4 \cdot 0.667\text{H}_2\text{O}$ was then checked by SEM and compared to the one before dissolution. The micrographs in **Figure III.18** suggest the needle-like morphology characteristic of the rhabdophane structure is maintained throughout the experiment. There is not evidence of secondary phases after the dissolution. This study assumes that the rhabdophane phase controls Nd, Eu and P concentrations at equilibrium and the associated solubility products can be determined.

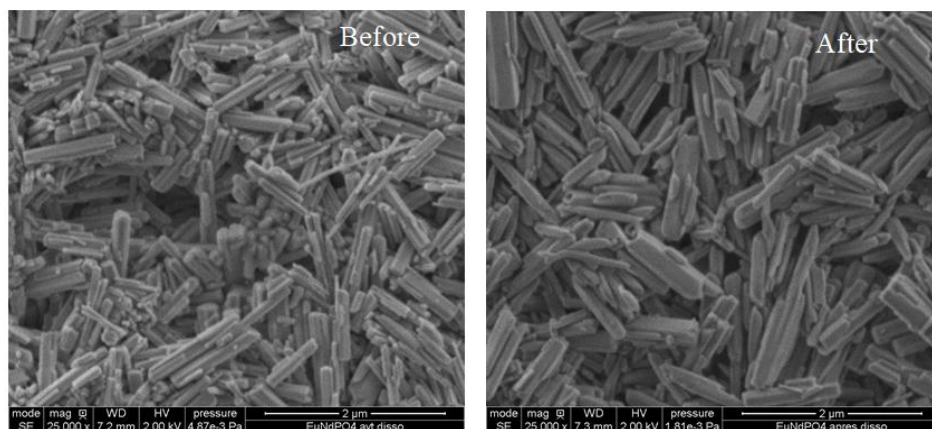


Figure III.18. SEM micrographs of $\text{Eu}_{0.01}\text{Nd}_{0.99}\text{PO}_4 \cdot 0.667\text{H}_2\text{O}$ before and after the dissolution experiments (0.1 M HCl, room temperature)

III.2.2.2. Dissolution of $\text{Eu}_{0.01}\text{Nd}_{0.99}\text{PO}_4 \cdot 0.667\text{H}_2\text{O}$ doped with ^{152}Eu

The dissolution experiments involving 50.1, 11.3, 6.9, 5.5, 2.2 and 1.8 mg $\text{Eu}_{0.012}\text{Nd}_{0.988}\text{PO}_4 \cdot 0.667\text{H}_2\text{O}$ doped with ^{152}Eu , were performed in 0.15 M HCl with mass/volume ratio to 1:1 mg/mL at 25°C. Monitoring of the dissolution was conducted by analysis of the aliquots that were taken off at regular time intervals by γ -spectrometry. **Figure III.19** shows a diagram of how the elemental concentrations were determined. This determination is described in **Appendix 3** using the efficiency calibration of HPGe detector presented in **II.1.2.3**.

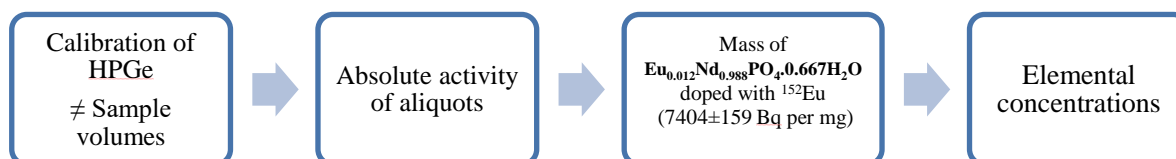


Figure III.19. Flowchart for the determination of elemental concentrations

The evolution of the dissolution of $\text{Eu}_{0.012}\text{Nd}_{0.988}\text{PO}_4 \cdot 0.667\text{H}_2\text{O}$ doped with ^{152}Eu is shown in **Figure III.20**. As can see the concentration of europium increased gradually and a plateau was reached after ~ 11 days regardless of the amount of mass used. The pH of the equilibrium was 0.82 and it was only measured for the systems with 50.1 mg.

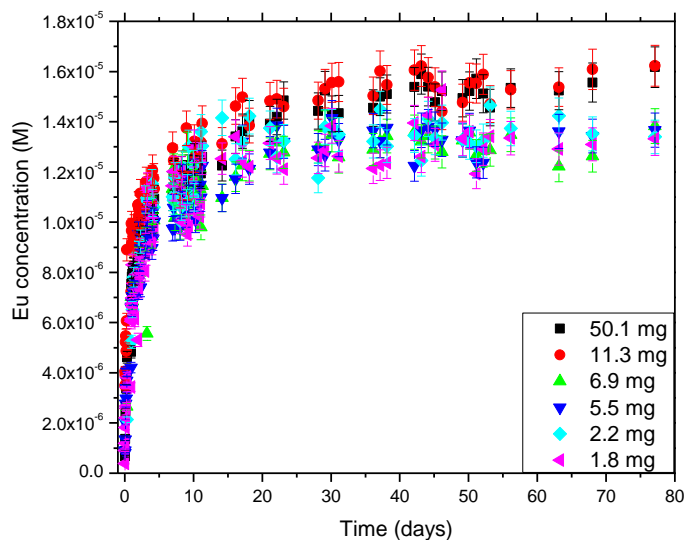


Figure III.20. Evolution of the dissolution of $\text{Eu}_{0.012}\text{Nd}_{0.988}\text{PO}_4 \cdot 0.667\text{H}_2\text{O}$ doped with ^{152}Eu in 0.15 M HCl at 25°C

The concentrations of Nd, Eu and P at the equilibrium involving $\text{Eu}_{0.012}\text{Nd}_{0.988}\text{PO}_4 \cdot 0.667\text{H}_2\text{O}$ and the one involving the solid doped with ^{52}Eu are listed in **Table III.11**. The concentrations of Nd and P were estimated as described in **Appendix 3**. It can be noted that the acidity of the medium has an impact on the dissolution of the solid. The elemental concentration of $\text{Eu}_{0.01}\text{Nd}_{0.99}\text{PO}_4 \cdot 0.667\text{H}_2\text{O}$ dissolved in 0.1 M HCl (pH=0.993) are higher than those of the system $\text{Eu}_{0.012}\text{Nd}_{0.988}\text{PO}_4 \cdot 0.667\text{H}_2\text{O}$ doped with ^{152}Eu in 0.15 M (pH=0.82). Moreover; the mole fractions of the elements in solution are equal to their mole fractions in the dissolving solid phase. Thus, the dissolution was stoichiometric and the solubility product can be calculated.

Table III.11. Concentration of Nd, Eu and P at the equilibrium

Component	Element concentration (M)		
	Eu _{0.01} Nd _{0.99} PO ₄ ·0.667H ₂ O	Eu _{0.012} Nd _{0.988} PO ₄ ·0.667H ₂ O with ¹⁵² Eu	
	in 0.1 M (pH=0.993)	in 0.15 M (pH=0.82)	
	50.2 mg	50.1 mg	1.8 mg
Eu	$7.9 \times 10^{-6} \pm 1.3 \times 10^{-6}$	$1.6 \times 10^{-5} \pm 7.8 \times 10^{-7}$	$1.3 \times 10^{-5} \pm 6.6 \times 10^{-7}$
Nd	$6.3 \times 10^{-4} \pm 5.1 \times 10^{-6}$	$1.3 \times 10^{-3} \pm 6.4 \times 10^{-5}$	$1.1 \times 10^{-3} \pm 5.4 \times 10^{-5}$
P	$6.5 \times 10^{-4} \pm 3.8 \times 10^{-6}$	$1.3 \times 10^{-3} \pm 6.5 \times 10^{-5}$	$1.1 \times 10^{-3} \pm 5.5 \times 10^{-5}$

The determination of the standard solubility products ($K_{s,0}^0$) as un-complexes species, the equilibrium constant ($*K_s$) and the standard solubility products ($*K_s^0$) as protonated species and associated standard Gibbs energy are calculated according to the strategy presented in part **II.3.1**.

The fundamental thermodynamic data obtained are summarized in **Table III.12**. $\log_{10} K_{s,0}^0$ value is found to be -25.11 ± 0.29 with $\Delta_r G^0(298 \text{ K}) = 144.2 \pm 5 \text{ kJ mol}^{-1}$ for Eu_{0.01}Nd_{0.99}PO₄·0.667H₂O and -24.92 ± 0.32 with $\Delta_r G^0(298 \text{ K}) = 141.5 \pm 7 \text{ kJ mol}^{-1}$ for the rhabdophane doped with ¹⁵²Eu. These values agree with those reported for NdPO₄·0.667H₂O ($\log K_{s,0}^0 = -25.6 \pm 0.02$ and $\Delta_r G^0(298 \text{ K}) = 145 \pm 3 \text{ kJ mol}^{-1}$) and EuPO₄·0.667H₂O ($\log K_{s,0}^0 = -24.3 \pm 0.3$ and $\Delta_r G^0(298 \text{ K}) = 142 \pm 10 \text{ kJ mol}^{-1}$)^[27]. However, the slight difference between Eu_{0.01}Nd_{0.99}PO₄·0.667H₂O and the one doped with ¹⁵²Eu can be attributed to the gamma measurements. Since only the peak at 121.8 keV had been considered for the estimation of the activity. Taking to account the other energies associated with ¹⁵²Eu could improve the accuracy of the measurement and lead to better estimation of $\log_{10} K_{s,0}^0$. Thus, this investigation discharge that $\log_{10} K_{s,0}^0$ of Eu_{0.012}Nd_{0.988}PO₄·0.667H₂O doped with ¹⁵²Eu belongs to a dissolution of pure EuPO₄·0.667H₂O. In addition, this investigation proved that regardless of the mass used in the dissolution experiments, it has not impact on the value of the solubility products. These results allow to conclude that this protocol can be applied for Pu-phosphate experiments where the amount of solid need to be reduced at least at 2 mg.

Table III.12. Elementary concentrations measured at the equilibrium, calculated molality of the predominant species, equilibrium constants form the predominant aqueous species ($\log_{10} {}^*K_s$) and standard solubility products obtained at $T=24\pm 1$ for the $\text{Eu}_{0.01}\text{Nd}_{0.99}\text{PO}_4\cdot 0.667\text{H}_2\text{O}$ in 0.1 M HCl and $\text{Eu}_{0.012}\text{Nd}_{0.988}\text{PO}_4\cdot 0.667\text{H}_2\text{O}$ with ^{152}Eu in 0.15 M HCl at different amount of solid

Mass (mg)	C_{Nd} M	C_{Eu} M	C_{P} M	$m_{\text{Nd}^{3+}}$ [m]	$m_{\text{H}_3\text{PO}_4}$ m	$\log_{10} {}^*K_s$	(Nd^{3+})	(H_3PO_4)	$\log_{10} {}^*K_{s,0}^0$	$\log_{10} K_{s,0}^0$	$\Delta_r G^\circ$ kJ mol $^{-1}$
$\text{Eu}_{0.01}\text{Nd}_{0.99}\text{PO}_4\cdot 0.667\text{H}_2\text{O}$ (pH=0.993, $\rho_{(\text{HCl})}=0.9989$ kg L$^{-1}$)											
50.2	6.30×10^{-4}	7.86×10^{-6}	6.51×10^{-4}	6.31×10^{-4}	1.32×10^{-3}	-3.32 ± 0.29	6.31×10^{-4}	1.32×10^{-3}	-3.61 ± 0.29	-25.11 ± 0.29	144.5 ± 7.4
$\text{Eu}_{0.012}\text{Nd}_{0.988}\text{PO}_4\cdot 0.667\text{H}_2\text{O}$ doped with ^{152}Eu (pH=0.82)											
50.1	1.28×10^{-3}	1.56×10^{-5}	1.30×10^{-3}	1.27×10^{-3}	2.60×10^{-3}	-3.00 ± 0.28	1.27×10^{-3}	2.60×10^{-3}	-3.00 ± 0.28	-24.71 ± 0.30	141.0 ± 7.2
11.3	1.38×10^{-3}	1.67×10^{-5}	1.39×10^{-3}	1.36×10^{-3}	2.79×10^{-3}	-2.94 ± 0.38	1.36×10^{-3}	2.79×10^{-3}	-2.94 ± 0.28	-24.65 ± 0.28	140.7 ± 7.2
6.9	1.09×10^{-3}	1.32×10^{-5}	1.10×10^{-3}	1.06×10^{-3}	2.17×10^{-3}	-3.16 ± 0.30	1.06×10^{-3}	2.17×10^{-3}	-3.16 ± 0.30	-24.86 ± 0.30	141.9 ± 7.2
5.5	1.13×10^{-3}	1.37×10^{-5}	1.14×10^{-3}	1.11×10^{-3}	2.26×10^{-3}	-3.12 ± 0.29	1.10×10^{-3}	2.26×10^{-3}	-3.12 ± 0.29	-24.83 ± 0.29	141.7 ± 7.2
2.2	1.12×10^{-3}	1.37×10^{-5}	1.14×10^{-3}	1.12×10^{-3}	2.30×10^{-3}	-3.11 ± 0.29	1.12×10^{-3}	2.30×10^{-3}	-3.11 ± 0.29	-24.81 ± 0.29	141.6 ± 7.2
1.8	1.07×10^{-3}	1.30×10^{-5}	1.09×10^{-3}	1.07×10^{-3}	2.20×10^{-3}	-3.15 ± 0.30	1.07×10^{-3}	2.20×10^{-3}	-3.15 ± 0.30	-24.85 ± 0.30	141.9 ± 7.2

III.2.3. Preliminary study in PuPO₄ monazite

III.2.3.1 Characterization

In order to apply the protocol developed in the previous section, Pu(III)-based rhabdophane was firstly synthesized by Paul ESTEVENON and Thomas DUMAS at CEA-Marcoule as described in **Chapter II**. Unfortunately, the powder obtained had a color blue which suggested a partial oxidation of Pu(III) to Pu(IV). With the aim to get pure Pu(III) a thermal treatment at 1100°C in argon flow was performed leading to formation of PuPO₄ monazite. Therefore, the characterization and dissolution experiments were performed with a monazite phase.

The solid was characterized by XRD confirming monazite phase and the cell parameters derived from X-Ray patterns (**Figure III.21**) are listed in **Table III.13** with data available in the literature. One could notice a remarkable consistency in the parameters determined, although the synthesis process was not strictly identical.

Table III.13. Cell parameters of PuPO₄ synthesized in the present work and data available in the literature

a (Å)	b (Å)	c (Å)	β (deg)	Volume (Å ³)	Reference
6.754(1)	6.981(1)	6.453(1)	103.63(1)	295.68	This work
6.76	6.98	6.44	103.66	295.27	[37]
6.759(1)	6.980(1)	6.447(1)	103.63(1)	295.6	[38]

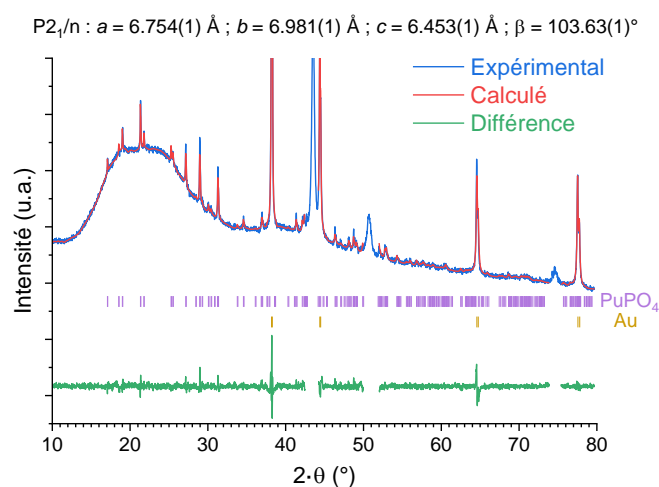


Figure III.21. X-Ray diffraction pattern of PuPO₄ monazite (experimental, calculated patterns and the difference between them are plotted)

The FTIR spectra recorded for PuPO_4 monazite is presented in **Figure III.22**. No bands associated with structural water vibrations were observed in the region $3000\text{-}1620\text{ cm}^{-1}$. Monazite structures present bands mainly in the region from 1200 to 500 cm^{-1} . The antisymmetric stretching mode $\nu_{\text{as}}(\text{PO}_4)$ is located at 1125 , 1084 and 1005 cm^{-1} and the symmetric stretching mode $\nu_{\text{s}}(\text{PO}_4)$ at 987 and 949 cm^{-1} . Then, bending mode is located $\delta_{\text{as}}(\text{PO}_4)$ at 611 cm^{-1} [28]. These bands confirm the good agreement with monazite structure.

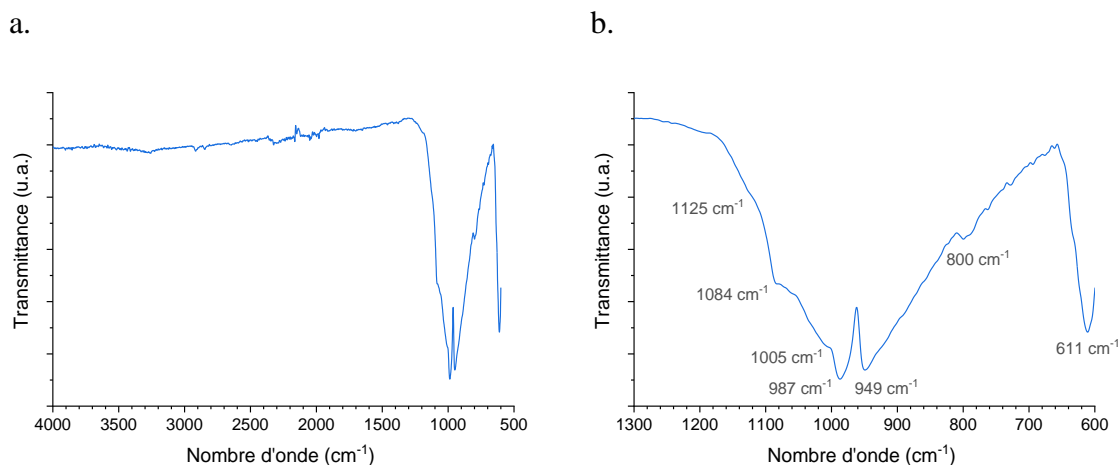


Figure III.22. FTIR spectra recorded for PuPO_4 monazite

III.2.3.1 Dissolution

The monazite PuPO_4 has been contacted during 4 to 6 months with de-aerated solutions whose composition is specified in **Table III.14**. Unlike studies performed with rhabdophane compounds, the solubility of PuPO_4 was also investigated in the presence of phosphate in the dissolution solution, in the same way as Rai *et al.*,^[39]. The aim of adding phosphate was to get information on the formation constant of phosphate complexes of Pu(III) in addition to the solubility in hydrochloric medium.

Table III.14. Composition of the solutions used for PuPO_4 dissolution studies (HA stands for hydroxylammonium hydrochloride $\text{NH}_2\text{OH}\cdot\text{HCl}$)

	$C_{\text{NaH}_2\text{PO}_4}$ (M)	C_{HA} (M)	C_{HCl} (M)	pH
S1	4×10^{-4}	10^{-3}	1.57×10^{-2}	2
S2	3×10^{-3}	10^{-3}	1.77×10^{-2}	2
S3	2×10^{-2}	10^{-3}	2.47×10^{-2}	2
S4	0.1	10^{-3}	6.14×10^{-2}	2
S5	0.5	10^{-3}	1.99×10^{-1}	2
S6	-	10^{-3}	0.1	1
S7	-	10^{-3}	0.01	2

UV Vis absorption spectra of centrifuged supernatants have been registered using the UV-Vis-NIR spectrophotometer UV-3100 from Shimadzu (nuclearized device, no optical fiber). For each sample, the baseline has been measured on the corresponding electrolyte. The absorption spectrum of the supernatant in 0.1 M HCl is illustrated in **Figure III.23**. Although the spectrum is extremely noisy one can identify the characteristic absorption fingerprint of Pu(III): bands at 561 and 601 nm ($\epsilon = 38 \text{ M}^{-1} \text{ cm}^{-1}$ in 1 M HClO_4 1M) and a less intense band at 665 nm ^[40].

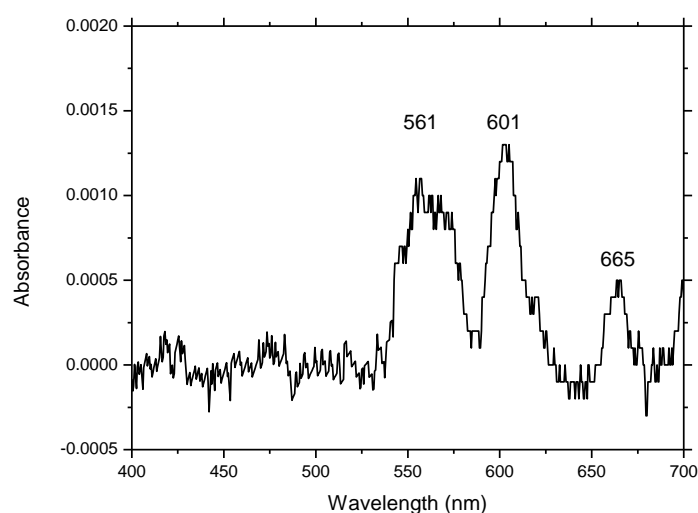


Figure III.23. Absorption spectra of the supernatant obtained from dissolution of PuPO_4 in 0.1 M HCl in the presence of 10^{-3} M $\text{NH}_2\text{OH}\cdot\text{HCl}$.

But the presence of higher oxidation states could not be detected. Obviously, the detection limit of the technique is not appropriate for speciation study of Pu in the supernatant. In the following, only the possible presence of Pu(IV) has been considered. The presence of hydroxylammonium hydrochloride (HA) and the use of de-aerated solutions indeed do not favour the formation of Pu(V) and Pu(VI). Concerning all samples at pH 2, no absorption bands could be observed, plutonium concentration being lower than the detection limit estimated to 2×10^{-4} M in Pu(III) and 10^{-5} M in Pu(IV).

Analysis of the supernatants have thus been conducted using radiometric techniques: PERALS and alpha spectrometry. The latter allows the quantification of the total plutonium. But PERALS that combines liquid-liquid extraction (chemical separation) and liquid scintillation (activity measurement), allows in principle to perform a selective determination of Pu(III).

The extractant in the scintillator cocktail ALPHAEX is HDEHP: an extraction at pH 3 favours a quantitative extraction of trivalent actinides, whereas in more acidic media, An(IV) are extracted from nitric acid solution [41, 42]. However, in the present work, de-aerated HCl containing HA, instead of HNO₃, has been used for dilution of the aliquots of supernatants in order to limit Pu(III) oxidation. According to Dacheux *et al.* extraction of trivalent actinides by ALPHAEX is quantitative from HNO₃ as well as HCl if pH is higher than 2.4 [42, 43]. In more acidic media, extraction efficiency of An(IV) remains close to 100% in HNO₃ but much lower in HCl [42].

A PERALS spectrum obtained after an extraction at pH 3 is presented in **Figure III.24**. This spectra is characterized by a broad peak and a shoulder. According to the isotopic composition and to the nuclear characteristics of radionuclides in PuPO₄ (**Table III.15**) and due to the poor energy resolution of PERALS (200-350 keV), the peak at channel 350 can be related to the energy of the main α -ray of ²³⁹Pu and ²⁴⁰Pu (5.157 and 5.168 MeV respectively). The shoulder can be attributed to ²³⁸Pu and also to ²⁴¹Am, a trivalent actinide that follows Pu(III) during extraction for the two pH values [44, 45]. A deconvolution procedure has been conducted to determine the absolute activity in ²³⁹Pu + ²⁴⁰Pu. But the net area in ²³⁸Pu cannot determine due to the overlapping of the peaks of ²³⁸Pu and ²⁴¹Am [40]. Results are reported in **Table III.16**.

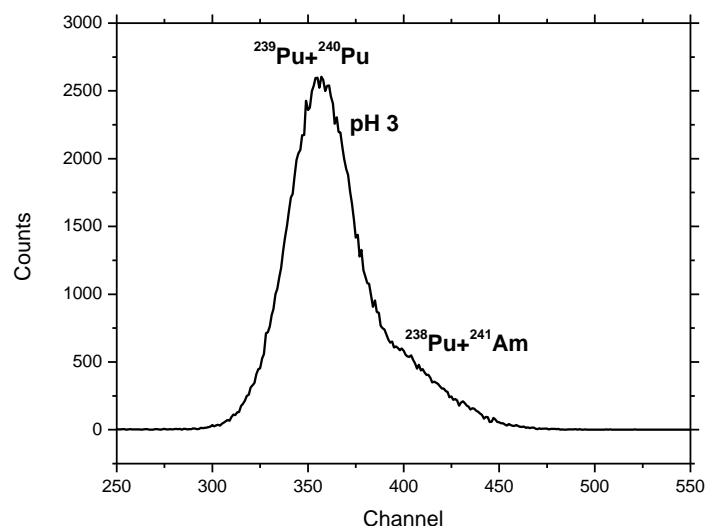


Figure III.24. PERALS spectra of the supernatant obtained from the dissolution of PuPO_4 in the mixture $4 \times 10^{-4} \text{ M NaH}_2\text{PO}_4$, 10^{-3} M HA and $1.57 \times 10^{-2} \text{ M HCl}$ (Counting time: 2000 s).

Table III.15. Isotopic composition of plutonium and nuclear characteristics of each isotope ^[46]

Isotope	%	Half-life (y)	Energy of the main alpha emission in MeV (emission %)
^{238}Pu (α)	0.040	87.74	5.499 (70.9) 5.456 (29.0)
^{239}Pu (α)	95.770	24090	5.157 (73.1) 5.144 (15.0) 5.105 (11.8)
^{240}Pu (α)	3.701	6563	5.168 (73.0) 5.124 (27.0)
^{241}Pu (β^- , α)	0.143	14.35	4.896 (83.2) 4.853 (12.2)
^{242}Pu (α)	0.350	376300	4.900 1 (77.5) 4.856 (22.4)
^{241}Am (α)	-	432.2	5.486 (84.0) 5.443 (13.1)

Table III.16. Alpha-measurements of Pu supernatant sampling

Sample	Counting time (s)	Counts in peak 1 $^{239}\text{Pu} + ^{240}\text{Pu}$	Counts in peak 2 $^{238}\text{Pu}(+^{241}\text{Am})$
Sample 1 pH 3	2000	103983 ± 845	26062 ± 881
Sample 2 pH 3	2000	37834 ± 559	29269 ± 612
Sample 3 pH3	4000	8879 ± 172	11812 ± 193
Sample 4 pH 3	4000	3450 ± 110	4104 ± 125
Sample 5 pH 3	2000	51738 ± 481	27158 ± 492

Unfortunately, alpha spectra recorded on the sources prepared by evaporation were of poor quality due to the presence of phosphate, except for sample 1. A procedure to remove phosphate is currently under study. A preliminary scheme about the PuPO_4 dissolution as a function of NaH_2PO_4 concentration is presented in **Figure III.25**. The experimental points indicates that the minimum of solubility is reached around $[\Sigma\text{PO}_4]=1.9\times 10^{-2}\text{ M}$, which is in a good agreement with the data reported by Rai *et. al.*,^[39] around $[\Sigma\text{PO}_4]=3\times 10^{-2}\text{ M}$ as shown in **Figure III.26**.

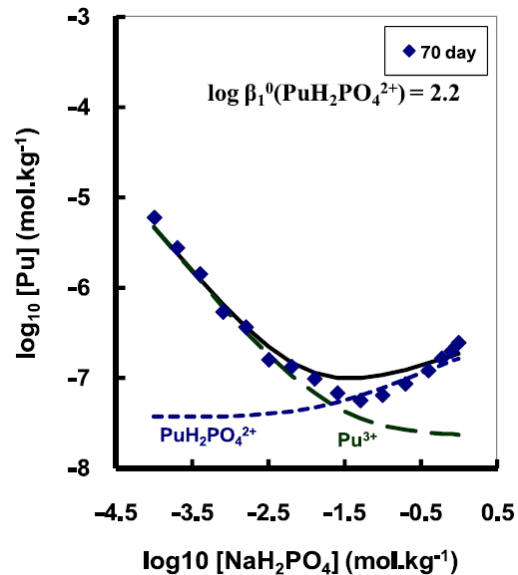
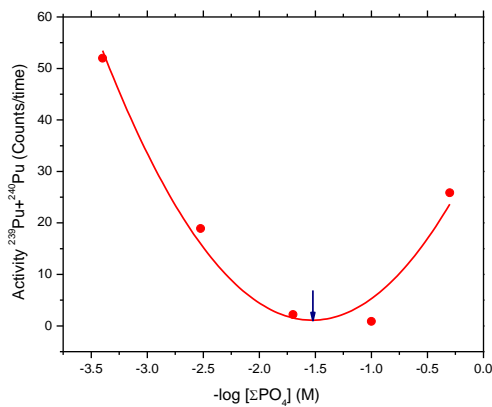


Figure III.25. PuPO_4 dissolution as a function of NaH_2PO_4 concentration obtained in this work ($4\times 10^{-4}\leq[\Sigma\text{PO}_4]\leq 0.5\text{ M}$, $1.57\times 10^{-2}\leq[\text{HCl}]\leq 1.99\times 10^{-1}$ in presence of $10^{-3}\text{ M NH}_2\text{OH HCl}$, $\text{pH}=2$ and $T=25^\circ\text{C}$)

Figure III.26. PuPO_4 dissolution as a function of NaH_2PO_4 concentration reported by Rai *et. al.*,^[39]

III.3. Conclusions and perspectives related to Ln(III)-phosphate systems

Due to the difficulties to manipulate plutonium, experimental protocols were developed with chemical analogs having stable oxidation state using Eu(III) and Nd(III) to simulate Pu(III) behavior. The study of the complexation followed two approaches: the determination of stability constants using very low concentration of Eu(III) to bypass the low solubility of the complexes and the second approach is the determination of solubility products at macro-amount of Nd(III) and Eu(III).

In homogeneous aqueous solution, the stability constants were determined by liquid-liquid extraction combined with γ -spectrometry using ^{152}Eu at trace scale and HDEHP as extractant. Complexes of maximum stoichiometry 1:3 have been identified in our experimental conditions. Firstly, the formation constants of two complexes $\text{Eu}(\text{H}_2\text{PO}_4)^{2+}$ and $\text{Eu}(\text{H}_2\text{PO}_4)_2^+$ were determined. The values obtained in our work, differ from one half of order of magnitude from data reported in the literature, but surprisingly, are close to the one of Gd and Cm. Then, the complexation constants of $\text{Eu}(\text{H}_2\text{PO}_4)_3^0$ complex was proposed for the first time. However results must take with caution since it was observed on a very narrow range of phosphate concentration. The protocol used with liquid-liquid extraction seems to be valid for further studies with Pu(III) in aqueous solution. However, performing liquid-liquid extraction experiments with Pu at tracer scale should include a step to avoid oxidation process.

In order to determine the solubility products of Pu(III)-phosphate solids, Nd-based rhabdophane were synthesized with 1% of Eu(III). After verifying that $\text{Eu}_{0.01}\text{Nd}_{0.99}\text{PO}_4 \cdot 0.667\text{H}_2\text{O}$ and the one with ^{152}Eu have similar dissolution behavior, a $\text{Eu}_{0.012}\text{Nd}_{0.988}\text{PO}_4 \cdot 0.667\text{H}_2\text{O}$ doped with ^{152}Eu were conducted with different masses of solid (from 50.1 to 1.8 mg) and different volumes of solution, keeping the mass-to-volume ratio constant. The solubility products obtained are very similar regardless of the mass employed. Thus, it allows concluding this protocol can be applied to low amount of solid for Pu experiments. Unfortunately, due to experimental difficulties in the synthesis of Pu rhabdophane, solubility experiments were performed using few mg of Pu(III) monazite. Dissolution experiments were performed in deaerated solutions of 0.1 M HCl with 10^{-3} M $\text{NH}_2\text{OH} \cdot \text{HCl}$. The analysis of the Pu concentration in solution are still in progress.

References

- [1] C. Jaussaud, Contribution a l'étude thermodynamique de l'hydrolyse de Pa(V) a l'échelle des traces par la technique d'extraction liquide-liquide avec la thenoyltrifluoroacetone (TTA). Ph.D Thesis, Orsay, France: Université Paris-Sud. U.F.R. Scientifique d'Orsay (2003).
- [2] S. Tsukahara, M. Fujiwara and H. Watarai, Ligand dissociation in the excited state of 2-thenoyltrifluoroacetone europium(III) ion in aqueous solution, *Chemistry Letters*, **29**, 412-413 (2000).
- [3] E. King and W. Reas, The hydration of thenoyltrifluoroacetone in benzene solution, *Journal of the American Chemical Society*, **73**, 1806-1808 (1951).
- [4] P. J. Elving and P. G. Grodzka, Thenoyltrifluoroacetone: Polarographic and spectrophotometric behavior, and dissociation equilibria. Mechanisms of electrolytic reduction, *Analytical Chemistry*, **33**, 2-11 (1961).
- [5] V. K. Manchanda and C. Allen Chang, Solvent extraction studies of lanthanum(III) and neodymium(III) with ionizable macrocyclic ligands and thenoyltrifluoroacetone, *Analytical Chemistry*, **58**, 2269-2275 (1986).
- [6] M. He, Complexation d'actinides et d'analogues par des ligands hydroxamates. Ph.D Thesis, Orsay, France: Université Paris Saclay (2019).
- [7] M. A. Lutoshkin, A. I. Petrov, Y. N. Mayar and A. S. Kazachenko, Interaction of rare-earth and some perfluorinated β -Diketones, *Inorganic Chemistry*, **60**, 3291-3304 (2021).
- [8] N. Ikeda, K. Kimura, H. Asai and N. Oshima, Extraction behavior of europium with thenoyltrifluoroacetone (TTA), *Radioisotopes*, **19**, 15-20 (1970).
- [9] P. Gans, A. Sabatini and A. Vacca, Investigation of equilibria in solution. Determination of equilibrium constants with the HYPERQUAD suite of programs, *Talanta*, **43**, 1739-1753 (1996).
- [10] P. Gans, A. Sabatini and A. Vacca, Determination of equilibrium constant from spectrophotometric data obtained from solutions of known pH: The program pHab, *Annali di Chimica*, **89**, 45-49 (1999).
- [11] J. Noro and T. Sekine, Solvent extraction of anionic chelate complexes of lanthanum(III), europium (III), lutetium (III), and indium (III) with 2-thenoyltrifluoroacetone as ion-pairs with tetrabutylammonium ions, *The Chemical Society of Japan*, **65**, 2729-2733 (1992).
- [12] V. Y. Buzco, I. V. Sukhno, L. D. Pettit and A. A. Polushin, Academic software, 2021. [Online]. Available: https://www.acadsoft.co.uk/aq_solutions.htm. [Accessed 13 12 2021].
- [13] N. Huittinen, I. Jessat, F. Réal, V. Vallet, S. Starke, M. Eibl and N. Jordan, Revisiting the complexation of Cm(III) with aqueous phosphates: What can we

- learn from the complex structures using luminiscence spectroscopy and Ab initio simulations, *Inorganic Chemistry*, **60**, 10656-10673 (2021).
- [14] N. Jordan, M. Demnitz, H. Lösch, S. Starke, V. Brendler and N. Huittinen, Complexation of trivalent lanthanides (Eu) and actinides (Cm) with aqueous phosphates at elevated temperatures, *Inorganic Chemistry*, **57**, 7015-7024 (2018).
- [15] I. A. Lebedev, V. Y. Frenkel, Y. M. Kulyako and B. F. Myasoedov, Investigation of the complex formation of americium (III) and americium (IV) in phosphoric acid solutions, *Soviet Radiochemistry*, **21**, 692-698 (1979).
- [16] A. Moskvin, Complex formation of the actinides with anions of acids in aqueous solutions, *Soviet Radiochemistry*, **11**, 447-449 (1969).
- [17] N. Jordan, T. Thoenen, S. Starke, K. Spahiu and B. Brendler, A critical review of the solution chemistry, solubility, and thermodynamics of europium: Recent advances on the Eu^{3+} aqua ion and the Eu(III) aqueous complexes and solid phases with the sulphate, chloride, and phosphate inorganic ligands, *Coordination Chemistry Reviews*, **473**, 214608 (2022).
- [18] X. Liu and R. H. Byrne, Rare earth and yttrium phosphate solubilities in aqueous solution, *Geochimica et Cosmochimica Acta*, **61**, 1625-1633 (1997).
- [19] L. S. Bingler and R. H. Byrne, Phosphate complexation of gadolinium(III) in aqueous solution, *Polyhedron*, **8**, 1315-1320 (1989).
- [20] H. Moll, V. Brendler and G. Bernhard, Aqueous curium (III) phosphate species characterized by time-resolved laser-induced fluorescence spectroscopy, *Radiochimica Acta*, **99**, 775-782 (2011).
- [21] V. K. Rao, G. R. Mahajan and P. R. Natarajan, Phosphate complexation of americium (III), *Radiochimica Acta*, **40**, 145-149 (1986).
- [22] R. M. Smith and A. E. Martell, Critical Stability Constants. Vol. 4: Inorganic Complexes, New York: Plenum Press (1976).
- [23] G. R. Choppin and A. Morgenstern, Thermodynamics of solvent extraction, *Solvent Extraction and Ion Exchange*, **18**, 1029-1049 (2000).
- [24] M. Mendes, S. Hamadi, C. Le Naour, J. Roques, A. Jeanson, C. Den Auwer, P. Moisy, S. Topin, J. Aupiais, C. Hennig and M. V. Di Giandomenico, Thermodynamical and structural study of protactinium(V) oxalate complexes, *Inorganic Chemistry*, **49**, 9962-9971 (2010).
- [25] C. Gausse, S. Szenknect, A. Meshbah, N. Clavier, S. Neumeier and N. Dacheux, Dissolution kinetics of monazite LnPO_4 (Ln=La to Gd): a multiparametric study, *Applied Geochemistry*, **93**, 81-93 (2018).
- [26] T. Y. Shvareva, J. B. Fein and A. Navrotsky, Thermodynamic properties of uranyl minerals: Constrains from calorimetry and solubility measurements,

Industrial and Engineering Chemistry Research, **51**, 607-613 (2012).

- [27] C. Gausse, S. Szenknect, D. W. Qin, A. Mesbah, N. Clavier, S. Neumeier, D. Bosbach and N. Dacheux, Determination of the solubility of rhabdophanes $\text{LnPO}_4 \cdot 0.667\text{H}_2\text{O}$ (Ln=La to Dy), *European Journal of Inorganic Chemistry*, **28**, 4615-4630 (2016).
- [28] N. Clavier, A. Meshbah, S. Szenknect and N. Dacheux, Monazite, rhabdophane, xenotime & churchite: Vibrational spectroscopy of gadolinium phosphate polymorphs, *Spectrochimica Acta Part A: Molecular and Biomolecular Spectroscopy*, **205**, 85-94 (2018).
- [29] J. Heuser, A. A. Bukaemskiy, S. Neumeier, A. Neumann and D. Bosbach, Raman and infrared spectroscopy of monazite-type ceramics used for nuclear waste conditioning, *Progress in Nuclear Energy*, **72**, 149-155 (2014).
- [30] P. V. Campos, A. R. L. Albuquerque, R. S. Angélica and S. P. A. Paz, FTIR spectral signatures of amazon inorganic phosphates: Igneous weathering, and biogenetic origin, *Spectrochimica Acta Part A: Molecular and Biomolecular Spectroscopy*, **251**, 1-12 (2021).
- [31] L. Berzina-Cimdina and N. Borodajenko, Infrared Spectroscopy-Materials Science, Engineering and Technology, *Materials Science, Engineering and Technology*, **12**, 251–263 (2012).
- [32] A. Meshbah, N. Clavier, E. Elkaim, C. Gausse, I. B. Kacem, S. Szenknect and N. Dacheux, Monoclinic form of the rhabdophane compounds: $\text{REEPO}_4 \cdot 0.667\text{H}_2\text{O}$, *Crystal growth and design*, **14**, 5090-5098 (2014).
- [33] M. R. Rafiuddin and A. P. Grosvenor, A structural investigation of hydrous and anhydrous rare-earth phosphates, *Inorganic Chemistry*, **55**, 9685-9695 (2016).
- [34] A. Mesbah, N. Clavier, E. Elkaim, S. Szenknect and N. Dacheux, In pursuit of the rhabdophane crystal structure: from the hydrated monoclinic $\text{LnPO}_4 \cdot 0.667\text{H}_2\text{O}$ to the hexagonal LnPO_4 (Ln = Nd, Sm, Gd, Eu and Dy), *Journal of Solid State Chemistry*, **249**, 221-227 (2017).
- [35] A. Shelyug, A. Mesbah, S. Szenknect, N. Clavier, N. Dacheux and A. Navrotsky, Thermodynamics and stability of rhabdophanes, hydrated rare earth phosphates $\text{REPO}_4 \cdot n\text{H}_2\text{O}$, *Frontiers in Chemistry*, **6**, 1-11 (2018).
- [36] R. G. Jonasson, DTA Study of the rhabdophane to monazite transformation in rare earth (La-Dy) phosphate, *Thermochimica Acta*, **108**, 65-72 (1986).
- [37] D. Bregiroux, R. Belin, P. Valenza, F. Audubert and D. Bernache-Assollant, Plutonium and americium monazite materials: Solid state synthesis and X-ray diffraction study, *Journal of Nuclear Materials*, **366**, 52–57 (2007).
- [38] K. Popa, P. E. Raison, L. Martel, P. M. Martin, D. Prieur, P. L. Solari, D. Bouëxière, R. J. M. Konings and J. Somers, Structural investigations of PuIII phosphate by X-ray diffraction, MAS-NMR and XANES spectroscopy, *Journal*

of *Solid State Chemistry*, **230**, 169-174 (2015).

- [39] D. Rai, D. A. Moore, A. R. Felmy, K. M. Rosso and H. Bolton Jr, PuPO₄ (cr, hyd.) Solubility product and Pu³⁺ complexes with phosphate and ethylenediaminetetraacetic acid, *Journal of Solution Chemistry*, **39**, 778-807 (2010).
- [40] D. L. Clark, S. S. Hecker, G. D. Jarvinen and M. P. Neu, Plutonium, *The chemistry of the actinide and transactinide elements*, vol. 2, Netherlands, Springer, **2**, 813-1264 (2010)
- [41] G. H. Coleman, The Radiochemistry of Plutonium, NSA-NS 358, Washington D. C: National Research Council, (1965).
- [42] N. Dacheux and J. Aupiais, Determination of uranium, thorium, plutonium, americium, and curium ultratraces by photon electron rejecting a liquid scintillation, *Analytical Chemistry*, **69**, 2275-2282 (1997).
- [43] N. Dacheux and J. Aupiais, Determination of low concentrations of americium and curium by photon/electron rejecting alpha liquid scintillation, *Analytica Chimica Acta*, **363**, 279-294 (1998).
- [44] J. R. Cadieux, S. Clark, R. A. Fjeld, S. Reboul and A. Sowder, Measurement of actinides in environmental samples by photon-electron rejecting alpha liquid scintillation, *Nuclear Instruments and Methods in Physics Research A*, **353**, 534-538 (1994).
- [45] M. Ayranov, L. Wacker and U. Krähenbühl, Plutonium separation by solvent extraction for the determination by photon electron rejecting alpha liquid spectrometry, *Radiochimica Acta*, **90**, 199-204 (2002).
- [46] W. Westmeier and A. Merklin, Catalog of alpha particles from radioactive decay, FRG-84-13714, Karlsruhe : Fachinformationszentrum Energie Physik Mathematik GmbH, 1-88 (1985)

Chapter IV

Systems An(VI)-phosphate

IV. System An(VI)-phosphate

The present chapter is devoted on the thermodynamic study of the complexation of uranium (VI) with phosphoric acid as well as EXAFS data on the U (VI)-phosphate complexes of maximum stoichiometry, with the aim of developing a protocol appropriate for Pu(VI).

IV.1. Study of the complexation of uranium(VI) with phosphoric acid by UV-Vis spectrophotometry

In order to develop an experimental protocol to study plutonium (VI)-phosphate interaction, we study the complexation of uranium (VI) in acidic media using UV-Vis absorption spectrophotometry. An additional experiment using x-ray absorption spectroscopy has also been conducted to get information about the coordination of uranium in the uranium(VI)-phosphate complex with a stoichiometry 1:2.

IV.1.1. Uranium(VI) in 1 M HClO₄ media

Due to the low solubility of U(VI) phosphate compounds, a compromise has to be found regarding the uranium concentration: sufficiently high to be quantified by UV-Vis spectrophotometry, and low enough to avoid precipitation. UV-Vis absorption spectra were registered at uranium (VI) concentration ranging from 1.74 to 17.5 mM in 1 M HClO₄ and at T=20°C. Experimental details are presented in **Chapter II**. These spectra were recorded in the visible range from 480 nm to 350 nm. The maximum absorption band is found at 413.8 nm, as can see in **Figure IV.1**, which is the same position reported by Meinrath ^[1]. **Figure IV.2** presents the variation of the absorbance at $\lambda_{\text{max}}=413.8$ nm according to the concentration of U(VI). The variation of the absorbance follows a linear trend, which confirms the use of the Lambert-Beer Law in the concentration range studied. From the linear regression of the absorbance vs. the concentration of U(VI), the molar absorption coefficient, ϵ , of U(VI) at I= 1 M HClO₄ can be determined and is equal to $10.69 \pm 0.23 \text{ M}^{-1} \text{ cm}^{-1}$. This value is close to $9.70 \pm 0.02 \text{ M}^{-1} \text{ cm}^{-1}$ reported by Meinrath ^[1] obtained at the same wavelength in the same medium.

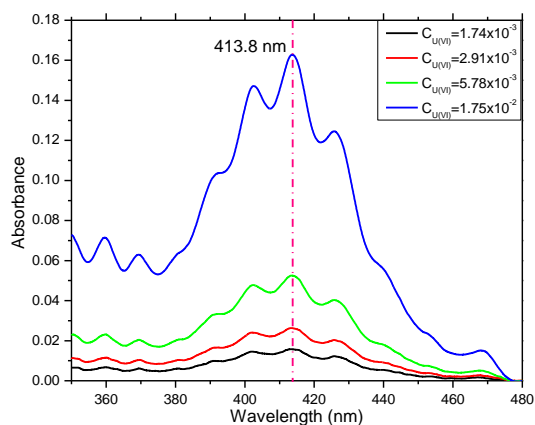


Figure IV.1. Absorption spectra of U(VI) at different concentration ($I=1\text{ M HClO}_4$)

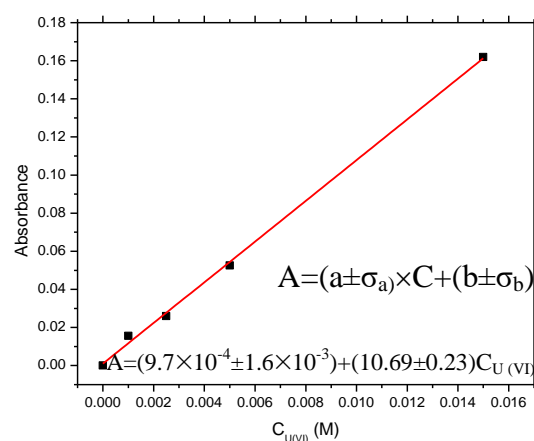


Figure IV.2. Evolution of the absorbance as a function of $C_{U(VI)}$ ($\lambda_{max}=413.8\text{ nm}$, $1.74 \times 10^{-3}\text{ M} \leq C_{U(VI)} \leq 1.75 \times 10^{-2}\text{ M}$, $I=1\text{ M HClO}_4$)

In order to find the lowest concentration that can be measured, the limit of detection (LOD) and quantification (LOQ) were determined according to equations **IV.1** and **IV.2** [2], where σ_a and σ_b are the standard deviation of the slope (ϵ) and intercept obtained from the linear regression of the absorbance vs. the concentration of U(VI). In our experimental conditions LOD is 0.45 mM and LOQ is 1.55 mM. The complexation study in this work was performed at two uranium concentrations: 5.22 and 7 mM.

$$LOD = \frac{3\sigma_b}{a} \quad \text{IV.1}$$

$$LOQ = \frac{10\sigma_b}{a} \quad \text{IV.2}$$

IV.1.2. Stability of U(VI)-phosphate complexes

Since Baes Jr. *et. al.*, [3] reported precipitation of U(VI)-phosphate compounds when working with a mixture of $\text{HClO}_4/\text{NaClO}_4$ at $I=1\text{ M}$ and $\text{pH}=1$, a preliminary study was performed to find optimal experimental conditions ensuring the use of homogeneous solutions. For that purpose, the stability was first studied in the same electrolyte that in Baes Jr.' study. This electrolyte is here called **electrolyte A**, and it is composed of 0.1 M HClO_4 and 0.9 M NaClO_4 . Then, three other electrolytes were also tested, either by decreasing the amount of NaClO_4 to bypass precipitation process, which is the case for **electrolyte B** (0.5 M $\text{HClO}_4/0.5\text{ M NaClO}_4$) and 1 M HClO_4 , or by decreasing the ionic strength with 0.1 M HClO_4 . The optimal conditions were determined by studying the

interaction of U(VI) with phosphates in the different electrolytes according to three criteria: formation of U(VI)-phosphate complexes, absence of precipitate and stability of the solutions over time.

From literature data, it is known that the complexation of uranium (VI) with phosphates leads to a red shift of the UV-Vis spectrum compared to the aquo species. This is what can be observed, for instance, in **Figure IV.3**. The figure shows the spectra of U(VI) aquo-ion and U(VI)-phosphate complex collected at ratio $\Sigma\text{PO}_4/\text{U}=40$. In presence of phosphate a shift at higher wavelength is observed and the intensity of the absorbance is higher. The maximum of absorbance is observed at 420 nm for the phosphate complex compared to 414 nm for the free uranyl. This behavior is an evidence of U(VI)-phosphate complexation in this medium.

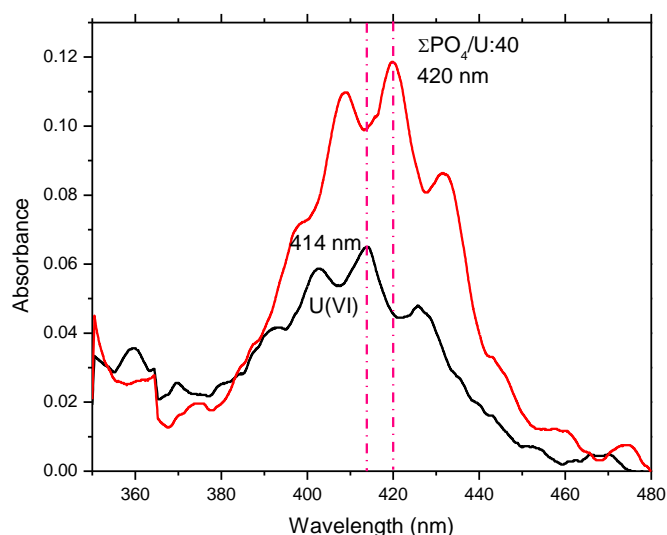


Figure IV.3. UV-Vis absorption spectra of U(VI) and U(VI)-phosphate in electrolyte A ($C_{\text{U(VI)}}=7 \times 10^{-3} \text{ M}$ and ratio $\Sigma\text{PO}_4/\text{U}=40$)

Considering first the **electrolyte A**, solutions at different ratio $\Sigma\text{PO}_4/\text{U}$: 1, 5, 7, 10, 20 and 40 were prepared to mimic conditions to study the complexation of uranium with phosphates. The stability of these solutions over time was followed by collecting the UV-Vis absorption spectra from them. Different behaviors were observed according to the ratio $\Sigma\text{PO}_4/\text{U}$. The equimolar sample, at ratio $\Sigma\text{PO}_4/\text{U}=1$, as presented in **Figure IV.4** is stable during the analysis time. However, no shift is observed on the spectrum of the sample. At higher ratio, for $\Sigma\text{PO}_4/\text{U}= 5-10$, even if a shift to higher wavelength is observed, fluctuations in the absorbance are observed over time, as illustrated in **Figure IV.5**, **Figure IV.6** and **Figure IV.7**, respectively. Then, at the highest ratio, $\Sigma\text{PO}_4/\text{U}=20$

and 40, the stability of the solutions seems better, as observed in **Figure IV.8** and **Figure IV.9**. However, after five hours of measurements, the solution in the cuvette had precipitates.

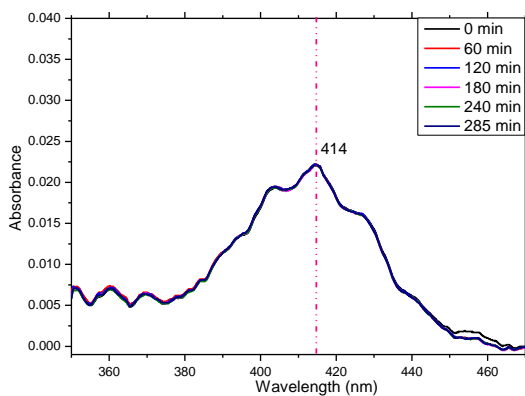


Figure IV.4. UV-Vis absorption spectra over the time of U(VI)-phosphate in electrolyte A at ratio 1:1.

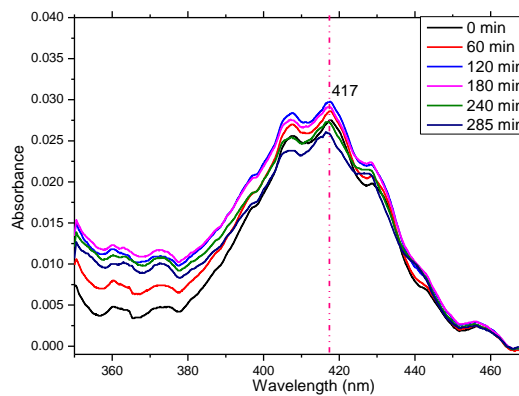


Figure IV.5. UV-Vis absorption spectra over the time of U(VI)-phosphate in electrolyte A at ratio 1:5.

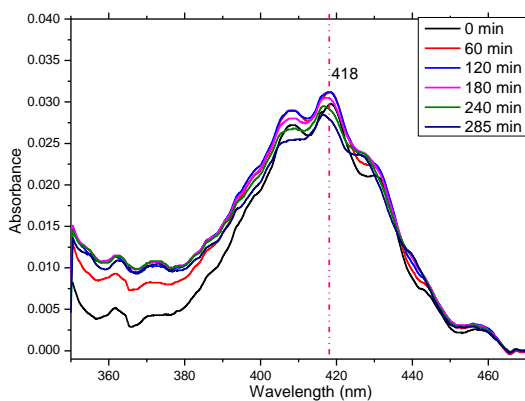


Figure IV.6. UV-Vis absorption spectra over the time of U(VI)-phosphate in electrolyte A at ratio 1:7.

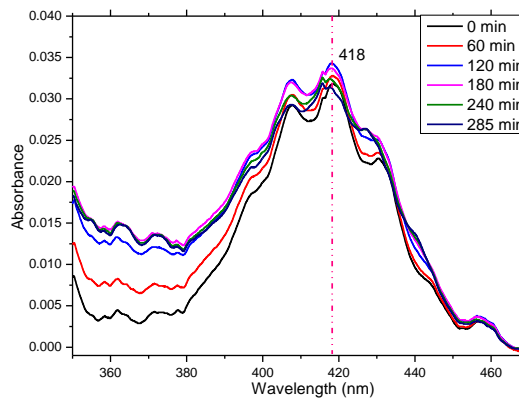


Figure IV.7. UV-Vis absorption spectra over the time of U(VI)-phosphate in electrolyte A at ratio 1:10.

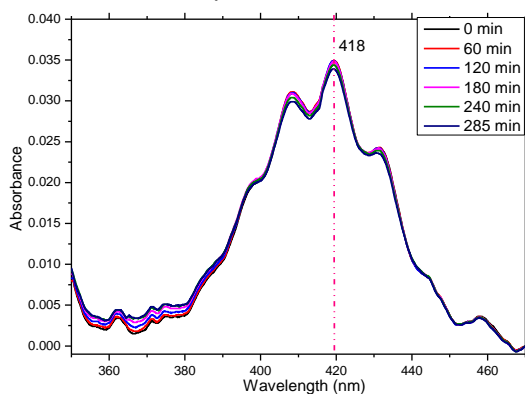


Figure IV.8. UV-Vis absorption spectra over the time of U(VI)-phosphate in electrolyte A at ratio 1:20.

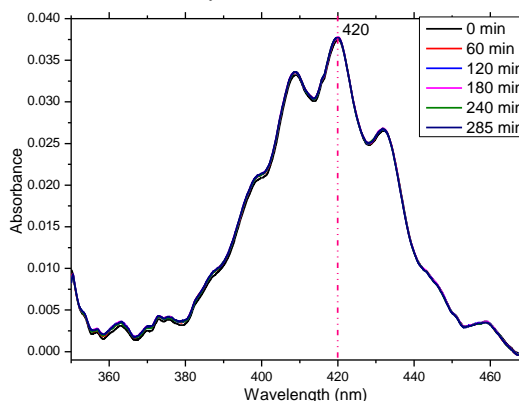


Figure IV.9. UV-Vis absorption spectra over the time of U(VI)-phosphate in electrolyte A at ratio 1:40.

Then, the samples were kept during 14 days. Visually, the solution of the samples at low ratio $\Sigma\text{PO}_4/\text{U}=0$ to 1 are cloudy. As the presence of phosphate increases, small amount of precipitates, with a light color, appears at the bottom of the tube (ratio $\Sigma\text{PO}_4/\text{U}=1$ to 20). This precipitate becomes more significant in the samples at ratio $\Sigma\text{PO}_4/\text{U}=20$ to 50. In order to better understand the phenomenon, solutions were centrifuged after 14 days, and supernatants were analyzed by UV-Vis spectrophotometry. The **Figure IV.10** corresponds to spectra of the solution at ratio $\Sigma\text{PO}_4/\text{U}=1$, showing a slight diminution in absorbance. This decrease is more evident when the ratio $\Sigma\text{PO}_4/\text{U}$ increases as illustrate in **Figure IV.11**. The decrease in absorbance is observed in all samples.

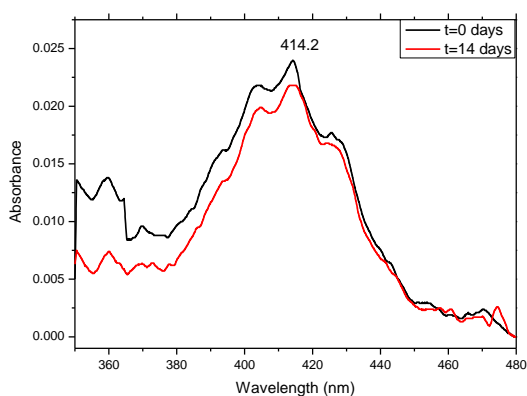


Figure IV.10. UV-Vis absorption spectra of U(VI)-phosphate in electrolyte A at ratio 1:1 registered at $t=0$ and 14 days of preparation.

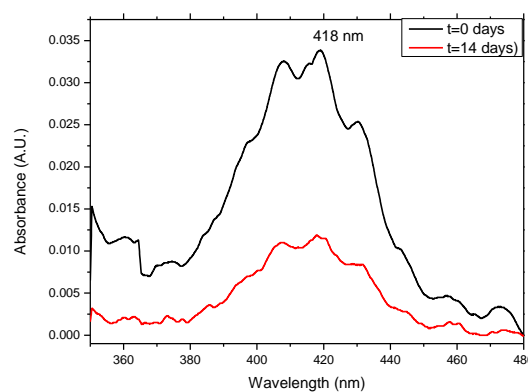


Figure IV.11. UV-Vis absorption spectra over the time of U(VI)-phosphate in electrolyte A at ratio 1:10.

From these results, it can be stated that the **electrolyte A** is not suitable to study the complexation of U(VI) with phosphates, according to our three initial criteria. Indeed, in those conditions, the solutions are not stable and are not homogeneous. The next step was then to perform the same study but with the three other electrolytes. Concerning the electrolytes 0.1 M HClO_4 , 1 M HClO_4 , and 0.5 M $\text{HClO}_4/0.5$ M NaClO_4 , the red shift due to the complexation of uranium with phosphates could be observed, and no changes were observed in the spectra overtime demonstrating the stability of the solutions whatever the ratio $\Sigma\text{PO}_4/\text{U}$. Moreover, no precipitates were observed in the solutions during the study.

The presence of precipitates was observed only in **electrolyte A**, which differs from the other electrolytes only by the concentration of NaClO₄ for the electrolyte 0.1 M HClO₄, but also by the pH for the others. In this electrolyte, the concentration of NaClO₄ is the highest (0.9 M). One hypothesis could be that Na⁺ plays a role in the precipitation. Baes Jr. *et al.*,^[3] did not mention any interaction with sodium, and assigned the formation of precipitates to UO₂HPO₄·4H₂O(cr) when the sum of the analytical concentrations of UO₂(ClO₄)₂-H₃PO₄ is higher than 0.14 M. However, other studies seem to indicate the influence of Na⁺. For instance, Weger and Reed, indicated that for solutions with sufficiently high Na⁺ concentration and low H⁺, UO₂(HPO₄)_m would be expected to precipitate as UO₂(NaPO₄)_m^[4]. A more recent study performed by Mehta *et al.*,^[5] prepared a U(VI)-phosphate solid with C_{U(VI)}=5×10⁻³ M and ΣPO₄/U=10 in NaNO₃/NaHCO₃ solutions. The author suggested that for solutions with Na⁺, the addition of phosphate induced the precipitation of sodium autunite Na₂(UO₂)₂(PO₄)₂ regardless of the pH conditions. According to Mehta *et al.*,^[5] Na⁺ is structurally incorporated into the U(VI)-phosphate complex making heavier gel and promoting the precipitation as observed in our experimental conditions.

In order to bypass the formation of precipitates due to the presence of Na⁺, This investigation study the U(VI)-phosphate complexation at low pH and two electrolytes were selected, 1 M HClO₄, and 0.5 M HClO₄/0.5 M NaClO₄ media, which demonstrate to be stable over the time.

IV.1.3. Complexation of U(VI) with phosphate in 1 M HClO₄, and electrolyte B

The study of the complexation of U(VI)-phosphate was performed in the two media selected previously. For that purpose, the ratio ΣPO₄/U was varying from 0 to 20.

The **Figure IV.12** and **Figure IV.13** present the UV-Vis absorption spectra collected at fixed C_{U(VI)}=5.2×10⁻³ M in 1 M HClO₄ medium and C_{U(VI)}=7.1×10⁻³ M in **electrolyte B**. In both systems, the addition of phosphoric acid increases the absorption of U(VI), and the main band at 414 nm is shifted to 418 nm. This variation can be related to the formation of the U(VI)-phosphate complexes.

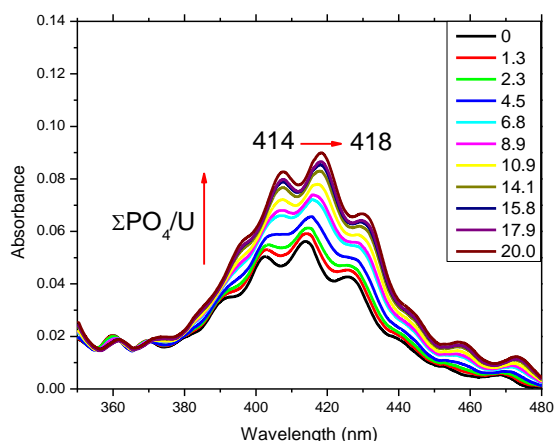


Figure IV.12. UV-Vis absorption spectra of U(VI)-phosphate system at $I= 1\text{ M}$ HClO_4 ($C_{U(VI)}=5.2 \times 10^{-3}\text{ M}$, $0 \leq \Sigma\text{PO}_4/\text{U(VI)} \leq 20$, $T=20^\circ\text{C}$)

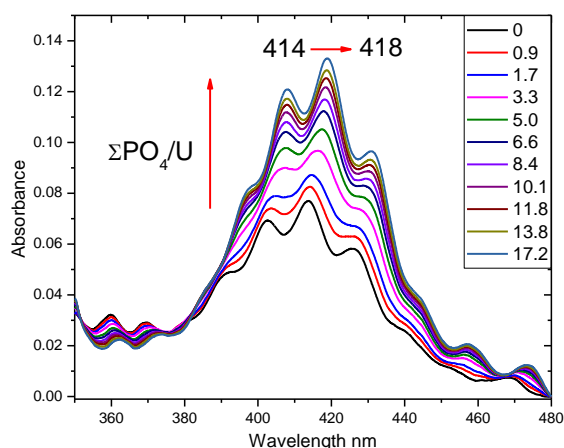


Figure IV.13. UV-Vis absorption spectra of U(VI)-phosphate system in electrolyte B ($C_{U(VI)}=7.1 \times 10^{-3}\text{ M}$, $0 \leq \Sigma\text{PO}_4/\text{U(VI)} \leq 20$, $T=20^\circ\text{C}$)

From these spectra, the stability constant of the U(VI)-phosphate complexes can be determined according to the following equilibrium:



In order to determine the corresponding stability constants from spectrophotometric data, the software HypSpec was used, assuming that the intensity of absorption of each species is proportional to its concentration in solution. In that way, the chemical species present in solution need to be defined, with other input data. These data are the dissociation constants of H_3PO_4 , the individual spectra corresponding to each ratio $\Sigma\text{PO}_4/\text{U}$ with the composition of each solution, and the equilibria considered. For the dissociation constants of H_3PO_4 , an ionic strength correction need first to be performed using the SIT method as explained in part II.2.1.

The data are then processed using HypSpec software, giving as output data the stability constants relative to equilibrium IV.3, as well as, individual spectra of species. From the Principal Component Analysis (PCA), it has been pinpointed that three species are present in the system, one of them being the aquo cation UO_2^{2+} (known data). On the basis of literature data, the two other species were assumed to be two uranium(VI)-phosphate complexes: $\text{UO}_2(\text{H}_2\text{PO}_4)^+$ and $\text{UO}_2(\text{H}_2\text{PO}_4)_2$. Figure IV.14 and Figure IV.15 show the individual spectra obtained from the refinement in both electrolytes. The

UO_2^{2+} aquo ion presents a maximum absorption band at 413.8 nm. Then, spectral shift were observed at 417.6 and 419.5 nm assigned to the species $\text{UO}_2(\text{H}_2\text{PO}_4)^+$ and $\text{UO}_2(\text{H}_2\text{PO}_4)_2$. The molar absorbance coefficient (ϵ) of the UO_2^{2+} aquo ion calculated by HypSpec software is around $10.71 \pm 0.06 \text{ M}^{-1} \text{ cm}^{-1}$ in 1 M HClO_4 and $10.83 \pm 0.08 \text{ M}^{-1} \text{ cm}^{-1}$ in electrolyte B. For $\text{UO}_2(\text{H}_2\text{PO}_4)^+$, ϵ slightly differ depending on the medium, 18.28 ± 0.18 in 1 M HClO_4 and 17.1 ± 0.1 in Electrolyte B. However, the variation is more significant for the complex $\text{UO}_2(\text{H}_2\text{PO}_4)_2$, with a higher ϵ in Electrolyte B, equal to 21.0 ± 0.1 , than 16.5 ± 0.3 for 1 M HClO_4 medium.

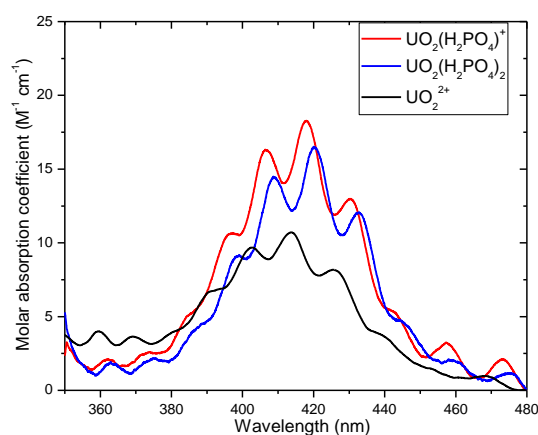


Figure IV.14. Molar absorption coefficient of UO_2^{2+} , $\text{UO}_2(\text{H}_2\text{PO}_4)^+$ and $\text{UO}_2(\text{H}_2\text{PO}_4)_2$ in 1 M HClO_4

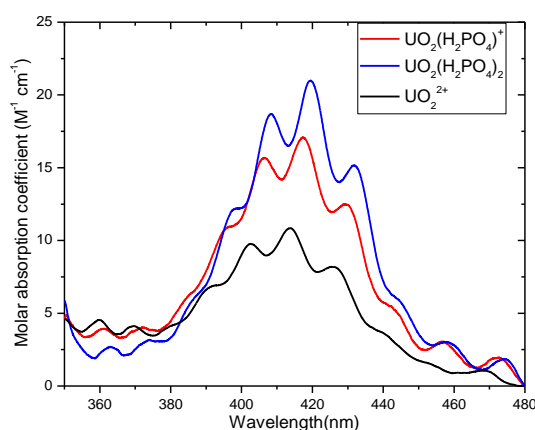


Figure IV.15. Molar absorption coefficient of UO_2^{2+} , $\text{UO}_2(\text{H}_2\text{PO}_4)^+$ and $\text{UO}_2(\text{H}_2\text{PO}_4)_2$ in 0.5M $\text{HClO}_4/0.5\text{M NaClO}_4$

For the purpose of comparison with literature, the constants associated to equation **IV.4** have been recalculated using the relationship:

$$\log \beta_i^H = \log \beta_i + i \times \log K_{a1} \quad \text{IV.4}$$

In order to correspond to equilibria in **Table I.16** involving H_3PO_4 as reactant. The recalculated values are reported in **Table IV.1** with the values of $\text{p}K_{a1}$ of H_3PO_4 that have been corrected to $I = 1 \text{ M}$ using the corresponding SIT coefficients and $\log_{10} K_{a1}^0$ available in NEA-TDB ^[6]. The uncertainty of our values comes from the error propagation from the calculations of the HypSpec software and the extrapolation of H_3PO_4 dissociation constants.

Table IV.1. Obtained stability constants for $UO_2(H_2PO_4)^+$ and $UO_2(H_2PO_4)_2$
(Equilibrium IV.3)

Medium	$\log_{10} \beta_1$	$\log_{10} \beta_2$	$\log_{10} \beta_1^H$	$\log_{10} \beta_2^H$	$\log_{10} K_{a1}$
1 M HClO ₄	2.83±0.06	5.18±0.11	0.96±0.02	1.44±0.03	-1.87±0.21
0.5 M HClO ₄ /0.5 M NaClO ₄	3.07±0.06	5.92±0.12	1.24±0.02	2.26±0.05	-1.83±0.28

High differences are observed in **Table IV.2** between the $\log_{10} \beta_i^H$ values obtained in 1 M HClO₄ and 0.5 M HClO₄/0.5 M NaClO₄. It suggested that the presence of Na⁺ seems to have an impact on the stability of 0.5 M HClO₄/0.5 M NaClO₄ medium. According to the studies performed by Baes Jr.^[3] and Mathur^[7], the $\log_{10} \beta_i^H$ values tends to be higher with increasing Na⁺ concentration in the solution. The stability constants $\log_{10} \beta_i^H$ obtained in this work and those reported in literature data are summarized in **Table IV.2**.

Table IV.2. Complexation constants according to equations in **Table I.16**.

Medium	$\log_{10} \beta_1^H$	$\log_{10} \beta_2^H$	T (°C)	Reference
1 M HClO ₄	0.96±0.02	1.44±0.03	20°C	This work
0.5 M HClO ₄ /0.5 M NaClO ₄	1.24±0.02	2.26±0.05	20°C	This work
1 M NaClO ₄	1.13±0.10 ^a	1.30±0.12 ^a	25°C	[7]
1.0 M HClO ₄ /NaClO ₄	0.72±0.04 ^b	0.41±0.10 ^b	25°C	[3]
1.06-1.07 M HClO ₄ /NaClO ₄	1.19±0.04 ^c		25°C	[8]

a. $\log \beta_i$ values taken from Mathur's work^[7] and recalculated using $\log K_{a1} = -1.81 \pm 0.16$ at 1 M NaClO₄ estimated in this work

b. $\log \beta_i^H$ recalculated at 1 M and 25°C by NEA-TDB^[6] based on the Baes Jr. 's work^[3]

c. $\log \beta_i^H$ recalculated at 1 M and 25°C by NEA-TDB^[6] based on the Thamer's work^[8].

IV.1.4. Temperature effect on the complexation of U(VI) with phosphate

UV-Vis absorption spectra have been registered at 30, 40, and 50°C on the same samples as those used in previous part. Samples were proved to be stable whatever the temperature. The spectra have been processed by HypSpec software in the same way as previously, using the acid dissociation constant of H₃PO₄ at the corresponding ionic

strength and temperature. Although all data have been obtained at the same ionic strength, differences are observed. In 1 M HClO₄, log β₁ and log β₂ seems to increase with the temperature. In contrast, with 0.5 M HClO₄/0.5 M NaClO₄ the temperature dependence of log β₁ and log β₂ is relatively small.

The stability constants obtained in the present work and the original data of Mathur^[7] are summarized in **Table IV.3**. In that case, the complexation constants correspond to equilibrium **IV.3**^[9]. Additionally, the presence of Na⁺ could also have an impact on the stability constants at different temperatures. The formation of ion pairs between Na⁺ and H₂PO₄⁻ can compete with the formation of [UO₂(H₂PO₄)_n]⁽²⁻ⁿ⁾⁺^[9, 10] decreasing the amount of available free H₂PO₄⁻ in solution. This competitive reaction could be more important in the work of Mathur^[7], performed at pH 2.5.

Table IV.3. Stability constant of U(VI)-phosphate complexes at different temperatures and 1 M HClO₄ and electrolyte B(0.5 M HClO₄/0.5 M NaClO₄)

T (°C)	1 M HClO ₄			0.5 M HClO ₄ /0.5 M NaClO ₄			1 M NaClO ₄ ^[7]		
	log ₁₀ β ₁	log ₁₀ β ₂	log ₁₀ K _{a1}	log ₁₀ β ₁	log ₁₀ β ₂	log ₁₀ K _{a1}	log ₁₀ β ₁	log ₁₀ β ₂	log ₁₀ K _{a1}
10	---	---	---	---	---	---	2.79±0.01	4.71±0.01	-1.64
20	2.83±0.06	5.18±0.11	-1.87±0.20	3.07±0.06	5.90±0.12	-1.83±0.28	---	---	---
25	---	---	---	---	---	---	2.94±0.02	4.93±0.02	-1.70±0.02
30	2.84±0.07	5.52±0.13	-1.92±0.21	3.14±0.06	5.92±0.11	-1.88±0.29	---	---	---
40	2.93±0.07	5.49±0.12	-1.96±0.22	3.19±0.06	6.02±0.11	-1.92±0.30	2.96±0.01	5.00±0.02	-1.77
50	3.94±0.05	6.95±0.11	-2.00±0.23	3.12±0.06	6.08±0.10	-1.96±0.31	2.99±0.03	5.11±0.01	-1.83

The variations of the constants $\log \beta_1$ and $\log \beta_2$ against $1/T$ are presented in **Figure IV.16** for the 1 M HClO_4 medium. It can be shown that the point at 50°C is out of the linear tendency, this can be attributed to either operating errors (preparation of samples, UV-Vis measurements, etc.) during the experiments, or to a ΔC_p not equal to zero. The linear variation from 20°C to 40°C allows the use of the simplified Van't Hoff equation ($\Delta C_p=0$). In this temperature range, $\log \beta_1$ seems to be athermic, and for $\log \beta_2$ a positive ΔH is observed which is related an endothermic formation reaction. In 0.5 M $\text{HClO}_4/0.5$ M NaClO_4 media the $\log \beta_1$ and $\log \beta_2$ vs $1/T$ plot in **Figure IV.17** indicates that the reactions for both complexes are athermic.

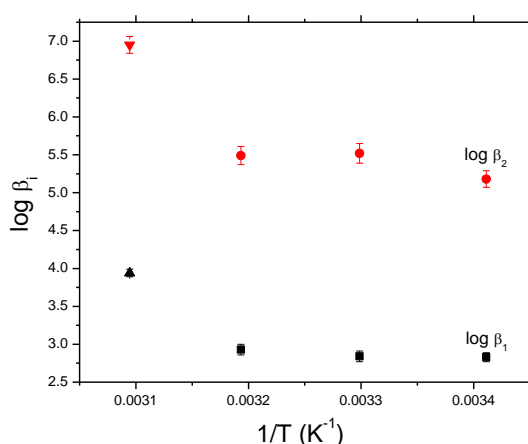


Figure IV.16. Variations of stability constant of $\text{UO}_2(\text{H}_2\text{PO}_4)^+$ and $\text{UO}_2(\text{H}_2\text{PO}_4)_2$ complexes as a function of inverse temperature at $I=1$ M HClO_4

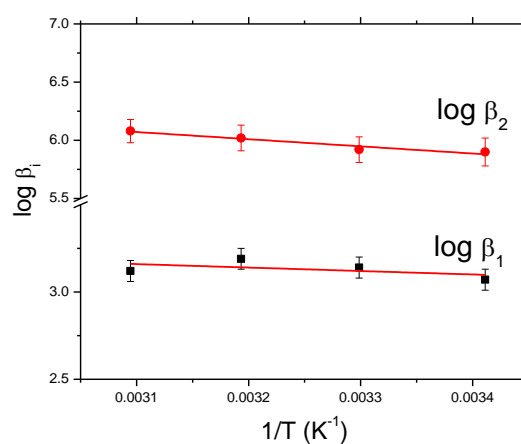


Figure IV.17. Variations of stability constant of $\text{UO}_2(\text{H}_2\text{PO}_4)^+$ and $\text{UO}_2(\text{H}_2\text{PO}_4)_2$ complexes as a function of inverse temperature at $I=0.5$ M $\text{HClO}_4/0.5$ M NaClO_4

The thermodynamic parameters ΔH , ΔS and ΔG for are summarized in **Table IV.4**. In 1 M HClO_4 medium, a positive enthalpy variations are obtained for the complexation of $\text{UO}_2(\text{H}_2\text{PO}_4)^+$ and $\text{UO}_2(\text{H}_2\text{PO}_4)_2$ indicates endothermic reactions with a large entropy contribution more energy is required to form complex 1:2. In case of 0.5 M $\text{HClO}_4/0.5$ M NaClO_4 medium, both complexes have a similar enthalpy indicates a slightly endothermic reactions and large positive entropy change, increasing the disorder in complex 1:2. In addition, the negative ΔG indicates that the reactions are spontaneous in the systems studied. Our thermodynamic parameters for $\text{UO}_2(\text{H}_2\text{PO}_4)^+$ in both media and the ones for $\text{UO}_2(\text{H}_2\text{PO}_4)_2$ in 0.5 M $\text{HClO}_4/0.5$ M NaClO_4 are similar with those

reported by Mathur ^[7]. However, the parameter estimated for $\text{UO}_2(\text{H}_2\text{PO}_4)_2$ in 1 M HClO_4 are larger than the ones in $I=0.5$ M $\text{HClO}_4/0.5$ M NaClO_4 and 1 M NaClO_4 . This difference can be attributed to the presence of sodium in the solution which competes with the formation of complex 1:2 and the formation of ion pairs between Na^+ and H_2PO_4^- decreasing the amount of available free H_2PO_4^- in solution^[9, 10].

Table IV.4. Thermodynamic parameters for $\text{UO}_2(\text{H}_2\text{PO}_4)^+$ and $\text{UO}_2(\text{H}_2\text{PO}_4)_2$ complexes at $T=25^\circ\text{C}$ in different media.

Parameter	1 M HClO_4		0.5 M $\text{HClO}_4/0.5$ M NaClO_4		1 M NaClO_4 ^[7]	
	$\log_{10} \beta_1$	$\log_{10} \beta_2$	$\log_{10} \beta_1$	$\log_{10} \beta_2$	$\log_{10} \beta_1$	$\log_{10} \beta_2$
ΔH (kJ mol^{-1})	8.5 ± 1.6^a	82 ± 31^a	10 ± 1^b	11 ± 1^b	9.5 ± 1.5^c	17 ± 1^c
ΔS ($\text{J K}^{-1}\text{mol}^{-1}$)	83 ± 6^a	376 ± 6^a	94 ± 2^b	150 ± 1^b	87 ± 6^c	151 ± 5^c
ΔG (kJ mol^{-1})	-34 ± 6^a	-31 ± 11^a	-38 ± 1^b	-33 ± 9^b	-33 ± 5^c	-27 ± 2^c

a. Values calculated for the range 20°C to 40°C in 1 M HClO_4

b. Values calculated for the range 20°C to 50°C in 0.5 M $\text{HClO}_4/0.5$ M NaClO_4

c. The thermodynamic parameters calculated for the range 10°C to 50°C using the $\log \beta_i$ values at $I=1$ M NaClO_4 reported by Mathur ^[7]

As a result of this work, from the stability constants obtained, we are able to propose a speciation diagram in our experimental conditions ($C_{\text{U(VI)}}=5.2 \times 10^{-3}$ or 7.1×10^{-3} M, $\Sigma\text{PO}_4/\text{U}=1$ to 20). **Figure IV.18** and **Figure IV.19** indicate that the three predominant species are UO_2^{2+} , $\text{UO}_2(\text{H}_2\text{PO}_4)^+$ and $\text{UO}_2(\text{H}_2\text{PO}_4)_2$ in both cases, but strong differences in their distribution between both media are observed. For U(VI)-phosphate complexation in 1 M HClO_4 media, as seen in **Figure IV.18**, the percentage of $\text{UO}_2(\text{H}_2\text{PO}_4)^+$ decrease as the temperature increases, opposite behavior for complex $\text{UO}_2(\text{H}_2\text{PO}_4)_2$. Nevertheless, the complex $\text{UO}_2(\text{H}_2\text{PO}_4)^+$ is formed at ratio $\Sigma\text{PO}_4/\text{U} < 10$ and then the complex $\text{UO}_2(\text{H}_2\text{PO}_4)_2$ appears at ratio $\Sigma\text{PO}_4/\text{U} > 10$. **Figure IV.19** showed the distribution of U(VI)-phosphate species in electrolyte B. The temperature effect is smaller; the curves follow mainly the same trend. The $\text{UO}_2(\text{H}_2\text{PO}_4)^+$ complex is formed

mainly at ratio $\Sigma\text{PO}_4/\text{U} < 5$ and as the presence of phosphate increase, $\text{UO}_2(\text{H}_2\text{PO}_4)_2$ appears.

These species were also determined by Kirishima *et al.*^[11], by studying the temperature effect on the U(VI)-phosphate complexation for samples at $C_{\text{U(VI)}} = 5 \times 10^{-5}$ M, $\text{pH} = 1$ and $I = 0.5$ M NaClO_4 . In this study, the first species formed is $\text{UO}_2(\text{H}_2\text{PO}_4)^+$ and as the concentration of phosphate increase the $\text{UO}_2(\text{H}_2\text{PO}_4)_2$ complex is formed. However, no significant variations occurred between 25°C and 100°C as illustrated in **Figure I.15** of the section **I.3.3.2.2**. This behavior supports our results and it suggests that the presence of Na^+ has also a strong impact at other temperatures.

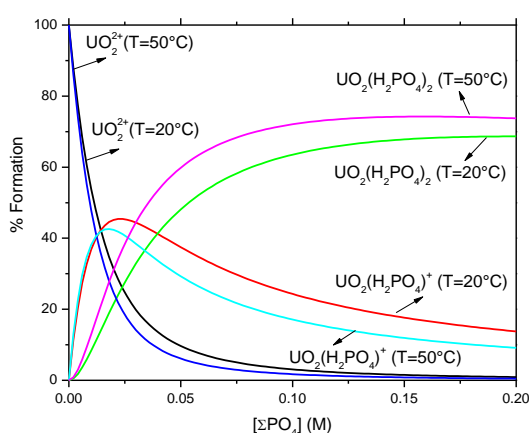


Figure IV.18. Speciation diagram of U(VI)-phosphate complexes in 1 M HClO_4 at $T = 20^\circ\text{C}$ and 50°C ($C_{\text{U(VI)}} = 5.2 \times 10^{-3}$ M, $\Sigma(\text{PO}_4)/\text{U} = 0$ to 20, $T = 20^\circ\text{C}$ and 50°C)

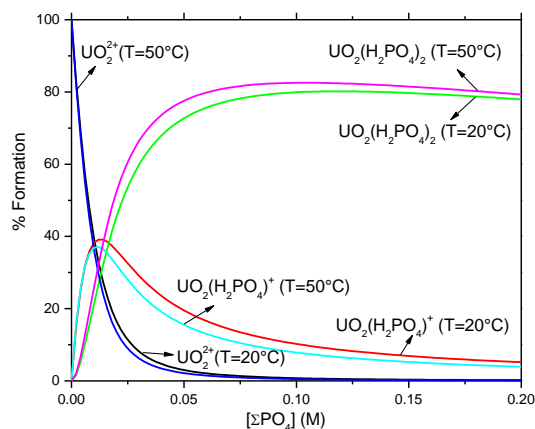


Figure IV.19. Speciation diagram of U(VI)-phosphate complexes in 0.5 M $\text{HClO}_4/0.5$ M NaClO_4 at $T = 20^\circ\text{C}$ and 50°C ($C_{\text{U(VI)}} = 7.1 \times 10^{-3}$ M, $\Sigma(\text{PO}_4)/\text{U} = 0$ to 20, $T = 20^\circ\text{C}$ and 50°C)

IV.1.5. Structural study of the complexation of $\text{UO}_2(\text{H}_2\text{PO}_4)_2$

The structure of the U(VI) complex in presence of 1 M phosphoric acid at pH 2 has been determined using X-ray absorption spectroscopy (XAS). In those conditions, the speciation of uranium(VI) expected in solution is the complex $\text{UO}_2(\text{H}_2\text{PO}_4)_2$ with a fraction of 94 % as illustrated in the speciation diagram in **Figure IV.20**.

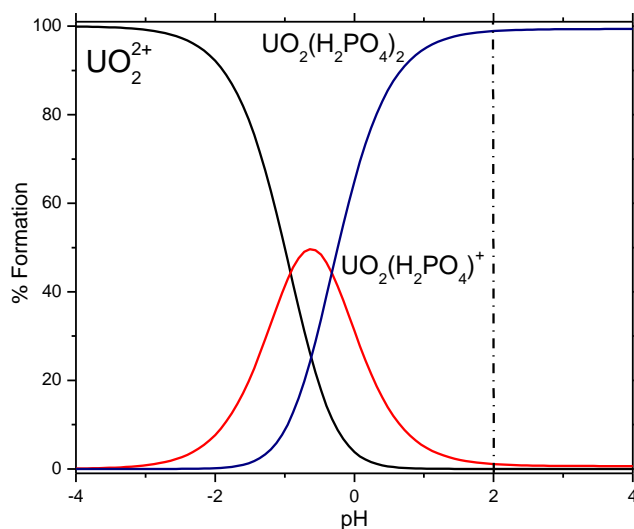


Figure IV.20. Speciation diagram of U(VI)-phosphate complexes calculated at standard conditions from stability constants determined in this work ($C_{U(VI)}=7\times 10^{-3}$ M, $[\Sigma PO_4]=1$ M, $T=25^\circ\text{C}$, $I=1$ M $HClO_4$)

To verify the stability over time of the sample in these conditions, the solution was analyzed by UV-Vis spectrophotometry during 12 days. The absorption spectra collected at different times after the preparation is presented in **Figure IV.21**, showing no significant variations even after 12 days. The same sample was analyzed by EXAFS, 8 days after the preparation. Thus, it was stable during the measurement.

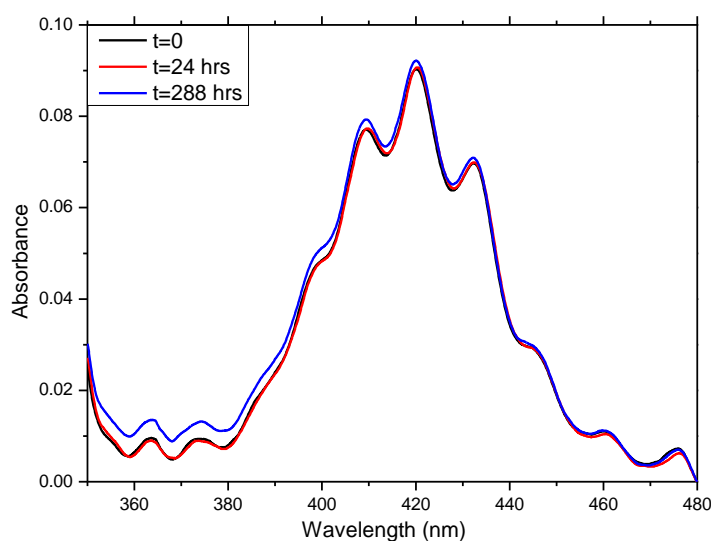


Figure IV.21. UV-Vis absorption spectra of $UO_2(H_2PO_4)_2$ ($C_{U(VI)}=7\times 10^{-3}$ M, $[\Sigma PO_4]=1$ M, $T=25^\circ\text{C}$)

The EXAFS spectrum, as well as its corresponding Fourier transform are presented in **Figure IV.22**. The Fourier transform of the EXAFS spectrum exhibits an intense peak at $R+\Phi \approx 1.3 \text{ \AA}$ (non-phase shift corrected distance), which is due to the contribution of the axial oxygen atoms. This contribution was fitted with two oxygen atoms at 1.76 \AA . The second peak, at around $R+\Phi \approx 1.9 \text{ \AA}$, corresponds to the equatorial oxygen atoms. The peak at $R+\Phi \approx 3 \text{ \AA}$ is due to backscattering from phosphorous atoms.

For the diphosphates complex, Jackson *et al.*,^[12] studied the geometry of the hydrated complexes, $\text{UO}_2(\text{H}_2\text{PO}_4)_2(\text{H}_2\text{O})_n$, with one to three water molecules by DFT calculations. They found out that whatever the number of water molecule, the coordination number for the equatorial oxygen is equal to five. The difference observed is about the coordination fashion of the phosphate groups. Thus, in presence of one water molecule, the bidentate coordination fashion of the phosphate groups is more prevalent and characterized by an average U-O(PO_4) and U-P distances around 2.40 \AA and 3.06 \AA respectively. For two water molecules, the uranium(VI) is coordinated to one bidentate and one monodentate H_2PO_4^- , whereas for three water molecules both are monodentate H_2PO_4^- . Monodentate coordination is featured in that case by a shorter U-O(PO_4) distance at $2.28\text{-}2.30 \text{ \AA}$, but a longer U-P distance equal to $\sim 3.60 \text{ \AA}$. All structures were used to fit the experimental data, but the best adjustment was found with the $\text{UO}_2(\text{H}_2\text{PO}_4)_2(\text{H}_2\text{O})_3$ structure.

The best fit parameters are reported in **Table IV.5**. The coordination sphere of the U(VI) is formed by the two axial oxygen atoms due to the actinyl moiety and by five oxygen atoms in the equatorial plane that are from both phosphate groups and water molecules. The U-O_{ax} distance is 1.76 \AA and the average U-O_{eq} is around 2.34 \AA . The coordination number of 5 around the uranyl moiety is in a good agreement with uranyl complexes under normal conditions with a coordination number around 4 and 6. The presence of a high Debye-Waller factor for this contribution, around 0.01 \AA^2 , features the presence of several oxygen distances. However, the radial resolution that can be obtained from this measurement ($\Delta R = \pi/2\Delta k \sim 0.15 \text{ \AA}$) prevents the distinction between the different oxygen shells. Then, the U-P distance is equal to 3.61 \AA

Table IV.5. EXAFS best fit parameters for the U(VI)-phosphate solutions at pH 2. s_0^2 is the EXAFS global amplitude factor ; $\Delta\chi^2$ is the quality factor and $R_f(\%)$ is the agreement factor of the fit.

	Shell	CN	R(Å)	$\sigma^2(\text{Å}^2)$
UO₂(H₂PO₄)₂ pH=2 [U(VI)] = 7×10^{-3} M, [ΣPO_4] = 1 M	O _{ax}	2	1.76(1)	0.0019
	O _{eq}	5.0(4)	2.34(1)	0.0099
	P	2	3.61(3)	0.0033
$S_0^2=0.86$, $e_0=-4.75$ eV, $r(\%)=0.87$ and $\Delta\chi^2=8.04$				

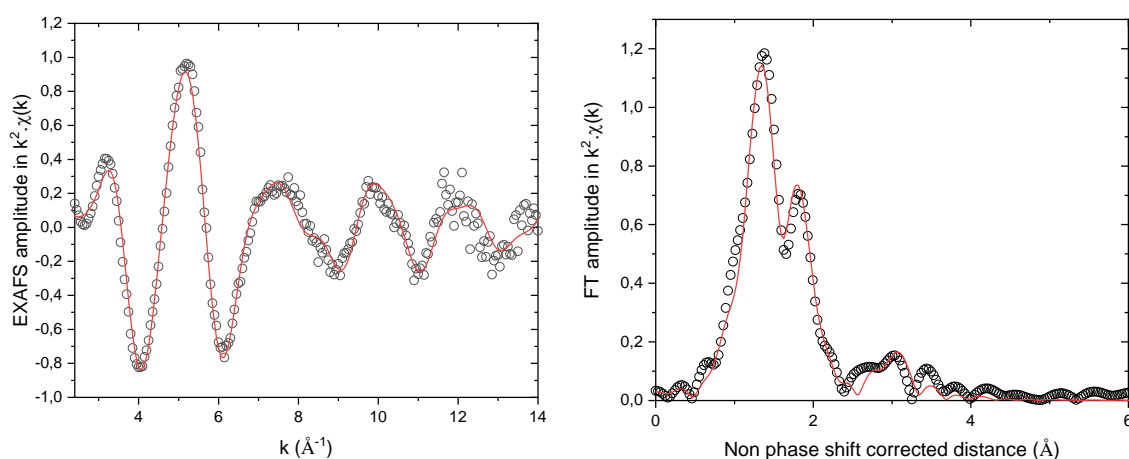


Figure IV.22. Experimental (open circles) and best adjustment (line) of the k^2 -weighted EXAFS spectrum and its corresponding Fourier transform at the U L_{III} edge for a solution of U(VI) at 7×10^{-3} M in presence of phosphates ($\Sigma\text{PO}_4=1$ M) at pH 2.

The U-O_{eq} and U-P distances are similar to the experimental and theoretical data published for monodentate coordination of U(VI) by phosphate ^[12-15]. Indeed, in those studies, with a relatively short U-O_{eq} distance between 2.28 and 2.33 Å and a U-P distance between 3.55 and 3.63 Å, corresponding to distances close to the one in the meta-autunite or uranyl hydrogen phosphate, they concluded that phosphate groups are in a monodentate binding mode, for instance in plants or in bacteria. Thus, from XAS

analysis, due to the number of phosphates determined, in this experimental conditions the complex formed seems to be the 1:2 complex as expected. In solution, the structure of the U(VI)-phosphate complex with a stoichiometry 1:2, can be proposed as shown in **Figure IV.23**, with two monodentate phosphate groups, as $\text{UO}_2(\text{H}_2\text{PO}_4)_2(\text{H}_2\text{O})_3$.

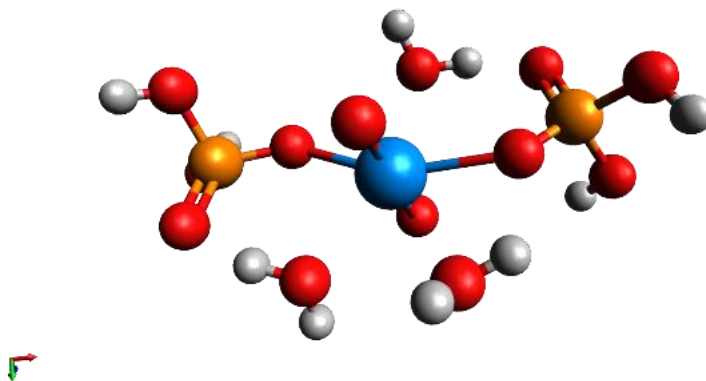


Figure IV.23. Proposed structure of the U(VI)-diphosphate complex

IV.2. Conclusions and perspectives related to An(VI)-phosphate systems

Chapter IV was devoted to the determination of fundamental data related to the complexation of Pu(VI) with phosphoric acid in order to improve models for predicted the plutonium behavior in the environment and industry. Nevertheless, the Pu(VI)-phosphate thermodynamic data reported in literature is still limited. Thus, most of the thermodynamic data available in literature have been obtained by analogy with U(VI)-phosphate systems and were used to interpret the behavior of Pu(VI)^[16-18].

A suitable experimental protocol was developed by UV-Vis spectrophotometry to get reliable data using small amounts of U(VI) and avoid the formation of precipitates for future applications with Pu(VI)-phosphate systems. Thus, the complexation of U(VI) with phosphates have been studied at $C_{U(VI)} \sim 5-7$ mM in 1 M HClO₄, and 0.5 M HClO₄/0.5 M NaClO₄ media, which ensure the use of homogeneous solutions. Stability constants were obtained at 20, 30, 40 and 50°C for the two phosphate complexes UO₂(H₂PO₄)⁺ and UO₂(H₂PO₄)₂. Slight differences can be observed with those reported in the literature that can be attributed to the phosphoric acid protonation used in our work, the experimental conditions (electrolyte, ionic strength) or the technique employed (partition methods or TRLFS). Moreover, the presence of Na⁺ seems to have an impact on the stability constants. The thermodynamic data determined indicate that the formation reactions of UO₂(H₂PO₄)⁺ and UO₂(H₂PO₄)₂ complexes whatever the medium are endothermic with a large entropic contribution. The values obtained in 0.5 M HClO₄/0.5 M NaClO₄ are similar with the ones reported by Mathur ^[7] and demonstrate once again that the presence of Na⁺ has strong influence even at higher temperatures. The structure of the complex UO₂(H₂PO₄)₂ was determined through X-ray absorption spectroscopy (XAS). This investigation suggests that the coordination sphere of the U(VI) is formed by the two axial oxygen atoms due to the actinyl moiety and by five oxygen atoms in the equatorial plane that are from both phosphate groups and water molecules and confirms the presence of a monodentate coordination of U(VI) by the two phosphates groups.

According to our results, this protocol can be validated to get thermodynamic data at low concentration of U(VI) and can therefore be applied to Pu(VI) systems. As a matter of fact, UV-Vis absorption spectroscopy is a suitable method to detect and quantify plutonium, since each oxidation state has a distinctive absorption spectrum with narrow

and intense bands (**Figure IV.24**). Pu(VI) presents a strong band at 831 nm with a larger molar absorption coefficient $\epsilon=550 \text{ M}^{-1} \text{ cm}^{-1}$ at $I=1 \text{ M HClO}_4$ ^[19] compared with the one of U(VI) equal to $10.69\pm 0.23 \text{ M}^{-1} \text{ cm}^{-1}$, leading to a lower limit of detection. Based on this fact and applying the Pu(VI) molar absorption coefficient to the calculation of limit of detection, the minimum concentration of Pu(VI) needed can be estimated to $5\times 10^{-4} \text{ M}$ of Pu(VI).

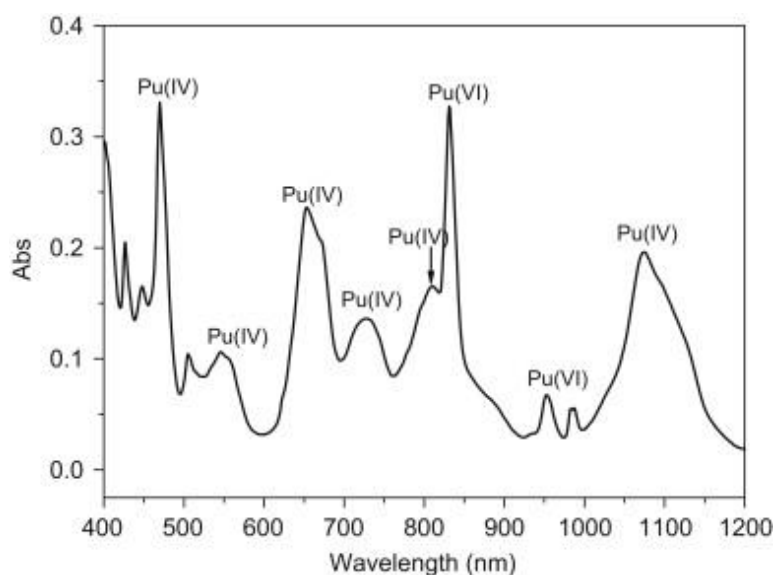


Figure IV.24. UV-Vis-NIR absorption spectra of Pu at different oxidation states in 1 M HCl-1 M NH₂OH HCl ^[20]

References

- [1] G. Meinrath, Uranium(VI) speciation by spectroscopy, *Journal of Radioanalytical and Nuclear Chemistry*, **224**, 119-126 (1997).
- [2] V. Thomsem, D. Schatzlein and D. Mercurio, Limits of detection in spectroscopy, *Spectroscopy*, **18**, 112-114 (2003).
- [3] C. F. Baes Jr., A spectrophotometric investigation of uranyl phosphate complex formation in perchloric acid solution, *Journal of Physical Chemistry*, **60**, 878-883 (1956).
- [4] H. T. Weger and D. Reed, Absorption spectra and speciation of plutonium (VI) with phosphate, *United States Department of Energy*, **40**, 1-27 (1996).
- [5] V. S. Mehta, F. Maillot, Z. Wang, J. G. Catalano and D. E. Giammar, Effect of co-solutes on the products and solubility of uranium (VI) precipitated with phosphate, *Chemical Geology*, **364**, 66-75 (2014).
- [6] I. Grenthe, J. Fuger, R. J. M. Konings, R. Lemire, R. Muller, C. Ngunyen-Trungh and H. Wanner, *Chemical Thermodynamics of Uranium*, Amsterdam: Elsevier Science, (1992).
- [7] J. N. Mathur, Complexation and thermodynamics of the uranyl ion with phosphate, *Polyhedron*, **1**, 47-53 (1991).
- [8] B. J. Thamer, Spectrophotometric and solvent-extraction studies of uranyl phosphate complexes, *Journal of the American Chemical Society*, **79**, 4298-4305 (1957).
- [9] A. D. Pethybridge, J. D. R. Talbot and W. A. House, Precise conductance measurements on dilute aqueous solutions of sodium and potassium hydrogenphosphate and dihydrogenphosphate, *Journal of Solution Chemistry*, **35**, 381-393 (2006).
- [10] P. G. Daniele, A. De Robertis, C. De Stefano, A. Gianguzza and S. Sammartano, Salt effects on the protonation of orthophosphate between 10 and 50°C in aqueous solution. A complex formation model, *Journal of Solution Chemistry*, **20**, 495-515 (1991).
- [11] A. Kirishima, T. Kimura, O. Tochiyama and Z. Yoshida, Speciation study on complex formation of uranium (VI) with phosphate and fluoride at high temperature and pressures by time-resolved laser induced fluorescence spectroscopy, *Radiochimica Acta*, **92**, 889-896 (2004).
- [12] V. E. Jackson, K. E. Gutowski and D. A. Dixon, Density Functional Theory Study of the complexation of the uranyl dication with anionic phosphate ligands with and without water molecules, *The journal of Physical Chemistry A*, **117**, 8939-8957 (2013).

- [13] M. Lopez-Fernandez, M. Romero-González, A. Günther, P. L. Solari and M. Merroun, Effect of U(VI) aqueous speciation on the binding of uranium by the cell surface of *Rhodotorula mucilaginosa*, a natural yeast isolate from bentonites, *Chemosphere*, **199**, 351-360 (2018).
- [14] J. Laurette, C. Larue, I. Llorens, D. Jaillard, P. H. Jouneau, J. Bourguignon and M. Carrière, Speciation of uranium in plants upon root accumulation and root-to-shoot translocation: A XAS and TEM study, *Environmental and Experimental Botany*, **77**, 87-95 (2012).
- [15] F. Morcillo, M. T. González-Muñoz, T. Reitz, M. E. Romero-González, J. M. Arias and M. L. Merroun, Biosorption and biomineralization of U(VI) by the marine bacterium *Idiomarina iohiensis* MAH1: effect of background electrolyte and pH, *PLOS ONE*, **9**, e91305 (2014).
- [16] R. J. Lemire, J. Fuger, H. Nitsche, P. Potter, M. H. Rand, J. Rydberg, K. Spahiu, J. C. Sullivan, W. J. Ullman, P. Vitorge and H. Wanner, Chemical Thermodynamics of neptunium and plutonium, vol 4, Amsterdam: Elsevier, (2001).
- [17] D. Rai, Y. Xia, L. Rao, N. J. Hess, A. R. Felmy, D. A. Moore and D. E. McCready, Solubility of $(\text{UO}_2)_3(\text{PO}_4)_2 \cdot 4\text{H}_2\text{O}$ in H^+ - Na^+ - OH^- - H_2PO_4^- - HPO_4^{2-} - PO_4^{3-} - H_2O and its comparison to the analogous PuO_2^{2+} system, *Journal of Solution Chemistry*, **34**, 469-498 (2005).
- [18] I. Grenthe, X. Gaona, L. Rao, V. Plyasunov, W. H. Runde, B. Grambow, R. J. M. Konings, A. L. Smith y E. E. Moore, Second update on the chemical thermodynamics of uranium, neptunium, plutonium, americium and technetium. Chemical thermodynamics, vol. 14, Paris: OECD/NEA, (2020).
- [19] M. H. Lee, Y. J. Park and W. H. Kim, Absorption spectroscopic properties for Pu(III, IV and VI) in nitric and hydrochloric acid media, *Journal of Radioanalytical and Nuclear Chemistry*, **273**, 375-382 (2007).
- [20] M. H. Lee, J. Y. Kim, W. H. Kim, E. C. Jung and K. Y. Jee, Investigation of the oxidation states of Pu isotopes in a hydrochloric acid solution, *Applied Radiation and Isotopes*, **66**, 1975-1979 (2008).

Conclusions and perspectives

V. Conclusions and perspectives

In this work, the aim was to develop suitable protocols for plutonium at different oxidation states in order to determine thermodynamic data on the complexation of plutonium with phosphates. In that way, we focused on analogs of Pu(III) and Pu(VI), such as Eu(III) and Nd(III), and also U(VI).

Until now, literature data concerning the interaction of phosphates with plutonium remain scarce, mainly due to the low solubility of phosphate compounds. Moreover, due to limited amount available in academic laboratory and the difficulties to manipulate plutonium (radiotoxicity and redox properties), there is a need to develop experimental protocols which allow to reduce the amount of plutonium used. By using chemical analogs, the new protocols can be validated before being applied to the plutonium. Thus, two approaches were followed to determine stability constants, first the use of homogeneous solutions and secondly the study of the solubility of phosphate compounds. In homogeneous solutions, the experimental conditions were always selected to avoid precipitation process: medium composition for U(VI) by UV-Vis spectrophotometry, and trace scale for Eu(III) by liquid-liquid extraction.

Before determining the thermodynamic data of U(VI) complexation, a preliminary study was performed in order to ensure the stability of the samples overtime (at least one month). Media with high amount of NaClO₄ (more than 0.5 M) have been discarded. The stability constants of the complexes of stoichiometry 1:1 and 1:2 were determined in two media (1M HClO₄, and 0.5M HClO₄/0.5M NaClO₄) and at different temperatures (from 20 to 50°C). The collected thermodynamic data agree well with literature data, which validate the protocol as suitable method for further studies on Pu(VI)-phosphate complexation by UV-Vis absorption spectrophotometry. Considering that Pu(VI) has a strong band at 831 nm with a larger molar absorption coefficient $\epsilon=550 \text{ M}^{-1} \text{ cm}^{-1}$ at I=1 M HClO₄,^[1] a lower detection limit than U(VI) ($\epsilon=10.69\pm 0.23 \text{ M}^{-1} \text{ cm}^{-1}$) is expected. Thus, the minimum concentration of Pu(VI) required to be detected and quantified can be estimated to $5\times 10^{-4} \text{ M}$. In addition, to avoid the formation of precipitates, it is suggested to work at low pH (<1.0) and in 1 M HClO₄ media.

At the +III oxidation state, a new protocol was developed for the determination of stability constants in homogeneous solution, with ¹⁵²Eu at trace level by liquid-liquid

extraction, using HDEHP as extractant, combined with γ -spectrometry. In presence of phosphates, complex of stoichiometry 1:1 and 1:2 are formed by increasing the phosphate concentration. It seems that at higher phosphate concentration, a complex 1:3 can be formed. However, due to the lack of experimental points at this concentration range, the stability constants determined in this work should be considered as an estimation. The stability constants calculated for the two other complexes, $\text{Eu}(\text{H}_2\text{PO}_4)^{2+}$ and $\text{Eu}(\text{H}_2\text{PO}_4)_2^+$, are in good agreement with the literature data. Further studies with ^{152}Eu should be considered at higher phosphate concentrations in order to get a more reliable stability constant of the complex 1:3 and verify the existence of the complex 1:4 as mentioned by Moksvin ^[2]. This protocol validates the use of liquid-liquid extraction to study the complexation of Pu(III) with phosphates at trace scale. However, it will be necessary to include a reductant in aqueous phase to maintain Pu at the +III oxidation state and use α -spectrometry.

Concerning the interaction in aqueous solution between phosphates ions and plutonium at other oxidation states (+IV and +V), two different approach can be suggested. A new experimental protocol could be developed for Pu(IV) using $^{227}\text{Th}(\text{IV})$ as analog and liquid-liquid extraction at tracer scale combined with γ -spectroscopy. In another hand, for Pu(V) a protocol could be implemented with $^{237}\text{Np}(\text{V})$ as analog using UV-Vis-NIR spectrophotometry or capillary electrophoresis coupled to inductively coupled plasma mass spectrometry (CE-ICP-MS). In addition, for all oxidation states, further thermodynamic studies should be performed at different temperatures, to get the corresponding thermodynamic data (ΔH and ΔS). It would also be interesting to increase the ionic strength, to be able to reach complexes of higher stoichiometry, by increasing the phosphate concentration.

Regarding the determination of the solubility products of Pu(III)-phosphate compounds, a method was elaborated involving amount of Nd-based rhabdophane containing 1% of europium suitable for Pu handling in our laboratory. The influence of the Eu doping on the structure and the dissolution behavior was first evaluated, showing similar properties. Then, the solid $\text{Eu}_{0.012}\text{Nd}_{0.988}\text{PO}_4 \cdot 0.667\text{H}_2\text{O}$ was doped with ^{152}Eu . Dissolution experiments were performed with decreasing mass up to around 2mg of this compound and monitored using γ -spectrometry. Whatever the mass of solid used, the solubility products were similar and are in good agreement with literature data.

This protocol using only few milligrams of phosphate compounds can then be applied to Pu(III) with the monazite PuPO_4 . The dissolution experiments are still in progress. First results seem to indicate that the plutonium remains mainly as Pu(III) in solution. The minimum of solubility is observed at the same phosphate concentration as the one observed by Rai *et al.* [4]. However, to get reliable data there is a need to improve α -spectrometry measurement since the presence of high concentration of phosphate in solution prevent obtaining good evaporated and electrodeposited sources. As it was performed for Nd-based rhabdophane sample, a physical-chemical characterization of the PuPO_4 solid after the dissolution experiments could be performed to evaluate the morphology of the solid and verify the absence of secondary phases after dissolution.

The determination of solubility products of plutonium phosphate at other oxidation states, could also be investigated. The same protocol could be applied for Pu(IV) using $\text{Pu}(\text{HPO}_4)_2 \cdot n\text{H}_2\text{O}$ as solid compound. For Pu(VI), it is suggested to perform dissolution experiments on $(\text{PuO}_2)_3 \cdot (\text{PO}_4)_2 \cdot 4\text{H}_2\text{O}$ (am) solid. In addition, the effect of the temperature on the solubility constants at all Pu oxidation state could also be studied.

References

- [1] M. H. Lee, Y. J. Park and W. H. Kim, Absorption spectroscopic properties for Pu(III, IV and VI) in nitric and hydrochloric acid media, *Journal of Radioanalytical and Nuclear Chemistry*, **273**, 375-382 (2007).
- [2] A. Moskvina, Complex formation of the actinides with anions of acids in aqueous solutions, *Soviet Radiochemistry*, **11**, 447-449 (1969).
- [3] G. R. Choppin, Utility of oxidation state analogs in the study of plutonium behaviour, *Radiochimica Acta*, **65**, 89-95 (1999).
- [2] D. Rai, D. A. Moore, A. R. Felmy, K. M. Rosso and H. Bolton Jr, «PuPO₄ (cr, hyd.) Solubility product and Pu³⁺ complexes with phosphate and ethylenediaminetetraacetic acid, *Journal of Solution Chemistry*, **39**, 778-807 (2010).

Appendix

Appendix

Appendix 1. Calculation of the density of the solutions at different temperatures

The calculation of the density as a function of the temperature was calculated with the parameters reported by Novotný *et. al.*,^[1]. The density of the aqueous solution as a function of their temperature and concentration can be expressed as equation A.1.

$$\rho = \rho_w + Ac + Bct + Cct^2 + Dc^{3/2} + Ec^{3/2}t + Fc^{3/2}t^2 \quad \text{A.1}$$

Where A through F are adjustable constant, c is the solute concentration in M, t is the temperature in °C, and ρ is the density of the solution in kg m^{-3} . The density of water, ρ_w is calculated according with the empirical equation A.2.

$$\rho_w = 999,65 + 2,0438 \times 10^{-1}t - 6,174 \times 10^{-2}t^{3/2} \quad \text{A.2}$$

The parameters for the density calculation of NaClO_4 , NaCl , HClO_4 and HCl reported by Novotný *et. al.*,^[1] used in this work are summarized in **Table A.1**.

Table A.1. Parameters for density calculation in aqueous solution

Parameter	Factor	Medium				Substance
		NaClO_4	NaCl	HClO_4	HCl	H_3PO_4
A	100	0.8462	0.4485	0.5985	0.2046	0.5574
B	-0.1	3.788	0.9634	3.334	0.9435	5.606
C	0.001	3.966	0.6136	3.190	1.090	0.2366
D	-1.0	3.025	2.712	-0.05668	1.227	2.050
E	0.01	9.968	1.009	8.249	1.269	0.3387
F	-0.0001	11.13	0	9.076	1.980	-0.5906

Appendix 2. Preparation of the solutions

A.2.1. Preparation of the stock solutions

All the stock solutions were prepared from analytical grade reagents and deionized water purified by milli-Q gradient system from Millipore Corporation with a resistivity equal to 18.2 M Ω .cm. The reagents and starting materials used are summarized in **Table A.2**.

Table A.2. Summary of the reagents and starting materials

Reagent	Quality (%)	Supplier
HCl	37	Merck
HClO₄	70	Sigma Aldrich
H₃PO₄	85	Sigma Aldrich
NaOH STD (0.1 mol dm⁻³)		Merck
NaCl	99	Sigma Aldrich
CH₃OONa		Sigma Aldrich
EuCl₃·6H₂O	99	Sigma Aldrich
NdCl₃·6H₂O	99	Sigma Aldrich
NaH₂PO₄	100	Sigma Aldrich
TTA	99%	Sigma Aldrich
HDEHP	97%	Sigma Aldrich
NaClO₄·H₂O		Fluka
HCl STD (0.1 mol dm⁻³)		Merck
Toluene	99	Fisher
NH₂OH·HCl	99	Sigma Aldrich
ALPHAEX		Etrac

The acidic stock solutions of **HClO₄**, **H₃PO₄** and **HCl** were prepared by dilution of concentrated reagents in deionized water. In order to get the desired concentration, successive dilutions in deionized water were performed. The concentration was determined by acid-base titration with fresh standard solution of 0.1 M NaOH.

The **NaCl**, **NaClO₄**, **CH₃OONa**, **NaH₂PO₄**, **NH₂OH·HCl** solutions were prepared by dissolution of the reagent in deionized water. The **NaClO₄** stock solution was filtered in Millipore Stericup Unit (0.2 μ m) and the final concentration was determined by gravimetric method taking 500 μ L of the solution, then it was dried in an oven. The solid remaining was weighted (generally after three days the mass does not change).

The concentration and associated error were determined from the main value of the 3 weighted masses of the monohydrate salt.

Because of the highly hygroscopic character of $\text{NdCl}_3 \cdot 6\text{H}_2\text{O}$ and $\text{EuCl}_3 \cdot 6\text{H}_2\text{O}$, an appropriate amount of the metal salts were dissolved in 1 M HCl. The final concentration was determined by ICP- using an Agilent 720-ES. The calibration was done with Inorganic Ventures standard solutions of Eu ($1001 \pm 4 \mu\text{g/mL}$, 7% HNO_3 v/v) and Nd ($1001 \pm 3 \mu\text{g/mL}$, 2% HNO_3 v/v). The wavelengths used for the calibration are listed in **Table A.3**. The estimated concentrations of the stock solutions are 0.034 M for Eu and 0.445 M for Nd.

Table A.3. Selected wavelengths for the determination of the element concentrations by ICP-MS

Wavelength positions (nm)	
Nd	Eu
386.341	272.778
396.310	381.967
401.224	390.771
406.108	397.197
410.945	412.972
430.357	420.504

A.2.2. Preparation of the electrolytes

The electrolytes used for the study of U(VI)-phosphate, Eu(III)-TTA, $^{152}\text{Eu(III)}$ -phosphate/TTA-Toluene, $^{152}\text{Eu(III)}$ -HDEHP, $^{152}\text{Eu(III)}$ -phosphate/HDEHP-Toluene were prepared by mixing NaClO_4 or NaCl with HClO_4 , HCl or CH_3OONa stock solutions in order to fix the ionic strength and pC_H . The electrolytes used for Nd-based rhabdophane for dissolution experiments were prepared by dilution of HCl stock solution. The electrolytes for PuPO_4 monazite dissolution were prepared by mixing HCl and $\text{NH}_2\text{OH} \cdot \text{HCl}$ stock solutions with and without $\text{Na}_2\text{H}_2\text{PO}_4$. In the presence of phosphate, the pH was adjusted to 2 with HCl . A summary of the composition of the electrolytes, the ionic strength and pC_H of each system is presented in **Table A.4**.

Table A.4. Preparation of the electrolytes at fixed ionic strength

Technique	System	Electrolyte
UV-Vis spectrophotometry	Eu(III)-TTA	0.5 M NaClO ₄ /CH ₃ OONa pC _H =3.91
	U(VI)-phosphate	1 M HClO ₄ , pC _H =0
		0.1 M HClO ₄ pC _H =1
		0.1 M HClO ₄ /0.9 M NaClO ₄ , pC _H =0.89
	0.5 M HClO ₄ /0.5 M NaClO ₄ pC _H =0	
LLE combined with γ-spectrometry	¹⁵² Eu(III)- phosphate/TTA-Toluene	0.5 Mdm ⁻³ NaClO ₄ /HClO ₄ pC _H =3.9
	¹⁵² Eu(III)-HDEHP	1 M NaCl/HCl pC _H =1, 2, 3, 4 and 5
	¹⁵² Eu(III)- phosphate/HDEHP- Toluene	1 M NaCl/HCl pC _H =3.1
ICP-OES γ-spectrometry	Eu _{0.01} Nd _{0.99} PO ₄ ·0.667H ₂ O	0.1 M HCl pH=1
	Eu _{0.012} Nd _{0.988} PO ₄ ·0.667H ₂ O with ¹⁵² Eu	0.15 M HCl pH=0.82
UV-Vis absorption spectrophotometry PERALS α-spectroscopy	PuPO ₄	0.1 M HCl 10 ⁻³ M NH ₂ OH·HCl pH=0.966
		0.01 M HCl 10 ⁻³ M NH ₂ OH·HCl pH=2.079
		4×10 ⁻⁴ , 3×10 ⁻³ , 2×10 ⁻² , 0.1 and 0.5 M of NaH ₂ PO ₄ 10 ⁻³ NH ₂ OH.HCl HCl (to adjust pH) pH=2.0

A.2.3. Preparation of aqueous phases

Depending of the system under investigation the aqueous phases were prepared as described below. The proton concentrations of the solutions were measured as described in **Chapter 2** part **II.1.1**.

TTA/NaClO₄-CH₃OONa

Due to the low solubility of TTA, 3×10^{-3} M of The hydrated form of TTA (keto-hydrate) was dissolved in 0.5 M NaClO₄-CH₃OONa in order to get a total TTA concentration equal 3×10^{-3} M. The pC_H of the solution was adjusted to 3.91 with HClO₄ solution.

NaH₂PO₄ solution

The preparation of the ligand solution for liquid-liquid extraction experiments requires taking into account the deprotonation of the phosphoric acid at the pC_H studied. According to phosphoric acid speciation diagram in, the predominant specie is H₂PO₄⁻ with small percentage of H₃PO₄. In this pC_H range, the deprotonation into HPO₄²⁻ and PO₄³⁻ species can be neglected. The total concentration of the species in solution under our experimental conditions can be calculated as **A.3**, where the species HPO₄²⁻ and PO₄³⁻ species are set to zero. The concentration of H₂PO₄⁻ anion was calculated by substitution of the total concentration (**A.3**) in the first dissociation reaction (**Table I.6**) of phosphoric acid, give us equation **A.4**. In our experiments, C_{Tot} refers to the known concentration of NaH₂PO₄. The pH is 3.9 for ¹⁵²Eu(III)-phosphate/TTA-Toluene system and 3.1 for ¹⁵²Eu(III)-phosphate/HDEHP-Toluene system. The log values of the first dissociation constant Ka₁ of H₃PO₄ at the corresponding ionic strength, media and temperature are tabulated in **II.2.1.1**.

$$C_{Total} = [H_3PO_4] + [H_2PO_4^-] + [HPO_4^{2-}] + [PO_4^{3-}] \quad \text{A.3}$$

$$[H_2PO_4^-] = \frac{C_{Total} \cdot Ka_1}{Ka_1 + [H^+]} \quad \text{A.4}$$

Ligand solution for ¹⁵²Eu(III)-phosphate/TTA-Toluene system

The ligand solutions in ¹⁵²Eu(III)-phosphate/TTA-Toluene system was prepared by dilution of 0.0993 mol NaH₂PO₄ in 0.45 M in order to get a final ionic strength equal to

0.5 M. The proton concentration was adjusted to $pC_H=3.9$ with $HClO_4$ concentrated solution. Then sample solutions were prepared by successive dilution of this solution in 0.5 M $HClO_4/NaClO_4$.

Ligand solution for $^{152}Eu(III)$ -phosphate/HDEHP-Toluene system

In order to reduce the variation of pC_H and ionic strength of the samples used in $^{152}Eu(III)$ -phosphate/HDEHP-Toluene system, two ligand solutions were prepared. The **solution A** was prepared at 0.5 M NaH_2PO_4 (or 0.48 M $H_2PO_4^-$ anion) in 0.76 M of $NaCl$. The intermediate **solution B** was prepared at 0.1 M NaH_2PO_4 (or 0.09 M $H_2PO_4^-$ anion) in 0.95 M $NaCl$. The pC_H of both solutions was adjusted to 3.1 with HCl concentrated solution. The successive dilution to get other NaH_2PO_4 concentration was carried out with 1 M $NaCl/HCl$ electrolyte.

Isotope ^{152}Eu solution for liquid-liquid extraction experiments

For experiments in perchloric medium, part of the standard solution of ^{152}Eu in 1 N HCl (CERCA-LEA, 524 ± 9 kBq g^{-1} , see **Table II.2** for details about this source) was evaporated to dryness in PTFE beaker. The residue was taken up in 1 mL 0.01 M $HClO_4$. For liquid-liquid extraction experiments, between 10 and 50 μL of this solution was evaporated in a PTFE crucible and taken up in 1.3 mL of 10^{-4} M $HClO_4$. For experiments in hydrochloric acid, 10 and 50 μL of the ^{152}Eu source were evaporated and the residue taken up in 1.3 mL 10^{-3} M HCl . This Eu solution was distributed (50 μL) over twenty samples used for extraction and three references for mass balance. The concentration of ^{152}Eu europium is around 10^{-10} M.

A.2.4. Preparation of organic phases

For liquid-liquid extraction experiments, organic phases must be pre-equilibrated with the electrolyte under investigation in order to limit changes in ionic strength, acidity or variation volume during the extraction.

TTA in Toluene

The hydrated form of 2-thenoyl-trifluoroacetone (TTA) was prepared from TTA reagent contacted with deionized water during seven days at room temperature in the dark ^[23]. The TTA keto-hydrate (M. W. 240 g mol⁻¹) obtained was dried and recrystallized two times with diethyl ether. the white powder obtained was stored in a glass bottle in the dark at 8°C ^[24]. The toluene was pre-equilibrated with electrolyte (0.5 M NaClO₄-HClO₄ at pC_H to 3.9) during 72 hours. The TTA stock solution was prepared by dissolution of TTA-hydrate in pre-equilibrated toluene, This solution was filtered on WHATMAN filter (No. 3) and it was used immediately.

HDEHP in Toluene

Commercially HDEHP reagent may contain inorganic and organic impurities, especially mono- (2-ethylhexyl)phosphoric acid (H₂MEHP)) that can affect the extraction properties of HDEHP ^[2]. Different purification methods, involving copper salt precipitation or various extraction and washings, more or less time-consuming, are described in the literature ^[3, 4]. In the present work, the purity of HDEHP was verified by acid-base titration. An aliquot of HDEHP was diluted ten-fold in ethanol and the solution was titrated with 0.1 M NaOH standard solution. The titration curve in **Figure A.1** displays only one equivalence point. The presence of significant amount of H₂MEHP leads to the presence of two equivalence points as illustrated in **Figure A.2** ^[5]. These are due to the HDEHP reagent can be contain impurities such iron(III) that can be interfere in the extraction process. Since our reagent just has a one equivalent point, it had been used without further purification. The absence of a second equivalence point has also been used by Kandil *et al.* as purity criteria ^[6].

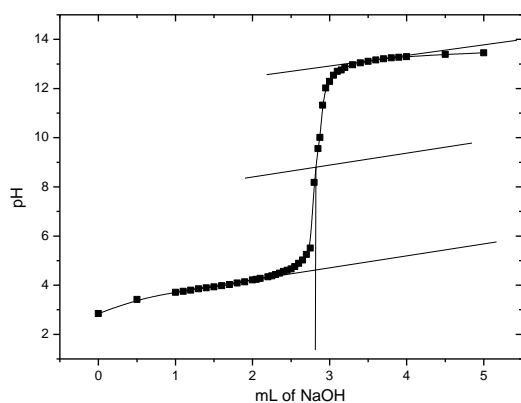


Figure A.1. Titration curve of HDEHP purified 10-fold diluted in ethanol (reagent used in this work)

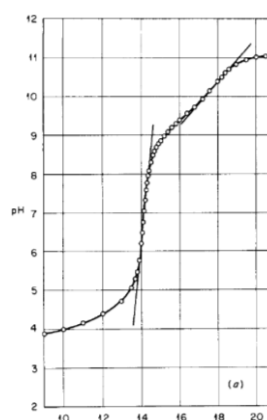


Figure A.2. Titration curve of non-purified HDEHP^[5]

Based in the study performed by Aguilar *et. al.*,^[7], a suitable D value is obtained at low concentration of HDEHP as also seen in experiments using TTA as extractant. For the experiments aiming at the determination of extraction conditions of ¹⁵²Eu, a solution of 0.01M HDEHP in toluene was pre-equilibrated with 1 M NaCl-HCl at pC_H=1, 2, 3, 4, 5 during 2 hours. Then, the aqueous phases were replaced by fresh ones and contacted with HDEHP solution during 24h. For experiments aiming at complexation constants determination, the same procedure was performed with 1M NaCl-HCl solution of pC_H to 3.1 and 0.075 M HDEHP in toluene

Appendix 3. Determination of the amount ^{152}Eu in rhabdophane (on HPGe 4000 detector)

In order to determine the total activity on $\text{Eu}_{0.012}\text{Nd}_{0.988}\text{PO}_4 \cdot 0.667\text{H}_2\text{O}$ doped with ^{152}Eu , a dissolution experiments were performed with 5.9 mg of solid in 5.9 mL of a mixture of 1 M HNO_3 (75%) and 1 M HCl (25%). The dissolution was prepared in PTFE-Saville containers and stirred in an orbital shaking incubator (IKA KS 4000i control) at 150 rpm and room temperature until total dissolution. Then, the absolute activity of the sample of 90 μL (20 μL of dissolution solution diluted in 70 μL HCl) and 250 μL (60 μL diluted in 190 μL HCl) has been obtained using the corresponding calibration data. The activity was deduced from the mean value of seven energies, the values obtained are summarized in **Table A.5**. Therefore, the amount of ^{152}Eu found in $\text{Eu}_{0.012}\text{Nd}_{0.988}\text{PO}_4 \cdot 0.667\text{H}_2\text{O}$ was equal to 7404 ± 159 Bq per mg of solid.

Table A.5. Absolute activity calculated in total dissolution samples (90 μL and 250 μL samples)

Sample	Activity (Bq)	Bq mg^{-1} of dissolution
90 μL	133 \pm 6	6.4 \pm 0.3
250 μL	397 \pm 14	6.7 \pm 0.2
Mean value		6.5 \pm 0.4

- **Determination of the concentration of Eu(III)**

In order to deduce the concentration Eu(III) during the dissolution experiments. The first step is determining the activity of the **Aliquot B** (see **section II.3.2.2.**) as described in equation **A.5**, where the counts and time are from gamma measurements, ε^{FEP} is tabulated in **Table II.4** at the corresponding aliquot volume and $P_{E\gamma}$ at 121.7817 keV obtained from **Table II.3**.

$$\text{Activity of aliquot B (Bq)} = \frac{\text{Counts}}{(\text{Time})(\varepsilon^{\text{FEP}})(P_{E\gamma})} \quad \text{A.5}$$

The second step consists on calculate the absolute activity corresponding to rhabdophane dissolved in each system according to equation **A.6**. The total mass of rhabdophane refers to 50.1-1.8 mg employed in the dissolutions systems.

Activity of sample (Bq) A.6

$$= \frac{\text{Activity of aliquot B (Bq)} * \text{Total mass of rhabdophane (mg)}}{\text{Mass of aliquot B (mg)}}$$

The mass of rhabdophane dissolved is calculated by equation A.7, which is derived from the total activity on rhabdophane previously calculated as $7404 \pm 159 \text{ Bq mg}^{-1}$.

$$\text{Mass of rhabdophane dissolved (mg)} = \frac{\text{Activity of sample (Bq)}}{7404 \pm 159 (\text{Bq mg}^{-1})} \quad \text{A.7}$$

The concentration of Eu(III), Nd(III) and P can be deduced as described in equation A.8, where the molar weight of each element, molar fraction used in this work are presented in Table A.6.

Concentration (M) A.8

$$= \frac{\text{Molar fraction} * \text{Mass rhabdophane dissolved (mg)}}{\text{Molar weight (g mol}^{-1}) * \text{Total volume rhabdophane (mL)}}$$

Table A.6. Parameters used for calculation of concentration in dissolution experiments^[8]

Element	Molar weight g mol ⁻¹	Stoichiometry	Molar fraction
Nd	144.242	0.988	0.57
Eu	151.964	0.012	0.01
P	30.97	1	0.12
O	15.99	4	0.25
H₂O	18.01	0.667	0.05
Total	361.17		1

Appendix 4. Experimental techniques

Inducted Couple Plasma-Optical Emission Spectrometry (ICP-OES)

The ICP-OES is an analytical technique used for the determination of trace elements. The technique consists of subjecting a sample to temperatures high enough to cause the dissociation of atoms and produce significant amounts of excitation or ionization of the sample's atoms. One the atoms are in their excited stated, they decay to lower states thermal or radioactive emission or energy transition. In OES, the intensity of the light emitted at specific wavelength is measured and used to determinate the concentration of the elements of interest ^[9, 10].

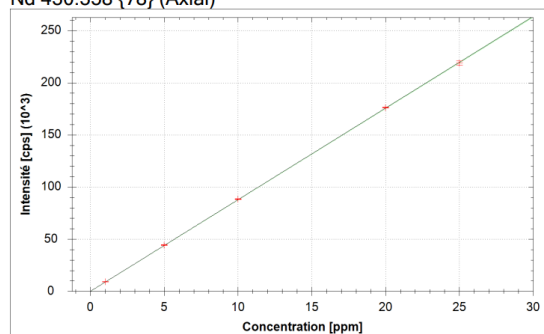
The elemental concentration of Nd, Eu and P were estimated after initial calibration with SPEX standards solutions. The selected wavelengths used for the calibration are summarized in **Table A.7**. The measurements were performed at ICSM laboratory

Table A.7. Selected wavelength for the determination of Nd(III), Eu(III) and P concentration by ICP-OES in dissolution experiments.

Wavelength positions (nm)		
Nd	Eu	P
378.425	393.048	177.495
401.225	412.970	178.284
430.358	420.505	213.618

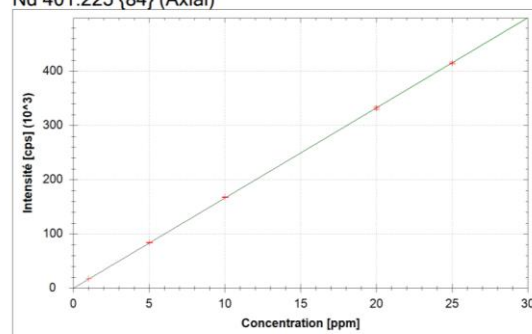
The calibrations curves for Nd, P and Eu are presented in **Figure A.3**, **Figure A.4** and **Figure A.5**, respectively.

Nd 430.358 {78} (Axial)



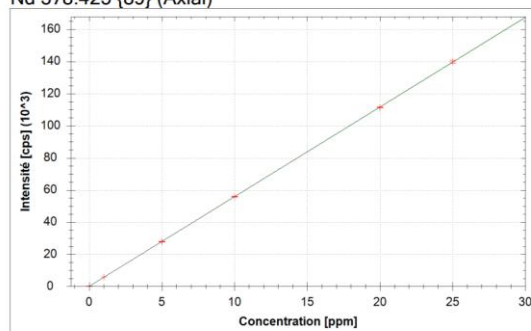
$f(x) = 8781,7090 \cdot x + 6,0245$
 $R^2 = 1,0000$
 BEC = 0,001 ppm
 LoD = 0,0042 ppm

Nd 401.225 {84} (Axial)



$f(x) = 16619,7143 \cdot x + -51,1927$
 $R^2 = 1,0000$
 BEC = -0,003 ppm
 LoD = 0,0106 ppm

Nd 378.425 {89} (Axial)



$$f(x) = 5581,3530 \cdot x + 93,1836$$

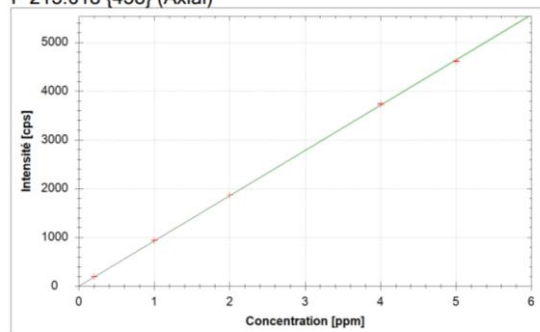
$$R^2 = 1,0000$$

$$\text{BEC} = 0,017 \text{ ppm}$$

$$\text{LoD} = 0,0083 \text{ ppm}$$

Figure A.3. ICP-OES calibration curve for Nd

P 213.618 {458} (Axial)



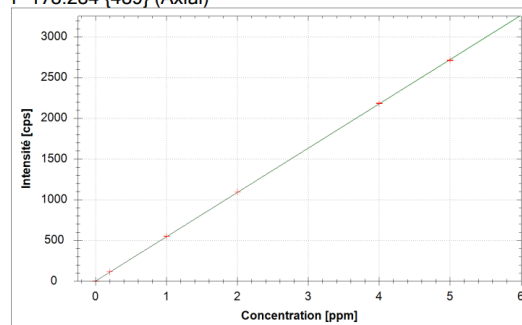
$$f(x) = 928,3936 \cdot x + -0,6684$$

$$R^2 = 0,9999$$

$$\text{BEC} = -0,001 \text{ ppm}$$

$$\text{LoD} = 0,0016 \text{ ppm}$$

P 178.284 {489} (Axial)



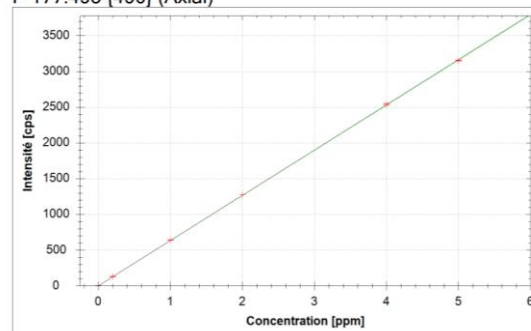
$$f(x) = 543,9079 \cdot x + 1,8586$$

$$R^2 = 1,0000$$

$$\text{BEC} = 0,003 \text{ ppm}$$

$$\text{LoD} = 0,0046 \text{ ppm}$$

P 177.495 {490} (Axial)



$$f(x) = 632,7051 \cdot x + 0,7084$$

$$R^2 = 0,9999$$

$$\text{BEC} = 0,001 \text{ ppm}$$

$$\text{LoD} = 0,0018 \text{ ppm}$$

Figure A.4. ICP-OES calibration curve for P

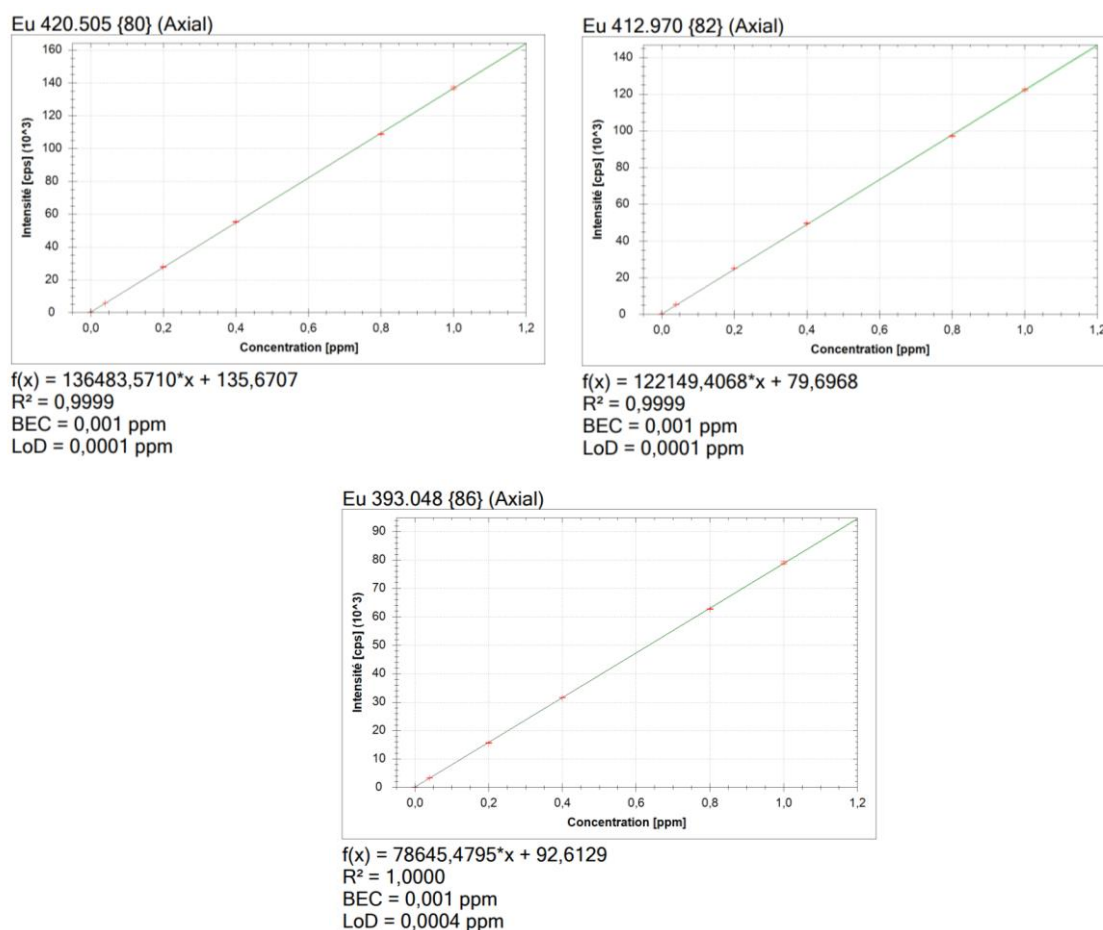


Figure A.5. ICP-OES calibration curve for Eu

Fourier-Transform Infrared Spectroscopy (FTIR)

Infrared spectroscopy is an absorption method which is used in the infrared region of the electromagnetic spectrum. The analysis of the interaction of infrared light with molecules allows getting some information about functional groups present in molecules (organic or inorganic) ^[11]. This is a vibrational spectroscopy. The common used region for infrared absorption spectroscopy is $4000\text{-}400\text{ cm}^{-1}$ ^[12].

X-Ray diffraction (XRD)

X-ray diffraction is an analytical technique uses for phase identification of a crystalline material and can provide information about unit cell parameters. This is based on constructive interference of monochromatic x-rays and crystalline sample when the conditions satisfy the Bragg's Law (equation A.9). This law links the wavelength (λ) of an electromagnetic radiation to the diffraction angle (θ), and the lattice spacing (d), in a

crystalline sample. These diffracted x-ray are then detected, processed and countered. By scanning the sample through a range of 2θ angle, all possible diffraction directions of the lattice should be attained due to the random orientation of the powdered material. Conversion of the diffraction peaks to d-spacing allows identification of the mineral because each mineral has a set of unique d-spacing. Typically, this is achieved by comparison of d-spacing with standards patterns ^[13].

$$n\lambda = 2d \sin \theta$$

A.9

Thermogravimetric analysis (TGA)

Thermogravimetric analysis (TGA) is a method in which the mass of a sample is monitored as function of temperature or time in a controlled atmosphere. A plot of mass or mass percentage as a function of time is called a thermogram or a thermal decomposition curve. TGA is used to determine the loss in mass at particular temperatures, but TGA cannot identify the involved species ^[10]. TGA can provide information about physical or chemical changes, such as secondary phases, transition including vaporization, sublimation, dehydration and decomposition ^[14].

Scanning Electron Microscopy (SEM) and X-EDS analysis

Scanning Electron Microscopy (SEM) is a technique to observe the surface phenomena of materials by scanning an electron beam across the sample surface. The electrons interact with the atoms of the sample producing signals that give information about topography, morphology, composition, orientation of grains, crystallographic information of the material. Energy-disperse spectroscopy (EDS) is a supplementary tool of SEM for identifying and quantifying elemental composition among of the SEM image ^[15].

Appendix 5. Supplementary data relative to Eu

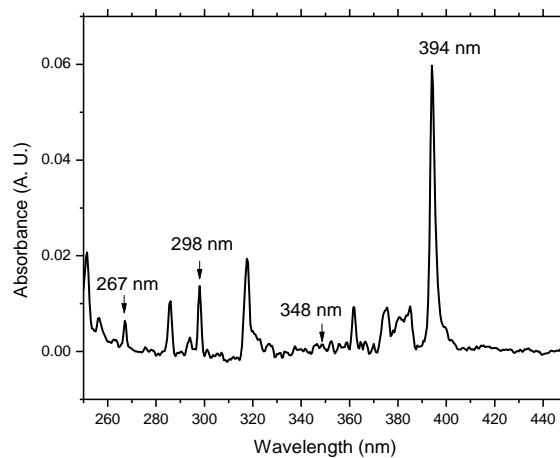
a. UV-Vis absorption spectra of Eu(NO₃)

Figure A.6. UV-Vis absorption spectra of Eu(III) ($C_{Eu(III)}=2.5 \times 10^{-2} M$, $T=25^{\circ}C$, $pC_H=3.52$, $I=0.5 M NaClO_4/CH_3OONa$)

b. UV-Vis absorption spectra of Eu-TTA complexation at different temperatures

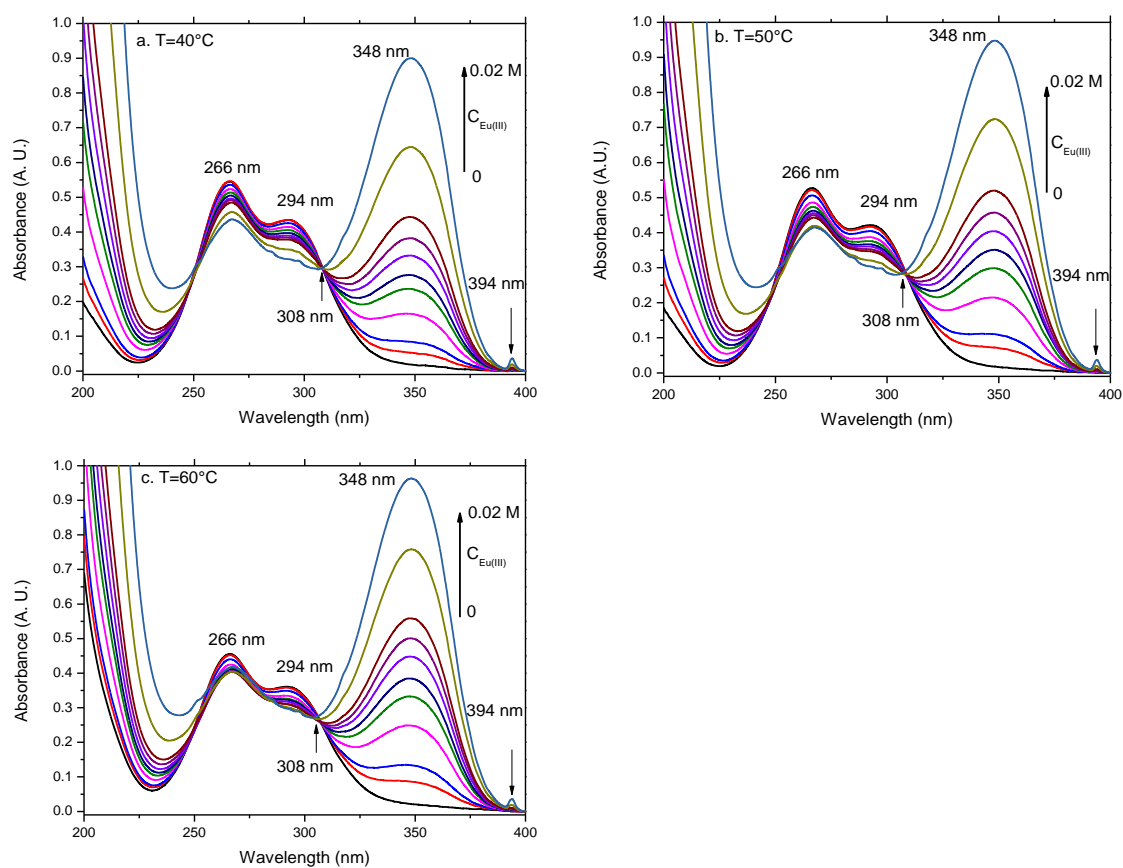


Figure A.7. UV-Vis absorption spectra of Eu(III)-TTA (keto-hydrate form) complexation ($C_{TTA}=5 \times 10^{-5} \text{ M}$, $0 \leq C_{Eu(III)} \leq 0.02 \text{ M}$, $pC_H=3.7$, $I=0.5 \text{ M NaClO}_4/\text{CH}_3\text{OONa}$ at $T=$ a. 40°C , b. 50°C and c. 60°C

c. Complexation of Eu(III)-phosphate using liquid-liquid extraction with HDEHP as extractant

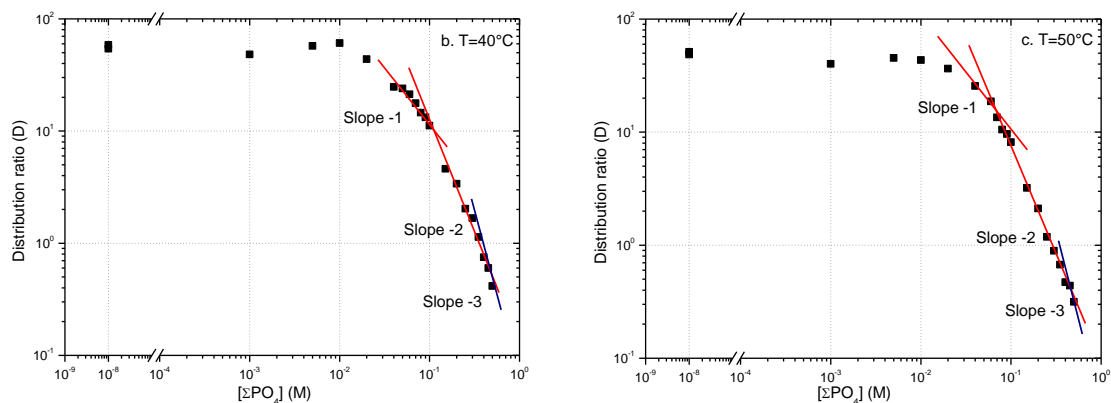


Figure A.8. Variation of the distributions coefficients of ^{152}Eu as a function of total phosphate concentration ($C_{\text{Eu}} \approx 10^{-8} \text{ M}$, $0 \leq [\Sigma\text{PO}_4] \leq 0.5 \text{ M}$, $C_{\text{HDEHP}} = 0.0075 \text{ M}$, $I = 1 \text{ M NaCl-HCl}$, $pC_{\text{H}} = 3.1$, $T = 40^*$ and $50^* \text{ }^\circ\text{C}$)

*The real temperatures measured by a conventional thermometer in our experimental conditions were 38, 46 and 56°C

d. Determination of $\log \beta_1$ at different temperatures in Eu(III)-phosphate using liquid-liquid extraction with HDEHP as extractant

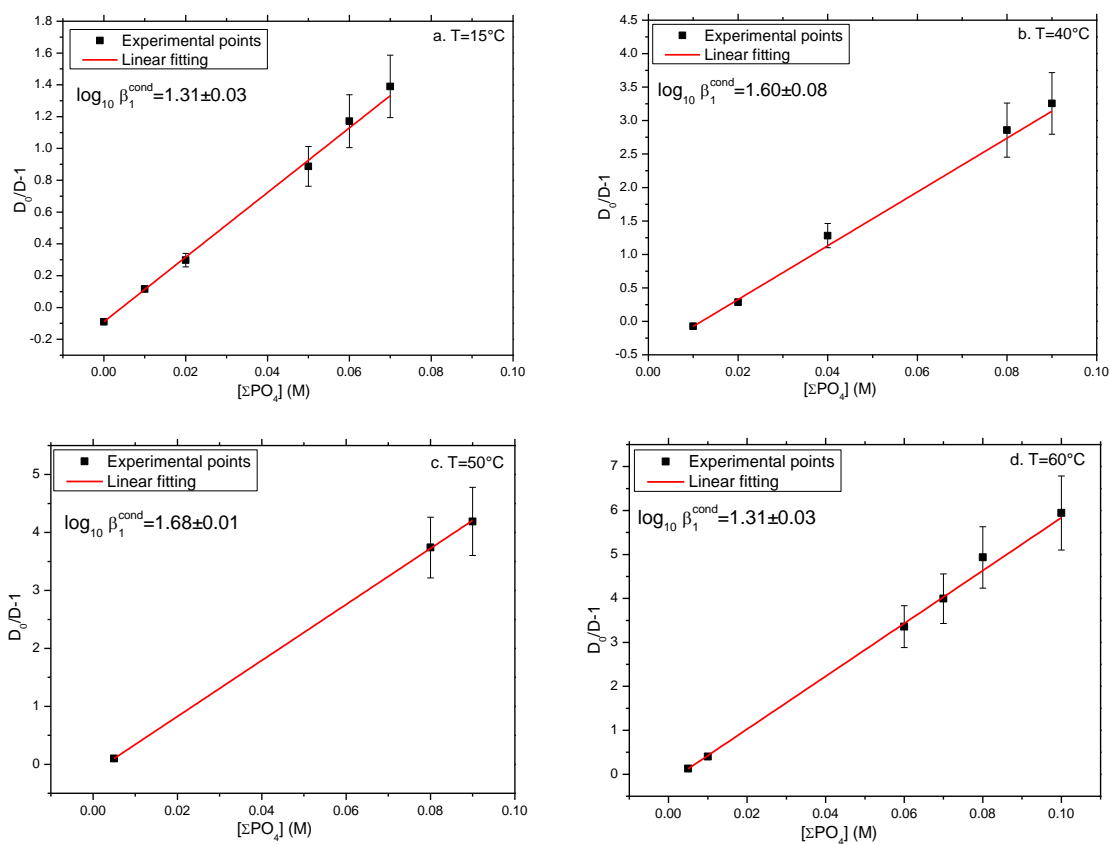


Figure A.9. Deduction of $\log \beta_1^{\text{cond}}$ by fitting $(D_0/D)-1$ as a function of total phosphate concentration ($C_{\text{Eu}} \approx 10^{-8}$ M, $C_{\text{HDEHP}} = 0.0075$ M, $10^{-2} \leq [\Sigma \text{PO}_4] \leq 0.1$ M, $I = 1$ M NaCl-HCl, $pC_{\text{H}} = 3.1$ and $T = 15, 40^*, 50^*$ and 60^*°C)

*The real temperatures measured by a conventional thermometer in our experimental conditions were 38, 46 and 56°C

e. Determination of $\log \beta_2$ at different temperatures in Eu(III)-phosphate using liquid-liquid extraction with HDEHP as extractant

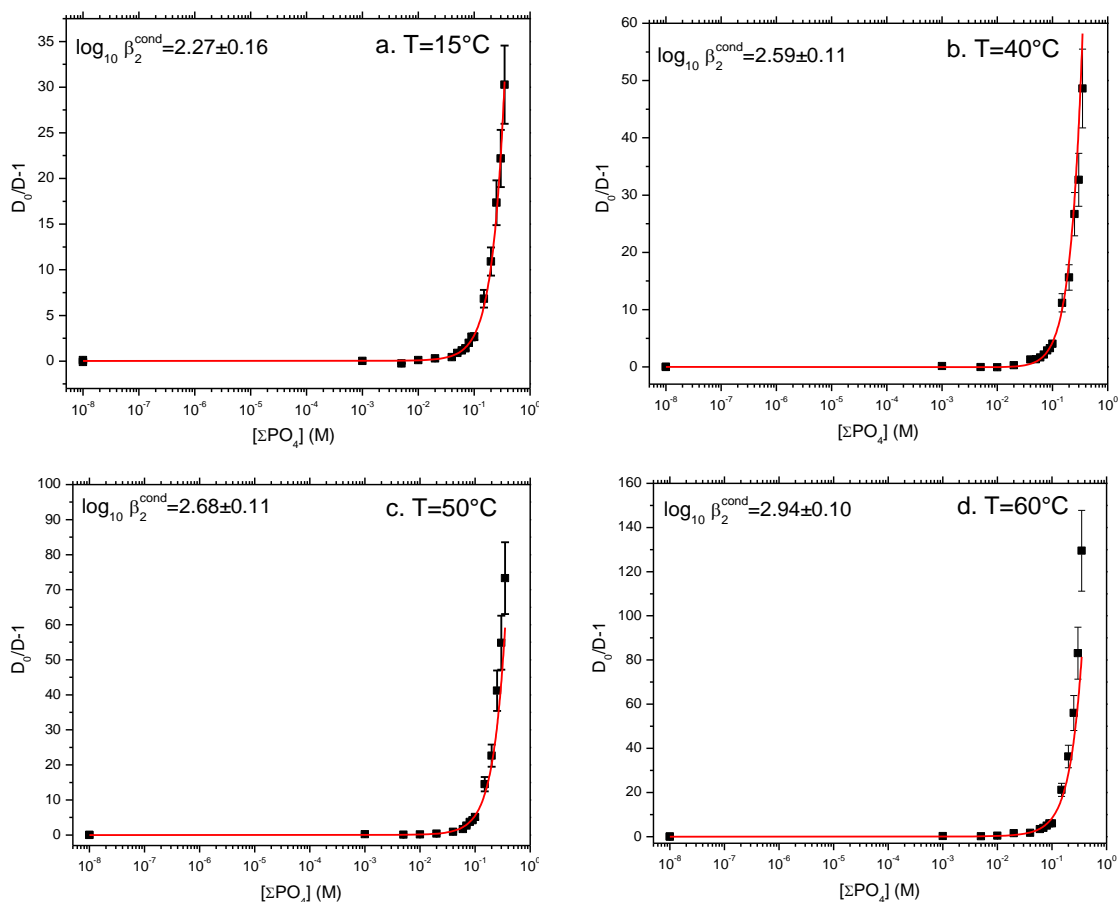


Figure A.10. Deduction of $\log \beta_2^{\text{cond}}$ by fitting $(D_0/D)-1$ as a function of total phosphate concentration to second order polynomial ($C_{\text{Eu}} \approx 10^{-8}$ M, $C_{\text{HDEHP}} = 0.0075$ M, $10^{-2} \leq [\Sigma PO_4] \leq 0.1$ M, $I = 1$ M NaCl-HCl, $pC_H = 3.1$ and $T = 15, 40^*, 50^*$ and $60^* (\text{C})$)

*The real temperatures measured by a conventional thermometer in our experimental conditions were 38, 46 and 56°C

f. Determination of $\log \beta_3$ at different temperatures in Eu(III)-phosphate using liquid-liquid extraction with HDEHP as extractant

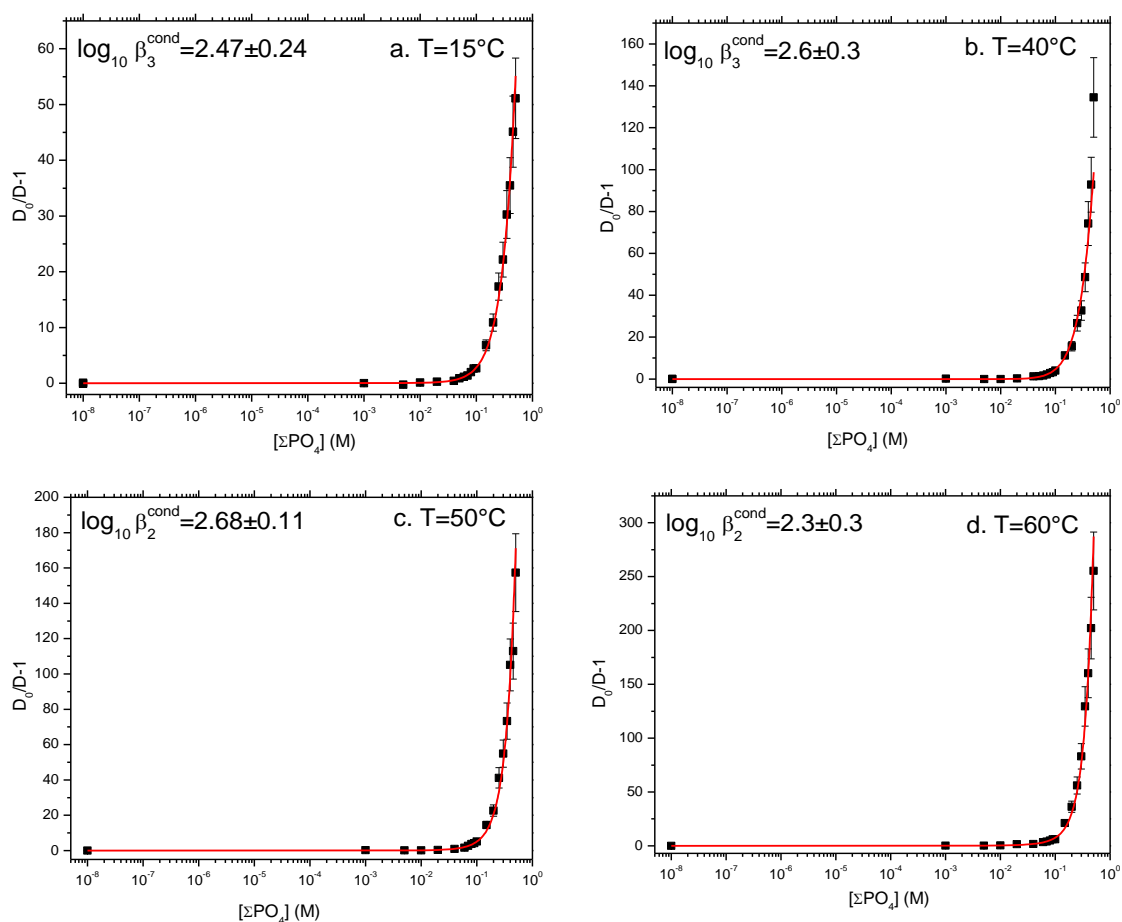


Figure A.11. Deduction of $\log \beta_3^{\text{cond}}$ by fitting $(D_0/D)-1$ as a function of total phosphate concentration to third order polynomial ($C_{Eu} \approx 10^{-8}$ M, $C_{HDEHP} = 0.0075$ M, $10^{-2} \leq [\Sigma PO_4] \leq 0.1$ M, $I = 1$ M NaCl-HCl, $pC_H = 3.1$ and $T = 15, 40^*, 50^*$ and $60^* (\text{C})$)

*The real temperatures measured by a conventional thermometer in our experimental conditions were 38, 46 and 56°C

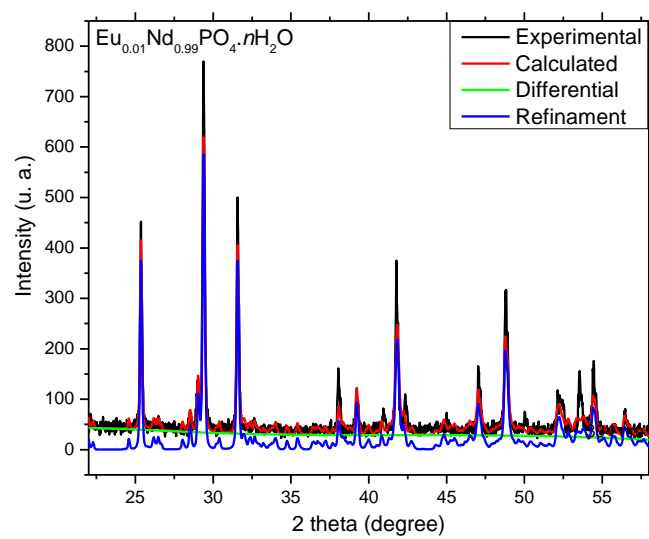
g. Rietveld refinement of X-Ray patterns of $\text{Eu}_{0.01}\text{Nd}_{0.99}\text{PO}_4 \cdot n\text{H}_2\text{O}$ 

Figure A.12. Experimental and calculate XRD patterns and Rietveld refinement obtained for $\text{Eu}_{0.01}\text{Nd}_{0.99}\text{PO}_4 \cdot n\text{H}_2\text{O}$

References

- [1] P. Novotný and O. Sönel, Density of binary aqueous solutions of 306 inorganic substances, *Journal of Chemical and Engineering Data*, **33**, 49-55 (1988).
- [2] D. F. Peppard, G. W. Mason, J. L. Maier and W. J. Driscoll, Fractional extraction of the lanthanides as their di-alkyl orthophosphates, *Journal of Inorganic and Nuclear Chemistry*, **4**, 334-343 (1957).
- [3] C. B. Honaker and W. W. Shulz, Ion exchange purification of bis-(2-ethylhexyl)phosphoric acid, *Journal of Inorganic and Nuclear Chemistry*, **39**, 1703-1704 (1977).
- [4] J. Partridge and R. Jensen, Purification of di-(2-ethylhexyl)phosphoric acid by precipitation of copper(II) di-(2-ethylhexyl)phosphate, *Journal of Inorganic and Nuclear Chemistry*, **31**, 2587-2589 (1969).
- [5] W. J. McDowell, P. T. Perdue and G. N. Case, Purification of di-(2-ethylhexyl)phosphoric acid, *Journal of Inorganic and Nuclear Chemistry*, **38**, 2127-2129 (1976).
- [6] A. T. Kandil and K. Farah, The solvent extraction of terbium and europium by di-(2-ethylhexyl)-phosphoric acid and various organophosphorous compounds, *Journal of Inorganic and Nuclear Chemistry*, **42**, 277-280 (1980).
- [7] M. Aguilar and D. H. Liem, Studies on the solvent extraction of europium (III) by di-(2-ethylhexyl)phosphoric acid (HDEHP) in toluene, *Acta Chemica Scandinavica*, **30**, 313-321 (1976).
- [8] T. Prohaska, J. Irrgeher, J. Benefield, J. K. Böhlke, L. A. Chesson, T. B. Coplen, T. Ding, P. Dunn, M. Gröning, N. E. Holden, H. A. J. Meijer, H. Moossen, A. Possolo, Y. Takahashi, J. Vogl, T. Walczyk, J. Wang, M. E. Wieser, S. Yoneda, X. K. Zhu and J. Meija, Standard atomic weights of the elements 2021 (IUPAC technical report), *Pure and Applied Chemistry*, **94**, 573-600 (2022).
- [9] C. B. Boss and J. K. Fredeen, Concepts, Instrumentation and Techniques in Inductively Couple Plasma Optical Emission Spectroscopy, 3 ed., USA: Pekin Elmer, (2004).
- [10] D. Skoog, J. F. Holler y S. R. Crouch, Principles of Instrumentation Analysis, 7 ed., USA: CENGAGE Learning (2018).
- [11] F. A. Settle, Handbook of instrumental techniques for analytical chemistry, New Jersey: Prentice Hall PTR (1997).
- [12] W. D. Perkins, Fourier Transform-Infrared Spectroscopy. Part I. Instrumentation. Topics in Chemical Instrumentation, *Journal of Chemical Education*, **63**, A5-A10 (1986).
- [13] B. D. Cullity and S. R. Stock, Elements of X-Ray Diffraction, 3 ed., USA:

Pretince Hall (2001).

- [14] M. Nasrollahzadeh, M. Atarod, M. Sajjadi, S. M. Sajadi and Z. Issaabadi, Plant-mediated green synthesis of nanostructures: mechanisms, characterization, and applications, *Interface Science and Technology*, Elsevier, **28**, 199-322 (2019).
- [15] K. Akhtar, S. A. Khan, S. B. Khan and A. M. Asiri, Scanning Electron Microscopy: Principle and Applications in Nanomaterials Characterization, *Handbook of Materials Characterization*, Springer International Publishing , **4** , 113-145 (2018)

Abstract in French

Abstract in French

Les actinides sont susceptibles d'intervenir avec des espèces phosphatées (acide phosphorique et anions dérivés) dans l'environnement ainsi que dans certains domaines liés à l'industrie nucléaire.

Les phosphates sont des espèces ubiquistes d'origine naturelle et anthropique. Il existe plusieurs centaines de minéraux phosphatés, comme par exemple l'apatite, la monazite, le rhabdophane ou l'autunite. L'érosion peut conduire à la dissémination de particules et dans une moindre mesure, à des espèces solubilisées, ces deux formes pouvant être assimilées par les plantes. Mais la majeure partie des composés phosphatés présents dans l'environnement provient de la production industrielle d'acide phosphorique pour la fabrication d'engrais phosphatés, de détergents, d'additifs pour l'alimentation animale... Or des actinides ont également été disséminés dans l'environnement suite à des essais nucléaires, des accidents de satellites et de centrales.

Dans l'industrie nucléaire, l'extractant mis en jeu dans le procédé PUREX de retraitement du combustible usé, le TBP (tributylphosphate) subit des dégradations chimiques et radiolytiques conduisant à la formation d'acide phosphorique. Cette espèce est susceptible d'interagir notamment avec les éléments valorisables U et Pu entraînant une diminution de l'efficacité d'extraction, voire une perte de matière significative. Par ailleurs, la stabilité des minéraux phosphatés permet d'envisager leur utilisation comme matrice de stockage spécifique de déchets radioactifs.

Dans la littérature, les données thermodynamiques et structurales sur l'interaction des actinides avec les espèces phosphatées sont peu nombreuses, en raison de la très faible solubilité des phosphates d'actinides et ce, quel que soit le degré d'oxydation considéré. Or ce type de données est essentielle pour prédire le comportement de ces éléments, et en particulier du plutonium, dans l'environnement et dans le cycle.

Le plutonium est un élément à la chimie redox extrêmement complexe puisque les degrés d'oxydation +III à +VI peuvent exister simultanément en solution aqueuse. Pour pallier cette difficulté, des analogues chimiques de chaque degré d'oxydation du plutonium sont souvent utilisés: lanthanides, Am, Cm pour Pu(III), Th, Ce(IV) pour Pu(IV), Np(V) pour Pu(V) et U(VI) pour Pu(VI). Dans ce travail, nous nous sommes intéressés aux degrés +III et +VI du plutonium, l'objectif étant de développer des protocoles expérimentaux permettant de déterminer des constantes de stabilité de phosphato-complexes et des produits de solubilité de composés phosphatés, pouvant par

la suite être appliqués au plutonium. En effet, aux difficultés inhérentes à la chimie de cet élément, vient s'ajouter une difficulté supplémentaire liée aux quantités manipulables limitées dans un laboratoire académique.

Dans la **première partie** de ce manuscrit, après un bref aperçu des propriétés des actinides, est présenté un état de l'art sur les données thermodynamiques relatives au système Pu-phosphate. Etant donné le peu d'information disponible dans la littérature, l'étude bibliographique a été étendue aux analogues de Pu(III), *i.e.* Am, Cm et les lanthanides, et à U(VI) en tant qu'analogue de Pu(VI).

Le **deuxième chapitre** est axé sur la méthodologie, la description des techniques expérimentales et de leur mise en œuvre. La détermination des constantes de formation des phosphato-complexes d'euporium et d'uranium(VI) a été réalisée à l'échelle des traces pour Eu (10^{-8} M) et à l'échelle millimolaire pour U(VI). C'est la technique d'extraction liquide-liquide combinée avec la spectrométrie gamma qui a été utilisée pour quantifier l'interaction Eu-phosphate. L'exploitation des données de partage obtenues à force ionique et température constante permet en effet d'accéder à la stoechiométrie maximale des complexes formés et à leur constante de formation. L'étude de la complexation de U(VI) a été conduite par spectrophotométrie d'absorption UV-Vis, et les données spectrales analysées en utilisant le logiciel Hypspec.

Pour les mesures de solubilité, notre choix s'est porté sur le rhabdophane à base néodyme, un composé dont la structure, la cinétique de dissolution et le produit de solubilité sont parfaitement connus. Par ailleurs, cette phase est également impliquée dans la dissolution de la monazite. Des phases rhabdophane à base Nd ont été dopés avec 1% d'euporium stable, puis avec Eu stable et ^{152}Eu pour permettre un suivi de la dissolution par spectrométrie gamma en mettant en jeu de faibles quantités de matière (de 50 à 1,8 mg). Les premières mesures de solubilité de PuPO_4 synthétisé au CEA de Marcoule, sont également décrites.

L'étude thermodynamique des systèmes Eu/Nd/Pu(III)-phosphate présentée dans le **troisième chapitre**, a été réalisée en milieu homogène et en milieu hétérogène.

En milieu homogène, les expériences ont été conduites avec l'euporium à l'échelle des traces en utilisant l'isotope ^{152}Eu , les coefficients de distribution D pouvant s'identifier au rapport d'activité dans chaque phase (mesures dans des conditions géométriques strictement identiques). Dans un premier temps, c'est la thénoltrifluoroacétone qui a été utilisée comme extractant. Les variations

logarithmiques de D ont été établies en fonction de la concentration totale de phosphate à pH 3 et à une force ionique de 1M imposée par NaClO_4 pour différentes températures. Mais un défaut dans le bilan de matière a été systématiquement observé dès le début de formation du complexe 1:1, avec une perte pouvant aller jusqu'à 90% de l'activité introduite initialement. Un autre extractant a alors été mis en jeu: l'acide di(2-éthylhexyl)phosphorique (HDEHP). Les variations logarithmiques de D en fonction de la concentration totale en phosphate ΣPO_4 , établies à différentes températures, présentent toutes la même allure: un plateau suivi d'une diminution de D avec l'augmentation de ΣPO_4 ce qui traduit la formation progressive de phosphato-complexes d'euporium en phase aqueuse. Des segments de pente -1 et -2, clairement observables sur la **Figure S1** permettent de conclure sans ambiguïté à la formation de complexes de stoechiométrie 1:1 et 1:2. Il faut toutefois souligner la possibilité de formation d'un complexe de stoechiométrie supérieure aux concentrations élevées de phosphate. Même si l'existence de cette espèce a déjà été suggérée dans la littérature, notre interprétation peut néanmoins être sujette à caution en raison du très faible nombre de points expérimentaux dans ce domaine de concentration.

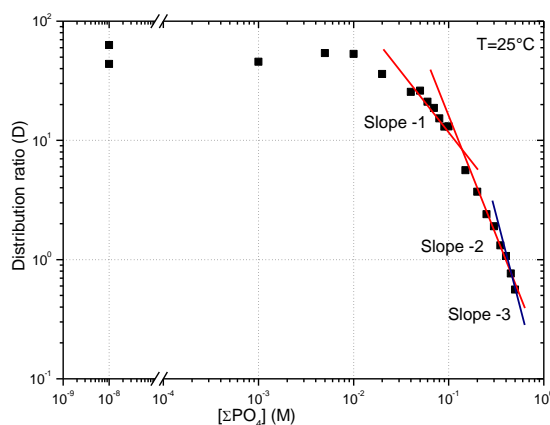
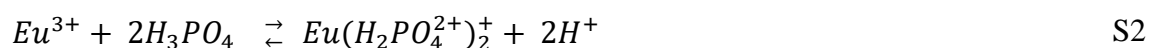
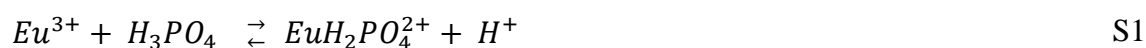


Figure S.1. Variations du coefficient de distribution de ^{152}Eu en fonction de la concentration totale de phosphate ($C_{\text{Eu}} = 10^{-8} \text{ M}$; $C_{\text{HDEHP}} = 0.0075 \text{ M}$; $I = 1 \text{ M}$ (H, NaCl); $pC_{\text{H}} = 3,1$; 25°C)

Les constantes associées aux deux équilibres suivants:



ont été déterminées à différentes températures. Les deux réactions s'avèrent endothermiques avec une contribution entropique modérée, en accord avec les données de la littérature.

En milieu hétérogène, l'objectif était de vérifier la possibilité de déterminer des produits de solubilité en mettant en jeu une petite quantité de matière (2 mg) en vue de la réalisation d'expériences avec un composé de plutonium. Dans un premier temps, les propriétés structurales, morphologiques et le comportement à la dissolution ont été établis pour $\text{Eu}_{0.01}\text{Nd}_{0.99}\text{PO}_4 \cdot 0.667 \text{H}_2\text{O}$ comparativement au rhabdophane $\text{NdPO}_4 \cdot 0.667 \text{H}_2\text{O}$. La similitude des deux composés, et notamment une dissolution congruente, ont été clairement démontrées. Ensuite, la synthèse de $\text{Eu}_{0.012}\text{Nd}_{0.988}\text{PO}_4 \cdot 0.667 \text{H}_2\text{O}$ a été réalisée en présence de ^{152}Eu conduisant à une phase rhabdophane à base Nd dopée à 7.4 kBq per mg en ^{152}Eu . Les expériences de dissolution ont alors été effectuées avec des masses de composé s'échelonnant entre 50 et 2 mg, avec un rapport masse (mg) /volume (ml) égal à 1. Contrairement aux expériences d'extraction où il s'agissait de mesures d'activité relatives, le suivi de la dissolution par spectrométrie gamma, a nécessité un étalonnage du détecteur pour chaque géométrie d'échantillon, *i.e* chaque volume analysé afin d'en déterminer l'activité absolue. L'évolution de la concentration d'euprimum de même que les produits de solubilité se sont avérés indépendants de la masse initiale de rhabdophane mise en jeu, permettant ainsi d'envisager des expériences avec un composé de Pu(III).

Le composé de plutonium a été synthétisé au CEA de Marcoule par Paul Estevenon et Thomas Dumas. Malheureusement, en raison d'une instabilité de Pu(III) dans la phase rhabdophane, c'est la monazite PuPO_4 qui a été synthétisée et caractérisée. C'est donc sur ce composé qu'ont été effectuées les études de solubilité. L'analyse des surnageants par spectroscopie PERALS a permis d'obtenir les variations de l'activité en $^{239+240}\text{Pu}$ en fonction de la concentration de phosphate présentées sur la **Figure S2**. La quantification du produit de solubilité nécessite le développement d'un protocole d'électrodépôt pour des mesures par spectrométrie alpha. La technique PERALS fait en effet intervenir une étape d'extraction dont l'efficacité dépend de l'acidité et du degré d'oxydation de l'actinide. Néanmoins, le minimum de solubilité observée que la **Figure S2** est en très bon accord avec la seule donnée existante de la littérature.

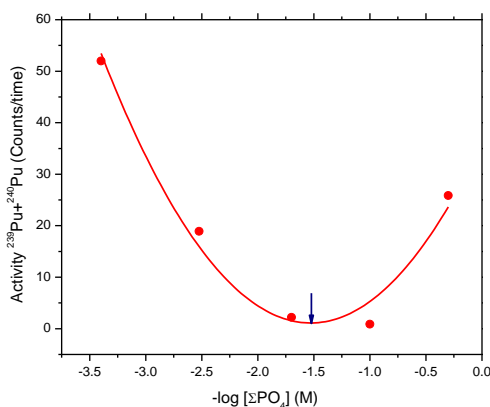


Figure S.2. Dissolution de PuPO_4 en fonction de la concentration de phosphate (mesures PERALS)

L'étude de la complexation de U(VI) par les ions phosphate en solution aqueuse est décrite dans le **quatrième chapitre**. Les variations des spectres d'absorption UV-Vis de U(VI) en fonction de la concentration en espèces phosphatées ont été déterminées dans deux électrolytes: HClO_4 1 M et NaClO_4 0.5 M/ HClO_4 0.5 M à différentes températures. L'augmentation de la concentration de phosphate se traduit par un décalage des bandes d'absorption de l'uranium vers les plus grandes longueurs d'onde, et une augmentation de l'absorbance (**Figure S3**). L'analyse des spectres par le logiciel Hypspec a permis de déterminer les constantes de formation des complexes $\text{UO}_2(\text{H}_2\text{PO}_4)^+$ et $\text{UO}_2(\text{PO}_4)_2$ et les variations d'enthalpie et d'entropie associée. Les données collectées sont du même ordre de grandeur que les données de la littérature.

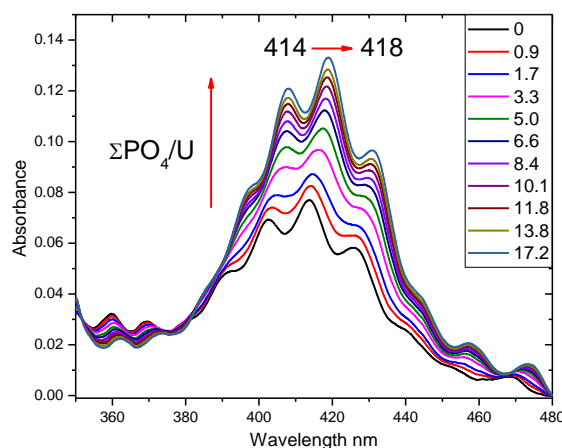


Figure S.3. Spectres d'absorption de U(VI) 7 mM pour différents ratio phosphate/métal à 20°C en milieu NaClO_4 0.5 M/ HClO_4 0.5 M

L'étude thermodynamique a été complétée par des mesures par absorption des rayons X sur la ligne MARS du synchrotron SOLEIL. L'analyse des spectres EXAFS tend à montrer une coordination monodente des deux ligands phosphate dans le complexe $\text{UO}_2(\text{PO}_4)_2$ avec 3 molécules d'eau dans le plan équatorial.

Les **perspectives** de ce travail relatives aux études de complexation en solution homogène peuvent se décliner selon 3 axes:

- confirmer ou infirmer l'existence d'un complexe Eu-phosphate de stoechiométrie 1:3 en augmentant la force ionique
- étudier la complexation de Pu(VI) de façon similaire à l'étude sur U(VI) en utilisant la bande caractéristique à 830 nm
- développer un protocole pour l'étude ultérieure de Pu(IV) en utilisant le radionucléide ^{227}Th à l'échelle des ultra-traces.

En solution hétérogène, l'analyse des surnageants issus de la dissolution de PuPO_4 se poursuit, notamment en développant une procédure d'électrodépôt compatible avec la présence de phosphate. Etant donné que le rhabdophane est susceptible d'apparaître en phase néoformée lors de la dissolution de la monazite, des études sur le rhabdophane de Pu(III) seraient nécessaires.